## QUANTUM LIQUIDS AND QUANTUM CRYSTALS

# Mutual influence of quantum vortices and heat pulses in superfluid helium

L. P. Kondaurova, S. K. Nemirovskiĭ,*) and M. V. Nedoboiko

*S. Kutateladze Institute of Thermophysics, Siberian Branch of the Russian Academy of Sciences, 630090 Novosibirsk, Russia*

(Submitted November 17, 1998; revised February 16, 1999)
Fiz. Nizk. Temp. **25**, 639–649 (July 1999)

The problem of evolution of strong heat pulses in He II interacting with quantum vortices induced by these pulses is investigated numerically on the basis of equations of hydrodynamics of superfluid turbulence. In order to study nonlinear effects, the initial equations are expanded to the second order in the amplitudes of pulses. The one-dimensional case in the absence of mass transport (second sound) is considered. The initiation of vortices was simulated by the generation term in the Vinen equation. The results on the dynamics of pulses in various temperature ranges are presented. It is shown that the Feynman–Vinen theory is applicable in the phase-transition region. © *1999 American Institute of Physics.* [S1063-777X(99)00107-3]

### INTRODUCTION

Quantum turbulence is a manifestation of quantum effects in superfluid helium. This concept is used for an aggregate of chaotic quantized filaments (vortex tangle) formed when the superfluid helium flux (or counterflow) exceeds a certain critical value. Ever since the evolution of the vortex filament density was described by Feynman,[1] the interest of physicists in this object remains undiminished. Most of experimental methods of investigation of superfluid turbulence (ST), such as probing by first and second sounds, measurement of hydrodynamic parameters as well as heat and mass fluxes, are of hydrodynamic type. On the other hand, all known methods of creating ST (ST generation by a flow or counterflow, acoustic waves, etc.) are also hydrodynamic methods. This means that we are dealing with mutual influence of hydrodynamic quantities and parameters of a vortex tangle.

At the beginning of the eighties, a series of publications concerning the study of interaction of high-intensity second-sound waves with a vortex tangle induced by this sound appeared. Commings *et al.*,[2] Lutset *et al.*,[3] and Turner[4] were the first to discover a disagreement in the dynamics of high-intensity second-sound waves with the theory of nonlinear waves. The results of these publications indicated indirectly the formation of a vortex structure. Nemirovskii and Tsoi[5] verified these assumptions directly. They proved that a vortex tangle (VC) evolves in the bulk of a liquid (rather than at the shock front as was assumed earlier) during the propagation of the pulse. A similar experiment was carried out by Torczynskii[6] who demonstrated convincingly the generation of a VC in the bulk of a liquid.

Another series of experiments on the study of intense short heat pulses revealed boiling of helium. According to the Landau two-fluid hydrodynamic model, temperature perturbation does not exceed $\delta T \sim 0.05-0.1$ K even for very strong heat pulses of $100\ \mathrm{W/cm^2}$ (see Khalatnikov[7] and Putterman[8]). This temperature perturbation is insufficient for attaining the ''liquid–vapor'' phase equilibrium curve. Boiling of He II was studied, for example, by Van-Sciver,[9] Tsoi and Lutset,[10] Miklaev *et al.*,[11] Sidyganov *et al.*,[12] Ruppert *et al.*,[13] and Danil'chenko *et al.*[14] These experiments also confirmed indirectly the formation of a vortex structure that changes radically the hydrodynamic properties of superfluid helium.

In order to describe the above experiments quantitatively, we must take into account the effect of ST on the dynamics of hydrodynamic variables. The inclusion of this effect modifies significantly the hydrodynamic parameters, which in turn affects the dynamics of a vortex tangle. A consistent approach to this problem follows from the hydrodynamics of superfluid turbulence (HST) combining the ''conventional'' two-velocity hydrodynamics of superfluid helium (see, for example, Ref. 7) and the macroscopic phenomenological theory of a vortex tangle. The phenomenological theory of the vortex tangle dynamics described in terms of the vortex filament density $L(t)$ was developed by Feynman and Vinen. According to this theory, the dynamics of the quantity $L$ is determined by the value of $L$ itself and satisfies the Vinen equation[15]

$$\frac{dL}{dt}=\alpha_v|\mathbf{W}|L^{3/2}-\beta_v L^2,$$

where $\mathbf{W}=\mathbf{V}_n-\mathbf{V}_s$, and $\mathbf{W}$, $\mathbf{V}_n$, and $\mathbf{V}_s$ are the relative, normal, and superfluid velocities respectively, and $\alpha_v$ and $\beta_v$ are the phenomenological coefficients. The increase in the value of $L$ can be associated with the action of the Magnus force, while its decrease is due to the reconnection of vortex filaments, leading to a cascade fragmentation of loops and their subsequent conversion into thermal excitations. In the Vinen theory, a problem associated with the time $\tau_v$ of formation of a vortex tangle is considered. If, following Vinen, we define $\tau_v$ as the time required for the evolution of the

 

density of vortex filaments to its half value $L_\infty/2 = \alpha_v^2 W^2/(2\beta_v^2)$ corresponding to the stationary case, the Vinen equation gives

$$\tau_v = \int_0^{L_\infty/2} \frac{dL}{\alpha_v |\mathbf{W}| L^{3/2} - \beta_v L^2}.$$

This integral diverges at the lower limit, i.e., $\tau_v \to \infty$. This divergence is due to the fact that the Vinen equation as the equation of the balance between the growth and decomposition of the existing tangle gives no information concerning the initiation of vortices. Experiments made in Ref. 16 prove that $\tau_v$ (which is naturally finite) is a function of the applied counterflow. The empirical dependence has the form $\tau_v = a(T) W^{-3/2}$ In order to correct the emerging discrepancy, Vinen proposed that a generating term $\gamma |\mathbf{W}|^{5/2}$, where $\gamma$ is a certain quantity depending strongly on temperature, should be introduced to account for the mechanism of the initiation of a vortex tangle. The inclusion of this generating term in the equation has made it possible to describe satisfactorily the experimental results for low-intensity heat fluxes.

The next step in the construction of the macroscopic theory was made in the eighties, when the Feynman–Vinen phenomenological theory was included in the two-velocity hydrodynamics of superfluid helium. Three different methods, viz., phenomenological (Nemirovskii–Lebedev[17]), variational (Guerst[18]), and stochastic method (Jamada *et al.*[19]), were used to obtain a complete system of equations describing the hydrodynamics of superfluid turbulent helium. This system essentially combines the classical equations of two-velocity hydrodynamics and the Vinen equation and is quite cumbersome. The problem was mainly solved numerically even in the simplified case when only the second sound is investigated. An attempt at an analytic description was made by one of the authors (see Nemirovskii[20]), who explained (qualitatively and even semi-quantitatively) many results and also described the mechanisms leading to certain effects. Numerical solutions of these equations are given in some publications devoted to boiling of He II and to the dynamics of thermal pulses. For example, linearized HST equations were solved in Refs. 21–23 for describing the propagation of small-amplitude thermal pulses, for which the vortex tangle density has time to tune itself to the change in hydrodynamic parameters. For example, the dependence of the time of He II boiling on the heat flux, which successfully describes experiments made in Ref. 9 was obtained in Ref. 21. However, in the above publications, an approximation is used which presumes that the initial evolution of a vortex tangle does not affect the processes occurring in this case. For this reason, the Vinen equation is not used in the above calculations to the fullest extent.

A more interesting case is the propagation of a large-amplitude heat pulse (see experimental work[24–28]), which can be described only by taking into account the entire dynamics of a vortex tangle. Besides, nonlinear distortions also become significant, and hence we must take into account second-order terms in HST equations. The corresponding calculations were made by Fiszdon *et al.* (Gottingen, FRG), Nemirovskii *et al.* (Novosibirsk, USSR), and Murakami and Iwashita (Tsukuba, Japan). The research made by the Gottingen group, in which calculations were supplemented by experimental measurements, deserve special attention.

Fiszdon *et al.*[25,29] analyzed in detail the influence of various factors for which the HST theory developed earlier failed to give an unambiguous answer, e.g., the effect of drift velocity of VC and the generating term in the Vinen equation. Since the mechanism of the initiation of a vortex tangle remains unclear, two approaches are used for an analysis of dynamics of heat pulses: (a) it is assumes that a certain background density of VC already exists in the bulk of helium, and in this case the balance equation for $L$ is used for describing the experimental data, and (b) it is assumed that VC evolves in the bulk of He II according to a certain (yet unknown) mechanism, and this evolution is described by the generating term introduced by Vinen in the equation for $L$. Among other things, Fiszdon *et al.*[25,29] found out that the expression proposed by Vinen for the generating term is insignificant and does not lead to any significant change in the pulse dynamics. For this reason, they chose a different approach, assuming that an initial vortex tangle density (VTD) already exists in the bulk of helium. It should be noted that Fiszdon *et al.*[25,29] used in their calculations the fitting parameters for an adequate description of experimental data, such as the preset initial VTD level, an appropriate choice of boundary conditions, and the variation of parameters in the Vinen equation.

The HST equations were also analyzed numerically by Murakami and Iwashita.[23] In contrast to the above-mentioned publications by the Göttingen group, they did not expand the system of HST equations into a power series in deviations from equilibrium. Such an approach, however, requires the knowledge of the dependence of thermodynamic quantities on $W^2$, which are known only in the first order (this was used by the authors in complete equations). The results of these publications are close quantitatively.

In spite of the fact that the interaction of second sound pulses and VC were analyzed quite intensely, both numerically and analytically some problems remain unsolved. In particular, the temperature region in which the second sound nonlinearity coefficient is negative or assumes zero value was not considered at all, although corresponding experimental results are available.[27,28] For example, Goldner *et al.*[28] observed the behavior of nonlinear second sound pulses near the λ-point, which differs significantly from the dynamics of heat pulses in the low-temperature region. It is unclear whether this is due to superfluid turbulence or the closeness to $T_\lambda$, and hence peculiarities typical of the given region. However, this is important from the point of view of applicability of the Feynman–Vinen theory in the vicinity of the phase-transition region. In addition, the mechanism of initiation of the vortex structure in the bulk of He II remains unclear.

In connection with what has been said above, we made an attempt to clarify some aspects in the description of the accumulated experimental results. We derived HST equations in the second approximation in the deviation of $W$, $L$, and $T$ from their equilibrium values. It was found, however,

that these equations differ slightly from the equations presented in Refs. 25 and 29. Namely, it will be proved below that several significant expansion terms are omitted in the hydrodynamic equations used in Ref. 25. In this connection, we solved the problem on propagation of low-intensity heat discontinuities in the absence of a vortex tangle. We derived a formula for the velocity of propagation of these heat discontinuities coincides with the familiar Khalatnikov expression,[7] confirming the correctness of our equations. On the other hand, the equations proposed in Ref. 25 cannot be used for obtaining such a solution. This circumstance necessitated repeated numerical calculations for interpreting the experimental data obtained in Ref. 25.

In Sec. 1 of this paper, we derive the HST equations in the second order for a planar geometry in the absence of mass transfer and solve the problem on propagation of a finite-amplitude temperature perturbation in vortex-free helium. In Sec. 2, the results of numerical solutions of the obtained system of equations by the ''discontinuity decay'' method (Godunov method[30]) are considered. This system of equations describes the propagation of high-intensity heat pulses in various temperature regions of unperturbed helium. The effect of the generating term in the Vinen equation on the dynamics of a heat pulse is analyzed simultaneously.

## 1. HYDRODYNAMIC EQUATIONS OF SUPERFLUID TURBULENCE

The HTS equations derived by different authors are slightly different. However, these differences are insignificant when we describe the evolution of high-intensity heat pulses. We write the system of equations derived when the phenomenological method of constructing HST was used[17]:

$$\frac{\partial S}{\partial t}+\operatorname{div}(S\mathbf{V}_n)=\frac{1}{T}\left|\alpha_1 L\mathbf{W}^2+\varepsilon_\beta\beta L^2\right|, \tag{1}$$

$$\frac{\partial \mathbf{V}_s}{\partial t}+\nabla\left(\mu(p,\sigma,\mathbf{W})+\frac{\mathbf{V}_s^2}{2}\right)=\frac{\alpha_1 L}{\rho_s}\mathbf{W}+\frac{\varepsilon_\beta\alpha}{\rho_s}L^{3/2}\frac{\mathbf{W}}{|\mathbf{W}|}, \tag{2}$$

$$\frac{\partial \mathbf{j}_i}{\partial t}+\frac{\partial(\pi_{ik}+\tau_{ik})}{\partial r_k}=0, \tag{3}$$

$$\frac{\partial \rho}{\partial t}+\operatorname{div}\mathbf{j}=0, \tag{4}$$

$$\frac{\partial L}{\partial t}+\operatorname{div}\mathbf{V}_L L=\chi_1\frac{B\rho_n}{\rho}|\mathbf{W}|L^{3/2}-\chi_2\kappa L^2. \tag{5}$$

In these relations, the following notation has been used: $S=\rho\sigma$ ($\sigma$ is the entropy per unit mass), $\rho=\rho_s+\rho_n$ ($\rho$, $\rho_s$, and $\rho_n$ are the density of liquid and the superfluid and normal densities of liquid, respectively, $\mathbf{j}=\rho_n\mathbf{V}_n+\rho_s\mathbf{V}_s$; $\pi_{ik}=\rho_n\mathbf{V}_{ni}\cdot\mathbf{V}_{nk}+\rho_s\mathbf{V}_{si}\cdot\mathbf{V}_{sk}+p\,\delta_{ik}$:

$$\tau_{ik}=-\eta\left(\frac{\partial \mathbf{V}_{ni}}{\partial r_k}+\frac{\partial \mathbf{V}_{nk}}{\partial r_i}-\frac{2}{3}\delta_{ik}\frac{\partial \mathbf{V}_{nl}}{\partial r_l}\right)$$
$$-\delta_{ik}[\xi_1\operatorname{div}(\mathbf{j}-\rho\mathbf{V}_n)+\xi_2\operatorname{div}\mathbf{V}_n];$$

$$\sigma_T=\partial\sigma/\partial T,\quad \sigma_{TT}=\partial^2\sigma/\partial T^2;\quad \alpha=\chi_1 B\rho_n/2\rho;$$

$$\alpha_1=A\rho_s\rho_n\beta^2/\alpha^2;\quad \beta=\kappa\chi_2/2\pi;\quad \varepsilon_\beta=\rho_s\kappa^2;$$

$A=\chi_1^2\pi B^3\rho_n^2 m_{\mathrm{HE}}/6\chi_2^2\rho^3 h$ is the Gorter–Mellinck constant, $V_L$ the velocity of a vortex tangle, $\chi_1$ and $\chi_2$ are the parameters in the Vinen equation, $B$ is the Hall–Vinen coefficient, and $\kappa=2\pi\hbar/m_{\mathrm{He}}$ the circulation quantum.

Putting further $\sigma=\sigma_0+\sigma'$, $T=T_0+T'$ ($T'$ and $\sigma'$ are the deviations from equilibrium values) and using the well-known relations $\sigma(p,T,\mathbf{W})=\sigma(p,T)+(1/2)\mathbf{W}^2\partial(\rho_n/\rho)/\partial T$ and $d\mu=-\sigma dT+dp/\rho-(\rho_n/\rho)\mathbf{W}d\mathbf{W}$, we obtain the system of equations in the absence of a mass flux ($\mathbf{j}=\rho_n\mathbf{V}_n+\rho_s\mathbf{V}_s=0$ is the condition satisfied in our experiments) in the second order of deviations in the planar geometry:

$$\frac{\partial T'}{\partial t'}-\left(\frac{\sigma_0(\rho+\rho_n)}{\sigma_T\rho_n\rho}\frac{\partial\rho_n}{\partial T}-\frac{\rho_s}{\rho}\right)\mathbf{W}'\frac{\partial T'}{\partial \mathbf{x}'}-\frac{\rho_s}{\rho}$$
$$\times\left(\frac{\sigma_0\sigma_{TT}}{\sigma_T^2}-1\right)T'\frac{\partial \mathbf{W}'}{\partial \mathbf{x}'}+\frac{\sigma_0\rho_s}{\sigma_T\rho}\frac{\partial \mathbf{W}'}{\partial \mathbf{x}'}$$
$$=\frac{1}{\rho\sigma_T T_0}(\alpha_1 L W'^2+\varepsilon_\beta\beta L^2); \tag{6}$$

$$\frac{\partial \mathbf{W}'}{\partial t'}+\frac{\rho_s}{2\rho}\left(3-\frac{\sigma_0}{\sigma_T\rho_n}\frac{\partial\rho_n}{\partial T}\right)\frac{\partial \mathbf{W}'^2}{\partial \mathbf{x}'}+\frac{\rho\sigma_0}{\rho_n}\frac{\partial T'}{\partial \mathbf{x}'}$$
$$+\frac{\rho\sigma_T}{2\rho_n}\frac{\partial T'^2}{\partial \mathbf{x}'}=-\frac{\rho\alpha_1}{\rho_s\rho_n}L\mathbf{W}'-\frac{\rho\varepsilon_\beta\alpha}{\rho_s}L^{3/2}\frac{\mathbf{W}'}{|\mathbf{W}'|}; \tag{7}$$

$$\frac{\partial L}{\partial t'}-\frac{\rho_n}{\rho}\frac{\partial \mathbf{W}' L}{\partial \mathbf{x}'}=\chi_1\frac{B\rho_n}{\rho}|\mathbf{W}'|L^{3/2}-\chi_2\kappa L^2. \tag{8}$$

In these equations, we consider that $\mathbf{V}_L=\mathbf{V}_s$ according to the available data of measurements.[31]

It can be seen that these equations do not coincide with those given in Refs. 25 and 29. Namely, the equation for the velocity $\mathbf{W}'$ does not contain the terms

$$\frac{\rho\sigma_T}{\rho_n}\frac{\partial T'^2}{\partial x'^2}\quad\text{and}\quad-\frac{\sigma_0\rho_s}{2\sigma_T\rho\rho_n}\frac{\partial\rho_n}{\partial T}\frac{\partial \mathbf{W}'^2}{\partial x'^2},$$

while the expression for the temperature $T'$ does not contain the terms

$$\left(\frac{\sigma_0}{\sigma_T\rho_n}\frac{\partial\rho_n}{\partial T}+\frac{\sigma_0}{\sigma_T\rho}\frac{\partial\rho_n}{\partial T}\right)\mathbf{W}'\frac{\partial T'}{\partial \mathbf{x}'}$$

and

$$\left(1-\frac{\sigma_0\sigma_{TT}\rho_s}{\sigma_T^2\rho}\right)T'\frac{\partial \mathbf{W}'}{\partial \mathbf{x}'}.$$

In order to verify the validity of the derived equations, we consider the propagation of the finite-amplitude perturbation in vortex-free helium. We shall find the velocity $c_2$ of a point corresponding to the deviation of $T'$ from the equilibrium temperature. In the one-dimensional case, all parameters of motion with a constant amplitude obey the relation $\partial/\partial t=-c_2(\partial/\partial x)$. Substituting this relation into the system of equations (6) and (7), from the compatibility condition we obtain

$$c_2=\left(\frac{\rho_s\sigma_0^2}{\rho_n\sigma_T}\right)^{1/2}+\left[\frac{3\rho_s}{\rho}-3\sigma\left(\frac{\partial\rho_n}{\partial T}\right)\frac{1}{2\rho_n\sigma_T}-\frac{\sigma_0\sigma_{TT}\rho_s}{2\sigma_T^2\rho}\right]W'=c_{20}+\alpha_2 W',$$

where $c_{20}^2=\rho_s\sigma_0^2/\rho_n\sigma_T$, and $\alpha_2=3\rho_s/\rho-3\sigma(\partial\rho_n/\partial T)/2\rho_n\sigma_T-\sigma_o\sigma_{TT}\rho_s/2\sigma_T^2\rho$ is the second sound nonlinearity coefficient. The convolution of this expression gives the well-known Khalatnikov formula.[7,8] At temperatures above 1.884 K and in the temperature range 0.4–0.9 K, the coefficient $\alpha_2<0$, while in the remaining region $\alpha_2>0$. In temperature regions where $\alpha_2>0$, the discontinuity surfaces are formed at the leading front of the wave, in the temperature region where $\alpha_2<0$, they are formed at the trailing edge of the wave, while the shape of the pulse does not change at temperature for which $\alpha_2$ assumes zero value. It can be verified easily by analyzing the system of equations used in Refs. 25 and 29 that this expression for the velocity of second sound cannot be derived.

Thus, the propagation of heat pulses of various amplitudes and duration can be analyzed numerically on the basis of the set of equations (6)–(8) by the discontinuity decay method[30] at the unperturbed helium temperatures 1.4, 1.7, and 1.884 K for $t=(T_\lambda-T)/T_\lambda=10^{-5}$, i.e., in the regions in which the second sound nonlinearity coefficient is positive, negative, or equal to zero, respectively. The influence of the generating term in the Vinen equation on the dynamics of temperature pulse is also studied.

## 2. NUMERICAL ANALYSIS OF DYNAMICS OF HIGH-INTENSITY HEAT PULSES IN VARIOUS TEMPERATURE REGIONS

### 2.1. Propagation of strong heat pulses in the temperature range where $\alpha_2>0$

It should be recalled that discontinuities are formed at the leading front of the wave in the temperature range in which the second sound nonlinearity coefficient assumes positive values. Fiszdon *et al.*[25] found that the temperature evolution at points separated by different distances from the heater proceeds in different ways (see Fig. 1c). Such a behavior of pulses is due to the mutual influence of VC and hydrodynamic quantities. In the description of the obtained experimental results presented in Ref. 25, we solved the problem under the following initial and boundary conditions corresponding to the experimental conditions:a rectangular heat pulse is supplied at one end of a long channel filled with unperturbed helium:

$$T'(x')=0,\quad W'(x')=0\quad \text{for } t'=0,$$

$$W'(t')=Q/\rho ST\quad \text{for } x'=0,\quad 0<t'<t_H,$$

$$W'(t')=0\quad \text{for } x'=0,\quad t'>t_H,$$

where $Q$ is the heat flux and $t_H$ the pulse duration. In our analysis of the influence of the initial level of the VTD as well as the generating term in the Vinen equation on the dynamics of heat pulse during the solution of the problem formulated above, we used the following two approaches: (a) we assumed that a certain initial distribution of the vortex tangle density $L(x',t'=0)=L_0$ already exists in the bulk of the liquid at the initial stage, and in this case the Vinen balance equation was used for describing the dynamics of $L$; and (b) we assumed that $L_0=0$ in unperturbed helium, and the initial evolution of the VC is described completely by the generating term, i.e., the Vinen equation with this extra term is used in the solution.

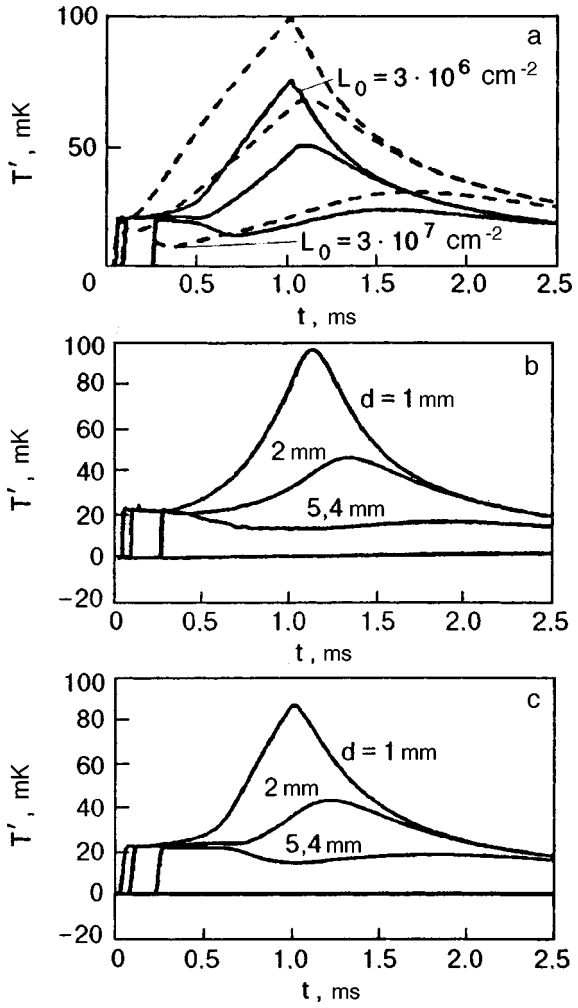


FIG. 1. Temperature evolution at points located at distances 1, 2, and 5.4 mm from the heater. The temperature of unperturbed helium is $T_0=1.4$ K, heat flux $Q=5$ W/cm$^2$, and pulse duration $t_H=1$ ms. The $T(t)$ dependences obtained by us (a) and in Ref. 25: experimental (b) and theoretical (c).

Case (a). In order to find the distributions of temperature $T'$, velocity $W'$, and the vortex tangle density $L'$ as functions of time and coordinate, we used (as in Ref. 25), a certain preset value $L_0$ as a fitting parameter. Figure 1a shows the results of numerical calculations of time dependence of temperature at the points separated by 1, 2, and 5.4 mm from the heater for $L_0=3\times10^6$ cm$^{-2}$ (solid curves) and $L_0=3\times10^7$ cm$^{-2}$ (dashed curves) for $T=1.4$ K, $Q=5$ W/cm$^2$ and $t_H=1$ ms. Figures 1b and 1c show experimental data and the results of numerical calculations[25] for the same parameters. It can be seen that the theoretical curves obtained by us (for $L_0=3\times10^6$ cm$^{-2}$) and in Ref. 25 are close: the dependences have the same typical form, the peaks on the curves are observed at the same instant of time,

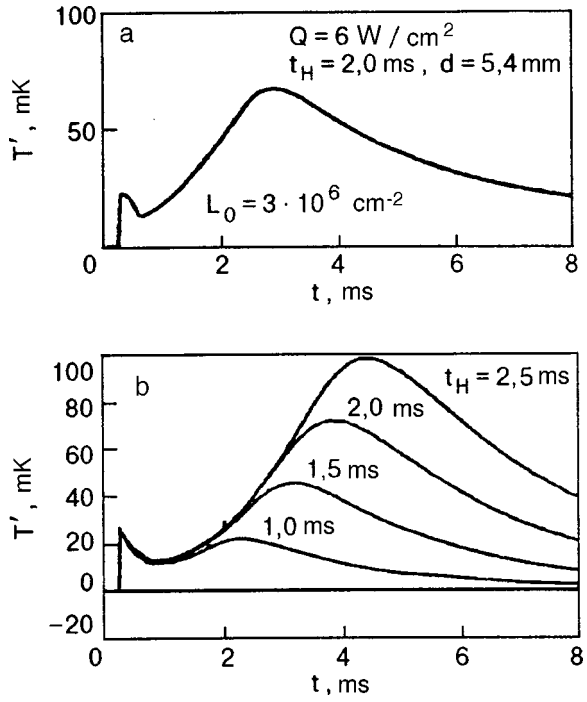


FIG. 2. Time dependence of temperature for different times of heating at a point located at a distance of 5.4 mm from the heater. The theoretical curve obtained by us (a) and experimental results obtained in Ref. 25 (b).

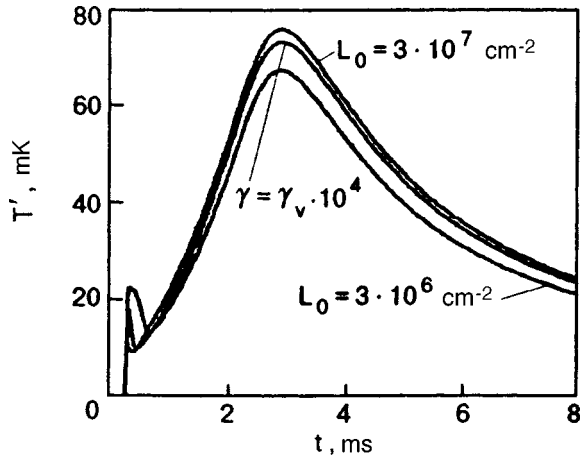


FIG. 3. Comparison of theoretical curves obtained using different approaches to the description of the initial evolution of vortex filament density. The temperature of unperturbed helium is $T_0=1.4$ K, heat flux $Q=5$ W/cm$^2$, pulse duration $t_H=1$ ms, and the distance to the heater $d=5.4$ mm.

and the curves attain the same asymptote. At the same time, a certain difference is observed: the peaks on the reduced curves differ numerically. Both these theoretical curves describe experimental results qualitatively. However, the positions and heights of the peaks on the curves do not coincide. Figure 2 shows the experimental curve[25] and numerical curve obtained by us, which describe the $T'(t')$ dependence at a point located at a distance of 5.4 mm from the heater for a heat pulse of the amplitude $Q=6$ W/cm$^2$ and duration $t_H=2$ ms for $L_0=3\times10^6$ cm$^{-2}$. A comparison of these curves demonstrates a discrepancy similar to that in the previous case, i.e., the positions and heights of the peaks on the curves do not coincide. Having analyzed the effect of all dissipative terms in the equations, we conclude that since the dissipation of the temperature pulse (see the experimental curve) is observed at a later instant of time, and the values of the amplitude are quite close, the discrepancy is rather due to inaccuracy in determining the Gorter–Mellinck constant.

Case (b). Varying the coefficient $\gamma$ of $W'^{5/2}$ in the Vinen equation, namely, increasing its value by a factor of $10^4$ as compared to the coefficient proposed by Vinen (since the characteristic time $\tau_v$ of evolution of a vortex tangle behaves approximately as a reciprocal cubic root of heat flux, this increase approximately corresponds to a decrease in $\tau_v$ approximately by a factor of 30), we obtained good agreement between the theoretical curves with the calculated curves described above (Fig. 3).

Thus, numerical and experimental curves are in accord with one another if we use in calculations the background VTD value $L_0=3\times10^6$ cm$^{-2}$ or a coefficient in the generating term exceeds the value proposed by Vinen by four orders of magnitude. Naturally, these situations do not correspond to physical reality, i.e., neither of these approaches to the solution of the problem of initiation of vortex filaments in the bulk of the liquid lead to reasonable physical results. In our opinion, the presence of such a strong background turbulence in the bulk of the liquid is due to the fact that heat pulses in the experiments described above were initiated under periodic conditions. For this reason, the dynamics of each pulse is determined by the conditions of generation of the entire series of pulses, in particular, the ''duty factor'' of the sequence of pulses. It should be noted that the attempts of numerical calculations on the basis of periodic conditions[25,29] did not lead to reasonable results. This is apparently due to the fact that the Vinen equation fails to describe free decay of a vortex tangle.[32]

Generation of pulses under periodic conditions is complicated by experimental difficulties in the observation of solitary pulses. This difficult problem was solved by Shimazaki *et al.*[33] who observed the evolution of virtually solitary heat pulses. The time of expectation between two consecutive pulses was 120 s. This time is quite sufficient for the decay of a vortex tangle. Unfortunately, the results of experiments made in Refs. 25 and 33 cannot be compared since the experiments were made at different temperatures of unperturbed helium. Shimazaki *et al.*[33] found that the time of evolution of a vortex tangle for strong second sound pulses is approximately one third the time period proposed by Vinen. We used this fact to describe the experimental data, correcting appropriately the generating term. Figure 4 shows the numerical results and experimental data[33] on the time dependence of temperature for a point located at 30 mm from the heater at bath temperature $T=1.7$ K for various densities of the heat flux $Q$ for the heat pulse duration $t_H=500$ $\mu$s. It can be seen that the numerical and experimental values of the pulse amplitude are approximately the same.

We also made calculations using the background value $L_0$ of the VTD as well as the combinations of the background value and the initial term. Figure 5 shows the numerical results obtained for different combinations of the back-

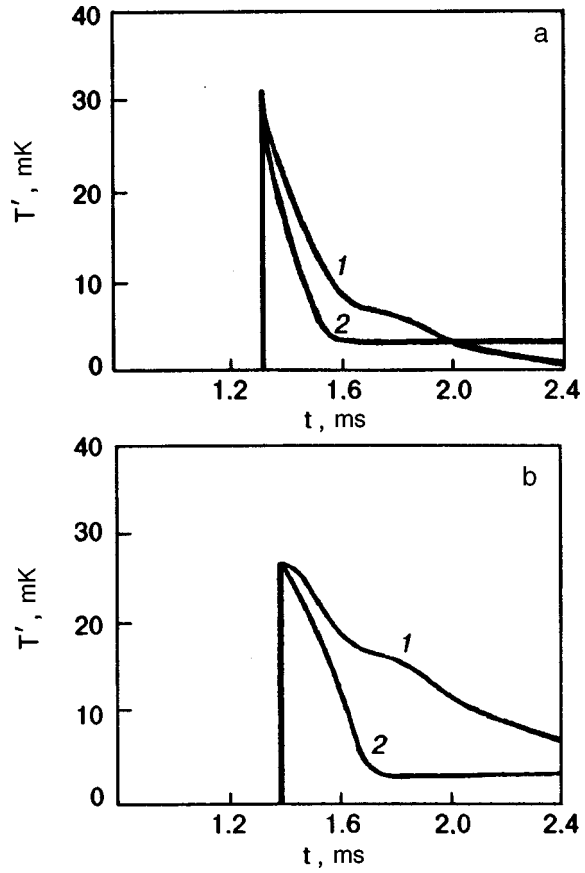


FIG. 4. Comparison of experimental data obtained in Ref. 33 (*1*) and the time dependence of temperature (*2*) obtained numerically: $Q=40$ W/cm$^2$ (a) and $Q=20$ W/cm$^2$ (b).

ground value of $L_0$ and $\gamma$. It can be seen that these curves differ significantly from the curve described above.

Thus, the obtained results can be regarded as a proof of the fact that the additional generating term increased in accordance with the experimental data[33] describes the initiation of a vortex tangle. The shape of pulses matches with the remaining coefficients in the Vinen equations, which can be different for powerful heat pulses.

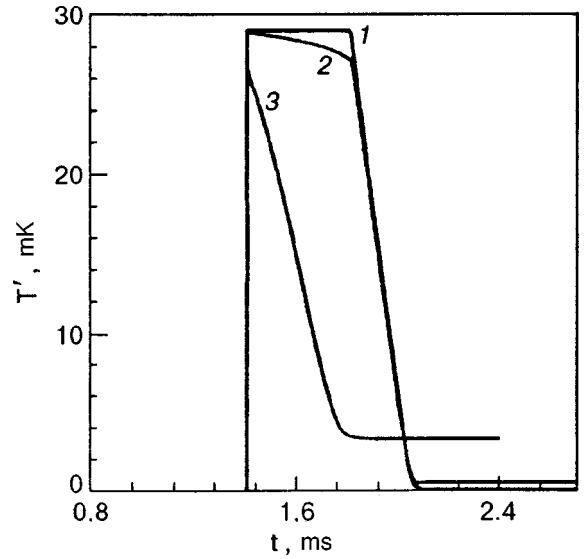


FIG. 5. Calculated time dependences of temperature. The temperature of unperturbed helium is $T_0=1.7$ K, heat flux $Q=20$ W/cm$^2$, pulse duration $t_H=0.5$ ms, and the distance to the heater $d=30$ mm; $\gamma=\gamma_v$, $L_0=0$ (*1*); $\gamma=\gamma_v$, $L_0=100$ cm$^{-2}$ (*2*); $\gamma=\gamma_v\times 25$, $L_0=0$ (*3*).

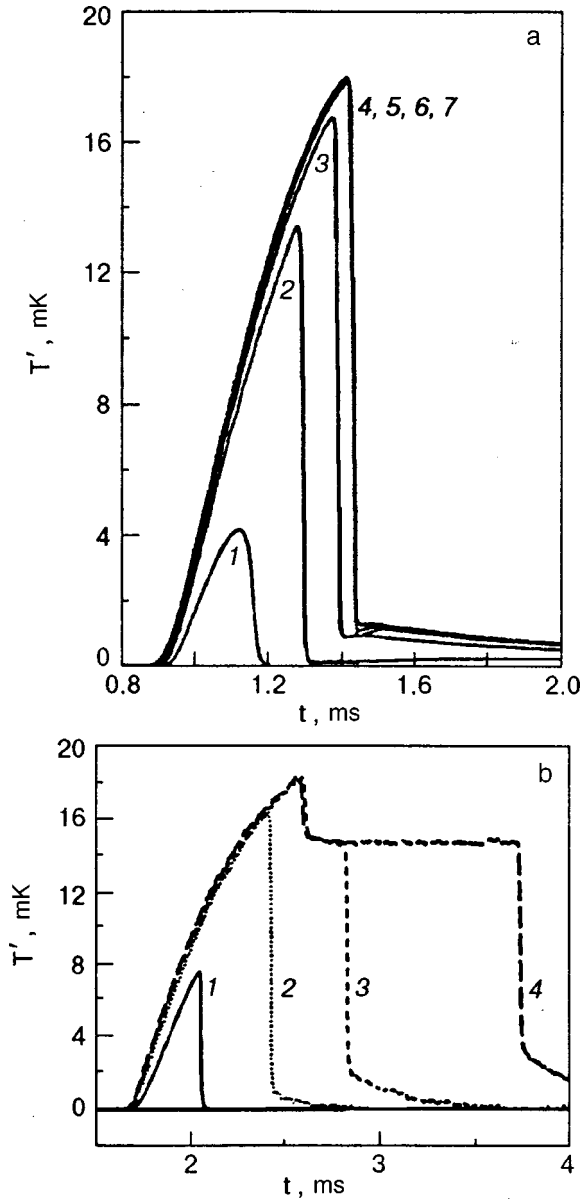


FIG. 6. Calculated (a) and experimental[28] (b) results: $T_0/T_\lambda=2\times10^{-5}$ (curve *1*). The shape of the pulse generated at the heater is half sinusoidal with frequency $\nu=1387$ Hz. The peaks of heat fluxes $Q$, mW/cm$^2$: 0.81 (curve *1*), 4.01 (curve *2*), 8.12 (curve *3*), 15.6 (curve *4*), 20 (curve *5*), 25 (curve *6*), and 30 (curve *7*).

### 2.2. Propagation of powerful heat pulses in the region of negative nonlinearity, $\alpha_2<0$

It was noted above that the temperature region in which the second sound nonlinearity coefficient is negative was not considered in the above-mentioned publications where the numerical method was used. As regards experimental works, the only publication[28] known to us covers the temperature range near $T_\lambda$, $t=1-T/T_\lambda=10^{-5}$, where $\alpha_2$ assumes a negative value. Shock front had time to be formed at the

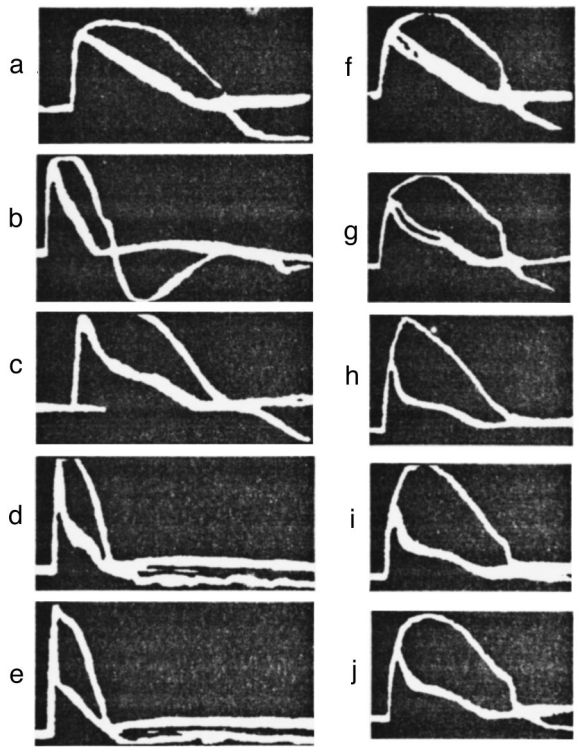


FIG. 7. Oscillograms of second sound waves[27]: pulse duration $t_H = 100\ \mu$s, distance from the heater is 2.7 mm (a–e) and 15.1 mm (f–g); $Q$, W/cm$^2$: 21.7 (a), 24.6 (b), 30.3 (c), 37.1 (d), 51.2 (e), 21.7 (f), 24.9 (g), 30.2 (h), 37.1 (i), and 52 (j); 20 and 50 $\mu$s/div.

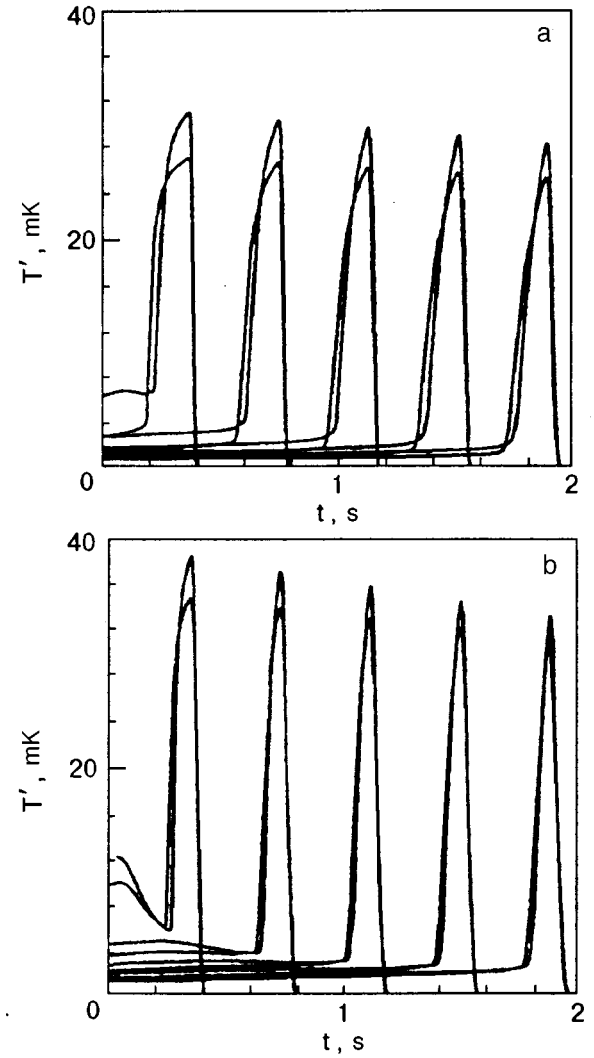


FIG. 8. Propagation of a heat pulse along the channel; $Q$, W/cm$^2$: 30, 35 (a) and 40, 45 (b).

trailing edge of high-intensity second sound pulses generated in these experiments when the detector arranged on the opposite side of the channel was reached. It can be seen (Fig. 6b) that experimental dependences of temperature on time differ significantly from those obtained earlier in the region of positive nonlinearity. The region near $T_\lambda$ is known to have typical singularities, and it is hence unclear whether such a behavior of pulses is due to proximity to $T_\lambda$ or due to superfluid turbulence. However, this is important to determine the applicability of the Feynman–Vinen theory in the vicinity of the phase-transition region.

In order to find answers to these questions, we solved the problem under the following initial and boundary conditions corresponding to the experimental conditions[28]: a heat pulse of frequency $\nu = 2387$ Hz having a shape of half-sinusoid is supplied at one end of a long channel filled with unperturbed helium. Numerical count was made on the basis of the Vinen equation with an additional generating term. The coefficients used in the first two terms on the right-hand side of this equation were obtained by direct extrapolation of the temperature dependences of $B$, and thermodynamic parameters to the region of $T_\lambda$ according to Refs. 34 and 35 The coefficient of $W^{5/2}$ was chosen so that the heights of the peaks of the theoretical and experimental dependences of $T'$ on $t'$ coincided for $Q = 15.6$ mW/cm$^2$. Figure 6a shows the theoretical curves of the time dependence of temperature at the point of location of the detector for the following values of heat flux: $Q_1 = 0.81$ mW/cm$^2$, $Q_2 = 4.01$ mW/cm$^2$, $Q_3 = 8.12$ mW/cm$^2$, $Q_4 = 15.6$ mW/cm$^2$, $Q_5 = 20$ mW/cm$^2$, and $Q_6 = 25$ mW/cm$^2$. It can be seen from the figure that discontinuity of pulses corresponding to different values of $Q$ occurs for close values of time. This can be explained as follows. In the temperature range under investigation, the leading fronts of pulses with different amplitudes are almost identical, and hence the evolution of a vortex tangle occurs virtually under the same conditions. According to the Vinen equation, the density of the vortex tangle at first increases slowly, and then its increase becomes very rapid. Consequently, the tangles generated by pulses of different amplitudes grow to size virtually terminating the temperature increase during the same time. Goldner *et al.*[28] also observed the termination of temperature increase for pulses of different amplitudes approximately during the same time periods (see Fig. 6b). However, the subsequent time dependence of temperature differs from the theoretical dependence. It was mentioned above that the shape of pulses is determined by the coefficients in the Vinen equation, which were not defined exactly for high-intensity heat fluxes. The obtained theoretical curves describe experimental data only qualitatively. However, we can conclude that such a peculiar behavior of

pulses is associated with superfluid turbulence, and the Vinen equation is applicable in this region, although the extrapolation of coefficients to the region of $T_\lambda$ is only of qualitative nature. Besides, the additional generating term in this equation describes the initiation of vortex filaments.

### 2.3. Propagation of high-intensity heat pulses in the temperature region where $\alpha_2=0$

No numerical calculations have been made earlier at temperatures at which the nonlinearity coefficient assumes zero value. It was mentioned above that Lutset and Tsoi[27] studied experimentally powerful heat pulses at the helium bath temperature $T=1.884$ K. Figure 7 shows oscillograms of second sound waves.[27] It should be noted that the observed experimental dependence $T'(t')$ (see Fig. 7) has the shape of the curves obtained in the region of negative nonlinearity of second sound. Such a qualitative coincidence of the observed dependences can be explained as follows. At first, the authors sent a moderate-amplitude heat pulse along the channel, and the second pulse whose dynamics was investigated was sent in the wake of the first pulse. The first heat pulse propagating along the channel generated a vortex structure in the bulk of helium, simultaneously heating it to a certain extent. This led to a departure from the initial value of helium temperature of 1.884 K to the region of negative nonlinearity. Besides, the error in determining the temperature of unperturbed helium (see Ref. 27 for details of experiments) also leads to the conclusion that their measurements were made in the negative nonlinearity region.

The results of numerical calculations of the coordinate dependence of temperature at various instants of time are shown in Fig. 8 for the following values of heat flux $Q$ (in W/cm$^2$): 30, 35, 40, and 45 and for $t_H=0.001$ s. Note that the two peaks are observed for heat fluxes of 40 and 45 W/cm$^2$, while for smaller heat fluxes the temperature decreases monotonically. It should be recalled that such a behavior of pulses is observed in the region of positive nonlinearity coefficient.

## CONCLUSION

The numerical analysis based on the equations of hydrodynamics of superfluid turbulence proved that

(1) the mutual influence of the vortex tangle parameters and hydrodynamic quantities leads to a change in the dynamics of high-intensity heat fluxes observed in a series of experiments;
(2) the generating term introduced by Vinen and additionally corrected according to experimental data[33] describes the initial evolution of vortex filaments in the bulk of the liquid, and
(3) the Feynman–Vinen theory can be used in the vicinity of the phase-transition temperature.

This research was carried out under the support of Russian Fund for Fundamental Research (Grant No. 96-02-19414).

*)E-mail: nemirov@otani.thermo.nsk.su

[1] R. P. Feynman, *Progress in Low Temperature Physics*, vol. 1 (ed. by C. J. Gorter), North Holland, Amsterdam (1955).
[2] J. C. Cumming, D. W. Schmidt, and W. J. Wagner, Phys. Fluids **21**, 713 (1978).
[3] M. O. Lutset, S. K. Nemirovskiĭ, and A. N. Tsoĭ, Zh. Éksp. Teor. Fiz. **81**, 249 (1981) [Sov. Phys. JETP **54**, 127 (1981)].
[4] T. N. Turner, Phys. Fluids **26**, 3227 (1983).
[5] S. K. Nemirovskiĭ, and A. N. Tsoĭ, JETP Lett. **35**, 286 (1982).
[6] J. R. Torczynskii, Phys. Fluids **27**, 2636 (1984).
[7] I. M. Khalatnikov, *Theory of Superfluidity* [in Russian], Nauka, Moscow (1971).
[8] C. Putterman, *Superfluid Hydrodynamics*, North-Holland, Amsterdam (1974).
[9] S. W. Van Sciver, Cryogenics **19**, 385 (1979).
[10] A. N. Tsoĭ and M. O. Lutset, Inzh.-Fiz. Zh. **51**, 5 (1984).
[11] V. M. Miklaev, I. A. Sergeev, and Yu. P. Filippov, Preprint Joint Inst. Nucl. Res. P8-87-33, Dubna (1987).
[12] V. U. Sidyganov and I. A. Klyuchnikov, *Abstracts of Papers to the Vth All-Union School of Young Scientists and Specialists ''Contemporary Problems in Thermal Physics''*, Novosibirsk (1988).
[13] U. Ruppert, W. Z. Yang, and K. Luders, Jpn. J. Appl. Phys., Suppl. **26**, Suppl. 26-3 (1987).
[14] B. A. Danil'chenko and V. N. Porpshin, Cryogenics **23**, 546 (1983).
[15] W. F. Vinen, Proc. R. Soc. London, Ser. A **240**, 128 (1957).
[16] W. F. Vinen, Proc. R. Soc. London, Ser. A **242**, 493 (1957).
[17] S. K. Nemirovskiĭ and V. V. Lebedev, Zh. Éksp. Teor. Fiz. **84**, 1729 (1983) [Sov. Phys. JETP **57**, 1009 (1983).
[18] J. A. Guerst, Physica B **154**, 327 (1989).
[19] K. Yamada, S. Kashiwamura, and K. Miyake, Physica B **154**, 318 (1989).
[20] S. K. Nemirovskiĭ, Zh. Éksp. Teor. Fiz. **91**, 1363 (1986) [Sov. Phys. JETP **64**, 803 (1986)].
[21] S. K. Nemirovskii, L. P. Kondaurova, and A. Ja. Baltsevich, Cryogenics **32**, 47 (1992).
[22] D. Gentile and J. Pakleza, Numer. Heat Transfer **6**, 317 (1983); Arch. Mech. **38**, 585 (1986).
[23] A. Murakami and K. Iwashita, *Proc. ICEC 13*, Butterworths, Guiford, UK (1990).
[24] W. F. Fiszdon and M. von Schwerdtner, J. Low Temp. Phys. **75**, 253 (1989).
[25] W. F. Fiszdon, M. von Schwerdtner, G. Stamm, and W. Popper, J. Fluid Mech. **212**, 663 (1990).
[26] A. Yu. Iznankin and L. P. Mezhov-Deglin, in *Abstracts of Papers to 17th Int. Conf. on Low Temp. Phys.*, Vol. 1, Elsevier Sci. Publ. B. V., Amsterdam (1984).
[27] M. O. Lutset and A. N. Tsoĭ, in *Boiling and Condensation (Fluid Dynamics and Heat Transfer)* (ed. by I. I. Gogonin and I. G. Malenkov), Novosibirsk (1986).
[28] L. S. Goldner, N. Mulders, and G. Ahlers, J. Low Temp. Phys. **93**, 131 (1993).
[29] W. F. Fiszdon, J. Piechna, and W. A. Poppe, *A Qualitative Numerical Analysis of Some Features of Propagation of Counterflow Temperature Waves in Superfluid Helium*, MPI Stromungsforsch, Gottingen (1988).
[30] S. K. Godunova (ed.), *Numerical Solution of Multidimensional Gasdynamic Problems* [in Russian], Nauka, Moscow (1976).
[31] R. T. Wang, C. E. Swanson, and R. J. Donnelly, Phys. Rev. B **36**, 5240 (1987).
[32] S. K. Nemirovskii and W. Fiszdon, Rev. Mod. Phys. **67**, 37 (1995).
[33] T. Shimazaki, M. Murakami, and T. Iida, Cryogenics **35**, 645 (1995).
[34] C. F. Barenghi and R. J. Donelly, J. Low Temp. Phys. **52**, 189 (1983).
[35] K. W. Schwartz, Phys. Rev. B **38**, 2398 (1988).

Translated by R. S. Wadhwa

# On the influence of drag effect on acoustic modes in two-condensate relativistic superfluid systems

S. I. Vil'chinskiĭ*)

*Taras Shevchenko University, 252022 Kiev, Ukraine*
(Submitted January 27, 1999; revised March 5, 1999)
Fiz. Nizk. Temp. **25**, 650–656 (July 1999)

Expressions for the velocities of acoustic excitations in relativistic two-condensate superfluid systems are derived taking into account the reciprocal drag of superfluid motions (drag effect). The influence of drag effect on acoustic modes in this system is considered. It is shown that the inclusion of drag effect does not change the nature of acoustic excitation vibrations, but changes the velocities of second, third and fourth sounds. © *1999 American Institute of Physics.* [S1063-777X(99)00207-8]

Although the nonrelativistic theory of superfluidity has been developed for over fifty years since its creation, the question of its relativistic generalization has recently become significant.[1–9] Characteristic velocities in superfluid helium, including critical velocity, are much smaller than the velocity of light. Consequently, ''relativization'' of the theory of superfluidity remained a trivial problem until the time when it was established reliably that the core of a neutron star contains a superfluid phase associated with the Cooper pairing of nucleons.[10] The parameters of neutron stars (radius of the order of 10 km, density of the inner liquid core $\sim 10^{14}-10^{15}\,\mathrm{g/cm^3}$) are such that the ratio of gravitational radius to the radius of the star is of the order of unity. In other words, neutron stars have a strong gravitational field, and relativistic effects must be taken into consideration in the investigation of such stars. Owing to the high density of the neutron star core, the Fermi velocity of the nucleons as well as the velocity of sound become of the order of the velocity of light $c$. These circumstances necessitate an analysis of relativistic equations of the theory of superfluidity with one condensate. As a result of accretion, the evolution of a binary star may lead to the coexistence and interaction of two relativistic superfluid phases with different order parameters in the case when the binary star is formed by neutron stars and the equations of two-condensate relativistic superfluidity theory are used for describing this process. Nonrelativistic superfluid systems in which two or more types of condensates can coexist were considered in Refs. 7, and 11–18. Equations for describing a multicondensate relativistic superfluid system were derived in Refs. 7, 19, and 20. Historically, the main attention in two-condensate theories of superfluidity was paid to fundamental problems while the applied problems remained practically untouched. The aim of the present research is to study the reciprocal drag of superfluid motions (drag effect), which was first predicted by Andreev and Bashkin[13] and analyzed for nonrelativistic and relativistic superfluid systems,[7,13,14] and its effect on the nature and velocity of acoustic excitations in a relativistic quantum system in which normal and two superfluid components (condensates) coexist. Equations describing the propagation of acoustic waves in such a system were derived and solved by us[21] using the approach developed in our earlier work[19] and not taking into account the drag effect. In a separate publication,[20] the author has derived phenomenologically the equations of relativistic theory of superfluidity with two types of condensates in the nondissipative approximation taking into account the reciprocal drag of superfluid motions. In the present work, these equations are used, together with the approach and notation of Ref. 21, to determine and analyze the expressions for the velocities of acoustic excitations in such a system. The results are compared with those obtained in Ref. 21.

## BASIC EQUATIONS

Let us write down the equations describing a relativistic quantum system in the state of local equilibrium below the critical point containing two superfluid components (two condensates), each with its own gas of ''excitations.'' The gas of ''excitations'' has densities $\rho_{n1}$ and $\rho_{n2}$, and hence two flows are conserved. The velocities of the gas of ''excitations'' are equalized by viscosity. We use the following notation: $P(x)$ is the pressure, $T(x)$ the temperature, $\mathbf{v}_n(x)$ the normal velocity, $\mu_1(x)$ and $\mu_2(x)$ are the chemical potentials, $E(x)$ is the energy density, $g(x)$ the momentum density, and $\rho_1$, $\rho_2$ are the mass densities of the components of the system. The condensates are described by complex scalar order parameters, viz., by the effective wave functions

$$\psi_1(x^\mu)=\eta_1(x^\mu)\exp[i\alpha_1(x^\mu)],$$
$$\psi_2(x^\mu)=\eta_2(x^\mu)\exp[i\alpha_2(x^\mu)]. \tag{1}$$

The two superfluid velocities $\mathbf{v}_{s1}$ and $\mathbf{v}_{s2}$ are connected with the phases of the corresponding wave functions in such a way that the following relations are observed in the absence of vortices:

$$\mathbf{v}_{s1}=\nabla\alpha_1(x), \quad \mathbf{v}_{s2}=\nabla\alpha_2(x). \tag{2}$$

Here, we put $c=1$, $\hbar=1$ and choose the Lorentz metric

 

$$g_{\mu\nu}=\begin{pmatrix}1 & 0\\ 0 & -\delta_{ik}\end{pmatrix}.$$

Let us write the equations that we shall be requiring later.[20] The two continuity equations have the form

$$\nabla_\mu j_1^\mu=0,\quad \nabla_\mu j_2^\mu=0. \tag{3}$$

Here we have introduced the four-dimensional notation $j^\mu=(\rho,\mathbf{j})$:

$$j_1^\mu=j_{11}^\mu+j_{21}^\mu=\left(\frac{\partial\Psi}{\partial I_1}\right)v_1^\mu+\left(\frac{\partial\Psi}{\partial I_3}\right)v_2^\mu+\left(\frac{\partial\Psi}{\partial I_4}\right)w^\mu,$$

$$j_2^\mu=j_{12}^\mu+j_{22}^\mu=\left(\frac{\partial\Psi}{\partial I_2}\right)v_2^\mu+\left(\frac{\partial\Psi}{\partial I_3}\right)v_1^\mu+\left(\frac{\partial\Psi}{\partial I_5}\right)w^\mu,$$

where the four-dimensional vectors are defined as follows:

$$\begin{aligned}v_{1\nu}&=(\mu_1+\mathbf{v}_{s1}\cdot\mathbf{v}_n,-\mathbf{v}_{s1}),\\ v_{2\nu}&=(\mu_2+\mathbf{v}_{s2}\cdot\mathbf{v}_n,-\mathbf{v}_{s2}),\\ w_\nu&=(T+\mathbf{v}_n\cdot\mathbf{w},-\mathbf{w}).\end{aligned} \tag{4}$$

In view of invariance, the pressure $P$ can be presented in the form

$$P=\Psi(I_1,I_2,I_3,I_4,I_5,I_6), \tag{5}$$

where

$$\begin{aligned}&I_1=1/2g^{\mu\nu}v_{1\mu}v_{1\nu},\quad I_2=1/2g^{\mu\nu}v_{2\mu}v_{2\nu},\\ &I_3=g^{\mu\nu}v_{1\mu}v_{2\nu},\quad I_4=g^{\mu\nu}v_{1\mu}w_\nu,\\ &I_5=g^{\mu\nu}v_{2\mu}w_\nu,\quad I_6=1/2g^{\mu\nu}\omega_\mu w_\nu.\end{aligned}$$

In this case,

$$\frac{\partial\Psi}{\partial I_1}=\rho_{11},\quad \frac{\partial\Psi}{\partial I_2}=\rho_{22}$$

and

$$\rho_{12}=\rho_{21}=\frac{\partial\Psi}{\partial I_3}$$

are three independent quantities appearing in the three-velocity relativistic hydrodynamics instead of the densities of superfluid parts. The quantities $\rho_{12}=\rho_{21}$ describe the drag effect. The density of the ''gas of excitations'' in the components of the system can be presented in the form

$$\frac{\partial\Psi}{\partial I_4}=\rho_1-\rho_{11}-\rho_{21}=\rho_{n1},$$

$$\frac{\partial\Psi}{\partial I_5}=\rho_2-\rho_{22}-\rho_{12}=\rho_{n2}.$$

The quantity

$$\frac{\partial\Psi}{\partial I_6}=s$$

describes the entropy density. The vector $\mathbf{w}$ is introduced in accordance with the expression

$$\mathbf{g}=\rho_{11}\mathbf{v}_{s1}+\rho_{22}\mathbf{v}_{s2}+s\mathbf{w}+\rho_{21}\mathbf{v}_{s1}+\rho_{12}\mathbf{v}_{s2}. \tag{6}$$

The equation of entropy conservation has the form

$$\nabla_\mu(S^\mu)=0, \tag{7}$$

where $S^\mu=(s,s\mathbf{v}_n)$ is the 4-flux density of entropy, which is defined as

$$S^\mu=\left(\frac{\partial\Psi}{\partial I_4}\right)v_1^\mu+\left(\frac{\partial\Psi}{\partial I_5}\right)v_2^\mu+\left(\frac{\partial\Psi}{\partial I_6}\right)w^\mu.$$

The energy–momentum conservation law is defined by the equation

$$\nabla_\mu T_\nu^\mu=0, \tag{8}$$

where

$$\begin{aligned}T^{\mu\nu}=&\frac{\partial\Psi}{\partial I_1}v_1^\mu v_1^\nu+\frac{\partial\Psi}{\partial I_2}v_2^\mu v_2^\nu+\frac{\partial\Psi}{\partial I_3}(v_1^\mu v_2^\nu+v_1^\nu v_2^\mu)\\ &+\frac{\partial\Psi}{\partial I_4}(v_1^\mu w^\nu+v_1^\nu w^\mu)+\frac{\partial\Psi}{\partial I_5}(v_2^\mu w^\nu+v_2^\nu w^\mu)\\ &+\frac{\partial\Psi}{\partial I_6}w^\mu w^\nu-g^{\mu\nu}P.\end{aligned} \tag{9}$$

The equations

$$\nabla_\mu v_{1\nu}-\nabla_\nu v_{1\mu}=0,\quad \nabla_\mu v_{2\nu}-\nabla_\nu v_{2\mu}=0 \tag{10}$$

for velocities of the superfluid components together with the equation

$$s^\mu(\nabla_\mu w_\nu-\nabla_\nu w_\mu)=0 \tag{11}$$

contain the conditions $\operatorname{curl}\mathbf{v}_{s1}=0$ and $\operatorname{curl}\mathbf{v}_{s2}=0$. The following thermodynamic equations hold:

$$dP=j_1^\mu dv_{1\mu}+j_2^\mu dv_{2\mu}+s^\mu dw_\mu, \tag{12}$$

$$dE=v_{1\mu}dj_1^\mu+v_{2\mu}dj_2^\mu+w_\mu ds^\mu. \tag{13}$$

## SOUNDS

We shall seek the solution of the system of equations (1)–(13) for acoustic processes in the linear approximation. The superscript ''0'' will indicate the equilibrium values of the quantities, while the superscript ''1'' reflects small departures from the equilibrium values. The equilibrium values are assumed to be independent of coordinates and time. In addition, we shall assume that

(i) the superfluid and normal components have the same velocity in the equilibrium state:

$$w^{0\nu}=v_1^{0\nu}=v_2^{0\nu};$$

(ii) in the linear approximation, $w^{1\nu}$, $v_1^{1\nu}$, and $v_2^{1\nu}$ are orthogonal to $w^{0\nu}$:

$$w_\nu^0 w^{1\nu}=w_\nu^0 v_1^{0\nu}=w_\nu^0 v_2^{0\nu}=0.$$

After linearization of equations and elimination of derivatives of $w^{1\nu}$, $v_1^{1\nu}$, and $v_2^{1\nu}$, we arrive at a system of three equations describing the propagation of acoustic excitations in this system:

$$\partial_\nu^2\varepsilon^1+\Theta P^1=0;$$

$$\partial_\nu^2 s^1+\beta\Theta P^1+\alpha_1\Theta\mu_1^1+\alpha_2\Theta\mu_2^1=0;$$

$$\partial_\nu^2(\rho_1^1+\rho_2^1)+\nu\partial_\nu^2 s^1+\frac{\rho_1^0}{\mu_1^0}\Theta\mu_1^1+\frac{\rho_2^0}{\mu_2^0}\Theta\mu_2^1=0. \tag{14}$$

Here, $\varepsilon$ is the invariant energy density defined by the equality $\varepsilon\equiv v_\nu^0 v_\mu^0 T^{\nu\mu}$, and

$$\partial_\nu^2\equiv v_\nu^0\partial^\nu,\quad \Theta\equiv(g_{\nu\mu}-v_\nu^0 v_\mu^0)\partial^\nu\partial^\mu;$$

$$\beta\equiv\frac{s^0\sigma_1(\rho_{11}^0+\rho_{12}^0)+s^0\sigma_2(\rho_{22}^0+\rho_{21}^0)}{(\rho_1^0+\rho_2^0)(T^0s^0+\mu_1^0\rho_{n1}^0+\mu_2^0\rho_{n2}^0)};$$

$$\sigma_1\equiv 1-\frac{\rho_{n1}^0}{\rho_1^0};\quad \sigma_2\equiv 1-\frac{\rho_{n2}^0}{\rho_2^0};\quad \nu\equiv-\frac{\rho_{n1}^0+\rho_{n2}^0}{s^0};$$

$$\alpha_1\equiv-\frac{s^0(\rho_{11}^0+\rho_{12}^0)}{\mu_1^0(\rho_1^0+\rho_2^0)}\left[1+\frac{\mu_1^0(\rho_{11}^0+\rho_{12}^0+\rho_{21}^0+\rho_{22}^0)}{T^0s^0+\mu_1^0\rho_{n1}^0+\mu_2^0\rho_{n2}^0}\right];$$

$$\alpha_2\equiv-\frac{s^0(\rho_{21}^0+\rho_{22}^0)}{\mu_2^0(\rho_1^0+\rho_2^0)}\left[1+\frac{\mu_2^0(\rho_{11}^0+\rho_{12}^0+\rho_{21}^0+\rho_{22}^0)}{T^0s^0+\mu_1^0\rho_{n1}^0+\mu_2^0\rho_{n2}^0}\right].$$

We shall consider the solution of the system (14) in the form of plane waves (all thermodynamic quantities vary according to the law $\exp(ik^\nu x_\nu)$, where $k^\nu$ is a four-dimensional wave vector). We choose $P$, $\mu_1$, and $\mu_2$ as independent variables. The compatibility condition for the system (14) leads to a dispersion equation in the wave vector $k$ which defines the square of the velocity of sound and can be reduced to the following form after cumbersome transformations:

$$\begin{aligned}
&k^6-k^4\left\{\frac{\partial T}{\partial s}s^2(\rho_{11}+2\rho_{12}+\rho_{22})(Ts+\mu_1\rho_1+\mu_2\rho_2)}{\mu_1\rho_1+\mu_2\rho_2}+\left(\frac{\partial P}{\partial\varepsilon}\right)+\frac{(\rho_{11}\rho_{22}-\rho_{12}\rho_{21})\left(\mu_1\rho_1\dfrac{\partial\mu_1}{\partial\rho_2}+\mu_2\rho_2\dfrac{\partial\mu_2}{\partial\rho_1}\right)}{\sigma_1^2(\rho_1-\rho_{n1})+\sigma_2^2(\rho_2-\rho_{n2})+\rho_1\rho_2\left(\dfrac{\partial\mu_1}{\partial\rho_1}+\dfrac{\partial\mu_2}{\partial\rho_2}\right)}\right\}\\
&+k^2\left\{\left(\frac{\partial P}{\partial\varepsilon}\right)\frac{\dfrac{\partial T}{\partial s}s^2(\rho_{11}+2\rho_{12}+\rho_{22})(Ts+\mu_1\rho_1+\mu_2\rho_2)}{\mu_1\rho_1+\mu_2\rho_2}+\left(\frac{\partial P}{\partial\varepsilon}\right)\frac{(\rho_{11}\rho_{22}-\rho_{12}\rho_{21})\left(\mu_1\rho_1\dfrac{\partial\mu_1}{\partial\rho_2}+\mu_2\rho_2\dfrac{\partial\mu_2}{\partial\rho_1}\right)}{\sigma_1^2(\rho_1-\rho_{n1})+\sigma_2^2(\rho_2-\rho_{n2})+\rho_1\rho_2\left(\dfrac{\partial\mu_1}{\partial\rho_1}+\dfrac{\partial\mu_2}{\partial\rho_2}\right)}\right.\\
&\left.+\left[\frac{\dfrac{\partial T}{\partial s}s^2(\rho_{11}+2\rho_{12}+\rho_{22})(Ts+\mu_1\rho_1+\mu_2\rho_2)}{\mu_1\rho_1+\mu_2\rho_2}\right]\left[\frac{(\rho_{11}\rho_{22}-\rho_{12}\rho_{21})\left(\mu_1\rho_1\dfrac{\partial\mu_1}{\partial\rho_2}+\mu_2\rho_2\dfrac{\partial\mu_2}{\partial\rho_1}\right)}{\sigma_1^2(\rho_1-\rho_{n1})+\sigma_2^2(\rho_2-\rho_{n2})+\rho_1\rho_2\left(\dfrac{\partial\mu_1}{\partial\rho_1}+\dfrac{\partial\mu_2}{\partial\rho_2}\right)}\right]\right\}+\left(\frac{\partial P}{\partial\varepsilon}\right)\\
&\times\left[\frac{\dfrac{\partial T}{\partial s}s^2(\rho_{11}+2\rho_{12}+\rho_{22})(Ts+\mu_1\rho_1+\mu_2\rho_2)}{\mu_1\rho_1+\mu_2\rho_2}\right]\left[\frac{(\rho_{11}\rho_{22}-\rho_{12}\rho_{21})\left(\mu_1\rho_1\dfrac{\partial\mu_1}{\partial\rho_2}+\mu_2\rho_2\dfrac{\partial\mu_2}{\partial\rho_1}\right)}{\sigma_1^2(\rho_1-\rho_{n1})+\sigma_2^2(\rho_2-\rho_{n2})+\rho_1\rho_2\left(\dfrac{\partial\mu_1}{\partial\rho_1}+\dfrac{\partial\mu_2}{\partial\rho_2}\right)}\right]=0.
\end{aligned}\tag{15}$$

if we assume, as in Ref. 21, that

$$\frac{1}{\rho_i}\frac{\partial\rho_i}{\partial T}\ll 1,\quad \frac{T}{\mu_i}\ll 1,\quad \left[1-\frac{\partial P}{\partial\varepsilon}\frac{\partial s}{\partial\mu_i}\right]\ll 1,$$

$$\frac{T}{\mu_1\rho_1+\mu_2\rho_2}\frac{\dfrac{\partial P}{\partial\varepsilon}\dfrac{\partial P}{\partial T}}{\left(1+\dfrac{T_s}{\mu_1+\mu_2}\right)}\ll 1. \tag{16}$$

This equation has the following roots:

$$\kappa_1^2=\left(\frac{\partial P}{\partial\varepsilon}\right) \tag{17}$$

viz., the square of the first sound velocity,

$$\kappa_2^2=\left[\frac{\dfrac{\partial T}{\partial s}s^2(\rho_{11}+2\rho_{12}+\rho_{22})(Ts+\mu_1\rho_1+\mu_2\rho_2)}{\mu_1\rho_1+\mu_2\rho_2}\right] \tag{18}$$

the square of the second sound velocity, and

$$\kappa_3^2=\left[\frac{(\rho_{11}\rho_{22}-\rho_{12}\rho_{21})\left(\mu_1\rho_1\dfrac{\partial\mu_1}{\partial\rho_2}+\mu_2\rho_2\dfrac{\partial\mu_2}{\partial\rho_1}\right)}{\sigma_1^2(\rho_1-\rho_{n1})+\sigma_2^2(\rho_2-\rho_{n2})+\rho_1\rho_2\left(\dfrac{\partial\mu_1}{\partial\rho_1}+\dfrac{\partial\mu_2}{\partial\rho_2}\right)}\right] \tag{19}$$

the square of the third sound velocity.

In order to determine the nature of vibrations in the acoustic modes obtained above, we consider the dependence between the thermodynamic variables in an acoustic wave. For this purpose, we substitute the expressions for variables in the form of plane waves into the linearized equations (3),

(7)–(13). After elimination of $\rho_1^1$, $\rho_2^1$, $\mu_1^1$ and $\mu_2^1$, we arrive at the following relations between $P^1$, $T^1$, $v_1^{1\nu}k_\nu$, $v_2^{1\nu}k_\nu$ and $w^{1\nu}k_\nu$.

$$k_uP^1=-\kappa^2(w_n^0w^{1\nu}k_\nu+w_{s1}^0v_1^{1\nu}k_\nu+w_{s2}^0v_2^{1\nu}k_\nu),$$

$$w^{1\nu}k_\nu=\frac{1}{w_n^0}\left(\frac{a\kappa^2+1}{b\kappa^2-1}\right)(w_{s1}^0v_1^{1\nu}k_\nu+w_{s2}^0v_2^{1\nu}k_\nu),$$

$$k_uT^1=-\kappa^2\frac{(\rho_{n1}^0+\rho_{n2}^0)}{(\rho_1^0+\rho_2^0)}\left(\frac{w_{s1}^0v_1^{1\nu}k_\nu}{\rho_{11}^0+\rho_{12}^0}+\frac{w_{s2}^0v_2^{1\nu}k_\nu}{\rho_{21}^0+\rho_{22}^0}-\frac{w_n^0w^{1\nu}k_\nu}{\rho_{n1}^0+\rho_{n2}^0}\right), \tag{20}$$

where

$$k_u\equiv w_\nu^0k^\nu,\quad \omega_n\equiv Ts+\mu_1\rho_{n1}+\mu_2\rho_{n2};$$

$$\omega_{s1}\equiv\mu_1(\rho_{11}+\rho_{12}),\quad \omega_{s2}\equiv\mu_2(\rho_{21}+\rho_{22}),$$

$$a\equiv\frac{1}{s}\left(\frac{\rho_{n1}^0}{\rho_{s1}^0}+\frac{\rho_{n2}^0}{\rho_{s2}^0}\right)\left(\frac{\partial\varepsilon}{\partial T}\right)_P-\left(\frac{\partial\varepsilon}{\partial P}\right)_T,$$

$$b\equiv\frac{1}{s}\left(\frac{\partial\varepsilon}{\partial T}\right)_P-\left(\frac{\partial\varepsilon}{\partial P}\right)_T.$$

Substituting formula (17) for the first sound velocity into (20) and disregarding small terms in accordance with (16), we obtain

$$P^1\simeq-\left(\frac{\partial P}{\partial\varepsilon}\right)_T\left[\frac{(\rho_1^0+\rho_2^0)w_n^0}{k_u(\rho_{n1}^0+\rho_{n2}^0)}\right]w^{1\nu}k_\nu,\quad T^1\simeq0,$$

$$\frac{\omega_{s1}^0}{\rho_{11}^0+\rho_{12}^0}v_1^{1\nu}k_\nu+\frac{\omega_{s2}^0}{\rho_{21}^0+\rho_{22}^0}v_2^{1\nu}k_\nu\simeq\frac{\omega_n^0}{\rho_{n1}^0+\rho_{n2}^0}w^{1\nu}k_\nu. \tag{21}$$

It follows from here that the first sound waves are small oscillations of density and pressure and are analogous to ordinary sound waves in which temperature oscillations do not occur. The last equation indicates that the superfluid ''liquid'' oscillates in the first sound wave as a single entity, the normal and superfluid components moving together. Substituting formula (18) into (20) for the second sound velocity and disregarding small terms, we obtain

$$T^1\simeq\frac{s^2}{k_u}\left(\frac{\partial s}{\partial T}\right)\left(\frac{\omega_{1s}^0}{\rho_{s1}^0}v_1^{1\nu}k_\nu+\frac{\omega_{2s}^0}{\rho_{s2}^0}v_2^{1\nu}k_\nu\right)\times\left[1+\frac{Ts}{\mu_1\rho_1+\mu_2\rho_2}\right],\quad P^1\simeq0, \tag{22}$$

$$\frac{\omega_{s1}^0}{\rho_{11}^0+\rho_{12}^0}v_1^{1\nu}k_\nu+\frac{\omega_{s2}^0}{\rho_{21}^0+\rho_{22}^0}v_2^{1\nu}k_\nu\simeq-\frac{\omega_n^0}{\rho_{n1}^0+\rho_{n2}^0}w^{1\nu}k_\nu.$$

Consequently, temperature and entropy oscillate in second sound waves, there are no pressure oscillations, and the normal and superfluid components in second sound waves move towards each other. Similarly, substitution of formula (19) for the third sound velocity into (20), we arrive at the expression

$$\rho_1^1\rho_2^1\left(\frac{\partial\mu_1}{\partial\rho_2}+\frac{\partial\mu_2}{\partial\rho_1}\right)\simeq\left(\mu_1^0\rho_1^0\frac{\partial\mu_1}{\partial\rho_1}+\mu_2^0\rho_2^0\frac{\partial\mu_2}{\partial\rho_2}\right)\times\left(\frac{\omega_{1s}^0}{\rho_{s1}^0}v_1^{1\nu}k_\nu+\frac{\omega_{2s}^0}{\rho_{s2}^0}v_2^{1\nu}k_\nu\right),$$

$$k_u\mu_1^1\simeq\frac{\left(\rho_1^0\frac{\partial\mu_1}{\partial\rho_1}\right)\left(\frac{\alpha_1\alpha_2\omega_n^0}{(\alpha_1+\alpha_2)\beta}w^{1\nu}k_\nu\right)}{\left[\sigma_1^2(\rho_1^0-\rho_{n1}^0)+\sigma_2^2(\rho_2^0-\rho_{n2}^0)+\rho_1^0\rho_2^0\left(\frac{\partial\mu_1}{\partial\rho_1}+\frac{\partial\mu_2}{\partial\rho_2}\right)\right]},$$

$$k_u\mu_2^1\simeq\frac{\left(\rho_2^0\frac{\partial\mu_2}{\partial\rho_2}\right)\left(\frac{\alpha_1\alpha_2\omega_n^0}{(\alpha_1+\alpha_2)\beta}w^{1\nu}k_\nu\right)}{\left[\sigma_1^2(\rho_1^0-\rho_{n1}^0)+\sigma_2^2(\rho_2^0-\rho_{n2}^0)+\rho_1^0\rho_2^0\left(\frac{\partial\mu_1}{\partial\rho_1}+\frac{\partial\mu_2}{\partial\rho_2}\right)\right]}, \tag{23}$$

whence it can be concluded that the third sound consists of density and chemical potential oscillations.

Let us now consider the propagation of the fourth sound waves emerging in the system when the normal component is retarded. While linearizing the system (1)–(13) in this case, we must take into account the fact that $w_\nu^1=0$ due to the retardation of the normal component, and only two thermodynamic variables are independent. Omitting cumbersome calculations, we can directly write the expressions for the squares of fourth sound velocities:

$$\kappa_{4_1}^2=\frac{\rho_{11}(1+\rho_1\sigma_1\xi_1)}{\mu_1\rho_1\left(\frac{\partial\rho_1}{\partial P}-\xi_1\frac{\partial\rho_1}{\partial T}\right)}+\frac{2\rho_{12}\rho_{21}(1+\rho_2\sigma_2\xi_2)}{\mu_2\rho_2^2\left(\frac{\partial\rho_1}{\partial P}-\xi_2\frac{\partial\rho_2}{\partial T}\right)},$$

$$\kappa_{4_2}^2=\frac{\rho_{22}(1+\rho_2\sigma_2\xi_2)}{\mu_2\rho_2\left(\frac{\partial\rho_2}{\partial P}-\xi_2\frac{\partial\rho_2}{\partial T}\right)}+\frac{2\rho_{12}\rho_{21}(1+\rho_1\sigma_1\xi_1)}{\mu_1\rho_1^2\left(\frac{\partial\rho_2}{\partial P}-\xi_1\frac{\partial\rho_1^2}{\partial T}\right)}, \tag{24}$$

where

$$\xi_1\equiv\frac{\sigma_1\left(\frac{\partial\rho_1}{\partial P}\right)+\rho_1\left(\frac{\partial\sigma_1}{\partial P}\right)}{\sigma_1\left(\frac{\partial\rho_1}{\partial T}\right)+\rho_1\left(\frac{\partial\sigma_1}{\partial T}\right)},\quad \xi_2\equiv\frac{\sigma_2\left(\frac{\partial\rho_2}{\partial P}\right)+\rho_2\left(\frac{\partial\sigma_2}{\partial P}\right)}{\sigma_2\left(\frac{\partial\rho_2}{\partial T}\right)+\rho_1\left(\frac{\partial\sigma_2}{\partial T}\right)}, \tag{25}$$

and the expression

$$k_uT^1\simeq\frac{\xi_1(\rho_{11}+\rho_{12})\mu_1}{1+\alpha_1\sigma_1(\rho_{11}+\rho_{12})}v_{1\nu}^1k^\nu+\frac{\xi_2(\rho_{21}+\rho_{22})\mu_2}{1+\alpha_2\sigma_2(\rho_{21}+\rho_{22})}v_{2\nu}^1k^\nu, \tag{26}$$

according to which the fourth-sound waves are oscillations of temperature, entropy and density for the case when the normal component is retarded.

## DISCUSSION OF RESULTS

The following conclusions can be drawn from the results obtained in this work. The drag effect does not influence the nature or the magnitude of the first sound velocity. Nor does

the drag effect change the nature of oscillations of second, third and fourth sound waves, but the velocities of propagation of these sounds may change. A comparison of the obtained expressions for the velocities with the analogous results obtained in Ref. 21 (where the drag effect was not taken into consideration) allows us to conclude that as a result of the drag effect, the square of the second sound velocity changes by an amount

$$\kappa_{2d}^2=2\rho_{12}\left[\frac{\dfrac{\partial T}{\partial s}s^2(Ts+\mu_1\rho_1+\mu_2\rho_2)}{\mu_1\rho_1+\mu_2\rho_2}\right],$$

while the square of the third sound velocity decreases:

$$\kappa_{3d}^2=(\rho_{12}\rho_{21})\times\left[\frac{\left(\mu_1\rho_1\dfrac{\partial\mu_1}{\partial\rho_2}+\mu_2\rho_2\dfrac{\partial\mu_2}{\partial\rho_1}\right)}{\sigma_1^2(\rho_1-\rho_{n1})+\sigma_2^2(\rho_2-\rho_{n2})+\rho_1\rho_2\left(\dfrac{\partial\mu_1}{\partial\rho_1}+\dfrac{\partial\mu_2}{\partial\rho_2}\right)}\right].$$

The ratio $\kappa$ of the contribution of the drag effect in the square $\kappa_d^2$ to the square $\kappa_n^2$ of the velocity of sound calculated without taking the drag effect into consideration has the following form for the second sound:

$$\kappa_2\equiv\frac{\kappa_{d2}^2}{\kappa_{n2}^2}=\frac{\rho_{12}+\rho_{21}}{\rho_{11}+\rho_{22}},$$

For the third sound, this ratio is defined as

$$\kappa_3\equiv\frac{\kappa_{d3}^2}{\kappa_{n3}^2}=\frac{\rho_{12}\rho_{21}}{\rho_{11}\rho_{22}}.$$

In other words, the influence of the drag effect on the magnitude of the velocities depends on the ratio of the drag density $\rho_{12}=\rho_{21}$ to the densities $\rho_{11}$ and $\rho_{22}$.

The velocities of fourth sounds change by

$$\frac{2\rho_{12}\rho_{21}(1+\rho_2\sigma_2\xi_2)}{\mu_2\rho_2^2\left(\dfrac{\partial\rho_1}{\partial P}-\xi_2\dfrac{\partial\rho_2}{\partial T}\right)}\quad\text{and}\quad\frac{2\rho_{12}\rho_{21}(1+\rho_1\sigma_1\xi_1)}{\mu_1\rho_1^2\left(\dfrac{\partial\rho_2}{\partial P}-\xi_1\dfrac{\partial\rho_1}{\partial T}\right)},$$

while the value of $\kappa$ for each velocity is defined by the following relations:

$$\kappa_{4_1}=\frac{2\rho_{12}\rho_{21}\mu_1\rho_1}{\rho_{11}\rho_2\mu_2\rho_2}\left(\frac{1+\rho_2\sigma_2\xi_2}{1+\rho_1\sigma_1\xi_1}\right)\frac{\left(\dfrac{\partial\rho_1}{\partial P}-\xi_2\dfrac{\partial\rho_2}{\partial T}\right)}{\left(\dfrac{\partial\rho_1}{\partial P}-\xi_1\dfrac{\partial\rho_1}{\partial T}\right)},$$

$$\kappa_{4_2}=\frac{2\rho_{12}\rho_{21}\mu_2\rho_2}{\rho_{22}\rho_1\mu_1\rho_1}\left(\frac{1+\rho_1\sigma_1\xi_1}{1+\rho_2\sigma_2\xi_2}\right)\frac{\left(\dfrac{\partial\rho_2}{\partial P}-\xi_1\dfrac{\partial\rho_1}{\partial T}\right)}{\left(\dfrac{\partial\rho_2}{\partial P}-\xi_2\dfrac{\partial\rho_2}{\partial T}\right)}.$$

In the absence of a drag effect ($\rho_{12}=\rho_{21}=0$), the above corrections vanish and the expressions for velocities coincide with the results obtained in Ref. 21.

Thus, reciprocal drag by superfluid components in the system does not change the number or nature of oscillations of acoustic excitations of the system, but leads to a variation of the second, third and fourth sound velocities.

The author is indebted to P. I. Fomin for fruitful discussions.

*)E-mail: sivil@ap3.bitp.kiev.ua

[1] W. Israel, Phys. Lett. A **86**, 79 (1981).
[2] V. V. Lebedev and I. M. Khalatnikov, Zh. Éksp. Teor. Fiz. **83**, 1601 (1982) [Sov. Phys. JETP **56**, 923 (1982)].
[3] A. F. Prozorkevich, S. A. Smolyanskiĭ and V. A. Samorodov, Teor. Mat. Fiz. **52**, 292 (1982).
[4] P. I. Fomin and V. N. Shadura, Dokl. Akad. Nauk USSR, Ser. A, No. 6 (1985).
[5] S. I. Vil'chinskiĭ, Zh. Éksp. Teor. Fiz. **105**, 106 (1994) [JETP **78**, 56 (1994)].
[6] Yu. Vlasov, Zh. Éksp. Teor. Fiz. **111**, 1320 [JETP **84**, 729 (1997)].
[7] N. N. Bogoliubov, Jr., M. Yu. Kovalevskiĭ, A. M. Kurbatov *et al.*, Usp. Fiz. Nauk **159**, 585 (1989) [Sov. Phys. Usp. **32**, 1041 (1989)].
[8] B. Carter and I. M. Khalatnikov, Phys. Rev. D **45**, 4536 (1992).
[9] B. Carter and D. Langlois, Phys. Rev. D **51**, 5855 (1995).
[10] P. Anderson, D. Pines, J. Shahan, and M. Alpar, Prog. Theor. Phys. **69**, 376 (1980).
[11] I. M. Khalatnikov, Zh. Éksp. Teor. Fiz. **32**, 653 (1957) [Sov. Phys. JETP **5**, 542 (1957)].
[12] V. P. Mineev, Zh. Éksp. Teor. Fiz. **67**, 263 (1974) [Sov. Phys. JETP **40**, 132 (1974)].
[13] A. F. Andreev and E. P. Bashkin, Zh. Éksp. Teor. Fiz. **69**, 319 (1975) [Sov. Phys. JETP **42**, 164 (1975)].
[14] M. Yu. Kovalevskii and N. M. Lavrinenko, Fiz. Nizk. Temp. **8**, 341 (1982) [Sov. J. Low Temp. Phys. **8**, 169 (1982)].
[15] I. N. Adamenko and Yu. M. Poluektov, Fiz. Nizk. Temp. **8**, 912 (1982) [Sov. J. Low Temp. Phys. **8**, 458 (1982)].
[16] S. I. Shevchenko, Fiz. Nizk. Temp. **4**, 1410 (1982) [Sov. J. Low Temp. Phys. **4**, 663 (1978)].
[17] G. E. Volovik, Zh. Éksp. Teor. Fiz. **74**, 67 (1978) [Sov. Phys. JETP **47**, 34 (1978)].
[18] V. L. Pokrovskiĭ and I. M. Khalatnikov, JETP Lett. **23**, 599 (1976).
[19] S. I. Vil'chinskiĭ and P. I. Fomin, Fiz. Nizk. Temp. **21**, 729 (1995) [Low Temp. Phys. **21**, 566 (1995)].
[20] S. I. Vil'chinskiy, to be published in Physica Scripta (1999).
[21] S. I. Vil'chinskiĭ and P. I. Fomin, Fiz. Nizk. Temp. **24**, 8 (1998) [Low Temp. Phys. **24**, 5 (1998)].

Translated by R. S. Wadhwa

# Three-phonon interactions and initial stage of phonon pulse evolution in He II

M. A. H. Tucker and A. F. G. Wyatt*)

*School of Physics, University of Exeter, EX4 4QL, UK*

I. M. Adamenko,**) A. V. Zhukov, and K. E. Nemchenko

*Kharkov State University, 310077 Kharkov, Ukraine*
(Submitted February 1, 1999)
Fiz. Nizk. Temp. **25**, 657–663 (July 1999)

An expression for the characteristic rate of three-phonon processes in superfluid $^4$He, which is valid in the entire range of phonon energies where three-phonon processes are allowed is derived proceeding from the hydrodynamic Landau Hamiltonian. Possible limiting cases are analyzed and compared with the results of previous investigations. It is found that three-phonon processes completely govern the initial relaxation of a phonon pulse injected into He II by a heated solid. As a result, the equilibrium form of phonon distribution is established in the anomalous region of phonon dispersion over a time interval of the order of $10^{-10}$ s.
 [S1063-777X(99)00307-2]

## 1. INTRODUCTION

It is well known that the phonon spectrum in He II is of the decay type in the range of low energies right to a certain critical energy $\varepsilon_c \simeq 10$ K,[1,2] three-phonon processes (3pp) being allowed for energies $0 < \varepsilon < \varepsilon_0 \simeq 8.5$ K.[3] In the region of intermediate energies $\varepsilon_0 < \varepsilon < \varepsilon_c$, higher-order processes with nonconserved number of phonons are allowed.

The prediction of the decay type of the phonon spectrum made by Maris and Massey[4] and the experimental confirmation of this prediction[1,5] necessitated a revision of the existing concepts concerning collective processes in He II. In particular, all dissipative processes in superfluid $^4$He were investigated previously on the basis of the concepts of a decisive role of the four-phonon relaxation time[6] since decay processes (including 3PP) are forbidden by the momentum and energy conservation laws in the case of a normal spectrum. It should be noted that even before the result of Maris and Massey were published,[4] the phonon lifetime determined by the decay processes was obtained by Beliaev[7] on the basis of the model of a weakly nonideal Bose gas in which the quasiparticle spectrum is known to be of the decay type in the low-frequency range. The characteristic frequency 3PP obtained by Beliaev[7] turned out to be proportional to the fifth power of the phonon energy. For a real phonon spectrum in He II, such a problem was apparently solved by Havlin and Luban,[8] who obtained an expression for the 3PP characteristic rate in the form

$$\nu_3^{(HL)}(\varepsilon) = \frac{(u+1)^2}{240c^5\rho_0}\varepsilon^5, \tag{1}$$

where the Grüneisen constant is $u = (\rho_0/c)(\partial c/\partial \rho_0) \approx 2.84$ under the saturated vapor pressure,[9] $\rho_0$ the equilibrium density of He II, and $c$ the velocity of first sound. It is natural that formula (1) has the same energy dependence as the result obtained by Beliaev,[7] but the computational technique used by Havlin and Luban[8] unfortunately did not allow to establish the conditions of applicability of the results. For example, the dependence of three-particle relaxation time on the characteristic temperature of the thermal phonon field distribution remains unclear. Further progress in the study of 3PP was associated with attempts to explain experimental data concerning various dissipative processes in He II.[10–13] Maris[10,11] obtained the characteristic relaxation frequency associated with 3PP in the form

$$\nu_3^{(M)}(\varepsilon) = \frac{\pi^3(u+1)^2}{15c^5\rho_0}T^4\varepsilon, \tag{2}$$

where $T$ is the characteristic temperature of background thermal phonons. As regards the region of applicability of formula (2), the method of calculations used by Maris[10,11] indicates that it describes the absorption of an ultrasonic phonon in the gas of equilibrium thermal phonons. It is clear from these considerations that the region of applicability of the result (2) is limited to energies $\varepsilon \ll T$.

Processes occurring in phonon beams injected by a solid heater to He II were analyzed systematically in Refs. 14–16 Among other things, the effect of generation of high-energy phonons ($\varepsilon \simeq 10$ K) by a cold phonon beam with the characteristic temperature $T \simeq 1$ K during its propagation through a He II bath having a temperature of the order of $10^{-2}$K was discovered in Ref. 14. In order to explain this astonishing effect, we must analyze in detail all the stages of evolution of such a beam. For example, the description of initial relaxation of the phonon being injected requires the knowledge of the expression for the 3PP characteristic rate, which is valid in the entire range of admissible energies (i.e., in the anomalous spectral region). It is this necessity that stimulated the present research. In Sec. 3, we derive the most general relation for the 3PP rate on the basis of the kinetic equation using the Landau Hamiltonian of the quantized phonon field in He II. Section 4 is devoted to an analysis of various limiting cases and to a comparison with the results of previous

 

investigations.[7,8,10,11] Finally, the initial relaxation of a phonon beam in superfluid $^4$He is considered in Sec. 5.

## 2. QUANTIZATION OF PHONON FIELD IN He II

In order to study various processes occurring in the phonon subsystem of superfluid $^4$He, the Landau Hamiltonian[17]

$$\mathcal{H}_L=\int_V\left\{\frac{1}{2}\rho(\mathbf{r})\mathbf{v}^2(\mathbf{r})+E(\rho)\right\}d^3r, \tag{3}$$

suitable for describing He II dynamics in the hydrodynamic limit as traditionally used, where $\mathbf{v}(\mathbf{r})$ and $\rho(\mathbf{r})$ are the velocity and local density of helium and $E(\rho)$ is the internal energy per unit volume in He II, which is a function of local density. An explicit expression for $E(\rho)$ can be derived from simple thermodynamic considerations. Indeed, the work done during isothermal compression of helium must be equal to the change in its internal energy. In the differential form, this can be written as $d(VE)=-PdV$, which leads after elementary transformation to the following relation:

$$E(\rho)=\rho\int\frac{P}{\rho^2}d\rho.$$

In order to describe the dynamics of long-wave excitations, we can use the smallness of deviations from equilibrium and expand Hamiltonian (3) into a power series in fluctuations of density and velocity field. In this case, we use the well-known relation $\partial P/\partial P=c^2$. After the formal quantization procedure, the Hamiltonian correct to the fourth-order term in the expansion has the form

$$\hat{\mathcal{H}}_{\rm ph}=\hat{\mathcal{H}}_0+\hat{\mathcal{H}}_{\rm int},\quad \hat{\mathcal{H}}_{\rm int}=\hat{V}_3+\hat{V}_4. \tag{4}$$

Here

$$\hat{\mathcal{H}}_0=\frac{1}{2}\int_V\left\{\rho_0\hat{\mathbf{v}}^2+\frac{c^2}{\rho_0}(\delta\hat{\rho}(\mathbf{r}))^2\right\}d^3r \tag{5}$$

is the Hamiltonian describing a gas of noninteracting phonons confined in volume $V$ and $\delta\hat{\rho}=\hat{\rho}(\mathbf{r})-\rho_0$ is the operator of local deviation of density from its equilibrium value $\rho_0$. In the component $\hat{\mathcal{H}}_{\rm int}$ describing the interaction in the phonon system, we retained the terms containing the third

$$\hat{V}_3=\frac{1}{2}\int_V\left\{\hat{\mathbf{v}}(\mathbf{r})\,\delta\hat{\rho}(\mathbf{r})\hat{\mathbf{v}}(\mathbf{r})+\frac{1}{3}\left(\frac{\partial}{\partial\rho_0}\frac{c^2}{\rho_0}\right)[\delta\hat{\rho}(\mathbf{r})]^3\right\}d^3r \tag{6}$$

and fourth

$$\hat{V}_4=\frac{1}{24}\left(\frac{\partial^2}{\partial\rho^2}\frac{c^2}{\rho_0}\right)\int_V[\delta\hat{\rho}(\mathbf{r})]^4d^3r \tag{7}$$

powers of the small quantities $\hat{\mathbf{v}}(\mathbf{r})$ and $\delta\hat{\rho}(\mathbf{r})$.

The quantization of the phonon field described by Hamiltonian (4) was carried out in the conventional way using a transition to the phonon creation $\hat{a}_{\mathbf{p}}^+$ and annihilation $\hat{a}_{\mathbf{p}}$ operators in the state with momentum $\mathbf{p}$:

$$\delta\hat{\rho}(\mathbf{r})=\sum_{\mathbf{p}}\left(\frac{\rho_0}{2\varepsilon_{\mathbf{p}}V}\right)^{1/2}p(\hat{a}_{\mathbf{p}}e^{i\mathbf{p}\cdot\mathbf{r}}+\hat{a}_{\mathbf{p}}^+e^{-i\mathbf{p}\cdot\mathbf{r}}), \tag{8}$$

$$\hat{\mathbf{v}}(\mathbf{r})=\sum_{\mathbf{p}}\left(\frac{\varepsilon_p}{2\rho_0V}\right)^{1/2}\mathbf{n}(\hat{a}_{\mathbf{p}}e^{i\mathbf{p}\cdot\mathbf{r}}+\hat{a}_{\mathbf{p}}^+e^{-i\mathbf{p}\cdot\mathbf{r}}), \tag{9}$$

where $\varepsilon_{\mathbf{p}}\approx cp$ is the phonon energy and $\mathbf{n}=\mathbf{p}/p$ the unit vector in the direction of the phonon momentum. After the substitution of Eqs. (8) and (9) into (4)–(7), we obtain the Hamiltonian of the phonon subsystem of He II in the representation of secondary quantization. The Hamiltonian component $\hat{V}_3$ (6) describes the three-phonon interaction we are interested in, while $\hat{V}_4$ (7) corresponds to four-phonon processes.[18]

## 3. THREE-PHONON PROCESS RATE

In order to obtain the characteristic time of 3PP, we use the kinetic equation method. The equation describing the evolution of the phonon distribution function $n(\mathbf{p})$ in the presence of 3PP can be written in the form[6,13]

$$\begin{aligned}\frac{dn}{dt}=&\frac{1}{2}\sum_{\mathbf{p}',\mathbf{p}''}2\pi|\langle\mathbf{p}'\cdot\mathbf{p}''|\hat{V}_3|\mathbf{p}\rangle|^2\delta(\varepsilon_{\mathbf{p}'}+\varepsilon_{\mathbf{p}''}-\varepsilon_{\mathbf{p}})\\&\times[n'n''(1+n)-n(1+n')(1+n'')]\\&+\sum_{\mathbf{p}',\mathbf{p}''}2\pi|\langle\mathbf{p}'|\hat{V}_3|\mathbf{p}\cdot\mathbf{p}''\rangle|^2\delta(\varepsilon_{\mathbf{p}}+\varepsilon_{\mathbf{p}''}-\varepsilon_{\mathbf{p}'})\\&\times[n'(1+n'')(1+n)-nn''(1+n')],\end{aligned} \tag{10}$$

where $n'=n(\mathbf{p}')$ and $n''=n(\mathbf{p}'')$. It should be noted that we take into account only 3PP processes on the right-hand side of Eq. (10), i.e., we disregard higher-order interactions, assuming that the rate of 3PP is the highest in the system. Three-phonon processes are allowed only at angles that are small in view of the smallness of deviation of the phonon spectrum from linearity. In this case, superdiffusion in the space of angles[19,20] takes place, which is not considered here.

Using Eqs. (6), (8), and (9), we obtain the following expression for the matrix element:

$$\begin{aligned}\langle\mathbf{p}'\mathbf{p}''|\hat{V}_3|\mathbf{p}\rangle=&\left(\frac{1}{8\rho_0V}\right)^{1/2}\left\{\left(\frac{\varepsilon_{\mathbf{p}}\varepsilon_{\mathbf{p}''}}{\varepsilon_{\mathbf{p}'}}\right)^{1/2}p'\mathbf{n}\cdot\mathbf{n}''\right.\\&+\left(\frac{\varepsilon_{\mathbf{p}}\varepsilon_{\mathbf{p}'}}{\varepsilon_{\mathbf{p}''}}\right)^{1/2}p''\mathbf{n}\cdot\mathbf{n}'+\left(\frac{\varepsilon_{\mathbf{p}'}\varepsilon_{\mathbf{p}''}}{\varepsilon_{\mathbf{p}}}\right)^{1/2}p\mathbf{n}'\cdot\mathbf{n}''\\&\left.+c^2(2u-1)\frac{pp'p''}{(\varepsilon_{\mathbf{p}}\varepsilon_{\mathbf{p}'}\varepsilon_{\mathbf{p}''})^{1/2}}\right\}\delta_{\mathbf{p},\mathbf{p}'+\mathbf{p}''}.\end{aligned} \tag{11}$$

In order to determine the 3PP characteristic rate, we put in Eq. (10)

$$n=n_0+\delta n,\quad n'=n_0',\quad n''=n_0'', \tag{12}$$

where the subscript ''0'' indicates the equilibrium distribution and $\delta n$ the deviation of distribution function from linearity. In particular, the latter can be due to phonons injected by a heater to the bulk of He II. Substituting relations (12) into the kinetic equation (10) and going over from summation to integration [$\varepsilon_{\mathbf{p}}\equiv\varepsilon(\mathbf{p})$ is now a function of continuous argument], we obtain the following relation:

$$-\frac{d}{dt}\ln(\delta n)=\frac{1}{2n_0}\int W(\mathbf{p}|\mathbf{p}'\cdot\mathbf{p}'')\,\delta(\varepsilon_{\mathbf{p}}-\varepsilon_{\mathbf{p}'}-\varepsilon_{\mathbf{p}''})n_0'n_0''d\Gamma'+\int W(\mathbf{p}'|\mathbf{p}\cdot\mathbf{p}'')\times\delta(\varepsilon_{\mathbf{p}'}-\varepsilon_{\mathbf{p}}-\varepsilon_{\mathbf{p}''})\{n_0''-n_0'\}d\Gamma', \quad (13)$$

where

$$W(\mathbf{p}|\mathbf{p}'\cdot\mathbf{p}'')=2\pi V|\langle\mathbf{p}'\cdot\mathbf{p}''|\hat{V}_3|\mathbf{p}\rangle|^2 \quad (14)$$

is the transition probability density in the phase space and $d\Gamma=d^3p/(2\pi)^3$ is an element of the phase volume of the system.

It was mentioned above that 3PP processes are allowed only in a small angular range close to zero. This allows us to assume that all scalar products of unit vectors in Eq. (11) are equal to unity. As a result, we obtain the following simple expression for the transition probability density appearing in (13):

$$W(\mathbf{p}|\mathbf{p}'\cdot\mathbf{p}'')=\frac{c\pi}{\rho_0}(u+1)^2pp'p''\Delta(\mathbf{p},\mathbf{p}'+\mathbf{p}''), \quad (15)$$

where $\Delta(\mathbf{p},\mathbf{p}'+\mathbf{p}'')$ is the Kronecker symbol of a continuous argument.

Further, the 3PP characteristic rate can be naturally determined by the relation

$$\nu_3(\mathbf{p})=-\frac{d}{dt}\ln(\delta n). \quad (16)$$

Equations (13)–(16) lead to

$$\nu_3(\mathbf{p})=\frac{(u+1)^2}{4\pi\rho_0}\left\{\frac{1}{2}J_1(\mathbf{p})+J_2(\mathbf{p})\right\}, \quad (17)$$

where

$$J_1(\mathbf{p})=\frac{cp}{n_0(p)}\int_0^p dp'\int_{\cos\theta_c}^1 d(\cos\theta')\times p'^3|\mathbf{p}-\mathbf{p}'|n_0(p')n_0(p-p')\times\delta(\varepsilon(p)-\varepsilon(p')-\varepsilon(|\mathbf{p}-\mathbf{p}'|)); \quad (18)$$

$$J_2(\mathbf{p})=cp\int_p^{p_0}dp'\int_{\cos\theta_c}^1 d(\cos\theta')p'^3|\mathbf{p}'-\mathbf{p}|\{n_0(p'-p)-n_0(p')\}\delta(\varepsilon(p)-\varepsilon(p')-\varepsilon(|\mathbf{p}-\mathbf{p}'|)). \quad (19)$$

Here $\theta'$ is the angle between the vectors $\mathbf{p}$ and $\mathbf{p}'$, $\theta_c$ is the maximum angle for which 3PP are still allowed, and $p_0\approx\varepsilon_0/c$ is the momentum above which 3PP are forbidden, It should be noted that, in view of the asymptotic smallness of the Bose–Einstein distribution function in the momentum range $p>p_0$, the integration with respect to $p'$ in relation (19) can be extended to infinity to an exponential accuracy.

Eliminating $\delta$-functions in Eqs. (18) and (19) by integrating with respect to the angle $\theta'$ and introducing dimensionless variables, we obtain the following expression for $\nu_3(\mathbf{p})$ from (16):

$$\nu_3(x)=\frac{(u+1)^2}{4\pi\rho_0}\left(\frac{T}{c}\right)^5\left\{\frac{1}{2}\zeta(x)+\beta(x)\right\}, \quad (20)$$

where $x=\varepsilon(p)/T$, and

$$\zeta(x)=\int_0^x y^2(x-y)^2\frac{n_0(y)}{n_0(x)}n_0(x-y)dy; \quad (21)$$

$$\beta(x)=\int_x^\infty y^2(y-x)^2\{n_0(y-x)-n_0(y)\}dy. \quad (22)$$

Expression (20) taking into account (21) and (22) completely determines the characteristic rate of three-phonon relaxation. It should be noted that the final result (20) does not contain parameters of nonlinearity of the phonon spectrum in He II in spite of the fact that 3PP processes are due to the deviation of the spectrum from linearity. This fact can be expressed analytically as the existence of a nonzero volume of possible states in the space of angles $\theta'$ [see Eqs. (18) and (19)], which resulted in the appearance of a zero in the $\delta$-functions. In the next section, we shall analyze some limiting cases following from formula (20).

## 4. THREE-PHONON PROCESSES FOR HIGH AND LOW ENERGIES

According to our method of calculating the 3PP characteristic time, result (20) can be interpreted as the reciprocal lifetime of a phonon with momentum $p<p_0$ (energy $\varepsilon(\mathbf{p})<\varepsilon_0$), which is determined for 3PP in the equilibrium field of thermal phonons with temperature $T$. Let us consider the limiting cases following from the general formula (20). First of all, we consider the hyperacoustic limit. For this purpose, we must put $x\gg1$ $(\varepsilon(\mathbf{p})\gg T)$ in formula (20). This gives

$$\beta(x)\simeq0 \quad (23)$$

and

$$\zeta(x)\simeq\int_0^x y^2(x-y)^2dy=\frac{x^5}{30}. \quad (24)$$

Substituting relations (23) and (24) into (20), we obtain

$$\nu_3^{(\infty)}(\mathbf{p})=\nu_3^{(HL)}(\mathbf{p}), \quad (25)$$

which coincides with the result (1) obtained for the first time by Havlin and Luban.[8] This explains why formula (1) does not contain the temperature of background. A hyperacoustic phonon just ''does not feel'' the difference between a decay to zero and to a finite temperature. This fact was also presumed by Beliaev,[7] and naturally led to the same momentum dependence. Relations (23) and (24) show that such a limiting case corresponds to purely decay processes of the type $\mathbf{p}\rightarrow\mathbf{p}',\mathbf{p}''$. It should be noted that formula (25) actually has a limited applicability region. This is due to the fact that two conditions must be satisfied simultaneously: $\varepsilon(\mathbf{p})\gg T$, but $\varepsilon(\mathbf{p})<\varepsilon_0$. For this reason, formula (25) can be actually used

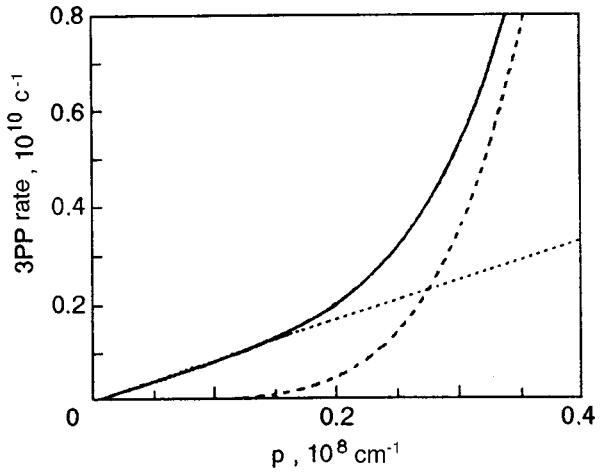


FIG. 1. Dependence of the rate of three-phonon processes on the phonon momentum (solid curve) calculated by formula (20) for $T=0.8$ K. The dashed curve and dotted line correspond to the limiting cases (1) and (2) respectively.

for obtaining numerical estimates only at ultralow temperatures.

Another limiting case $x \ll 1$ ($\varepsilon(\mathbf{p}) \ll T$) corresponds to absorption of an acoustic wave by an equilibrium phonon field with temperature $T$. In this case, we have

$$\zeta(x) \simeq 0 \tag{26}$$

and

$$\beta(x) \simeq x \int_0^\infty \frac{y^4 e^y}{(e^y-1)^2}\, dy = \frac{4\pi^4}{15} x. \tag{27}$$

While deriving relation (27), we have used the expansion

$$n_0(y-x) \approx n_0(y) + x n_0(y)[1+n_0(y)], \tag{28}$$

which is valid for small $x$. The substitution of (26) and (27) into (20) gives

$$\nu_3^{(0)}(\mathbf{p}) = \nu_3^{(M)}(\mathbf{p}), \tag{29}$$

i.e., we arrive at the result (2) obtained by Maris.[10,11] In contrast to the absorption of a high-energy phonon considered above, the limiting result (29) corresponds, according to relations (26) and (27), only to the capture processes $\mathbf{p}', \mathbf{p} \rightarrow \mathbf{p}''$. Formula (29) was used many times for describing various relaxation processes both in pure He II and in superfluid $^3$He–$^4$He mixtures (see the review in Ref. 21).

Figure 1 shows the dependence of the 3PP rate on the phonon momentum at 0.8 K. The same figure shows for comparison the curves corresponding to limiting cases (1) and (2). It can be seen clearly from Fig. 1 that the range of applicability of formula (1) is limited at relatively high temperatures.

Concluding the section, we must mention that the neutron scattering technique was used quite recently for measuring the phonon lifetime in He II determined by the 3PP processes.[22] A comparison with the theoretical result (1) showed a discrepancy by a factor greater than two, In our opinion, this is due to the fact that the measurements in Ref. 22 were made at a temperature of the order of 0.9 K, at which all relaxation processes in helium are virtually determined by interactions in the roton gas. The phonon lifetime in this case can depend considerably on the interaction between the phonon and roton subsystems and on the relaxation in the roton gas. Result (20) can be directly verified in experiments on sound absorption for various ratios between its frequency and helium temperature. For example, the absorption of sound of frequency $10^9$ Hz at a helium temperature below 10 mK is determined by formula (1), while at temperatures above 100 mK it is determined by formula (2). For intermediate temperatures, relation (20) should be used.

## 5. INITIAL EVOLUTION OF A PHONON BEAM INJECTED BY A SOLID INTO He II

A number of extremely interesting effects were observed in experiments[14–16] on propagation of phonon pulses injected by a solid heater into superfluid $^4$He at a temperature for which the interaction of the phonons in the pulse with thermal phonons can be neglected. In order to describe the observed phenomena theoretically, we must study consistently all the interactions determining the dynamics of the system. The results described in the previous sections give the idea of processes occurring in the phonon pulse at the initial stage of its propagation in He II.

Phonons injected by the heater into superfluid $^4$He can be divided into two groups depending on the emission channel. First, these are phonons emitted along the elastic channel and propagating in a narrow cone of angles $\Omega_{\mathbf{p}}$, whose axis is perpendicular to the heater surface. These phonons just form the main pulse propagating to the detector. Phonons of the second group are emitted almost isotropically in the entire half-space and are known as background phonons. The existence of the first group of phonons was predicted theoretically by Khalatnikov[23] and soon confirmed experimentally.[24] The possibility of the existence of an inelastic channel was investigated theoretically in Refs. 25 and 26. This channel was discovered independently by Sherlock *et al.*[24,27] in experiments on phonon emission by cleaved crystals. Experiments made in Ref. 28 proved that the total energy carried out by background phonons is an order of magnitude higher than the energy in the pulse, but the energy density in the pulse is much higher than in the gas of background phonons in view of the smallness of the solid angle $\Omega_{\mathbf{p}}$. The energy of emitted phonons is equal to or smaller than the temperature of the heater depending on the emission channel (elastic or inelastic).[29] It was found in the experiments[15] in which a gold film was used as a heater that the phonons emitted through the elastic channel propagate within the cone angle $\Omega_{\mathbf{p}}=0.115$ srad. In order to estimate the final temperature of such a pulse in helium (after the establishment of the Bose energy distribution), we must use the formula

$$gW = \frac{\Omega_{\mathbf{p}} \pi T^4}{120 c^2}, \tag{30}$$

where $g$ is the relative part of the energy $W$ supplied to the heater, which is emitted within the cone angle $\Omega_{\mathbf{p}}$, and $T$ the temperature of the thermalized pulse. For $\Omega_{\mathbf{p}}=0.115$ srad and $gW=0.7\,\mathrm{mW/mm^2}$, relation (30) gives $T=0.81$ K. Calculations based on formula (20) show that the entire pulse attains the equilibrium distribution over a time of the order of $10^{-10}$ s, which is more than three orders of magnitude smaller than the time of pulsation $\tau_p=l_p/c$ ($l_p$ is the pulse length) and the remaining characteristic times of experiments.[14–16] For this reason, the initial physical object in these experiments is a phonon beam with a Bose distribution characterized by the temperature determined in accordance with relation (30).

## CONCLUSION

We investigated three-phonon processes in superfluid $^4$He. Proceeding from the Landau hydrodynamic Hamiltonian (3), the general expression (20) is obtained for the rate of 3PP processes, which is valid for any phonon energy in the spectral range where 3PP processes are allowed. Expressions (25) and (29) obtained in the limiting cases of high and low energies are in accord with the results (1) and (2) obtained by using earlier theories.[8,9,11] The general approach developed by us has made it possible to define more precisely the range of applicability of the limiting formulas (1) and (2) derived earlier. An experiment for a direct verification of the results of the theory is proposed.

The derived general formula (20) has made it possible to describe the initial evolution of a phonon beam injected by a solid heater into He II. It is found that the energy distribution function for the emitted phonons attains equilibrium form over a time much shorter than the characteristic times in experiments with phonon pulses.[14–16]

The results of this research were partially reported at the XXXI Conference on Low Temperature Physics in Moscow.

The authors are grateful for the support offered by EPSRC (grants GR/M/22543 and GR/L/29149) and by ISEP foundation (grants QSU082002 (I.N.A), PSU082118 (A.V.Zh.), and YSU082037 (K.E.N.)).

*)E-mail: a.f.g.wyatt@exeter.ac.uk
**)E-mail: adamenko@pem.kharkov.ua

[1] R. C. Dynes and V. Narayanamurti, Phys. Rev. B **12**, 1720 (1975).
[2] T. Haavasoja, V. Narayanamurti, and M. A. Shin, J. Low Temp. Phys. **57**, 55 (1984).
[3] W. Stirling, in *Proc. 75th Jubilee Conf. on* $^4$He (ed. by J. G. M. Armitage), World Scientific, Singapore (1983), p. 109.
[4] H. J. Maris and W. E. Massey, Phys. Rev. Lett. **25**, 220 (1970).
[5] N. G. Mills, R. A. Sherlock, and A. F. G. Wyatt, J. Phys. C **8**, 2575 (1975).
[6] I. M. Khalatnikov, *Theory of Superfluidity* [in Russian], Nauka, Moscow (1971).
[7] S. T. Belyaev, Zh. Éksp. Teor. Fiz. **34**, 431 (1958) [*sic*].
[8] S. Havlin and M. Luban, Phys. Lett. A **42**, 133 (1972).
[9] B. M. Abraham, Y. Eckstein, J. B. Ketterson *et al.*, Phys. Rev. A **1**, 250 (1970).
[10] H. J. Maris, Phys. Rev. A **8**, 1980 (1973).
[11] H. J. Maris, Phys. Rev. A **9**, 1412 (1974).
[12] D. Benin, Phys. Rev. B **11**, 145 (1975).
[13] C. I. Um, S. Y. Lee, S. K. Yoo *et al.*, Fiz. Nizk. Temp. **23**, 537 (1997) [Low Temp. Phys. **23**, 397 (1997)].
[14] M. A. H. Tucker and A. F. G. Wyatt, J. Phys. C **6**, 2813 (1994).
[15] M. A. H. Tucker and A. F. G. Wyatt, J. Phys. C **6**, 2825 (1994).
[16] M. A. H. Tucker and A. F. G. Wyatt, *Proceedings of Quantum Fluids and Solids*, Amherst (1998).
[17] L. D. Landau, Zh. Éksp. Teor. Fiz. **11**, 592 (1941).
[18] I. N. Adamenko, K. É. Nemchenko, M. A. H. Tucker *et al.*, in *Proc. of the XXXIth Conf. on Low Temp. Phys.* [in Russian], Moscow (1998), p. 72.
[19] V. L. Gurevich and B. D. Laĭkhtman, Zh. Éksp. Teor. Fiz. **69**, 1230 (1975) [Sov. Phys. JETP **42**, 628 (1975)].
[20] V. L. Gurevich and B. D. Laĭkhtman, Zh. Éksp. Teor. Fiz. **70**, 1907 (1976) [Sov. Phys. JETP **43**, 993 (1976)].
[21] I. N. Adamenko and É. Ya. Rudavskiĭ, Fiz. Nizk. Temp. **13**, 3 (1987) [Sov. J. Low Temp. Phys. **13**, 1 (1987)].
[22] F. Mezei, C. Lartigue, and B. Farago, in: *Excitations in Two-Dimensional and Three-Dimensional Quantum Fields* (ed. by A. F. G. Wyatt and H. J. Lauter), Plenum Press, New York (1991), p. 119.
[23] I. M. Khalatnikov, Zh. Éksp. Teor. Fiz. **22**, 687 (1952).
[24] R. A. Sherlock, A. F. G. Wyatt, N. G. Mills, and N. A. Lockerbie, Phys. Rev. Lett. **29**, 1299 (1972).
[25] I. N. Adamenko and I. M. Fuks, Zh. Éksp. Teor. Fiz. **59**, 2071 (1970) [Sov. Phys. JETP **32**, 1123 (1970)].
[26] I. M. Khalatnikov and I. N. Adamenko, Zh. Éksp. Teor. Fiz. **63**, 745 (1972) [Sov. Phys. JETP **36**, 391 (1972)].
[27] R. A. Sherlock, N. G. Mills, and A. F. G. Wyatt, J. Phys. C **8**, 300 (1975).
[28] A. F. G. Wyatt and G. J. Page, J. Phys. C **11**, 4927 (1978).
[29] A. F. G. Wyatt and G. N. Crisp, J. Phys. (Paris), Colloq. **39**, C6-244 (1978).

Translated by R. S. Wadhwa

# On transfer of motion in a system of two-dimensional superfluid Bose-gases separated by a thin layer

S. V. Terentjev and S. I. Shevchenko*)

*B. Verkin Institute for Low Temperature Physics and Engineering, National Academy of Sciences of the Ukraine, 310164 Kharkov, Ukraine*

(Submitted February 10, 1999)
Fiz. Nizk. Temp. **25**, 664–676 (July 1999)

The effect of transfer of motion between superfluid $2D$ Bose gases separated by a thin layer is predicted on the basis of microscopic calculations. It is shown that the effect exists at nonzero temperatures as well as at $T=0$ only for a closed secondary circuits. The dependence of the drag current on temperature and thickness of the layer is determined for charged Bose gases. An experiment is proposed for measuring the predicted effect. © *1999 American Institute of Physics.* [S1063-777X(99)00407-7]

Electron or electron–hole systems in which two two-dimensional conducting layers are separated by a thin insulating layer have aroused considerable interest during the last decade. Several interesting effects caused by the interaction of carriers separated in space were predicted for such systems. For example, the possibility of pairing of spatially separated electrons and holes, and a transition of the system to a peculiar superconducting state in which the supercurrent in the electron region is accompanied by an equal and opposite supercurrent in the hole region, were predicted way back in 1976 for the case when electrons are the carriers in one layer, and holes in the other layer.[1,2] Swierkowski and Nelson[3] observed mutual polarization of spatially separated carriers and proposed that correlations between layers can facilitate Wigner crystallization in adjacent layers. Shimshon[4] discussed the peculiarities of the mechanism of coupling between plane vortices in parallel superconducting films. A large number of publications were devoted to the effects of mutual friction or transfer of motion between adjacent conducting layers. Friction between two electron gases was studied experimentally in Refs. 5–8, between an electron gas and a hole gas in Ref. 9, and between electrons in normal and superconducting films in Refs. 10 and 11.

Theoretically, the problem of drag between two electron gases separated in space was first considered by Pogrebinskiĭ[12] and later by Price.[13] They studied the case when drag is caused by direct Coulomb interaction between electrons from different films. Gurzhi and Kopeliovich[14] predicted the possibility of transfer of motion between spatially separated carriers due to phonon exchange. Drag induced by Coulomb interaction was later studied in Refs. 15–23, while the drag induced by exchange of phonons, both real and virtual, was studied in Refs. 24 and 25.

While studying the transfer of motion from one superconducting film to another, it must be borne in mind that such a transfer may occur owing to two quite different mechanisms. One mechanism is effective in the case when the films are placed in a magnetic field exceeding the field $H_{c1}$. In this case, the transfer of motion is associated mainly with the entanglement of vortex lattices in the driving film and the driven film. The other mechanism is realized in the absence of vortices, when the motion is induced by direct (Coulomb) or indirect (through exchange phonons) interaction between electrons from different films. The first mechanism has been studied for a long time, starting from the pioneering work of Giaever.[26] In the present work, we shall consider only the second mechanism of transfer of motion.

To our knowledge, this mechanism was studied theoretically only in Refs. 27 and 28. Kamenev and Oreg[27] developed the diagrammatic technique for evaluating the current induced in film 2 by an external field applied to film 1. The authors detected a significant increase in the friction coefficient upon a transition of both films to the superconducting state. They studied only the case when the film temperature is close to the superconducting transition temperature. However, the authors failed to observe an important circumstance that the supercurrent flowing in the driving film 1 will induce a supercurrent in the driven film 2 only if the electric circuit in film 2 is closed. This important circumstance was first noted by Duan and Yip.[28] Besides, Kamener and Oreg did not take into account the collective modes associated with electron density oscillations. These oscillations, which do not exist in bulk superconductors due to the presence of a plasma gap in the spectrum, become possible in thin films since the electric fields accompanying density oscillations in films are mainly concentrated not in the superconductor but in the space surrounding it. The contribution of collective vibrations to the transfer of motion between superconducting films was determined by Duan and Yip.[28] However, they did not carry out a consistent microscopic computation, and hence a number of important problems like the dependence of the force of friction between superconducting films on the pairing potential of superconducting electrons remained unsolved.

We shall consider the problem of transfer of motion between two identical superconducting films at temperatures that are low in comparison with the superconducting transition temperature. At low temperatures, the number of one-particle excitations is exponentially small and such excitations can be neglected altogether in the first approximation.

 

In this case, qualitatively correct results can be obtained if the problem on the friction force between superconducting electron gases caused by collective excitation, is replaced by the problem on the friction force between superfluid charged Bose gases. Such a replacement allows us not only to obtain the exact solution of the problem in the limit of weak currents, but also to determine the variation of results obtained by Duan and Yip[28] upon an increase in the pairing potential.

A brief summary of the results obtained here was published earlier in Ref. 29.

### 1. DRAG CURRENT AT $T=0$

Let us consider the problem of transfer of momentum/motion between two two-dimensional superfluid Bose gases separated by a thin partition at zero temperature. Although we shall be interested in charged Bose gases, we shall not specify initially the form of the interaction potential between bosons and derive a number of expressions that are valid for the general case. We shall assume that Bose gases are identical, and proceed from the Hamiltonian

$$\hat{H}=\sum_{\alpha=1,2}\sum_{\mathbf{k}}\varepsilon(k)\hat{a}_\alpha^+(\mathbf{k})\hat{a}_\alpha(\mathbf{k}) + \frac{1}{2S}\sum_{\alpha,\beta=1,2}\sum_{\mathbf{k},\mathbf{p},\mathbf{q}}\gamma_{\alpha\beta}(k)\hat{a}_\alpha^+(\mathbf{p}-\mathbf{k})\hat{a}_\beta^+ \times(\mathbf{q}+\mathbf{k})\hat{a}_\beta(\mathbf{q})\hat{a}_\alpha(\mathbf{p}). \quad (1)$$

Here, $\varepsilon(k)=\hbar^2k^2/2M$ is the energy of a free boson, $\gamma_{\alpha\beta}(k)$ the Fourier component of boson interaction potential in a layer (for $\alpha=\beta$) and between layers (for $\alpha\neq\beta$), and $\hat{a}_\alpha^+(\mathbf{k})$, $\hat{a}_\alpha(\mathbf{k})$ are the creation and annihilation operators of a boson with momentum $\hbar\mathbf{k}$ in the layer $\alpha$.

We shall determine the energy spectrum of a two-layer Bose-system described by Hamiltonian (1). Since Bose-Einstein condensation takes place in a two-dimensional Bose gas at $T=0$, the energy spectrum can be determined by using the well-known Bogoliubov procedure of separating the condensate operators $\hat{a}_\alpha^+(0)$ and $\hat{a}_\alpha(0)$ of creation and annihilation of bosons in the state with momentum $\mathbf{p}=0$ and replacing them by $\sqrt{N_0}$, where $N_0$ is the number of bosons in the condensate. The obtained expression should be formally expanded in powers of small quantities $\hat{a}_\alpha^+(\mathbf{k})$, $\hat{a}_\alpha(\mathbf{k})$ $(\mathbf{k}\neq0)$ and only the quadratic terms should be retained in the expansion. Such an expansion implicitly assumes the smallness of the number of bosons over the condensate, and we shall formulate below the conditions under which such an expansion is valid.

It is convenient to go over to new creation and annihilation operators

$$\hat{a}_\pm(\mathbf{k})=\frac{1}{\sqrt{2}}[\hat{a}_1(\mathbf{k})\pm\hat{a}_2(\mathbf{k})]. \quad (2)$$

Like operators $\hat{a}_{1,2}(\mathbf{k})$, the operators $\hat{a}_\pm(\mathbf{k})$ satisfy Bose commutation relations. After transition to new operators, the Hamiltonian can be regarded as the sum of two components, each containing only one kind of operators $\hat{a}_\sigma(\mathbf{k})$, where $\sigma=\pm$ [the numerical factor is omitted in (3)]:

$$\hat{H}=\sum_\sigma\left\{\sum_{\mathbf{k}}\varepsilon(k)\hat{a}_\sigma^+(\mathbf{k})\hat{a}_\sigma(\mathbf{k}) + \frac{n}{2}\sum_{\mathbf{k}\neq0}[\gamma(k)+\sigma\gamma_{12}(k)][2\hat{a}_\sigma^+(\mathbf{k})\hat{a}_\sigma(\mathbf{k}) + \hat{a}_\sigma^+(\mathbf{k})\hat{a}_\sigma^+(-\mathbf{k})+\hat{a}_\sigma(\mathbf{k})\hat{a}_\sigma(-\mathbf{k})]\right\}. \quad (3)$$

Here $n$ is the number density of bosons, and $\gamma(k)=\gamma_{11}(k)=\gamma_{22}(k)$. Diagonalization in (3) is carried out with the help of Bogoliubov's standard $uv$ transformations:

$$\hat{a}_\sigma(\mathbf{k})=u_\sigma(\mathbf{k})\hat{b}_\sigma(\mathbf{k})+v_\sigma(\mathbf{k})\hat{b}_\sigma^+(-\mathbf{k}), \quad (4)$$

where $\hat{b}_\sigma^+(\mathbf{k})$, $\hat{b}_\sigma(\mathbf{k})$ are the creation and annihilation operators of Bose quasiparticles. As a result of diagonalization, we obtain

$$\hat{H}=E_0+\sum_{\sigma,\mathbf{k}\neq0}E_\sigma(k)\hat{b}_\sigma^+(\mathbf{k})\hat{b}_\sigma(\mathbf{k}), \quad (5)$$

where

$$E_0=\frac{N^2}{2S}[\gamma(0)+\gamma_{12}(0)]+\frac{1}{2}\times\sum_{\sigma,\mathbf{k}\neq0}[E_\sigma(k)-\varepsilon(k)-n\gamma(k)], \quad (6)$$

is the ground state energy, and

$$E_\sigma(k)=\sqrt{\varepsilon^2(k)+2n\varepsilon(k)[\gamma(k)+\sigma\gamma_{12}(k)]}. \quad (7)$$

is the energy of elementary excitations. The coefficients $u_\sigma(k)$ and $v_\sigma(k)$ are presented in terms of the energies $\varepsilon(k)$ and $E_\sigma(k)$ in the conventional manner:

$$u_\sigma^2(k)=\frac{1}{2}\left\{\frac{\varepsilon(k)+n[\gamma(k)+\sigma\gamma_{12}(k)]}{E_\sigma(k)}+1\right\},$$
$$v_\sigma^2(k)=\frac{1}{2}\left\{\frac{\varepsilon(k)+n[\gamma(k)+\sigma\gamma_{12}(k)]}{E_\sigma(k)}-1\right\}. \quad (8)$$

It follows from formulas (2), (4) and (5) that an elementary excitation belongs to the entire system, and cannot be attributed to an individual layer. As a result of interaction between layers, the system acquires a single coherent ground state in which the phases of superfluid Bose gases are correlated.

Let us consider in detail the case when both Bose gases are charged. In this case, the interaction potentials have the form

$$V_{\alpha\alpha}=\frac{Q^2}{\epsilon_0 r},\quad V_{\alpha\bar{\alpha}}=\frac{Q^2}{\epsilon_0\sqrt{r^2+d^2}}, \quad (9)$$

where $Q$ is the boson charge, $\epsilon_0$ the permittivity of the medium, and $d$ the separation between two-dimensional layers in which Bose gases are localized. The corresponding Fourier components are defined as

$$\gamma(k)=\frac{2\pi Q^2}{\epsilon_0 k},\quad \gamma(0)=0,$$
$$\gamma_{12}(k)=\frac{2\pi Q^2}{\epsilon_0 k}e^{-kd},\quad \gamma_{12}(0)=0. \quad (10)$$

The equalities $\gamma(0)=\gamma_{12}(0)=0$ reflect the existence of a positively charged substrate compensating the average boson charge in a layer in such a way that the system on the whole is electrically neutral. Substituting expression (10) into (7), we obtain the dispersion relation for elementary excitations of ''+'' and ''−'' modes. In the longwave limit (to be more precise, for $kd\ll 1$), it follows from (7) and (10) that

$$E_-=\left(\frac{2\pi\hbar^2 nQ^2 d}{M\epsilon_0}\right)^{1/2}k; \quad E_+=\left(\frac{4\pi\hbar^2 nQ^2}{M\epsilon_0}\right)^{1/2}\sqrt{k}. \tag{11}$$

It can be seen from the definition (2) of modes ''-'' and ''+'' that the mode ''+'' corresponds to vibrations of the Bose gas in two films as a single entity, while the mode ''-'' is associated with density oscillations in one film relative to another for a fixed value of the total density.

It is interesting to note that formulas (11) are identical to those obtained by Flensberg and Hu[30] for the spectrum of collective excitations in a two-layer normal Fermi system (in which the fermion charge $e$ and mass $m$ are replaced by the boson charge $Q=2e$ and mass $M=2m$). The authors of Ref. 30 took into account the renormalization of initial fermion interaction associated with screening effects. For the system under consideration, there is no need for additionally taking into account the screening effects owing to the fact that Hamiltonian (1) is exactly diagonalized.

It should be also observed that the spectrum of a charged two-dimensional (one-layer) Bose gas was studied by Apaja *et al.*[31] using the variation technique. They obtained an expression for plasma oscillations in the longwave limit coinciding with (11) after replacement of the two-dimensional density of bosons by double the boson density in a two-layer system considered in the present work.

Knowing the energy spectrum, we can easily determine the momentum distribution function for real bosons in the layer $\alpha$:

$$N_\alpha(k)=\langle\hat{a}_\alpha^+(\mathbf{k})\hat{a}_\alpha(\mathbf{k})\rangle=\frac{1}{2}\sum_\sigma\langle\hat{a}_\sigma^+(\mathbf{k})\hat{a}_\sigma(\mathbf{k})\rangle. \tag{12}$$

Here the angle brackets indicate averaging over the ground state. Replacing the operators $\hat{a}_\sigma$ by their expressions in terms of $\hat{b}_\sigma$ and $\hat{b}_\sigma^+$ from (4) and considering that there are no elementary excitations (i.e., $\langle\hat{b}_\sigma^+\hat{b}_\sigma\rangle=0$) in the case of zero temperature considered here, we obtain

$$N_\alpha(k)=\frac{1}{2}\sum_\sigma\nu_\sigma^2(\mathbf{k})=\frac{1}{8}\sum_\sigma\frac{[E_\sigma(k)-\varepsilon(k)]^2}{\varepsilon(k)E_\sigma(k)}. \tag{13}$$

The total number of bosons over the condensate in the layer $\alpha$ is given by

$$\delta N_\alpha=N_\alpha-N_{\alpha 0}=\sum_{\mathbf{k}\neq 0}N_\alpha(\mathbf{k})\equiv\frac{1}{2}\sum_\sigma\delta N_\sigma. \tag{14}$$

Let us find out the number of particles over the condensate for Coulomb-type Bose gases. In this case, the expression for the number of bosons over the condensate depends on the relation between the thickness $d$ of the insulator separating the Bose gases and the length $d_0$ defined by the expression

$$d_0^3=\frac{\hbar^2\epsilon_0}{8\pi MnQ^2}=\frac{a_0}{8\pi n}, \tag{15}$$

where $a_0$ is the effective Bohr radius. Using the expressions (13) and (14), we obtain the following relation for $d\gg d_0$:

$$\frac{\delta N_+}{N}=\frac{\delta N_-}{N}=(na_0^2)^{-1/3}. \tag{16}$$

The difference in the energy spectra for ''+'' and ''−'' modes is not manifested in this case since the part of the mode $E_-(k)$ linear in $k$ does not make a significant contribution to the integral in (14) for $d\gg d_0$. For $d\ll d_0$, we obtain

$$\delta N_+/N=(na_0^2)^{-1/3}, \tag{17}$$

$$\delta N_-/N=d/a_0. \tag{18}$$

The theory constructed here is based on the fact that the number of particles over the condensate is small in comparison with the number of particles in the condensate, and hence the theory is applicable for $\delta N_\alpha/N\ll 1$. It follows from (16)–(18) that this inequality is satisfied for

$$na_0^2\gg 1 \quad \text{and} \quad d/a_0\ll 1. \tag{19}$$

The constraint $d/a_0\ll 1$ appears only for $d\ll d_0$. It can be verified easily that for $na_0^2\gg 1$ and $d\ll d_0$, the condition $d/a_0\ll 1$ is automatically satisfied. Thus, for the two-layer system of charged Bose gases, the condition of applicability of the theory constructed here is a high density of the Bose gas: $na_0^2\gg 1$.

Let us now consider the transfer of motion from the superfluid Bose gas in one layer to the Bose gas in the other layer. If a superfluid flux emerges in layer 1, the field operator

$$\hat{\psi}_1(\mathbf{r})\equiv\frac{1}{\sqrt{S}}\sum_{\mathbf{k}}e^{i\mathbf{k}\cdot\mathbf{r}}\hat{a}_1(\mathbf{k}) \tag{20}$$

in this layer acquires an additional factor $\exp(i\mathbf{k}_{s1}\cdot\mathbf{r})$, where the wave vector $\mathbf{k}_{s1}$ is connected with the superfluid velocity $\mathbf{v}_{s1}$ through the relation $\mathbf{v}_{s1}=\hbar\mathbf{k}_{s1}/M$. This leads to the emergence of an additional term proportional to this flux in the Hamiltonian (1). Introducing the particle flux density vector in the layer $\alpha$

$$\hat{\mathbf{j}}_\alpha(\mathbf{r})=\frac{i\hbar}{2M}[(\nabla\hat{\psi}_\alpha^+(\mathbf{r}))\hat{\psi}_\alpha(\mathbf{r})-\hat{\psi}_\alpha^+(\mathbf{r})(\nabla\hat{\psi}_\alpha(\mathbf{r}))], \tag{21}$$

we can present the correction $\hat{H}_1$ to the Hamiltonian (1) in the form

$$\hat{H}_1=\int d^2r\hat{\mathbf{j}}_1(\mathbf{r})\cdot\mathbf{v}_{s1}. \tag{22}$$

Owing to the interaction between Bose gases in adjacent layers, the flow of current in layer 1 leads to the flow of current in layer 2. The drag current in layer 2 can be determined easily by calculating the linear response of the system to the perturbation (22). As a result, we arrive at the relation

$$\mathbf{j}_2=\langle 0|\hat{\mathbf{j}}_2|0\rangle-\sum_{n\neq 0}\frac{\langle 0|\hat{H}_1|n\rangle\langle n|\hat{\mathbf{j}}_2|0\rangle}{E_n-E_0}$$

$$-\sum_{n\neq 0}\frac{\langle 0|\hat{\mathbf{j}}_2|n\rangle\langle n|\hat{H}_1|0\rangle}{E_n-E_0}. \tag{23}$$

Going over from the operators $\hat{a}_\alpha^+$ and $\hat{a}_\alpha$ of creation and annihilation of bosons in the layer $\alpha$ to the operators $\hat{b}_\sigma^+$ and $\hat{b}_\sigma$ of creation and annihilation of elementary excitations in the expression for the current density operator $\hat{\mathbf{j}}_2(\mathbf{r})$ and considering that the ground state of operators $\hat{b}_\sigma$ is vacuum (i.e., $\hat{b}_\sigma|0\rangle=0$), we can easily show that the density of drag current is defined as

$$\mathbf{j}_2=\frac{\mathbf{v}_{s1}}{2S}\sum_{\mathbf{k}}\varepsilon(k)\frac{[v_+(k)u_-(k)-u_+(k)v_-(k)]^2}{E_+(k)+E_-(k)}. \tag{24}$$

Substituting the explicit expressions for the $uv$-transformation coefficients from (8), we obtain

$$\mathbf{j}_2=\frac{\mathbf{v}_{s1}}{8S}\sum_{\mathbf{k}}\frac{\varepsilon(k)[E_+^2(k)-E_-^2(k)]^2}{E_+(k)E_-(k)[E_+(k)+E_-(k)]^3}. \tag{25}$$

Subsequent calculations will be carried out for two charged Bose gases. We shall confine the analysis to the case when the thickness $d$ of the insulating layer separating the Bose gases and the length $d_0$ introduced above [see Eq. (15)] satisfy the inequality

$$d\gg d_0. \tag{26}$$

Numerical estimates show that this inequality will be satisfied for those values of $d$ for which tunneling of carriers from one layer to the other can be disregarded (see Sec. 3 for a detailed discussion of the constraints imposed on $d$ in real experiments).

If the inequality (26) is satisfied, the first term in the radicand in the expression (7) for energy $E_\sigma(k)$ can be disregarded. It can be shown easily that the density of the drag current is defined as

$$\mathbf{j}_2=C\left(\frac{\hbar^2}{2\pi^3MQ^2nd^2}\right)^{1/2}\frac{\mathbf{v}_{s1}}{8d^2}. \tag{27}$$

The coefficient $C$ appearing in this expression can be determined by numerical integration:

$$C\equiv\int_0^\infty dx\,\frac{x^{5/2}\mathrm{e}^{-2x}}{\sqrt{1-\mathrm{e}^{-2x}}(\sqrt{1+\mathrm{e}^{-x}}+\sqrt{1-\mathrm{e}^{-x}})^3}\approx 0.0406. \tag{28}$$

Thus, we have shown that even at zero temperature, one superfluid liquid must entrain during its movement another superfluid liquid from which it is separated by a partition through which tunneling does not take place, but interaction of particles belonging to different liquids is possible. It should be emphasized that, like formula (25), this conclusion is valid for all types of interaction between bosons.

It should be expedient to replace the expression (27) for drag current obtained from microscopic calculations for the case of Coulomb interaction by the expression derived by Duan and Yip[28] for the drag current between two superconductors from qualitative considerations. According to Duan and Yip,[28] the ratio of the drag current $j_2$ to the current $j_1$ flowing into layer 1 must be equal to $\sqrt{2}\hbar/(48\pi nmv_Fd^3)$ at zero temperature, where $m$ is the fermion mass and $v_F$ the velocity at the Fermi surface. In view of the fact that the mode $E_-$ is the acoustic mode for small $k$ and the velocity of sound for this mode $c_-=\sqrt{2\pi nQ^2d/M\epsilon_0}$ [see Eq. (11)], our results for the ratio $j_2/j_1$ can be written in the form $\hbar/(200\pi nMc_-d^3)$. In this connection, the result obtained in Ref. 28 seems to be valid only in the weak bond approximation. Upon an increase in the electron–electron attraction, the expression derived in Ref. 28 must be modified and the Fermi velocity of pairing electrons in the limit of two Bose gases should be replaced by the velocity of the mode $E_-$. Note that the results obtained by us and by Duan and Yip[28] differ not only numerically, but also in their functional dependence. In particular, since the velocity $c_-$ depends on the separation $d$ between Bose gases, $j_2/j_1\sim d^{-7/2}$ in our case, while the authors of Ref. 28 found that $j_2/j_1\sim d^{-3}$.

## 2. COLLECTIVE VARIABLES

The Bogoliubov technique becomes inapplicable at nonzero temperature since there is no Bose condensate in a two-dimensional system for $T\neq 0$. The absence of such a condensate is guaranteed by Bogoliubov's theorem on singularities of the type $1/q^2$. The applicability of Bogoliubov's technique is also limited by another circumstance. The terms not containing condensate operators and disregarded in the Hamiltonian (1) may make a significant contribution to the energy even at $T=0$, i.e., in the presence of a macroscopic number of particles in the condensate. This circumstance was first noted by Nepomnyashchii[32] who showed that the corrections to the eigenenergy parts associated with terms containing triples and quadruples of operators over the condensate diverge for small momenta. Thus, the behavior of the system for $k\to 0$ remains unclear.

The method of describing a Bose gas in terms of density and phase operators $\hat{\rho}$ and $\hat{\varphi}$ does not suffer from the above-mentioned drawbacks. In the coordinate representation, the relation between the new variables and field operators of Boson annihilation in the layer $\alpha$ has the form

$$\hat{\psi}_\alpha(\mathbf{r})=\exp\{i\hat{\varphi}_\alpha(\mathbf{r})\}\sqrt{\hat{\rho}_\alpha(\mathbf{r})}. \tag{29}$$

The most convincing arguments in favor of the description of the system in terms of operators $\hat{\rho}$ and $\hat{\varphi}$ can be formulated as follows. In the same way as the consideration of Pauli's exclusion principle is very important for degenerate Fermi systems, the symmetry requirements for the wave function or the density matrix upon a transposition of pairs of identical bosons are vital for degenerate Bose systems. This symmetry can be taken into account automatically by writing the density matrix in terms of the operators $\hat{\rho}$. Indeed, the Fourier component of the density operator can be represented in the form

$$\hat{\rho}(\mathbf{k})=\frac{1}{S}\sum_{j=1}^{N}\exp\{-i\mathbf{k}\cdot\mathbf{r}_j\}, \tag{30}$$

where $\mathbf{r}_j$ is the coordinate of the $j$th particle. This expression clearly indicates the symmetry of the operator $\hat{\rho}(\mathbf{k})$ relative to transposition of a boson pair. However, the Hamiltonian cannot be written in terms of the density operators, only, and phase operators $\hat{\varphi}$ conjugate to the operators $\hat{\rho}$ must also be taken into account. In a two-layer system, these operators satisfy the following commutation relations:

$$\hat{\rho}_\alpha(\mathbf{q})\hat{\rho}_\beta(\mathbf{p})-\hat{\rho}_\beta(\mathbf{p})\hat{\rho}_\alpha(\mathbf{q})=\hat{\varphi}_\alpha(\mathbf{q})\hat{\varphi}_\beta(\mathbf{p})-\hat{\varphi}_\beta(\mathbf{p})\hat{\varphi}_\alpha(\mathbf{q})=0, \tag{31}$$

$$\hat{\rho}_\alpha(\mathbf{q})\hat{\varphi}_\beta(-\mathbf{p})-\hat{\varphi}_\beta(-\mathbf{p})\hat{\rho}_\alpha(\mathbf{q})=\frac{i}{S}\delta_{\alpha\beta}\delta_{\mathbf{q},\mathbf{p}}, \tag{32}$$

where $\alpha$ is the layer number.

A transition to collective variables $\hat{\rho}$ and $\hat{\varphi}$ actually indicates a decomposition of excitations emerging in the system into density waves with wave vector $\mathbf{k}$. Collective variables correctly reflect the structure of excitations in the longwave region and are therefore quite effective for describing the properties associated with the inclusion of the long-range part of the interaction. In particular, this is valid for systems with Coulomb interaction.

Decomposition into density waves becomes inapplicable for describing one-particle excitations with wavelengths of the order of, or smaller than, the mean separation between particles. The most consistent solution of the problem involves the decomposition of the field operator $\hat{\psi}_\alpha(\mathbf{r})$ into two components corresponding to small and large boson momenta (see Refs. 32 and 33 for details). However, in the range of temperatures considered by us which are small compared to the critical temperatures, i.e.,

$$T\ll T_c, \tag{33}$$

the contribution of one-particle excitations (e.g., due to breaking of Cooper pairs) is small, and it is sufficient to consider excitations of collective type only for a correct description of the system.

The Hamiltonian of the system can be presented in terms of the density and phase operators (29) in the following form

$$\begin{aligned}H=&\frac{\hbar^2}{2M}\sum_{\alpha=1,2}\int d^2r\Bigg[\sqrt{\hat{\rho}_\alpha}(\nabla\hat{\varphi}_\alpha)^2\sqrt{\hat{\rho}_\alpha}+\frac{(\nabla\hat{\rho}_\alpha)^2}{4\hat{\rho}_\alpha}\\&+\frac{i}{2}\left(\frac{\nabla\hat{\rho}_\alpha}{\sqrt{\hat{\rho}_\alpha}}\nabla\hat{\varphi}_\alpha\sqrt{\hat{\rho}_\alpha}-\sqrt{\hat{\rho}_\alpha}\nabla\hat{\varphi}_\alpha\frac{\nabla\hat{\rho}_\alpha}{\sqrt{\hat{\rho}_\alpha}}\right)\Bigg]\\&+\frac{1}{2}\sum_{\alpha,\beta=1,2}\int\int d^2rd^2r'\hat{\rho}_\alpha(\mathbf{r})V_{\alpha\beta}(\mathbf{r}-\mathbf{r}')\hat{\rho}_\beta(\mathbf{r}')\\&-\frac{1}{2}\sum_{\alpha=1,2}\int d^2r\hat{\rho}_\alpha(\mathbf{r})V_{\alpha\alpha}(0).\end{aligned} \tag{34}$$

The density operator can be presented in the form of the sum

$$\hat{\rho}_\alpha(\mathbf{r})=n+\delta\hat{\rho}_\alpha(\mathbf{r}), \tag{35}$$

where the $C$-number $n=\langle\hat{\rho}_\alpha(\mathbf{r})\rangle$ describes the mean density of bosons in the layer. Representation (29) turns out to be useful if the fluctuations density in the system are small or, to be more precise, if

$$n^2\gg\langle[\delta\hat{\rho}(\mathbf{r})]^2\rangle. \tag{36}$$

If the system contains vortices, inequality (36) is obviously violated near the vortex core, where $n(\mathbf{r})\to 0$. Hence the density-phase representation is not valid if the system contains vortices. However, if the condition (33) is satisfied, the probability of emergence of vortices is exponentially low and we shall assume that there are no vortices in the system. Inequality (36) will also be violated if we take into account density oscillations with howsoever large vectors on the right-hand side of (36). Within the framework of the approach used here, this is due to the divergence of zero-point vibration in the system at small wavelengths. In a more consistent description, the contribution of zero-point vibration will be finite and condition (36) will be satisfied.

Inequality (36) allows us to expand the kinetic terms in the Hamiltonian (34) into powers of $\delta\hat{\rho}/n$. Retaining terms upto and including second-order terms, considering that $\langle\delta\hat{\rho}(\mathbf{r})\rangle=0$, and going over to the Fourier components of the operators $\hat{\rho}$ and $\hat{\varphi}$, we obtain

$$\begin{aligned}\hat{H}=&\frac{N^2}{2S}[\gamma(0)+\gamma_{12}(0)]-\sum_{\mathbf{k}}[\varepsilon(k)+n\gamma(k)]\\&+S\sum_{\mathbf{k}}\Bigg\{\sum_{\alpha=1,2}\Bigg[n\varepsilon(k)\hat{\varphi}^+_\alpha(\mathbf{k})\hat{\varphi}_\alpha(\mathbf{k})\\&+\frac{\varepsilon(k)}{4n}\hat{\rho}^+_\alpha(\mathbf{k})\hat{\rho}_\alpha(\mathbf{k})\Bigg]\\&+\frac{1}{2}\sum_{\alpha,\beta=1,2}\hat{\rho}^+_\alpha(\mathbf{k})\gamma_{\alpha\beta}(k)\hat{\rho}_\beta(\mathbf{k})\Bigg\}.\end{aligned} \tag{37}$$

As in the preceding section, we first go over to the sum and difference of the initial operators

$$\hat{\rho}_\pm(\mathbf{k})=\frac{1}{\sqrt{2}}[\hat{\rho}_1(\mathbf{k})\pm\hat{\rho}_2(\mathbf{k})],$$

$$\hat{\varphi}_\pm(\mathbf{k})=\frac{1}{\sqrt{2}}[\hat{\varphi}_1(\mathbf{k})\pm\hat{\varphi}_2(\mathbf{k})]. \tag{38}$$

In this case, the Hamiltonian is decomposed into a sum of two terms, each of which depends only on variables with the same value of $\sigma$:

$$\begin{aligned}\hat{H}_\sigma=&\frac{N^2}{2S}[\gamma(0)+\gamma_{12}(0)]-\frac{1}{2}\sum_{\mathbf{k}}[\varepsilon(k)+n\gamma(k)]\\&+S\sum_{\mathbf{k}}\Bigg\{n\varepsilon(k)\hat{\varphi}^+_\sigma(\mathbf{k})\hat{\varphi}_\sigma(\mathbf{k})+\Bigg[\frac{\varepsilon(k)}{4n}\frac{1}{2}[\gamma(k)\\&+\sigma\gamma_{12}(k)]\Bigg]\hat{\rho}^+_\sigma(\mathbf{k})\hat{\rho}_\sigma(\mathbf{k})\Bigg\}.\end{aligned} \tag{39}$$

Going over from operators $\hat{\rho}_\sigma(\mathbf{k})$ and $\hat{\varphi}_\sigma(\mathbf{k})$ to the operators $\hat{b}^+_\sigma$ and $\hat{b}_\sigma$ of creation and annihilation of elementary excitations with the help of the relations

$$\hat{\rho}_\sigma(\mathbf{k})=\left(\frac{\varepsilon(k)n}{E_\sigma(k)S}\right)^{1/2}[\hat{b}_\sigma(\mathbf{k})+\hat{b}^+_\sigma(-\mathbf{k})],$$

$$\hat{\varphi}_\sigma(\mathbf{k}) = \frac{1}{2i}\left(\frac{E_\sigma(k)}{\varepsilon(k)nS}\right)^{1/2}[\hat{b}_\sigma(\mathbf{k}) - \hat{b}^+_\sigma(-\mathbf{k})], \tag{40}$$

we can easily diagonalize the Hamiltonian $H = \Sigma_\sigma H_\sigma$ of the system to the form (5). The ground state energy $E_0$ and the energy of elementary excitations $E_\sigma(k)$ are described in this case by the same expressions (5) and (7), respectively.

Unlike the Bogoliubov technique, the applicability of this method is based on the smallness of the ratio

$$\frac{\langle|\delta\hat{\rho}|^2\rangle}{n^2} = \frac{1}{2}\sum_\sigma \int \frac{d^2k}{(2\pi)^2}\frac{1}{n}\frac{\varepsilon(k)}{E_\sigma(k)}[2\langle\hat{b}^+_\sigma(\mathbf{k})\hat{b}_\sigma(\mathbf{k})\rangle + 1]. \tag{41}$$

In contrast to the preceding section, the angle brackets in this equation indicate thermodynamic averaging. Neglecting density fluctuations caused by zero-point vibrations (which do not emerge in a more consistent approach), this expression is found to be small at temperatures that are low in comparison with the characteristic boson interaction energy.

We shall now consider the method of determining the density of particles in the condensate at $T=0$ by using the formalism described above. For this purpose, we shall derive the relation between the operators $\hat{\rho}(\mathbf{q})$ and $\hat{\varphi}(\mathbf{q})$ and the operators $\hat{a}^+_\alpha$ and $\hat{a}_\alpha$ of creation and annihilation of real bosons. The expression for the operator $\hat{\rho}$ apparently follows from the equality $\hat{\rho}(\mathbf{r}) = \hat{\psi}^+(\mathbf{r})\hat{\psi}(\mathbf{r})$. Going over to Fourier components, we obtain

$$\hat{\rho}_\alpha(\mathbf{q}) = \frac{1}{S}\sum_{\mathbf{p}} \hat{a}^+_\alpha(\mathbf{p}-\mathbf{q}/2)\hat{a}_\alpha(\mathbf{p}+\mathbf{q}/2). \tag{42}$$

The expression for the phase operator can be found as follows. The current density operator in the $\rho$–$\varphi$ representation has the form

$$\hat{\mathbf{j}}_\alpha(\mathbf{r}) = \frac{\hbar}{M}\sqrt{n+\delta\hat{\rho}_\alpha(\mathbf{r})}(\nabla\hat{\varphi}_\alpha(\mathbf{r}))\sqrt{n+\delta\hat{\rho}_\alpha(\mathbf{r})}. \tag{43}$$

If the assumption concerning the small value of density fluctuations (36) is valid, the current density operator can be expressed in the first approximation through the phase operator gradient and the average density $\hat{\mathbf{j}}_\alpha = (\hbar n/M)\nabla\varphi_\alpha$ of bosons in a layer. On the other hand, the relation between the current density operator and the operators of creation and annihilation of particles is defined by the familiar expression

$$\hat{\mathbf{j}}_\alpha(\mathbf{q}) = \frac{\hbar}{MS}\sum_{\mathbf{p}} \mathbf{q}\hat{a}^+_\alpha(\mathbf{p}-\mathbf{q}/2)\hat{a}_\alpha(\mathbf{p}+\mathbf{q}/2). \tag{44}$$

Equating both expressions for the current density operator, we can define the phase operator $\hat{\varphi}$ as a function of $\hat{a}^+_\alpha$ and $\hat{a}_\alpha$:

$$\hat{\varphi}_\alpha(\mathbf{q}) = -\frac{i}{nS}\frac{\mathbf{q}}{q^2}\sum_{\mathbf{p}} \mathbf{p}\hat{a}^+_\alpha(\mathbf{p}-\mathbf{q}/2)\hat{a}_\alpha(\mathbf{p}+\mathbf{q}/2). \tag{45}$$

Since this is an approximate expression, the phase operator defined by it satisfies commutation relations differing from (31) and (32). Considering that the operators $\hat{a}^+_\alpha$ and $\hat{a}_\alpha$ satisfy Bose commutation relations, we can easily find with the help of Eqs. (42) and (45) that

$$\hat{\varphi}(\mathbf{q})\hat{\varphi}(\mathbf{p}) - \hat{\varphi}(\mathbf{p})\hat{\varphi}(\mathbf{q}) = \frac{i}{N}\frac{(p^2-q^2)\mathbf{qp}}{q^2p^2}\hat{\varphi}(\mathbf{q}+\mathbf{p}), \tag{46}$$

$$\hat{\rho}(\mathbf{q})\hat{\varphi}(\mathbf{p}) - \hat{\varphi}(\mathbf{p})\hat{\rho}(\mathbf{q}) = -\frac{i}{N}\hat{\rho}(\mathbf{q}+\mathbf{p}). \tag{47}$$

We shall show that in the thermodynamic limit, i.e., for $N\to\infty$ and $S\to\infty$, $n = N/S$ is a finite quantity and commutation relations (46) and (47) are transformed into (31) and (32). For $\mathbf{q}\neq -\mathbf{p}$, the right-hand sides of formulas (46) and (47) contains a quantity of the same order as the quantity on the left-hand sides divided by the total number of particles. Hence in this case, the right-hand side of the equalities can be treated as equal to zero for $N\to\infty$. For the case $\mathbf{q} = -\mathbf{p}$, we obtain formula (32) from (47) since $\rho_0 = n \equiv N/S$. As $\mathbf{q}\to -\mathbf{p}$ in (46) it must be noted that for low values of momenta, the phase operator $\hat{\varphi}(\mathbf{q}) \sim 1/q$. This divergence of $\hat{\varphi}(\mathbf{q}+\mathbf{p})$ on the right-hand side of (46) is compensated by the factor $p^2 - q^2$. Hence, if $N\to\infty$, formula (46) is again transformed into (31) as $\mathbf{q}\to -\mathbf{p}$.

The obtained expressions for the operators $\hat{\rho}(\mathbf{q})$ and $\hat{\varphi}(\mathbf{q})$ can be simplified for $T=0$. Since the system as $T=0$ has a Bose condensate, and the number of particles over the condensate is small in comparison with the total number of particles, we can retain in the sums over $\mathbf{p}$ in (42) and (45) only terms for which the argument of one of the operators vanishes. In this case, the operator $\hat{a}^+_\alpha(0)$ or $\hat{a}_\alpha(0)$ can be replaced by the $C$-number $\sqrt{N_0} \approx \sqrt{N}$. hence it can easily be seen that

$$\hat{\rho}_\sigma(k) = \frac{\sqrt{N}}{S}[\hat{a}^+_\sigma(-\mathbf{k}) + \hat{a}_\sigma(\mathbf{k})], \tag{48}$$

$$\hat{\varphi}_\sigma(\mathbf{k}) = \frac{i}{2\sqrt{N}}[\hat{a}^+_\sigma(-\mathbf{k}) - \hat{a}_\sigma(\mathbf{k})]. \tag{49}$$

Using these relations, we arrive at the expression

$$\frac{1}{2S}[\hat{a}^+_\sigma(\mathbf{k})\hat{a}_\sigma(\mathbf{k}) + \hat{a}^+_\sigma(-\mathbf{k})\hat{a}_\sigma(-\mathbf{k}) + 1]$$

$$= n\hat{\varphi}^+_\sigma(\mathbf{k})\hat{\varphi}_\sigma(\mathbf{k}) + \frac{1}{4n}\hat{\rho}^+_\sigma(\mathbf{k})\hat{\rho}_\sigma(\mathbf{k}). \tag{50}$$

Averaging both sides of (50) over the ground state (it should be recalled that we are considering the case $T=0$) and considering that

$$N_\sigma(\mathbf{k}) \equiv \langle\hat{a}^+_\sigma(\mathbf{k})\hat{a}_\sigma(\mathbf{k})\rangle = \langle\hat{a}^+_\sigma(-\mathbf{k})\hat{a}_\sigma(-\mathbf{k})\rangle, \tag{51}$$

we obtain the following expression for the distribution function of real bosons:

$$N_\alpha(k) = \frac{S}{2}\sum_\sigma\left[n\langle\hat{\varphi}^+_\sigma(\mathbf{k})\hat{\varphi}_\sigma(\mathbf{k})\rangle + \frac{1}{4n}\langle\hat{\rho}^+_\sigma(\mathbf{k})\hat{\rho}_\sigma(\mathbf{k})\rangle - \frac{1}{2S}\right]. \tag{52}$$

Presenting $\hat{\rho}$ and $\hat{\varphi}$ in terms of the operators $\hat{b}$ and $\hat{b}^+$ of elementary excitations and considering that $\langle\hat{b}^+\hat{b}\rangle = 0$, we arrive at an expression for the distribution function of real bosons, which is identical to the distribution function (13) obtained by using the Bogoliubov technique.

Thus, we have shown that a transition to the $\rho$-$\varphi$ representation makes it possible to solve the problem about the energy spectrum of a $2D$ Bose gas for the case when the system does not contain a Bose condensate. At $T=0$, the results coincide with the results obtained by using the familiar Bogoliubov method.

### 3. DRAG CURRENT FOR $T\neq 0$

Before deriving an expression for the drag current at nonzero temperatures, we must note an important circumstance which distinguishes the drag in superfluid and superconducting systems from the drag in normal systems. It is well known that phase coherence in superfluid and superconducting systems allows us to introduce the $C$-number complex order parameter. The phase of the order parameter (to be more precise, its gradient) determines the value of the supercurrent flowing in the system. Earlier, we took into account the emergence of the $C$-number phase in layer 1 by introducing the factor $e^{i\mathbf{k}_{s1}\cdot\mathbf{r}}$ in the field operator $\hat{\varphi}_1$ acting in layer 1. In the general case, a similar factor $e^{i\mathbf{k}_{s2}\cdot\mathbf{r}}$ must also be introduced for the field operator $\hat{\varphi}_2$ acting in the second layer. The vector $\mathbf{k}_s$ must be determined from the condition of minimum energy (to be more precise, free energy) of the system.

The case of open circuit terminals in layer 2 must be distinguished from the case of closed circuit terminals, when layer 2 becomes a multiply connected system. It will be shown below that for the case of open circuit terminals, the value of $\mathbf{k}_{s2}$ following from the condition of minimum energy leads to zero drag current, i.e., $\mathbf{j}_{s2}\equiv 0$. In view of the circulation quantization $\oint\nabla\varphi\cdot d\mathrm{l}=2\pi n$, (where $n=0,1,2,\ldots$) for closed circuit terminals, the vector $\mathbf{k}_s$ can assume only a discrete series of values. Consequently, the current $\mathbf{j}_{s2}$ will be nonzero in the general case. In the following, we shall assume everywhere that the quantity $\mathbf{k}_{s1}$ is defined by external conditions while $\mathbf{k}_{s2}$ is defined by the system depending on whether the terminals are closed, and also on remaining parameters affecting the drag current.

The correction to the Hamiltonian (5), which is connected with the superconducting currents and is linear in $\mathbf{k}_{s1}$ and $\mathbf{k}_{s2}$ has the form

$$M\int d^2r[\mathbf{v}_{s1}\hat{\mathbf{j}}_1(\mathbf{r})+\mathbf{v}_{s2}\hat{\mathbf{j}}_2(\mathbf{r})]=\frac{\hbar^2}{M}\int d^2r[\mathbf{k}_{s1}\sqrt{\hat{\rho}_1(\mathbf{r})}\times[\nabla\hat{\varphi}_1(\mathbf{r})]\sqrt{\hat{\rho}_1(\mathbf{r})}+\mathbf{k}_{s2}\sqrt{\hat{\rho}_2(\mathbf{r})}[\nabla\hat{\varphi}_2(\mathbf{r})]\sqrt{\hat{\rho}_2(\mathbf{r})}]. \tag{53}$$

After transition to creation and annihilation operators of excitations $\hat{b}_\sigma^+$ and $\hat{b}_\sigma$, we can write the following expression for the Hamiltonian of the system, taking the current components (53) into consideration:

$$\hat{H}=\hat{H}_0+\hat{H}', \tag{54}$$

where

$$\hat{H}_0=E_0+\sum_{\sigma,\mathbf{k}}\left(E_\sigma(k)+\frac{\hbar^2\mathbf{k}\cdot(\mathbf{k}_{s1}+\mathbf{k}_{s2})}{2M}\right)\hat{b}_\sigma^+(\mathbf{k})\hat{b}_\sigma(\mathbf{k}), \tag{55}$$

$$\hat{H}'=\sum_{\mathbf{k}}\frac{\hbar^2\mathbf{k}\cdot(\mathbf{k}_{s1}-\mathbf{k}_{s2})}{4M\sqrt{E_+E_-}}\{(E_+-E_-)[\hat{b}_+^+(\mathbf{k})\hat{b}_-^+(-\mathbf{k})+\hat{b}_+(\mathbf{k})\hat{b}_-(-\mathbf{k})]+(E_++E_-)[\hat{b}_+^+(\mathbf{k})\hat{b}_-(\mathbf{k})+\hat{b}_-^+(\mathbf{k})\hat{b}_+(\mathbf{k})]\}. \tag{56}$$

Let us first consider the case when the terminals in layer 2 are closed. Assuming that $\mathbf{k}_{s2}=0$, we shall determine the current emerging in this layer as a response to the perturbation of the system induced by current in layer 1. At nonzero temperatures, the expression for the linear response to the perturbation (Kubo formula) has the form

$$\langle\hat{\mathbf{j}}_2\rangle=\langle\hat{\mathbf{j}}_2(t)\rangle_0+\int_{-\infty}^{t}\frac{dt'}{i\hbar}\langle(\hat{\mathbf{j}}_2(t)\hat{H}'(t')-\hat{H}'(t')\hat{\mathbf{j}}_2(t))\rangle_0, \tag{57}$$

where the angle brackets $\langle\ldots\rangle_0$ now stand for thermodynamic averaging with the Hamiltonian $\hat{H}_0$. The operators $\hat{\mathbf{j}}(t)$ and $\hat{H}'(t)$ can be written in terms of the interaction

$$\hat{A}(t)=e^{i\hat{H}_0t/\hbar}\hat{A}e^{-i\hat{H}_0t/\hbar}. \tag{58}$$

We introduce the following notation for the quasiparticle distribution functions:

$$\langle\hat{b}_\sigma^+(\mathbf{k})\hat{b}_\sigma(\mathbf{k})\rangle_0\equiv n_\sigma(\mathbf{k})=\left[\exp\left(\frac{E_\sigma(k)+\hbar^2\mathbf{k}\cdot\mathbf{k}_{s1}/2M}{T}\right)-1\right]^{-1}. \tag{59}$$

Expanding the distribution function in powers of $\mathbf{k}_{s1}$ up to linear terms

$$n_\sigma(\mathbf{k})\approx n_\sigma^0(\mathbf{k})+\frac{\hbar^2\mathbf{k}\cdot\mathbf{k}_{s1}}{2M}\frac{\partial n_\sigma^0}{\partial E_\sigma}, \tag{60}$$

we arrive at the following expression for the drag current density:

$$\mathbf{j}_2=\frac{1}{S}\sum_{\mathbf{k}}\frac{\hbar\mathbf{k}_{s1}}{4M}\varepsilon(k)\left\{\frac{\partial n_+^0}{\partial E_+}+\frac{\partial n_-^0}{\partial E_-}+\frac{(E_+-E_-)^2}{2E_+E_-(E_++E_-)}[n_+^0(\mathbf{k})+n_-^0(\mathbf{k})+1]-\frac{(E_++E_-)^2}{2E_+E_-(E_+-E_-)}[n_+^0(\mathbf{k})-n_-^0(\mathbf{k})]\right\}. \tag{61}$$

At $T=0$, there are no quasiparticles in the system (i.e., $n_\sigma^0(\mathbf{k})=0$), and formula (61) is transformed into the expression (25) obtained by the Bogoliubov method.

In order to compute the drag current for closed as well as open circuit terminals in the second layer, let us determine the free energy of the system. Nondiagonal components of $\hat{H}'$ are taken into account according to the perturbation theory

$$F=F_0-\sum_{n\neq m}\frac{\langle m|\hat{H}'|n\rangle\langle n|\hat{H}'|m\rangle}{E_n^0-E_m^0}\exp\frac{F_0-E_m^0}{T}, \tag{62}$$

where

$$F_0 = -T\ln\left[\mathrm{Tr}\exp\left(-\frac{\hat{H}_0}{T}\right)\right] = E_0 + T \times \sum_{\mathbf{k},\sigma} \ln\left[1-\exp\left(-\frac{E_\sigma(k)+\hbar^2\mathbf{k}\cdot(\mathbf{k}_{s1}+\mathbf{k}_{s2})/2M}{T}\right)\right], \tag{63}$$

$$E_m^0 = E_0 + \sum_{\mathbf{k},\sigma}\left(E_\sigma(k)+\frac{\hbar^2\mathbf{k}\cdot(\mathbf{k}_{s1}+\mathbf{k}_{s2})}{2M}\right)n_\sigma(\mathbf{k}), \tag{64}$$

$n_\sigma(\mathbf{k})$ being the occupancy of state $\sigma$ with momentum $\hbar\mathbf{k}$. After simple calculations, we arrive at the following expression for free energy:

$$F = E_0 + T\sum_{\mathbf{k},\sigma}\ln\left[1-\exp\left(-\frac{\hbar^2\mathbf{k}\cdot(\mathbf{k}_{s1}+\mathbf{k}_{s2})/2M}{T}\right)\right] - \sum_{\mathbf{k}}\left(\frac{\hbar^2\mathbf{k}\cdot(\mathbf{k}_{s1}-\mathbf{k}_{s2})}{4M}\right)^2\frac{1}{2E_+E_-} \times\left\{\frac{(E_+-E_-)^2}{E_++E_-}[n_+(\mathbf{k})+n_-(\mathbf{k})+1] - \frac{(E_++E_-)^2}{E_+-E_-}[n_+(\mathbf{k})-n_-(\mathbf{k})+1]\right\}. \tag{65}$$

The average flux density $\mathbf{j}_\alpha$ of particles in the layer $\alpha$ is expressed in terms of the free energy with the help of the familiar thermodynamic relation

$$\mathbf{j}_\alpha = \frac{1}{\hbar S}\frac{\partial F}{\partial \mathbf{k}_{s\alpha}}. \tag{66}$$

Differentiating (65) with respect to $\mathbf{k}_{s2}$, putting $\mathbf{k}_{s2}=0$ in the obtained expression (which corresponds to the regime with closed circuit terminals), and retaining only terms proportional to the first power of $\mathbf{k}_{s1}$, we arrive exactly at formula (61) for current in the layer 2.

In the case of open terminals, we proceed from the free energy minimum and consider the factor $e^{i\mathbf{k}_{s2}\mathbf{r}}$ as a response of the system to the current in layer 1. we must calculate the derivative $\partial F/\partial\mathbf{k}_{s2}$ and equate it to zero. The resulting equation will define the value of the wave vector $\mathbf{k}_{s2}$. In view of the relation (66), however, the condition $\partial F/\partial\mathbf{k}_{s2}=0$ means that the current in layer 2 will be equal to zero.

Let us dwell on this problem in greater detail. We shall describe the emerging situation in terms of two currents. If the field operator acting in the layer $\alpha$ has the form $\hat{\Psi}_\alpha = \exp\{i\mathbf{k}_{s\alpha}\cdot\mathbf{r}\}\hat{\psi}_\alpha$, we can go over in formula (21) for the particle flux density operator $\mathbf{j}$ from operators $\hat{\Psi}_\alpha$ and $\hat{\Psi}_\alpha^+$ to $\hat{\psi}_\alpha$ and $\hat{\psi}_\alpha^+$. This gives

$$\hat{\mathbf{j}}_\alpha[\hat{\Psi}(\mathbf{r})] = \frac{\hbar\mathbf{k}_{s\alpha}}{M}\hat{\psi}_\alpha^+(\mathbf{r})\hat{\psi}_\alpha(\mathbf{r}) + \hat{\mathbf{j}}_\alpha[\hat{\psi}(\mathbf{r})]. \tag{67}$$

The first term on the right-hand side of (67) depends on the quantity $\mathbf{k}_{s\alpha}$ and defines the superfluid current component in the layer $\alpha$, which is connected directly with the difference in the phases of the order parameter at the ends of the layer. The second term on the right-hand side of (67) does not depend on the quantity $\mathbf{k}_{s\alpha}$ and is determined by the interaction between the layers. In the case of open circuit terminals, it follows from the free energy minimum that these two terms exactly compensate each other. However, if the terminals of the structure are closed, the first term assumes a discrete series of values and the second term is continuous. In this case, their sum may not be equal to zero.

Let us determine the drag current density $\mathbf{j}_2$ for the case of Coulomb Bose gases. For this purpose, we shall assume that the following inequalities are satisfied:

$$d \gg d_0, \quad T \ll T_0 \equiv \left(\frac{2\pi n Q^2\hbar^2}{M\epsilon_0 d}\right)^{1/2}. \tag{68}$$

The first of these inequalities allows us to neglect the term $\varepsilon^2(k)$ under the radicand in the expressions for the energy spectrum (7). When the second inequality is satisfied, we can disregard the excitations of ''+'' modes at nonzero temperatures. The latter statement follows from the fact that modes with $E(k)\leqslant T$ are excited at a given temperature $T$. The limiting wave number satisfying this condition is defined as

$$k_c \approx \left(\frac{M\epsilon_0 T^2}{2\pi Q^2 n\hbar^2 d}\right)^{1/2}, \tag{69}$$

while the ratio $E_+^2/E_-^2 > T_0/2T \gg 1$ for $k<k_c$.

Estimates show that the condition (68) can be easily satisfied in experiments. Thus, for characteristic values $n=10^{15}\,\mathrm{cm}^{-2}$, $M=2m_0$, where $m_0$ is the mass of a free electron, $Q=2e$, $\epsilon_0=10$, $d=10^{-6}\,\mathrm{cm}$ we have $d_0=6\times10^{-9}\,\mathrm{cm}$, $T_0\approx 4\cdot10^3\,\mathrm{K}$.

Taking (68) into account, we obtain the following expression from (61) for the drag current density of charged Bose gases:

$$\mathbf{j}_2 = \frac{1}{8\pi n_s}\frac{\hbar^2}{Md^4}\frac{1}{T_0}\left\{0.0406 - 2\zeta(3)\left(\frac{T}{T_0}\right)^3\right\}\mathbf{j}_1. \tag{70}$$

Here $\zeta(y)$ is Riemann's zeta-function, and $T_0$ is the temperature introduced in (68).

Before discussing the experiments on the detection of drag between electrons in spatially separated superconducting systems, let us note the fundamental features of this effect. For normal systems, current is passed through one conducting layer, and the potential difference is measured in the other layer whose ends are open. This method is not applicable for superconducting layers since electric current cannot exist in superconductors. The closure of the secondary circuit is a necessary condition for the *existence* of the effect. Unlike normal systems, the effect of transfer of motion is associated not with the transfer of momentum from one layer to the other (the Hamiltonian does not contain dissipative components in the approximation under consideration), but with the redistribution of supercurrent between the layers. This statement follows from the fact that the correction to the current in layer 1 calculated in analogy with (61) is equal and opposite to the current in the layer (2).

The peculiarities of the drag effect in two-layer superconducting systems necessitate the experimental measurement of, say, the magnetic flux produced in the secondary circuit by the circular supercurrent. We shall determine the value of the flux for the case shown in Fig. 1. The complete expression for the electric current density $\mathbf{J}_2$ in layer 2 (we

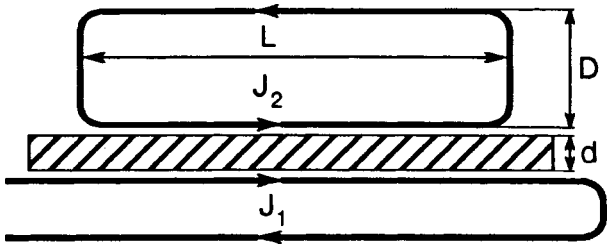


FIG. 1. Schematic diagram of the experiment for detecting the drag between superconducting layers. The lower superconducting layer is bent to prevent current excitation in the upper layer due to the magnetic field of the lower layer.

shall denote it by a capital letter to distinguish it from the particle flux density $j_2$) contains an additional term associated with the magnetic field produced by this current:

$$\mathbf{J}_2=\frac{Q\hbar\mathbf{k}_{s2}}{M}n_s+Q\mathbf{j}_2-\frac{Q^2n_s}{Mc}\mathbf{A}, \tag{71}$$

where $\mathbf{A}$ is the vector potential of this field. Estimates (70) show that the quantity $\mathbf{j}_2$ is quite small, and the energy minimum corresponds to $\mathbf{k}_{s2}=0$.

The total current in the lower and upper films must be equal to $-(Q^2n_s/Mc)\mathbf{A}_L+Q\mathbf{j}_2$ and $-(Q^2n_s/Mc)\mathbf{A}_H$ where $\mathbf{A}_L$ and $\mathbf{A}_H$ denote the vector potential in the lower and upper films. Solving the Maxwell equation curl$\mathbf{H}=4\pi\mathbf{J}/c$, we can easily find that

$$J_2=\frac{Qj_2}{2+\gamma}, \quad \text{where} \quad \gamma=\frac{4\pi n_sQ^2D}{Mc^2}. \tag{72}$$

Here $D$ is the separation between the upper and lower films in the secondary circuit (see Fig. 1). The magnetic flux between the films, which is related to the current $J_2$, is defined as

$$\Phi\equiv HDL=\frac{4\pi}{c}\frac{Qj_2}{2+\gamma}DL. \tag{73}$$

For $\gamma\ll 1$, the magnetic flux increases linearly with $D$. It attains saturation for $\gamma\approx 1$, and the flux $\Phi$ no longer depends on $D$ for $\gamma\gg 1$. In this case,

$$\Phi=\Phi_{\max}=\frac{0.02e\hbar LJ_1}{Q^2T_0(2\pi n_sd^2)^2}\Phi_0, \tag{74}$$

where $\Phi_0=hc/2e$ is the magnetic flux quantum.

Let us now present the numerical estimates. For $n_s=n=10^{15}\,\mathrm{cm}^{-2}$, $Q=2e$, $M=2m_0$ the dimensionless constant $\gamma$ is of the order of unity for $D\approx 10^{-4}$ cm. For $D\gg 10^{-4}$ cm, $\gamma\gg 1$ and the flux $\Phi=\Phi_{\max}$. While estimating the flux $\Phi_{\max}$, it must be remembered that it depends strongly on $d$ ($\Phi_{\max}\sim d^{-7/2}$), and hence the chosen value of $d$ should be as small as possible. At the same time, it must be large enough so that we can disregard the tunneling of electrons through the insulating layer separating the primary and secondary circuits. For $d\approx 50$ Å, $L=1$ cm, and $v_{s1}=10^4$ cm/s, the flux $\Phi_{\max}\approx 3\times 10^{-5}\cdot\Phi_0$.

Thus, microscopic computations carried out with the help of Bogoliubov's technique and by using the formalism of collective variables establish the existence of the effect of transfer of motion between two-dimensional Bose gases separated by a thin interlayer. The results are obtained for an arbitrary type of interaction between layers, and the case of charged Bose gases is considered in detail. We assume that the situation with charged Bose gases provides a qualitatively correct description of the drag between two-dimensional films from ''Cooper'' superconductors. The dependence of the drag current on temperature and thickness of the partition is determined for the case of charged Bose gases. The effect exists for zero and nonzero temperature for any type of interaction potential, the value of the drag current decreasing with increasing temperature in the case of Bose gases. Unlike normal systems, the transfer of motion between superfluid layers takes place only when the terminals of the secondary circuit are closed. It is associated not with the transfer of momentum from one layer to the other, but only with the establishment of a single coherent state as a result of interaction between layers, the phases of the order parameter being correlated in both layers in this coherent state. An experimental setup is proposed for detecting the predicted effect. Calculations show that the value of the magnetic flux emerging in the secondary circuit as a result of drag lies within the range that is accessible to measurements with the help of modern techniques.

This research was partially supported by an INTAS Grant No. 97-0972.

*)E-mail: shevchenko@ilt.kharkov.ua

[1] S. I. Shevchenko, Fiz. Nizk. Temp. **2**, 505 (1976) [Sov. J. Low Temp. Phys. **2**, 251 (1976)].
[2] Yu. E. Lozovik and V. I. Yudson, Zh. Éksp. Teor. Fiz. **71**, 738 (1976) [Sov. Phys. JETP **44**, 389 (1976)].
[3] L. Swierkowski and D. Nelson, Phys. Rev. Lett. **67**, 240 (1991).
[4] E. Shimshon, Phys. Rev. B **51**, 9415 (1995).
[5] P. M. Solomon, P. J. Price, D. J. Frank, and D. C. L. Tulipe, Phys. Rev. Lett. **63**, 2508 (1989).
[6] T. J. Gramila, J. P. Eisenstein, A. H. MacDonald *et al.*, Phys. Rev. Lett. **66**, 1216 (1991).
[7] T. J. Gramila, J. P. Eisenstein, A. H. MacDonald *et al.*, Phys. Rev. B **47**, 12957 (1993).
[8] H. Rubel, E. H. Linfield, D. A. Ritchie *et al.*, Semicond. Sci. Technol. **10**, 1229 (1995).
[9] U. Sivan, P. M. Solomon, and H. Shtrikman, Phys. Rev. Lett. **68**, 1195 (1992).
[10] N. Giordano and J. D. Monnier, Phys. Rev. B **50**, 9363 (1994).
[11] X. Huang, G. Bazan, and G. H. Bernstein, Phys. Rev. Lett. **74**, 4051 (1995).
[12] M. B. Pogrebinskiĭ, Fiz. Tekh. Poluprovod. **11**, 637 (1977) [Sov. Phys. Semicond. **11**, 372 (1977)].
[13] P. J. Price, Physica B **117**, 750 (1983).
[14] R. N. Gurzhi and A. I. Kopeliovich, JETP Lett. **26**, 140 (1977)].
[15] B. Laikhtman and P. M. Solomon, Phys. Rev. B **41**, 9921 (1990).
[16] I. I. Boiko and Yu. M. Sirenko, Phys. Status Solidi **159**, 805 (1990).
[17] A. G. Rojo and G. D. Mahan, Phys. Rev. Lett. **68**, 2074 (1992).
[18] Ji-Min Duan, Europhys. Lett. **29**, 489 (1995).
[19] L. Zheng and A. H. MacDonald, Phys. Rev. B **48**, 8203 (1993).
[20] A.-P. Jahuo and H. Smith, Phys. Rev. B **47**, 4420 (1993).
[21] K. Flensberg, B. Yu-Kuang Hu, A.-P. Jahuo and D. Huang, Phys. Rev. B **52**, 14761 (1995).
[22] K. Flensberg and B. Yu-Kuang Hu, Phys. Rev. B **52**, 14796 (1995).

[23] B. Tanatar, Solid State Commun. **99**, 1 (1996).
[24] H. C. Tso, P. Vasilopulos, and F. M. Peeters, Phys. Rev. Lett. **68**, 2516 (1992).
[25] J. Mao, Qi Huang, W. Cheng, and J. Zhon, J. Phys.: Condens. Matter **5**, 5019 (1993).
[26] I. Giaver, Phys. Rev. Lett. **15**, 825 (1965).
[27] A. Kamenev and Y. Oreg, Phys. Rev. B **52**, 7516 (1995).
[28] J.-M. Duan and S. Yip, Phys. Rev. Lett. **70**, 3647 (1993).
[29] S. I. Shevchenko and S. V. Terent'ev, Fiz. Nizk. Temp. **23**, 1088 (1997) [Low Temp. Phys. **23**, 817 (1997)].
[30] K. Flensberg and B. Yu-Kuang Hu, Phys. Rev. B **52**, 14796 (1995).
[31] V. Apaja, J. Halinen, V. Halonen *et al.*, Phys. Rev. B **55**, 12925 (1997).
[32] Yu. A. Nepomnyashchiĭ, Zh. Éksp. Teor. Fiz. **85**, 1244 (1983) [Sov. Phys. JETP **58**, 722 (1983)].
[33] V. N. Popov, *Functional Integrals in Quantum Field Theory and Statistical Physics* Reidel Dordrecht, 1983.

## SUPERCONDUCTIVITY, HIGH TEMPERATURE SUPERCONDUCTIVITY

# Power-law low-temperature asymptotics for spatially nonhomogeneous *s*-wave superconductors

A. M. Gabovich and A. I. Voitenko

*Institute of Physics, National Academy of Science of Ukraine, 46 Nauki Ave., 252022 Kiev, Ukraine**)
(Submitted December 21, 1998; revised February 23, 1999)
Fiz. Nizk. Temp. **25**, 677–684 (July 1999)

It is shown that low temperature asymptotics of various thermodynamic and transport properties of *s*-wave superconductors can become power-law ones if wide distributions of gap values exist, originating from structure domains, charge stripes, charge-density waves or other mesoscopic nonhomogeneities. The relevant experimental data for high-$T_c$ oxides are analyzed on the basis of the developed theory. © *1999 American Institute of Physics.* [S1063-777X(99)00507-1]

### 1. INTRODUCTION

The controversy over the order parameter symmetry in cuprates constitutes a great challenge to investigators and is far from being resolved,[1–3] contrary to what is sometimes claimed.[4,5] Really, the relevant experimental data may be divided into three main groups. The first group includes phase-sensitive methods, e.g., the phase-sensitive observations of the half-flux quantum spontaneous magnetization of the three-grain boundaries[4,6] and of the anomalous $\pi$-phase shift across the *c*-axis junction straddling a single twin.[7] These experimental results are often considered as an unequivocal evidence of the *d*-wave order parameter character. Nevertheless, as discussed in Ref. 2, the ordinary *s*-wave order parameter suppression at twin boundaries, the flux trapping there or in the corners, and meanderings of the grain boundaries on the scale of 100–1000 Å[8] can reproduce such a behavior as well. Moreover, the most recent measurements (see discussion in Ref. 9) of the *c*-axis (perpendicular to the layers)Josephson critical current $I_c$ between twisted bicrystals of $Bi_2Sr_2CaCu_2O_{8+y}$ ruled out the purported ''naive'' identification of the order parameter symmetry there with $d_{x^2-y^2}$ wave form. Namely, there was no dependence of $I_c$ on the twist angle $\varphi_0$, whereas in the *d*-wave case it would have been $I_c \propto \cos 2\varphi_0$. At the same time, *c*-axis tunneling between $Bi_2Sr_2CaCu_2O_{8+y}$ and Pb shows a distinct Fraunhofer pattern appropriate to *s*-wave order parameter, although the magnitude of the $I_c$ is very small.[10]

Two other groups are phase-insensitive. One of them probes the gap features, if any, at the Fermi surface (FS). It includes, in particular, the angle-resolved,[11] tunnel,[12] and point-contact[13] spectroscopies. The results obtained, making use of these methods for a number of specific hole-doped oxides, are also usually interpreted as manifestations of the *d*-wave pairing. However, this interpretation may be misleading. Namely, the emergence of the dielectric gap on the nesting FS sections due to the charge-density wave (CDW) formation may mimic the superconducting pseudogap above the critical temperature $T_c$ and severely hamper various measurements of the superconducting gap below $T_c$.[2,14–16] For example, the predicted current-voltage characteristics (CVC's) asymmetricity for junctions involving CDW superconductors with *s*-type pairing[16] resemble those of the *ab*-plane tunnel CVC's for $Bi_2Sr_2CaCu_2O_{8+y}$.[17] The same can be said about the persistence of the smeared pseudogap features in this experiment, so that the CDW's rather than the *d*-wave scenario with *V*-shaped conductance show themselves. The investigations[18] of inelastic Cooper pair tunneling for various phases of the Bi–Sr–Ca–Cu–O system clearly demonstrated the existence of the Riedel-like singularity and the subsequent steep reduction of the Josephson current inherent to Bardeen–Cooper–Schrieffer (BCS) isotropic superconductors,[19] whereas the *d*-wave picture lacks such a threshold behavior.[20] The indications of the *d*-wave inconsistency with measured photoexcited relaxation dynamics in $YBa_2Cu_3O_{7-x}$ were also found.[21] The direct evidence of the *s*-wave pairing in $YBa_2Cu_3O_{7-x}$ and $YbBa_2Cu_3O_{7-x}$ using tunnel and point-contact measurements was also obtained in Ref. 22, where clear classical gap features were seen.

It is also claimed that the type of pairing can be, in principle, deduced as well from the phase-insensitive experiments by analyzing the properties of high-$T_c$ oxides in the low-temperature limit. Indeed, the BCS theory leads to the following asymptotics for various thermodynamic and transport properties $P_s$ of superconductors at temperatures $T$ far below $T_c$:[23]

$$P_s^{\mathrm{asympt}}(\Delta_0, T) = A\Delta_0^m T^l \exp\left(-\frac{\Delta_0}{T}\right). \tag{1}$$

Here $k_B = \hbar = 1$, $\Delta_0$ is the value of the superconducting gap at $T=0$ and the quantities $m$ and $l$ are specific to the property concerned. Instead, a lot of investigations reveal power-law *T*-dependences.[1,2,4] Such a behavior was explained on the basis of the assumed *d*-wave symmetry of the order parameter with gap point or line nodes of the FS.[1,4] Our article is devoted just to this kind of experiment. However, in contrast to the traditional viewpoint, it is shown below that, if one

 

takes into account the wide distribution of the superconducting order parameter magnitudes always existing in complex nonhomogeneous structures of high-$T_c$ oxides,[24–26] the same results can be explained by the conventional *s*-wave pairing.

## 2. EXPERIMENTAL LOW-TEMPERATURE ASYMPTOTICS FOR CUPRATES

To be more specific, let us consider some experimental low-$T$ data for cuprates. In particular, for $YBa_2Cu_3O_{7-x}$ the specific heat $C_s \propto T$,[2] although the recent experiment[21] shows additional contribution $\propto T^2$ and Schottky anomalies $\propto T^{-2}$, making the whole picture uncertain. At the same time, the results for the *d*-wave gap function would have been proportional to $T^2$ for hexagonal or $T^3$ for cubic lattices.[27,28]

For $\delta\lambda_L(T)=[\lambda_L(T)-\lambda_L(0)]\lambda_L^{-1}(0)$, where $\lambda_L(T)$ is the constant magnetic field penetration depth, the experimental data are quite ambiguous. For nominally pure $YBa_2Cu_3O_{7-x}$ samples linear dependences on $T$ are observed,[29] whereas for Zn- and Ni-doped as well as nonhomogeneous crystals $\delta\lambda_L \propto T^2$[29–33] in a formal accordance with the theory of *d*-wave superconductors, either dirty ones[4] or those with surface-induced Andreev bound states.[33] There are also data showing two-gap low-$T$ asymptotics of $\delta\lambda_L(T)$ in $YBa_2Cu_3O_{7-x}$.[34] The authors of Ref. 34 claim that this dependence is intrinsic, whereas the results of Ref. 29 are due to a non-uniform sample oxygenation. For electron-doped oxide $Nd_{1.85}Ce_{0.15}CuO_{4-\delta}$ which always reveals *s*-wave features, $\delta\lambda_L(T)$ follows the exponential law.[1] At the same time, the initial *d*-wave picture with $\delta\lambda_L(T\to 0)\propto T$ was shown to be inconsistent with the third law of thermodynamics.[35] Further modifications[36,37] (see reply in Ref. 38) changed the electromagnetic response of the *d*-wave superconductor in such a way that the calculated in-plane dependence $\delta\lambda_{ab}(T\to 0)\propto T^2$ holds, not violating thermodynamics but destroying the apparent agreement with the experiment.

Unfortunately, it is hard to extract the electronic thermal conductivity component $\kappa_e$ from the experiment due to the complex action of electrons, phonons, and impurities.[39,40] Nevertheless, the experiments indicate that $\kappa_e \propto T$ in Zn-doped $YBa_2Cu_3O_{7-x}$[41] and below $T_c^* = 200$ mK in $Bi_2Sr_2Ca(Cu_{1-x}Ni_x)_2O_8$.[42] The ultrasonic attenuation coefficient $\alpha_s$ also exhibits a power-law $T^n$ decrease for $T \ll T_c$ both for $YBa_2Cu_3O_{7-x}$[43,44] and $La_{1.8}Sr_{0.2}CuO_{4-x}$[43] with a large scatter of the exponent $n$ for each substance. As for the nuclear relaxation rate $T_1^{-1}$, it demonstrates power-law dependences with $1 \leqslant n \leqslant 3$.[4]

This experimental material shows that the universal dependence for any phenomenon discussed does not exist. Moreover, the agreement with the theories based on the gap function with point or line nodes is superficial. Even with additional assumptions being made, the equality between experimental and theoretical power-law exponents still cannot be ensured. It is usually considered as a basis for the adoption of the *d*-wave concept.[1,4] At the same time, while analyzing local structures observed in the nonstoichiometric superconducting and nonsuperconducting oxides,[24–26,45] we drew the conclusion that there is a quite different solution to the problem. Our approach starts from the assumption of a wide distribution of order parameter $\Delta$ values in the bulk of the samples at each $T < T_c$.

## 3. THEORY

The key idea of the theory is that not only a polycrystalline but even a single crystal superconducting oxide sample can be considered as *mesoscopically nonhomogeneous*, i.e., consisting of domains. This domain structure is supposed to be $T$-independent, with each domain having the following properties:

(A) at $T=0$ it is described by a certain superconducting order parameter $\Delta_0$;

(B) up to the relevant critical temperature $T_{c0}(\Delta_0) = \gamma\Delta_0/\pi$, where $\gamma = 1.7810...$ is the Euler constant, it behaves as a true BCS superconductor, i.e., the temperature dependence $\Delta(T)$ of the superconducting order parameter is the Mühlschegel function $\Delta(T) = \delta_{\mathrm{BCS}}(\Delta_0, T)$; any property $P$ under investigation is characterized in this interval by the function $P_s(\Delta, T)$;

(C) at $T > T_{c0}$ it changes into the normal state, and the relevant property is $P_n(T)$.

At the same time, the values of $\Delta_0$ scatter for various domains. The current carriers move freely across domains and inside each domain acquire the respective properties. Thus, possible proximity effects resulting in the correlation of the properties of adjacent domains are neglected. The current carrier density is assumed constant all over the sample, so transient processes are excluded from consideration.

The averaging procedure considered below requires (i) the effective sample size $L$ to be much larger than the mean size of the domains $d_{\mathrm{mean}}$ and (ii) the size of each domain $d_i$ to be larger than the relevant coherence length $\xi_i$. The first condition is needed to regard the superconductor macroscopically homogeneous. The second one stems from the property (B) indicated above. In the opposite case, when $d_i \ll \xi_i$, we are led to the lattice model of superconductor with a local atomic disorder.[46,47] Such a model was applied to the description of $YBa_2Cu_3O_{7-x}$ in Ref. 48. In essence, the domain size there is comparable to that of the elementary cell. However, in this limiting case we go beyond the scope of the BCS *s*-wave picture based on the long-range character of the phonon-induced interaction between electrons[23] (see discussion in Sec. 4). In contrast, the actually adopted condition $d_i > \xi_i$ is fully in line with the basic concept.

Under these conditions, we consider the current carrier liquid to involve normal, $\rho_n(T)$, and superconducting, $\rho_s(T)$, fractions with $\rho_n(T)+\rho_s(T)=1$, and the superconducting fraction to be multicomponent. Each superconducting component corresponds to domains with a certain $\Delta_0$. They possess the properties (A), (B), (C) mentioned above. The superconducting fraction at $T=0$ can be described by a distribution function $f_0(\Delta_0)$ in the interval $0 \leqslant \Delta_0 \leqslant \Delta_0^{\max}$.

$$\rho_s(0) = \int_0^{\Delta_0^{\max}} f_0(\Delta_0)\, d\Delta_0 = 1 - \rho_n(0). \tag{2}$$

The distribution is assumed wide, i.e., $f_0(\Delta_0)$ is non-zero at every point of the interval. In principle, $f_0(\Delta_0)$ can be random or not, but the former case seems more frequently occurring.

At $T\neq 0$ the superconducting components with $T_{c0}<T$, i.e., with $\Delta_0<\Delta^*(T)=\pi T/\gamma$, lose their superconducting properties. The normal fraction of the current carriers in the sample is

$$\rho_n(T)=\rho_n(0)+\int_0^{\Delta^*(T)} f_0(\Delta_0)d\Delta_0, \tag{3}$$

whereas the remaining superconducting part is

$$\rho_s(T)=\int_{\Delta^*(T)}^{\Delta_0^{\max}} f_0(\Delta_0)d\Delta_0. \tag{4}$$

Due to the condition (B), the components, possessing at $T=0$ order parameters within the interval $[\Delta_0,\Delta_0+d\Delta_0]$, at $T\neq 0$ acquire order parameters within the interval $[\Delta,\Delta+d\Delta]$, where $\Delta=\Delta_{\rm BCS}(\Delta_0,T)$. This conversion is expressed by an equation

$$f(\Delta,T)d\Delta=f_0(\Delta_0)d\Delta_0. \tag{5}$$

Here $f(\Delta,T)$ is a function characterizing a new distribution of components in the interval $0<\Delta<\Delta^{\max}(T)$ where $\Delta^{\max}(T)=\Delta_{\rm BCS}(\Delta_0^{\max},T)$. This equation is a consequence of (i) the supposed domain structure permanence, (ii) the constant current carrier density, and (iii) the independence between superconducting components. Then, the function $\rho_s(T)$ takes the form

$$\rho_s(T)=\int_0^{\Delta^{\max}(T)} f(\Delta,T)d\Delta. \tag{6}$$

As for any investigated property $P$, each component, being superconducting or not, makes its contribution to the measured (averaged) value $\langle P\rangle$:

$$\langle P(T)\rangle=P_n(T)\rho_n(T)+\int_0^{\Delta^{\max}(T)} P_s(\Delta,T)f(\Delta,T)d\Delta. \tag{7}$$

This formula is valid (with restriction given above) for additive quantities, such as, e.g., the specific heat. But what about, for example, the penetration depth $\lambda_L$? Really, in the situation when the superconducting gap changes (and in fact goes to zero) on a very short length scale, even the notion of the penetration depth becomes questionable. Moreover, since each of our elementary volumes includes an ensemble of domains with different parameters $\lambda_{L,i}$'s, the matter becomes much more entangled. Nevertheless, even in this situation one may introduce an effective penetration depth $\lambda_L^{\rm eff}$ and measure its $T$-dependence. Really, the measured electromagnetic response of the nonhomogeneous superconductor is the sum of individual domain responses from the sample surface layer. The quantity $\lambda_L^{\rm eff}$ is a parameter that is extracted from the essentially averaged experimental data treated as obtained for a homogeneous BCS superconductor. In the specific case of cuprates the domain sizes $d_i$ are substantially smaller than the intrinsic penetration depths $\lambda_{L,i}$ for each domain and, therefore, the effective $\lambda_L^{\rm eff}$. We conceive that within such a context the calculation of $\lambda_L^{\rm eff}(T)$ as a weighted quantity is at least qualitatively reasonable.

The first term in Eq. (7) describes the contribution $\langle P(T)\rangle_n$ of the normal fraction. It is well-known and will not be considered below. The last term corresponds to the contribution $\langle P(T)\rangle_s$ of the superconducting electrons (holes). Since $f(\Delta=0,T)=f_0[\Delta_0=\Delta^*(T)]\neq 0$, for each $T$ there is a nonvanishing portion of superconducting components with $\Delta\to 0$. It is their contribution that leads to the deviation of the temperature behavior $\langle P(T)\rangle_s$ from the classical one. To make our statement even more sound, we suggest that the low-$T$ asymptotics (1) holds true for each superconducting component up to the relevant critical temperature $T_{c0}$, i.e.,

$$P_s(\Delta,T)=P_s^{\rm asympt}(\Delta_0,T). \tag{8}$$

The allowance for the exact dependences may only strengthen our standpoint.

Note that $P_s^{\rm asympt}(\Delta_0,T)$ in the framework of the BCS scheme depends on $T$ and on $\Delta_0$ rather than on $\Delta$ value. Accordingly, due to Eq. (5) the contribution $\langle P(T)\rangle_s$ can be rewritten as follows:

$$\langle P(T)\rangle_s=\int_{\Delta^*(T)}^{\Delta_0^{\max}} P_s^{\rm asympt}(\Delta_0,T)f_0(\Delta_0)d\Delta_0. \tag{9}$$

The distribution function $f_0(\Delta_0)$ can be expanded into the series

$$f_0(\Delta_0)=\frac{1}{\Delta_0^{\max}}\sum_{k=k_0}^{\infty} B_k\left(\frac{\Delta_0}{\Delta_0^{\max}}\right)^k, \tag{10}$$

where $k_0$ is the order of the leading expansion term. Substituting Eqs. (1) and (10) into Eq. (9) we obtain

$$\langle P(T)\rangle_s=\frac{AT^{l+m+1}}{\Delta_0^{\max}}\sum_{k=k_0}^{\infty} B_k\left(\frac{T}{\Delta_0^{\max}}\right)^k\int_{\frac{\Delta^*(T)}{T}}^{\frac{\Delta_0^{\max}}{T}} x^{m+k}{\rm e}^{-x}dx. \tag{11}$$

Within an accuracy of the made approximations and for temperatures $T\ll\Delta_0^{\max}$ we may extend the upper limit of integration to infinity, so

$$\langle P(T)\rangle_s\approx AT^{l+m}\left(\frac{T}{\Delta_0^{\max}}\right)\sum_{k=k_0}^{\infty} B_k\left(\frac{T}{\Delta_0^{\max}}\right)^k \times\Gamma\left[m+k+1,\frac{\Delta^*(T)}{T}\right], \tag{12}$$

where $\Gamma(a,x)$ is the incomplete gamma function.[49] Since $\Delta^*(T)/T=\pi/\gamma$, the apparently dominant exponential dependence of $\langle P(T)\rangle_s$ on $(-1/T)$ resulting from the second argument of $\Gamma(a,x)$ disappears altogether, whatever the particular value of $k_0$.

One more important result of this formula is that in the framework of the proposed model the measured properties of the superconducting components $\langle P(T)\rangle_s$ at low temperatures are insensible to the particular profile of the distribution function $f_0(\Delta_0)$ at large $\Delta_0$. Hence, for $T\ll\Delta_0^{\max}$ a few first terms of the series (12) constitute a good approximation. Restricting ourselves to the leading $k_0$-term we obtain

$$\langle P(T)\rangle_s = AB_{k_0}(\Delta_0^{\max})^{l+m}\Gamma\left(m+k_0+1,\frac{\pi}{\gamma}\right)\left(\frac{T}{\Delta_0^{\max}}\right)^M, \tag{13}$$

with $M=k_0+l+m+1$. The corrections to this expression are of the next order in $T/\Delta_0^{\max}$. This justifies the validity of substituting the upper limit of the integral in Eq. (11) by infinity. At the same time, this makes eligible the evaluating of the $\langle P(T)\rangle_s$ contribution in Eq. (7) using the low-$T$ asymptotics $P_s^{\text{asympt}}(\Delta_0,T)$ in the integrand instead of the exact value $P_s(\Delta,T)$. Indeed, the $T$-dependences of various parameters in the BCS theory are induced by the $T$-behavior of the gap $\Delta$,[23] e.g., the exponential multiplier in Eq. (1) originates from that in the low-$T$ asymptotics of $\Delta(T)$. Since $\Delta(T\to T_c)\propto(T_c-T)^{1/2}$ in the BCS theory, the considered parameters have at $T\to T_c$ the power-like asymptotics as well. Thus, the use of exact functional dependences $P_s(\Delta,T)$ results not in exponential but power-law dependences $\langle P(T)\rangle_s$.

One should note that in each specific experiment only a certain lowest temperature $T_{\lim}$ is accessible, so that, according to the Eq. (9), only gap values down to $\Delta_0^{\lim}=\pi T_{\lim}/\gamma$ are relevant. Hence, the restriction imposed above on the distribution function $f_0(\Delta_0)$ to extend down to $\Delta_0=0$ may be weakened. Namely, $f_0(\Delta_0)$ should be nonzero for $\Delta_0>\Delta_0^{\lim}$. In the case when the domain ensemble possesses the minimal value $\Delta_0^{\min}$ and the lowest accessible $T_{\lim}<\gamma\Delta_0^{\min}/\pi$, the value $\Delta_0^{\min}$ will manifest itself as the exponential factor $\exp(-\Delta_0^{\min}/T)$ in $\langle P(T)\rangle_s$ (cf. Ref. 23).

Returning to Eq. (13), we see that the actual distribution function reveals itself in the final result only through the expansion parameters $B_{k_0}$ and $k_0$. The most popular distribution functions,[50] namely, normal Gaussian

$$f_G(\Delta_0)=\frac{1}{\Delta_0^{\max}}\left(\frac{2}{\pi\sigma^2}\right)^{1/2}\left[2\Phi\left(\frac{1}{\sigma}\right)+1\right]^{-1}\times\exp\left[-\frac{1}{2}\left(\frac{\Delta_0-\Delta_0^{\max}}{\sigma\Delta_0^{\max}}\right)^2\right], \tag{14}$$

exponential $f_E(\Delta_0)=(\alpha/\Delta_0^{\max})\exp(-\alpha\Delta_0/\Delta_0^{\max})$, and uniform $f_U(\Delta_0)$ ones, where $\alpha$ and $\sigma$ are dimensionless parameters and $\Phi(x)$ is the error function,[49] have finite values at $\Delta_0=0$, so the leading term (13) in the series has the $k_0=0$ order of smallness. At the same time, different distribution functions have different values of coefficient $B_0$. Now it is impossible to make a choice in favor of one of them. The analysis of the heat capacity measurements for various oxides[51,52] makes us suggest that the function $f_0(\Delta_0)$ is mainly concentrated in a narrow interval near $\Delta_0=0$, which is beneficial for our hypothesis.

Applying the general approach to the properties concerned taking their actual low-$T$ expressions,[23] and comparing them with Eq. (1) we come to the following dependences for the chosen case $k_0=0$: for the specific heat

$$\langle C_s(T)\rangle\approx B_0\sqrt{2\pi}N(0)\Delta_0^{\max}\Gamma\left(\frac{7}{2},\frac{\pi}{\gamma}\right)\left(\frac{T}{\Delta_0^{\max}}\right)^2, \tag{15}$$

where $N(0)$ is the electron density of states at the Fermi level; for the penetration depth

$$\langle\delta\lambda_L(T)\rangle\approx B_0\sqrt{\pi/2}\,\Gamma\left(\frac{3}{2},\frac{\pi}{\gamma}\right)\frac{T}{\Delta_0^{\max}}; \tag{16}$$

for the thermal conductivity

$$\langle\kappa_e(T)\rangle\approx B_0\frac{2n_e\tau_{\text{tr}}}{m_e}\Delta_0^{\max}\Gamma\left(3,\frac{\pi}{\gamma}\right)\left(\frac{T}{\Delta_0^{\max}}\right)^2, \tag{17}$$

where $n_e$ is the normal state electron density, $\tau_{\text{tr}}$ is the transport collision time, and $m_e$ is the electron mass; for the ratio $\delta\alpha=\alpha_s/\alpha_n$ of the ultrasonic attenuation coefficients in superconducting, $\alpha_s$, and normal, $\alpha_n$, states

$$\langle\delta\alpha(T)\rangle\approx 2B_0\Gamma\left(1,\frac{\pi}{\gamma}\right)\frac{T}{\Delta_0^{\max}}. \tag{18}$$

These results correlate well with experimental data (see Sec. 4). For other possible distribution functions with $k_0>0$ the preceding results will remain power-law, although with larger $M$. In 2D-superconductors, such as cuprates, the value $k_0=0$ corresponds to linear objects, i.e., lines or edges of normal regions, consisting of ''nodes'' ($\Delta_0=0$) in the real space. Point-like zeros would lead to $k_0=1$, so that the relevant power-law exponents would increase by one.

From the methodological point of view it is of interest to indicate an analogy between our approach dealing with the $\Delta$-distribution in the real space and the Abrikosov's introduction[53] of the distribution function for the order parameter $\Delta$ anisotropic in the momentum space, with the anisotropy being quite general and including both *d*-wave and extended *s*-wave symmetries.

## 4. DISCUSSION

The inhomogeneities leading to the spread of $\Delta$ magnitudes over the sample may be of different nature. As the possible driven forces of these structural and/or electronic domains in high-$T_c$ oxides one should mention (i) composition irregularities, especially the inherent disorder in oxygen vacancy positions, observed, e.g., for $BaPb_{1-x}Bi_xO_3$,[51,54] $La_{2-x}[Sr(Ba)]_xCuO_{4-y}$[54,55] and $YBa_2Cu_3O_{7-x}$[26,54,56] and (ii) the phase separation of the electronic origin with impurity atoms frozen because of the kinetic barriers.[57] In oxides both mechanisms apparently act together.[45,56,58]

Vacancy disorder comprise point-like defects. As was indicated in Sec. 3, an attempt to allow for such irregularities was made in Ref. 48 where it was shown that only for an anomalously great dispersion $W$ of the site order parameters $\Delta_i$ it is possible to obtain the gapless-like behavior of the quasiparticle density of states. Considering the condition $W\gg\Delta_i^{\max}$ for the maximal quantity $\Delta_i^{\max}$ very improbable, the cited authors, in order to explain the experimental data, argued that $YBa_2Cu_3O_{7-x}$ is a *d*-wave object.

The inhomogeneities attributed above to the second group are of typical sizes exceeding the coherence length, the latter being extremely small in cuprates. The experimental evidence exists of the minority phase domains in $La_{2-x}Sr_xCuO_4$ being as large as several hundred Angströms in size.[58] For $YBa_2Cu_3O_{7-x}$ the x-ray and neutron diffraction

measurements supplemented by the lattice gas Monte Carlo simulations revealed not only tetragonal and ortho-I phases with the long range order but also a rich variety of structural phases with anisotropic correlation lengths of mesoscopic size.[56] The domain finiteness preserved even after annealing, and kinetic barriers turned out to be large enough to secure the logarithmic time ordering. The crystal field neutron spectra of $ErBa_2Cu_3O_{7-x}$[59] and the Raman spectra of $YBa_2Cu_3O_{7-x}$[60] which reflect the local region properties also revealed oxygen structure domains, indicating the phase separation and the percolation character of conductivity and superconductivity. It was pointed out in Ref. 61 as well that the percolative network of intermediate size hole-induced polarons (clusters) may lead to the difference between local and global (crystal) symmetry.

In contrast to $YBa_2Cu_3O_{7-x}$, the electron-doped superconducting oxide. $Nd_{2-x}Ce_xO_{4-y}$ is a random alloy.[62] Such an atomic-scale disorder may prevent the formation of structural domains, thus making our hypothesis of averaging inapplicable in this case. On the other hand, the in-plane coherence length in $Nd_{2-x}Ce_xO_{4-y}$ is $\xi_{ab}\approx 70-80$ Å. which exceeds substantially $\xi_{ab}\approx 10-15$ Å in $YBa_2Cu_3O_{7-x}$.[62] Also, making allowance that superconductivity of the former substance exists in the narrow range $0.14<x<0.15$ and $y\leqslant 0.01$,[63] it is natural to conclude that the spread of $\Delta$ assumed in our model is not large enough to validate the averaging procedure. Thus, $Nd_{2-x}Ce_xO_{4-y}$ should manifest its intrinsic exponential low-$T$ asymptotics which is indeed the case.[62]

At the same time, tunnel spectra of $YBa_2Cu_3O_{7-x}$ show a large spread of $\Delta$ magnitudes[64] which is favorable for our interpretation. The growth with $x$ of structural domains with different nonoptimal (for a nominal stoichiometry) $\Delta$'s and the attended widening of the distribution function $f(\Delta)$ may explain the increase of the numerical factor in the observed linear-$T$ term of $\delta\lambda_L(T)$ for $YBa_2Cu_3O_{7-x}$.[65] Another important source of the $\Delta$ scatter is the CDW emergence in superconducting oxides.[2,15,16,26,51] All factors listed above, taken together or separately, may be responsible for the transition from the exponential to the power-law behavior of the quantities under consideration.

To summarize the comparison with experiment, we may state that our theory accurately describes the respective power-law exponents. At the same time, at the quantitative level it is at least not worse than the $d$-wave picture of the low-$T$ asymptotics. To show this, let us compare our results for $\langle\delta\lambda_L\rangle$ with those of the $d$-wave approach. The choice of this quantity was made because it serves as a sensitive probe to test different pairing mechanisms. According to Ref. 4, $\delta\lambda_L\approx(T\ln 2)/\Delta_0$, which is consistent with the experiments for $YBa_2Cu_3O_{7-x}$,[29] and corresponds to the value $B_0\approx 1.96$ in Eq. (16). This value of $B_0$ is reproduced for $f_E(\Delta_0)$ and $\alpha\approx 0.69$, whereas $B_0\approx 0.29$ for $f_G(\Delta)$ if $\sigma=1$, and $B_0\equiv 1$ for $f_U(\Delta)$. These values of $\alpha$ and $\sigma$ seem quite realistic. The observations of different exponents for $\delta\lambda_L(T)$ in various samples[1,29–33] may reflect their dissimilar nonhomogeneous structures, leading to a change-over from one $f_0(\Delta_0)$ to another with different $k_0$'s.

Note that there is also another approach,[3] valid both for $s$- and $d$-order parameter symmetry, which is based on the proximity effect in the $S-N$ layer structures of cuprates and fits the experimental data on $\lambda_L(T)$. A possibility of the transformation of the dependence (1) into the power-law one with $M\leqslant 1$ due to the proximity effect was demonstrated in Ref. 66 for Nb/Al bilayer films.

Of course, the theory outlined above can be applied not only to cuprate oxides but to other materials as well. But the main requirement for them to exhibit power-law asymptotics remains the same, namely, the mesoscopic nonhomogeneity characteristic size ought to exceed the coherence length. Otherwise, the exponential behavior for $T\ll T_c$ would survive and the critical temperatures would be slightly renormalized in full accordance with the Anderson theorem.[23]

We are grateful to all colleagues who sent us the reprints of their works and especially to Niels Andersen and James Annett for useful discussions. This work was supported, in part, by the Ukrainian State Foundation for Fundamental Researches (Grant No. 2.4/100).

*)E-mail: collphen@marion.iop.kiev.ua

[1] J. F. Annett, N. D. Goldenfeld, and A. J. Leggett, in *Physical Properties of High Temperature Superconductors*, D. M. Ginsberg (Ed.), Vol. 5, World Scientific, Singapore (1996), p. 375.
[2] R. A. Klemm, in *Ten Years after Discovery*, *Proc. International Workshop on High Temperature Superconductivity*, Jaipur, India, S. M. Bose and K. B. Garg (Eds.), Narosa, New Delhi, India (1998), p. 179.
[3] R. A. Klemm and S. H. Liu, Phys. Rev. Lett. **74**, 2343 (1995).
[4] D. J. Scalapino, Phys. Rep. **250**, 329 (1995).
[5] G. G. Sergeeva, Yu. P. Stepanovskii, and A. V. Chechkin, Fiz. Nizk. Temp. **24**, 1029 (1998) [Low Temp. Phys. **24**, 771 (1998)].
[6] C. C. Tsuei, J. R. Kirtley, Z. F. Ren, J. H. Wang, H. Raffy, and Z. Z. Li, Nature (London) **387**, 481 (1997).
[7] K. A. Kouznetsov, A. G. Sun, B. Chen, A. S. Katz, S. R. Bahcall, J. Clarke, R. C. Dynes, D. A. Gajewski, S. H. Han, M. B. Maple, J. Giapintzakis, J.-T. Kim, and D. M. Ginsberg, Phys. Rev. Lett. **79**, 3050 (1997).
[8] H. Hilgenkamp, J. Mannhart, and B. Mayer, Phys. Rev. B **53**, 14586 (1996).
[9] R. A. Klemm, C. T. Rieck, and K. Scharnberg, in *Superconducting Superlattices II: Native and Artificial*, *Proc. of SPIE*, July 1998. I. Bozović and D. Pavuna (Eds.) (1998), Vol. 3480, p. 209; cond-mat/9811303 (Phys: Rev. B, to be published).
[10] M. Möble and R. Kleiner, in *Abstracts of the First Euro-conference on Anomalous Complex Superconductors*, Aghia Pelagia, 1998, G. Varelogiannis (Ed.) University of Crete, Heraklion (1998); Phys. Rev. B **59**, 4486 (1999).
[11] Z.-X. Shen and D. S. Dessau, Phys. Rep. **253**, 1 (1995).
[12] J. Lesueur, B. Leridon, M. Aprili, and X. Grison, *The Gap Symmetry and Fluctuations in High Temperature Superconductors*, J. Bok and G. Deutscher (Eds.), Plenum, New York (1998).
[13] I. K. Yanson, Fiz. Nizk. Temp. **17**, 275 (1991) [Sov. J. Low Temp. Phys. **17**, 143 (1991)].
[14] A. M. Gabovich, Fiz. Nizk. Temp **18**, 693, (1992) [Sov. J. Low Temp. Phys. **18**, 490 (1992)].
[15] A. M. Gabovich and A. I. Voitenko, Phys. Rev. B **55**, 1081 (1997).
[16] A. M. Gabovich and A. I. Voitenko, in *Symmetry and Pairing in Superconductors*, *Proc. NATO Advanced Research Workshop*, Yalta, Ukraine, M. Ausloos and S. P. Kruchinin (Eds.), Kluwer, Dordrecht. The Netherlands (1998), p. 187.
[17] A. K. Gupta and K.-W. Ng, Phys. Rev. B **58**, 8901 (1998).
[18] Ya. G. Ponomarev, M. E. Shabalin, A. I. Kuzmich, K. K. Uk, M. V. Sudakova, S. N. Chesnokov, B. A. Aminov, M. Lorenz, G. Müller, H. Piel, and M. Hein, in *Abstracts of the XXXI Workshop on Low Temperature Physics*, 2–3 December, 1998, Moscow (1998), p. 228.

[19] A. Barone and G. Paterno, *Physics and Applications of the Josephson Effect*, John Wiley and Sons, New York (1982).
[20] Yu. S. Barash and A. A. Svidzinskii, Zh. Éksp. Teor. Fiz. **111**, 1120 (1997) [JETP **84**, 619 (1997)].
[21] V. V. Kabanov, J. Demsar, B. Podobnlk, and D. Mihailovic, Phys. Rev. B **59**, 1497 (1999).
[22] Ya. G. Ponomarev, B. A. Aminov, N. B. Brandt, M. Hein, C. S. Khi, V. Z. Kresin, G. Müller, H. Piel, K. Rozner, S. V. Tchesnokov, E. B. Tsokur, D. Wehler, R. Winzer, Th. Wolfe, A. V. Yarygin, and K. T. Yusupov, Phys. Rev. B **52**, 1352 (1995).
[23] A. A. Abrikosov, *Fundamentals of the Theory of Metals*, North Holland, Amsterdam (1987).
[24] E. Kaldis, in *Ten Years after the Discovery, Proc. Workshop on High-$T_c$ Superconductivity*, 1996, E. Kaldis, E. Liarokapis, and K. A. Müller (eds.), Kluwer, Dordrecht, The Netherlands (1997), p. 411.
[25] J. D. Jorgensen, Phys. Today **44**, 34 (June 1991).
[26] T. Egami and S. J. L. Billinge, Prog. Mater. Sci. **38**, 359 (1994); in *Physical Properties of High Temperature Superconductors*, D. M. Ginsberg (Ed.), Vol. 5, World Scientific, Singapore (1996), p. 265.
[27] K. A. Moler, D. L. Sisson, J. S. Urbach, M. R. Beasley, A. Kapitulnik, D. J. Baar, R. Liang, and W. N. Hardy, Phys. Rev. B **55**, 3954 (1997).
[28] H. Monien, K. Scharnberg, L. Tewordt, and D. Walker, Solid State Commun. **61**, 581 (1987).
[29] W. N. Hardy, D. A. Bonn, D. C. Morgan, R. Liang, and K. Zhang, Phys. Rev. Lett. **70**, 3999 (1993).
[30] Z. Ma, R. C. Taber, L. W. Lombardo, A. Kapitulnik, M. R. Beasley, P. Merchant, C. B. Eom, S. Y. Hou, and J. M. Phillips, Phys. Rev. Lett. **71**, 781 (1993).
[31] J. Y. Lee, K. M. Paget, T. R. Lemberger, S. R. Foltyn, and X. Wu, Phys. Rev. B **50**, 3337 (1994).
[32] D. A. Bonn, S. Kamal, K. Zhang, R. Liang, D. J. Baar, E. Klein, and W. N. Hardy, Phys. Rev. B **50**, 4051 (1994).
[33] H. Walter, W. Prusseit, R. Semerad, H. Kinder, W. Assmann, H. Huber, H. Burkhardt, D. Rainer, and J. A. Sauls, Phys. Rev. Lett. **80**, 3598 (1998).
[34] N. Klein, N. Tellmann, H. Schulz, K. Urban, S. A. Wolf, and V. Z. Kresin, Phys. Rev. Lett. **71**, 3355 (1993).
[35] N. Schopohl and O. V. Dolgov, Phys. Rev. Lett. **80**, 4761 (1998).
[36] P. J. Hirschfeld, M.-R. Li, and P. Wölfle, Phys. Rev. Lett. **81**, 4024 (1998).
[37] G. E. Volovik, Phys. Rev. Lett. **81**, 4023 (1998).
[38] N. Schopohl and O. V. Dolgov, Phys. Rev. Lett. **81**, 4025 (1998).
[39] M. J. Graf, S.-K. Yip, J. A. Sauls, and D. Rainer, Phys. Rev. B **53**, 15147 (1996).
[40] M. Houssa and M. Ausloos, Phys. Rev. B **56**, 953 (1997).
[41] L. Taillefer, B. Lussier, R. Gagnon, K. Behnia, and H. Aubin, Phys. Rev. Lett. **79**, 483 (1997).
[42] R. Movshovich, M. A. Hubbard, M. B. Salamon, A. V. Balatsky, R. Yoshizaki, J. L. Sarrao, and M. Jaime, Phys. Rev. Lett. **80**, 1968 (1998).
[43] S. Bhattacharya, M. J. Higgins, D. C. Johnston, A. J. Jacobson, J. P. Stokes, J. T. Lewandowski, and D. P. Goshorn, Phys. Rev. B **37**, 5901 (1988).
[44] M.-F. Xu, H.-P. Baum, A. Schenstrom, B. K. Sarma, M. Levy, K. J. Sun, L. E. Toth, S. A. Wolf, and D. U. Gubser, Phys. Rev. B **37**, 3675 (1988).
[45] R. S. Markiewicz, J. Phys. Chem. Solids **58**, 1179 (1997).
[46] R. Oppermann, Z. Phys. B **70**, 49 (1988).
[47] K. Ziegler, Commun. Math. Phys. **120**, 117 (1988).
[48] J. F. Annett and N. Goldénfeld, J. Low Temp. Phys. **89**, 197 (1992).
[49] *Handbook of Mathematical Functions with Formulas, Graphs, and Mathematical Tables*, M. Abramowitz and I. A. Stegun (Eds.), National Bureau of Standards, New York (1964).
[50] W. Feller, *An Introduction to Probability Theory and Its Applications, Vol. 1*, John Wiley and Sons, New York (1952).
[51] A. M. Gabovich and D. P. Moiseev, Usp. Fiz. Nauk **150**, 599 (1986) [Sov. Phys. Usp. **29**, 1135 (1986)].
[52] D. A. Dikin, V. M. Dmitriev, A. P. Isakina, A. I. Prokhvatilov, O. D. Prikhod'ko, E. V. Khristenko, and L. D. Yantsevich, Fiz. Nizk. Temp. **14** 635 (1990) [Sov. J. Low Temp. Phys. **16**, 372 (1990)].
[53] A. A. Abrikosov, Physica C **214**, 107 (1993).
[54] A. W. Sleight, Phys. Today **44**, 24 (June 1991).
[55] V. K. Yanovskii, V. I. Voronkova, and I. V. Vodolazskaya, in *Physical Properties of High-$T_c$ Superconductors, Vol. 2*, Basis, Moscow (1991), p. 3.
[56] N. H. Andersen, M. von Zimmermann, T. Frello, M. Käll, D. Monster, P.-A. Lindgård, J. Madsen, T. Niemöller, H. F. Poulsen, O. Schmidt, J. R. Schneider, Th. Wolf, P. Dosanjh, R. Liang, and W. N. Hardy, Physica C (to be published).
[57] E. L. Nagaev, Usp. Fiz. Nauk **165**, 529 (1995) [Phys. Usp. **48**, 497 (1995)].
[58] M. K. Crawford, R. L. Harlow, E. M. McCarron, S. W. Tozer, Q. Huang, D. E. Cox, and Q. Zhu, *Ten Years after the Discovery*, E. Kaldis, E. Liarokapis, and K. A. Müller, (Eds.), Kluwer, Dordrecht (1997), p. 281.
[59] J. Mesot and A. Furrer, J. Supercond. **10**, 623 (1997); *Neutron Scattering in Layered Copper-Oxide Superconductors*, A. Furrer (Ed.), Kluwer, Dordrecht (1998), p. 335.
[60] M. N. Iliev, *Application of Spectroscopy to Superconducting Materials*, ACS, Washington (1999).
[61] A. Bill, V. Hizhnyakov, D. Nevedrov, G. Seibold, and E. Sigmund, Z. Phys. B **104**, 753 (1997).
[62] S. M. Anlage, D.-H. Wu, J. Mao, S. N. Mao, X. X. Xi, T. Venkatesan, J. L. Peng, and R. L. Greene, Phys. Rev. B **50**, 523 (1994).
[63] A. Yu. Ignatov, A. A. Ivanov, A. P. Menushenkov, S. Iacobucci, and P. Lagarde, Phys. Rev. B **57**, 8671 (1998).
[64] L. Ozyuzer, J. F. Zasadzinski, C. Kendziora, and K. E. Gray, Phys. Rev. B (to be published).
[65] C. Panagopoulos, J. R. Cooper, and T. Xlang T, Phys. Rev. B **57**, 13422 (1998).
[66] M. S. Pambianchi, S. N. Mao, and S. M. Anlage, Phys. Rev. B **52**, 4477 (1995).

This article was published in English in the original Russian journal. It was edited by R. T. Beyer.

# The influence of oxygen content on the $T_c$ of HTS Hg-1245

E. S. Itskevich*)

*Institute for High Pressure Physics, Russian Academy of Sciences, 142092 Troitsk, Moscow Region, Russia*
(Submitted December 21, 1998; revised February 19, 1999)
Fiz. Nizk. Temp. **25**, 685–689 (July 1999)

We have observed an extraordinary behavior of the $HgBa_2Ca_4Cu_5O_{12+\delta}$ layered HTS (phase 1245) in the overdoped state. Earlier we have synthesized the phase Hg-1245 with different oxygen content and consequently different values of the lattice parameter $a$. We have observed a coincidence of $a$ values when the $T_c(a)$ cupolas reach their maxima for phases Hg-1223, 1234, and 1245, and a merging of their overdoped parts together with abrupt falling off of the $T_c$ values. The Hg-1245 phase has shown the most unusual behavior. Contrary to other phases, this one contains three types of $CuO_2$ layers in a unit cell. We supposed that, in the case of the Hg-1245 phase, the holes coming from the reservoir, which is the Hg–O plane, cannot reach the ''far'' $CuO_2$ layer which is notable for this phase. We have calculated the hole concentration for each layer for 1223, 1234, and 1245 phases. The results obtained confirm our assumption. The hole concentration appears negligibly small for the overdoped 1245 phase. We can consider the ''fifth'' $CuO_2$ layer as not taking part in superconductivity. The analysis of the behavior of the $T_c(a)$ cupolas for the phases with different number of $CuO_2$ layers and of hole density distribution between the layers has been carried out. © *1999 American Institute of Physics.* [S1063-777X(99)00607-6]

## INTRODUCTION

The first goal in the study of the HTSC layered cuprates is to find out the optimum structure and content to reach the maximum possible critical temperature $T_c$. Up to now the maximum value of the $T_c = 135$ K was reached for Hg-based cuprates in their Hg-1223 phase. Numerous attempts at synthesis of layered cuprates with different elements added instead of mercury in recent years have failed to enlarge the $T_c^{\max}$.

We have synthesized the Hg-based cuprates with $n = 3$, 4, and 5[1,2] and measured the $T_c^{\max}$ and the $dT_c^{\max}/dp$ for phases with $n = 1-5$.[3] The largest $T_c^{\max}$ remained to be the value at $n = 3$.

To understand the nature of the HTSC the study of samples whose parameters lay far away from the optimal ones is necessary. Here we present and discuss the data on $T_c$ for phases Hg-1223, Hg-1234 and Hg-1245 with different oxygen content.

When studying the overdoped and underdoped cuprates the agreement was attained that different approaches should be used to describe their properties. The first—the overdoped state—may be considered as a Fermi liquid which is not true for the underdoped state. The problem of overdoped and underdoped states was considered by Laughlin[4] in a most impressive way. He proposed the existence of a quantum critical point on the way from an antiferromagnetic insulator (underdoped) to a normal metal (overdoped).

## EXPERIMENT

The phases Hg-1223, 1234, and 1245 were synthesized under high pressure at different pressures, temperatures and time intervals. The oxygen content in the starting mixtures was varied by changing the $BaO/BaO_2$ ratio, which allowed us to obtain the overdoped Hg-1223, 1234, and 1245 phases in as-preparated states. The technology of synthesis was described in detail in Refs. 1 and 2. Special attention was paid to getting single phase ceramic specimens. When the phases with $n \geqslant 3$ are synthesized, the kinetics of the process is important. First the previous phases are formed where then the fragments of $CaCuO_2$ take root. The phase composition was checked by the x-ray study.

The temperature dependence when an abrupt change of ac and dc susceptibility takes place was measured by the induction method. The temperature was measured by the (Cu+0.15%Fe)/Cu thermocouple. Measurements were carried out in the Institute for High Pressure Physics (IHPP) and at the Chemical Faculty of the Moscow University by different people and on different installations. The results obtained are qualitatively the same, having sometimes some unimportant quantitative difference. As was mentioned above, in all cases the maximum values of the $T_c$ were achieved for the phase Hg-1223.

Here we lay stress on the behavior of different phases in the overdoped states. The measured $T_c$ values as a function of lattice parameter $a$ (the spacing Cu–O in the layer) are shown in Fig. 1.

The underdoped states correspond to greater values of the parameter $a$. These states appear under heat processing of the as-preparated samples.[2] The change of $a$ is caused by oxidation of copper because of nonstoichiometric oxygen in the Hg–O layer (the reservoir), that is, because of the hole density $\delta$ in the sample. The $T_c$'s for phases Hg-1234 and Hg-1245 have a tendency in the overdoped state to merge with the overdoped phase Hg-1223 and to fall off abruptly.[2]

 

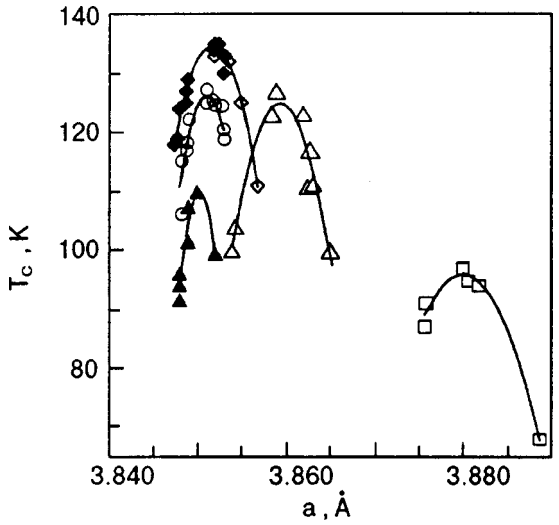


FIG. 1. The dependence of $T_c$ vs. parameter $a$ for Hg-based superconductors: Hg-1201 (□), Hg-1212 (△), Hg-1223 (♦), Hg-1223 (◇),[1] Hg-1234 (○), Hg-1245 (▲).

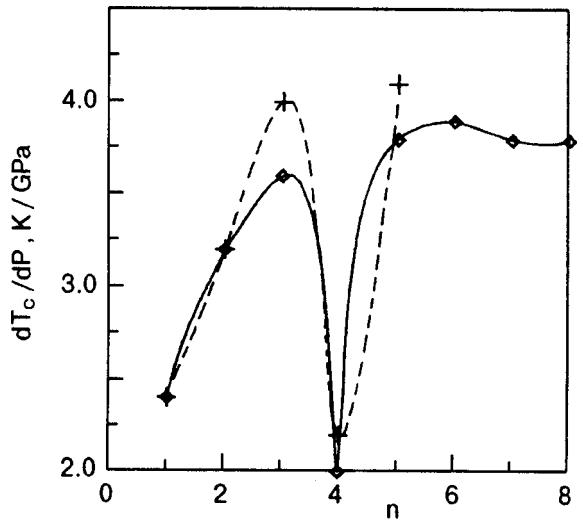


FIG. 3. Experimental (+) and calculated (◇) data for pressure derivative $dT_c^{\max}/dp$ as function of sublayers number $n$.[3]

## DISCUSSION

Earlier we have compared results for $T_c^{\max}$ for phases with $n=1-6$ and for $dT_c^{\max}/dp$ $(n=1-5)$[3] with data obtained from the model proposed by Anderson (the so-called RWB model[5]), see Figs. 2 and 3. In the RWB model the $T_c^{\max}$ is determined mainly by the coupling between $CuO_2$ layers and it is assumed that the holes, which are responsible for high $T_c$ values, are homogeneously distributed between all $CuO_2$ layers.

DiStasio, Müller, and Pietroneru in Ref. 6 have considered the charge distribution of holes among the various $CuO_2$ layers up to $n=4$ and found that this distribution is highly nonhomogenous for $n\geqslant 3$. ''A natural consequence of this distribution is that the density of states available for superconductivity can have a maximum as a function of $n$, as observed experimentally for $T_c$ ''.[6] Beginning with $n=3$ the nonequivalent $CuO_2$ layers exist—the outer ''$o$'' and inner ''$i$'' (see Fig. 4). The hole distribution inside the sheet is proposed to be homogeneous. In Ref. 6 the band (a parabolic band was assumed) and electrostatic energies were calculated. The total energy is minimized with respect to $x$—the fraction of charge in the $i$-layer ($1-x$ in the $o$-layer). If $\delta$ is the total density of holes coming from the reservoir then the concentration of charge carriers $n_h$ in the $i$-layer is equal to $x\delta/(n-2)$ and $(1-x)\delta/2$ in the $o$-layer. In the simplest empirical case

$$T_c(n_h)=T_c^{\max}[1-\beta(n_h-n_h^{\max})],$$

where $T_c^{\max}$ and $\beta$ do not depend on $n_h$ but on the structure parameters only.[7] This expression leads to the well known cupola-like dependence $T_c(n_h)$ that was observed in the experiment up to $n=5$.[2] The electrostatic interaction with the

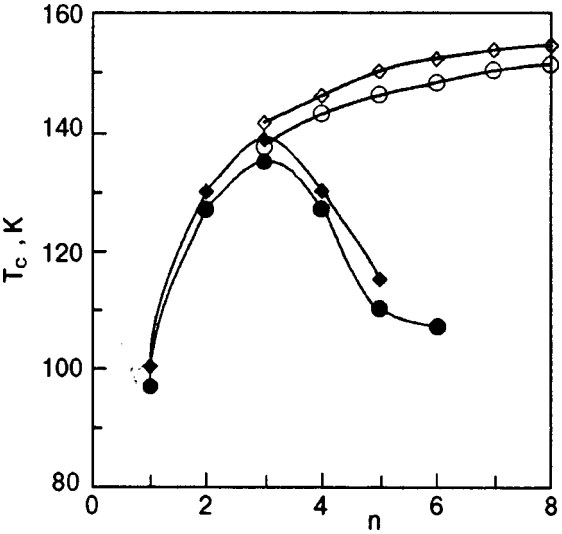


FIG. 2. Experimental and calculated values of $T_c^{\max}$ as a function of $CuO_2$ sublayers number $n$. Full circles and full rhombs—experiment at ambient pressure (■) and under pressure 1 GPa (♦), open circles and rhombs—the calculated data for ambient (○) and 1 GPa (◇) pressure, respectively.[3]

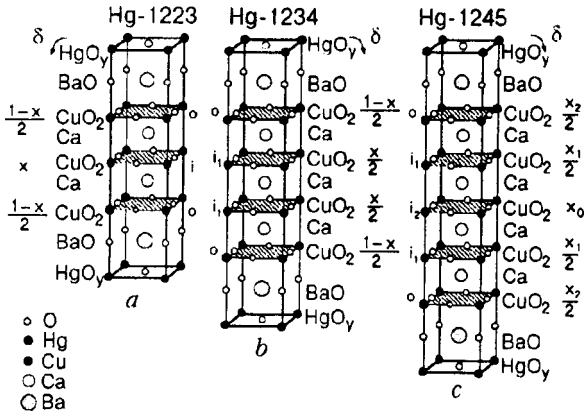


FIG. 4. Idealized structures of $HgBa_2Ca_2Cu_3O_{8+y}$ (Hg-1223) (a), $HgBa_2Ca_3Cu_4O_{10+y}$ (Hg-1234) (b), $HgBa_2Ca_4Cu_5O_{12+y}$ (Hg-1245) (c) with, respectively, three ($n=3$), four ($n=4$) and five ($n=5$) $CuO_2$ layers per unit cell. The structure with $n=5$ has inequivalent inner ($i_1$ and $i_2$) and outer ($o$) $CuO_2$ layers. The copper atoms of the inner $CuO_2$ layers have a fourfold oxygen coordination, the copper atoms of the outer $CuO_2$ layers have a fivefold oxygen coordination ○(1)—in the layer $i$, ○(2)—in the layer $o$. ○(3)—in the layer BaO; (4)—in the layer $HgO_y$.

layer—reservoir of holes is considered in Ref. 6 for the structure where all layers are equally spaced. Jover *et al.*[7] have considered the Hg-bearing cuprates up to $n=4$ on the basis of the model[6] (see Figs. 4a and 4b).

Let us consider the results shown in Fig. 1. The cupola-shaped dependence of the $T_c(a)$ for phases with $n=1-5$ is clearly seen. It can be assumed that these five first Hg-based cuprates have the same cupola-like shape of the $T_c(a)$ dependence due to the nonstoichiometric oxygen, like there is a reason for their structure identity. The implanting of an additional ($CaCuO_2$)-layer in the unit cell leads to contraction of layer parameters and to a stronger interaction in the $CuO_2$ plane. For phases with low number of layers in the unit cell the change of $T_c$ takes place in a rather extended range of $a$-values converging at larger $n$.

The last three phases show nearly the same $a$-values in their overdoped states in contrast with the two first of them (Fig. 1). The value of $T_c$ for phases Hg-1223, Hg-1234, and Hg-1245 appears to be very different at the same $a$. The $T_c(a)$ cupolas go down when $n$ changes from 3 to 5. Moreover, the left part of these $T_c(a)$ curves corresponding to overdoped states merge to a common curve where the $T_c$'s go down from a maximum value 135 K for $n=3$ to almost 90 K. The cupolas narrow down with $n$ increasing mostly because of their right sides.

Accumulating the experimental results we note the following peculiarities:

1) Critical temperature goes down both in underdoped and overdoped states showing a cupola-shaped $T_c(a)$ dependence;

2) The overdoped parts of the $T_c(a)$ curves merge to a common curve at $n=3$, 4, and 5;

3) The values of $T_c^{\max}$ most likely continue to fall off at $n>5$;

4) The pressure derivative $(dT_c^{\max}/dp)(n)$ shows a nonmonotonic behavior that can be described inside the RWB model.

All these peculiarities should be connected with some features of the crystal structure of the layered cuprates under consideration. The principal one of these is the fact that the holes cannot reach the sole inner $CuO_2$ layer in case of the 5th phase ($n=5$) and hence in case of phases with $n>5$.

We have carried out a calculation of the hole density in different layers similar to that of Ref. 6, generalizing the latter to the existence of third kind of $CuO_2$ layer in the unit cell of the system $HgBa_2Ca_4Cu_5O_{12}$ and taking into account hole reservoir distance. The main goal of the calculation was to find out the hole densities for the 5th phase. This phase should have two kinds of inner layers (see Fig. 4c) and the model[6] should be appropriate. We think as well that the ion model[8] describes correctly the phase Hg-1223 having a maximum $T_c$ within the entire Hg-cuprates series.[6] Both models Ref. 6 and Ref. 8 give the same expressions for the band energy as a function of $x$ for the phases Hg-1223 and Hg-1234 and different ones for the Madelung energy. The latter is of no importance for our problem.

Our calculation is based on the model.[6] For the band energy we get

for $n=3$

$$U_B=1/2A\delta^2(3x^2-2x+1)S \tag{1}$$

and for $n=4$

$$U_B=A\delta^2(x^2-x+1/2)S, \tag{2}$$

where $A=\pi h^2/2m^*a^2$; $S$ is the layer area.

The Madelung energy is the same for $n=3$ and 4:

$$U_M=B\delta^2(x^2+l/d)S. \tag{3}$$

Here $B=\pi e^2/\epsilon d$; $d$ is the distance between $CuO_2$ layers; $l$—the distance between the layer Hg–O(4) and the nearest $CuO_2$ plane; $\varepsilon$ is the dielectric constant. Minimizing the total energy with respect to $x$ we get

for $n=3$

$$x=A/(3A+2B) \tag{4}$$

and the concentration of the charge carriers (the holes $n_h$) in the layer

$$n_h^i=\delta x \quad \text{and} \quad n_h^o=\delta(1-x)/2.$$

For $n=4$

$$x=A/2(A+B) \tag{5}$$

and $n_h^i=\delta x/2$ (see Fig. 4).

In case of $n=5$ one more inner layer exists—the $i_2$ layer and two variational parameters should be put into consideration—$x_0$ and $x_1$ representing two kinds of inner layers.

That is: $n_h^i(5)=\delta x_0$—(layer $i_2$) and $n_h^i(3,4)=\delta x_1/2$ (two identical layers $i_1$).

In the outer layers

$$n_h^o=\delta/2(1-x_0-x_1)=\delta x_2/2,$$

where $x_2=(1-x_0-x_1)$ (see Fig. 4c).

Then for the band and Madelung energy we get

$$U_B=A\delta^2(1/2-x_0-x_1+3/2x_0^2+x_1^2+x_0x_1)S, \tag{6}$$

$$U_M=B\delta^2(2x_0^2+2x_0x_1+x_1^2+l/d)S. \tag{7}$$

Minimization of total energy gives

$$x_0=A^2/(5A^2+10AB+4B^2), \tag{8}$$

$$x_1=(2A^2+6AB+4B^2)A/(A+2B)(5A^2+10AB+4B^2)$$

$$=\frac{2x_0(A+3B+2B^2/A)}{(A+2B)}>2x_0. \tag{9}$$

Thus

$$x_2/2>x_1/2>x_0.$$

Our assumption that holes do not reach the inner layer $i_2$ gets a quantitative confirmation.

Considering the experimental and calculated results we conclude that the phase Hg-1223 is optimal for the high $T_c$. For this phase only the hole distribution between the $CuO_2$ layers is nearly uniform.[8]

Apparently this uniformity leads to the highest $T_c=135$ K within all layered HTSC. The inner layers of phases with $n=4$ and 5 contain much less carriers than the outer ones. For the phase with $n=5$ we find out that the inner $i_2$

layer contains a few of the carriers and all of them are concentrated in the outer layers. The distance between the outer layers increases with $n$ and that decreases the interaction between layers. Thus, the $T_c$'s fall off due to both the hole density decrease and the interaction weakening. There are experimental data on the $T_c^{\max}$ measured up to $n=8$.[9] In spite of a rather large spread the decrease in $T_c$ with $n$ is evident.

The real absence of holes in the inner layer of the phase Hg-1245 causes the disagreement between experimental values of $T_c^{\max}$ got for large $n$ and calculated ones in the frames of RWB model (see Fig. 2). The latter proposes a uniform carrier distribution on the $CuO_2$ layers.

A sharp increase of $dT_c^{\max}/dp$ for the 5th phase in comparison with the 4th one (Fig. 3) was explained in Ref. 3 within the frame of the RWB model.

Let some hole density $n_h^{\max}$ correspond to the $T_c^{\max}$. The hole densities less than $n_h^{\max}$ increase linearly with increase of $\delta$ in all layers.[6,8] The $T_c(a)$ shows a cupola-shaped dependence and $a$ is connected with $\delta$.[1] To each value of hole density for all the three kinds of layers of the phase Hg-1245 corresponds its own contribution of the ''layer—$T_c$'' to the $T_c^{\max}$.[7] The $T_c$ of the layer decrease with the hole density in the layer. The relative contribution of these $T_c$ to the $T_c^{\max}$ may be distinctly changed under pressure that leads to the nonmonotonic $n$ dependence of the $(dT_c^{\max}/dp)(n)$ observed.

The author is grateful to K. A. Lokshin, L. F. Kulikova, I. G. Morosov, and I. G. Kuzemskaya who participated in getting the results presented in Fig. 1, to E. V. Antipov for fruitful discussion, and to E. L. Nagaev for his help in calculation of hole densities for the phases Hg-1223, Hg-1234, and Hg-1245.

This research was supported by the State HTSC Program and by RFBR, Grant 96045 and Grant 96-02-16305.

*)E-mail: itskev@ns.hppi.troitsk.ru

[1] K. A. Lokshin, I. G. Kuzemskaya, L. F. Kulikova, E. V. Antipov, and E. S. Itskevich, Physica C **279**, 11 (1997).
[2] K. A. Lokshin, D. A. Pavlov, M. L. Kovba, E. V. Antipov, L. F. Kulikova, I. G. Kuzemskaya, I. V. Morosov, and E. S. Itskevich, Physica C **300**, 71 (1998).
[3] E. S. Itskevich and E. V. Zhasinas, Physica C **295**, 193 (1998).
[4] R. B. Laughlin, in ''Stripes-98,'' Univ. ''La Sapienza,'' Rome, Italy, Book of Abstracts, FR I-4 (1998).
[5] J. M. Wheatley, T. S. Hsu, and P. W. Anderson, Nature (London) **333**, 121 (1988).
[6] M. DiStasio, K. A. Müller, and L. Pietroneru, Phys. Rev. Lett. **64**, 2827 (1990).
[7] D. T. Jover, R. J. Wijngaarden, H. Wilbelmi, R. Griessen, S. M. Loureiro, J.-J. Capponi, A. Schilling, and H. R. Ott, Phys. Rev. B **54**, 4265 (1996).
[8] E. Helne, and J. Tallon, Phys. Rev. B **45**, 3172 (1992).
[9] B. A. Scott, E. Y. Suard, C. C. Tsuei, D. B. Mitzi, T. R. McGuire, B.-H. Chen, and D. Walker, Physica C **230**, 239 (1994).

This article was published in English in the original Russian journal. It was edited by R. T. Beyer.

## LOW-TEMPERATURE MAGNETISM

# Spectra of coupled magnetoelastic waves of a biaxial strongly anisotropic ferromagnet with biquadratic interaction

Yu. N. Mitsaĭ, Yu. A. Fridman, O. V. Kozhemyako, and O. A. Kosmachev

*Simferopol State University, 333036 Simferopol, Ukraine*
(Submitted October 13, 1998; revised February 23, 1999)
Fiz. Nizk. Temp. **25**, 690–698 (July 1999)

The spectra of coupled magnetoelastic waves in a biaxial ferromagnet with biquadratic interaction are investigated. The phase diagrams of the system under investigation are constructed as functions of biquadratic exchange. It is shown that for a strong Heisenberg exchange (exceeding the biquadratic interaction), phase transitions in the system occur only through a decrease in the magnitude of the magnetization vector. For a strong biquadratic exchange (exceeding the Heisenberg interaction), orientational phase transitions are possible, which are reduced to a reorientation of the principal axis of the tensor of quadrupole magnetic moments.
 [S1063-777X(99)00707-0]

**1.** Spectral and thermodynamic properties of magnets with a more complex interaction between magnetic ions than the Heisenberg exchange have recently become an object of intense investigation.[1–6] This interest is dictated primarily by the synthesis and experimental investigations of magnets in which the magnetic ordering temperatures are quite low. The Heisenberg interaction in such systems with the spin $S \geqslant 1$ of a magnetic ion can be comparable with or even weaker than the interaction described by higher-order invariants. Magnets possessing such properties include, for example, rare-earth intermetallides TmGd,[7,8] TmZn,[9] and some other compounds.

The role of carriers of magnetism in non-Heisenberg magnets is often played by rare-earth ions ($Tm^{3+}$ and $Ge^{2+}$).[1] The existence of a nonfrozen orbital angular momentum and spin-orbit coupling in such systems leads to large values of the one-ion anisotropy (OA) constant, which can compete with the exchange interaction constant. This special role of OA leads to the emergence of peculiar (purely quantum-mechanical) properties of magnets, such as the emergence of phases with a tensor order parameter,[1] viz., quadrupole (Q) phases. These effects are studied in detail for Heisenberg magnets with OA possessing different symmetries (see, for example, the review by Loktev and Ostrovskii[6]). In such systems, phase transitions occur with a simultaneous change in the modulus of magnetization vector and its rotation. The inclusion of the magnetoelastic (ME) interaction is known to result in a radical change in the spectral properties in the vicinity of orientational phase transitions. To be more precise, the phonon excitation branch becomes a soft mode, and the magnon spectrum acquires a ME gap.[10]

A similar situation also takes place for more complex moduli, e.g., biaxial ferromagnets with biquadratic exchange interaction.[11] However, Q phases can be realized in such models in zero magnetic field also,[5] i.e., phase transitions in material constants (OA constants as well as the constants of Heisenberg and biquadratic exchange) are possible in such systems. Although the OA and ME interaction have the same origin, the influence of ME interaction of the spectral properties of non-Heisenberg magnets is studied insufficiently.

In this communication, we consider the realization of coupled ME waves in a biaxial ferromagnet with biquadratic exchange. The spectra of the system are studied in zero magnetic field, i.e., the spectral properties of the magnet are analyzed in the vicinity of phase transitions (PT) in material constants.

**2.** The system under investigation has the form of a ferromagnetic crystal with biaxial OA and biquadratic exchange. The Hamiltonian of such a crystal can be written in the form

$$
\begin{aligned}
H = & -\frac{1}{2}\sum_{n,n'}\{I(n-n')\mathbf{S}_n\mathbf{S}_{n'}+K(n-n')(\mathbf{S}_n\mathbf{S}_{n'})^2\} \\
& -B_2^0\sum_n\{3(S_n^z)^2-S(S+1)\}-B_2^2\sum_n\frac{1}{2}\{(S_n^+)^2 \\
& +(S_n^-)^2\}+\nu\sum_n S_n^i S_n^j u_{ij}(n)+\int dr\Big\{\frac{\lambda+\eta}{2}(u_{xx}^2 \\
& +u_{yy}^2+u_{zz}^2)+\eta(u_{xy}^2+u_{xz}^2+u_{yz}^2)+\lambda \\
& \times(u_{xx}u_{xy}+u_{yy}u_{zz}+u_{xx}u_{zz})\Big\}, \qquad (1)
\end{aligned}
$$

where $S_n^\alpha$ are spin operators at the site $n(\alpha=+,-,z)$, $I(n-n')>0$ is the Heisenberg exchange constant, $K(n-n')>0$ the biquadratic exchange constant, $B_2^0$ and $B_2^2$ are the OA constants, $\nu$ is the ME coupling constant, $u_{ij}(n)$ are the strain tensor components, and $\lambda$ and $\eta$ elastic moduli.

It is proved in Refs. 12 and 13 that in the general case, Hamiltonian (1) must be written in the rotational-invariant

 

form. Among other things, the inclusion of rotational invariance leads to a new mechanism of ME coupling, which is directly associated with OA. For bulk samples, this is manifested only in the renormalization of coefficients in the frequency spectrum of ME waves and some material constants.[14] Even the presence of a strong OA leads to the same effects.[15] The inclusion of rotational invariance becomes significant, for example, for thin magnetic films or wires, or when we take into account mechanical boundary conditions.[16,17] For this reason, bulk samples are investigated here without taking into account rotational invariance.

In order to simplify calculations, we shall consider a system with spin $S=1$. However, the computational algorithm proposed by us is also valid for $S>1$.

Without any loss of generality, we can assume that $B_2^2>0$ since for $B_2^2<0$, after a rotation of the reference frame about the $z$-axis through an angle $\pi/2$ we would obtain Hamiltonian (1) in which the following substitution is made: $B_2^2\rightarrow|B_2^2|$.

The OA and ME interactions can be taken into account exactly by using the Hubbard operators technique. These operators are constructed on the basis of one-ion states defined by the one-ion Hamiltonian including the self-consistent field effects. In the general case, apart from the molecular field associated the magnetic moment ordering, additional molecular fields determined by quadrupole magnetic moments are induced in the magnet under investigation.[2–6]

Separating in the exchange component in (1) the self-consistent field $\langle S^x\rangle$ associated with magnetic moment ordering and the additional fields $q_2^p$ $(p=0,2)$ determined by the quadrupole magnetic moments, we obtain the following expression for the one-site Hamiltonian $\mathcal{H}_0(n)$:

$$\mathcal{H}_0(n)=-H_xS_n^x-\tilde{B}_2^0O_{2n}^0-\tilde{B}_2^2O_{2n}^2+\nu S_n^iS_n^ju_{ij}(n), \qquad (2)$$

where

$$H_x=\sum_{n'}\left\{I(n-n')-\frac{1}{2}K(n-n')\right\}\langle S^x\rangle;$$

$$\tilde{B}_2^0=B_2^0+\frac{1}{6}\sum_{n'}K(n-n')q_{2n}^0;$$

$$\tilde{B}_2^2=B_2^2+\frac{1}{2}\sum_{n'}K(n-n')q_{2n}^2;$$

$$q_{2n}^0=\langle O_{2n}^0\rangle;\quad q_{2n}^2=\langle O_{2n}^2\rangle;$$

$$O_{2n}^0=3(S_n^z)^2-2;\quad O_{2n}^2=\frac{1}{2}\{(S_n^+)^2+(S_n^-)^2\}.$$

It was proved by Val'kov *et al.*[5] and confirmed by the subsequent analysis that nonzero values of average values of other operators $O_{2n}^t$ $(t=xy,xz,yz)$ are not observed.

Hamiltonian (2) expressed in terms of Hubbard operators constructed on eigenfunctions of the operator $L=-H_xS_n^x-\tilde{B}_2^0O_{2n}^0-\tilde{B}_2^2O_{2n}^2$ assumes the form

$$\mathcal{H}_0(n)=\sum_n\left\{\sum_M P_MH_n^M+\sum_\alpha P_\alpha X_n^\alpha\right\}, \qquad (3)$$

where $X_n^{M'M}\equiv|\psi_n(M')\rangle\langle\psi_n(M)|$ is the Hubbard operator,[6,13] $H_n^M\equiv X_n^{MM}$ is the diagonal Hubbard operator, the index $M$ assumes the values $-$, 0, and $+$, $\alpha$ is the root vector, and $\psi_n(M)$ are the eigenfunctions of the operator $L$:

$$\psi_n(+)=\cos\theta|+\rangle+\sin\theta|0\rangle;$$

$$\psi_n(0)=-\sin\theta|+\rangle+\cos\theta|0\rangle;\quad \psi_n(-)=|-\rangle. \qquad (4)$$

Here, $|\pm\rangle=(1/\sqrt{2})(|1\rangle\pm|-1\rangle)$, $|0\rangle$, $|1\rangle$, $|-1\rangle$ are the eigenfunctions of the operator $S^z$, and

$$\sin\theta=\left(\frac{\chi_0-3\tilde{B}_2^0-\tilde{B}_2^2}{2\chi_0}\right)^{1/2};$$

$$\cos\theta=\frac{2H_x}{[2\chi_0(\chi_0-3\tilde{B}_2^0-\tilde{B}_2^2)]^{1/2}};$$

$$\chi_0^2=H_x^2+(3\tilde{B}_2^0+\tilde{B}_2^2)^2. \qquad (5)$$

For a magnet with $S=1$, the general form of the wave functions (4) was established in Refs. 18 and 19.

Since the $P_{M(\alpha)}$ in (3) have a cumbersome form, we do not write these expressions here (see Ref. 11).

Solving the one-ion problem with Hamiltonian (3), we obtain the energy levels for a magnetic ion taking into account the ME interaction (in the first nonvanishing approximation in $\nu$):

$$E_+=\frac{\tilde{B}_2^0-\tilde{B}_2^2}{2}+\nu\left(u_{xx}^{(0)}+\frac{u_{yy}^{(0)}+u_{zz}^{(0)}}{2}\right)-\frac{\chi}{2};$$

$$E_0=\frac{\tilde{B}_2^0-\tilde{B}_2^2}{2}+\nu\left(u_{xx}^{(0)}+\frac{u_{yy}^{(0)}+u_{zz}^{(0)}}{2}\right)+\frac{\chi}{2};$$

$$E_-=\tilde{B}_2^2-\tilde{B}_2^0+\nu(u_{yy}^{(0)}+u_{zz}^{(0)});$$

$$\chi^2=\{\chi_0-\nu(u_{zz}^{(0)}-u_{yy}^{(0)})\cos 2\theta\}^2+\nu^2(u_{yy}^{(0)}+u_{zz}^{(0)})^2\sin^2 2\theta+4\nu^2u_{xy}^{(0)^2}. \qquad (6)$$

Spontaneous deformations $u_{ij}^{(0)}$ are determined from the condition of the minimum density of free energy $F=F_0-T\ln Z$, where

$$F_0=\frac{\lambda+\eta}{2}\sum u_{ij}^2+\eta\sum_{i\neq j}u_{ij}^2(n)+\lambda\sum_{\substack{i\neq j\\ l\neq m}}u_{ij}u_{lm}$$

is the density of the elastic energy of the system and

$$Z=\sum_{M=+,0,-}\exp\left(-\frac{E_M}{T}\right)$$

is the partition function.

In the limit of low temperatures ($T\ll T_c$, $T_c$ is the Curie temperature), $u_{ij}^{(0)}$ have the simplest form and are defined by the formulas

$$u_{xx}^{(0)}=-\frac{\nu(\lambda+\eta)}{\eta(\eta+3\lambda)};\quad u_{yy}^{(0)}=-\frac{\nu(\eta-\lambda)}{\eta(\eta+3\lambda)}\sin^2\theta;$$

$$u_{zz}^{(0)}=-\frac{\nu(\eta-\lambda)}{\eta(\eta+3\lambda)}\cos^2\theta;\quad u_{ij}^{(0)}=0,\quad i\neq j. \qquad (6a)$$

It can be easily seen that Hamiltonian (3) is nondiagonal in the basis of the eigenfunctions of the operator $L$. In order to diagonalize this Hamiltonian, we introduce new Hubbard operators $Y_n^{M'M} \equiv |\tilde{\psi}_n(M')\rangle\langle\tilde{\psi}_n(M)|$ constructed on the eigenfunctions $\tilde{\psi}_n(M)$ of Hamiltonian (3):

$$\tilde{\psi}_n(+) = \cos\delta\psi_n(+) + \sin\delta\psi_n(0);$$
$$\tilde{\psi}_n(0) = -\sin\delta\psi_n(+) + \cos\delta\psi_n(0);$$
$$\tilde{\psi}_n(-) = \psi_n(-), \tag{7}$$

where

$$\cos\delta = \frac{\nu(u_{yy}^{(0)} - u_{zz}^{(0)})\sin 2\theta}{\{[\chi - \chi_0 - \nu(u_{yy}^{(0)} - u_{zz}^{(0)})\cos 2\theta]^2 + \nu^2(u_{yy}^{(0)} - u_{zz}^{(0)})^2 \sin^2 2\theta\}^{1/2}}.$$

The relation between the spin operators and ''new'' Hubbard operators has the form

$$S_n^+ = (Y_n^{++} - Y_n^{00})\sin 2\tilde{\theta} + (Y_n^{+0} + Y_n^{0+})\cos 2\tilde{\theta} + (Y_n^{-+} - Y_n^{+})\sin\tilde{\theta} + (Y_n^{-0} - Y_n^{0-})\cos\tilde{\theta};$$
$$S_n^- = (S_n^+)^+; \quad S_n^z = (Y_n^{+-} + Y_n^{-+})\cos\tilde{\theta} - (Y_n^{0-} + Y_n^{-0})\sin\tilde{\theta}; \quad \tilde{\theta} = \theta + \delta. \tag{8}$$

We write the components of the strain tensor in the form $u_{ij} = u_{ij}^{(0)} + u_{ij}^{(1)}$, where $u_{ij}^{(0)}$ are spontaneous deformations defined by formulas (6a), and $u_{ij}^{(1)}$ the dynamic component of the strain tensor, which describes vibrations of crystal lattice sites. Having quantized the dynamic component $u_{ij}^{(1)}$ in the standard manner,[20] we obtain from Hamiltonian (3) the following Hamiltonian describing the transformation of magnons into phonons and the inverse transformation:

$$\mathcal{H}_{\rm tr} = \sum_n \left\{ \sum_M \tilde{P}_M Y_n^M + \sum_\alpha \tilde{P}_\alpha Y_n^\alpha \right\}. \tag{9}$$

Here

$$\tilde{P}_{M(\alpha)} = \frac{1}{N^{1/2}} \sum_{k,\lambda} (b_{k,\lambda} + b_{-k,\lambda}^+) T_n^{M(\alpha)}(k,\lambda);$$

$b_{-k,\lambda}^+ (b_{k,\lambda})$ are the creation (annihilation) operators for phonons with polarization $\lambda$, $T_n^{M(\alpha)}(k,\lambda)$ transformation amplitudes, and $N$ is the number of sites in the crystal lattice.

**3.** Defining Green's function in the standard manner, i.e.,

$$G^{\alpha\alpha'}(n,\tau;n',\tau') = -\langle \hat{T}\tilde{Y}_n^\alpha(\tau)\tilde{Y}_{n'}^{\alpha'}(\tau')\rangle. \tag{10}$$

we obtain the following equation of the Larkin type for this function[11]:

$$G^{\alpha\alpha'}(k,\omega_n) = \Sigma^{\alpha\alpha'}(k,\omega_n) - \frac{1}{2}\Sigma^{\alpha\alpha_1}(k,\omega_n) \times \{\mathbf{c}(-\alpha_1), \hat{A}(k)\mathbf{c}(\alpha_2)\} G^{\alpha_2\alpha'}(k,\omega_n) + \Sigma^{\alpha\alpha_1}(k,\omega_n) T^{-\alpha_1}(k,\lambda) D_\lambda(k,\omega_n) \times T^{\alpha_2}(-k,\omega_n) G^{\alpha_2\alpha'}(k,\omega_n),$$

where

$$D_\lambda(k,\omega_n) = \frac{2\omega_\lambda(k)}{\omega_n^2 - \omega_\lambda^2(k)}$$

is the Green's function of a free $\lambda$-polarized phonon with the dispersion relation $\omega_\lambda(k) = c_\lambda k$ ($c_\lambda$ is the velocity of the $\lambda$-polarized sound). The eight-dimensional vector $\mathbf{c}(\alpha)$ has the following components:

$$\mathbf{c}(\alpha) = \{\gamma_1^\parallel(\alpha), \gamma_1^\perp(\alpha), \gamma_1^{\perp *}(-\alpha), \gamma_2^\parallel(\alpha), \gamma_2^\perp(\alpha), \times \gamma_2^{\perp *}(-\alpha), \gamma_3^\perp(\alpha), \gamma_3^{\perp *}(-\alpha)\}$$

and the $8\times 8$ matrix $\hat{A}_{nn'}$ splits into the direct sum of two matrices:

$$\hat{A}_{nn'} = \hat{A}_{nn'}^{(3)} \oplus \hat{A}_{nn'}^{(5)};$$

$$\hat{A}_{nn'}^{(3)} = \left\{ I(n-n') - \frac{1}{2}K(n-n') \right\} \begin{pmatrix} 1 & 0 & 0 \\ 0 & 0 & 1/2 \\ 0 & 1/2 & 0 \end{pmatrix};$$

$$\hat{A}_{nn'}^{(5)} = \frac{K(n-n')}{2} \begin{pmatrix} 1 & 0 & 0 & 0 & 0 \\ 0 & 0 & 1/2 & 0 & 0 \\ 0 & 1/2 & 0 & 0 & 0 \\ 0 & 0 & 0 & 0 & 1/2 \\ 0 & 0 & 0 & 1/2 & 0 \end{pmatrix}. \tag{11}$$

The functions $\gamma_i^{\parallel(\perp)}(\alpha)$ are determined from the relation between the spin operators and Hubbard operators.

The inclusion of the biquadratic interaction is formally manifested in the increase in the dimensions of the vectors $\mathbf{c}(\alpha)$ and the matrix $\hat{A}_{nn'}$ as compared to the Heisenberg exchange. The eight-dimensionality of the vectors $\mathbf{c}(\alpha)$ is due to the fact that the number of linearly independent operators for the biquadratic exchange is five, while in the presence of biquadratic and Heisenberg interaction (the structure of the latter is determined by three independent spin operators $S_n^i$), we must use the eight-dimensional basis.

This equation can be solved from the split dependence on $\alpha$. Considering that the component irreducible in the Larkin sense in the mean-field approximation has the form

$$\Sigma^{\alpha\alpha'} = \delta_{\alpha\alpha'} b(\alpha) G_0^\alpha(\omega_n); \quad b(\alpha) = \langle \boldsymbol{\alpha}\mathbf{Y}\rangle_0,$$

where $G_0^{\alpha}(\omega_n)=[i\omega_n+(\boldsymbol{\alpha}\cdot\mathbf{E})]^{-1}$ is the zero-order Green's function, we obtain the dispersion equation for coupled ME waves:

$$\det\|\delta_{ij}+x_{ij}\|=0; \quad i,j=1,2,3,...,8, \tag{12}$$

where

$$x_{ij}=G_0^{\alpha}b(\alpha)c_{ij}(\alpha)$$
$$+B^0(k,\lambda,\lambda')T^{-\alpha}(k,\lambda)G_0^{\alpha}(\omega_n)b(\alpha)$$
$$\times T^{\beta}(-k,\lambda)G_0^{\beta}(\omega_n)b(\beta)c_{ij}(\alpha,\beta);$$

$$B^0(k,\lambda,\lambda')=\frac{D_{\lambda}(k,\omega_n)}{1-Q_{\lambda\lambda'}D_{\lambda}(k,\omega_n)};$$

$$Q_{\lambda\lambda'}=T^{\alpha}(-k,\lambda)G_0^{\alpha}(\omega_n)b(\alpha)T^{-\alpha}(k,\lambda');$$

$$c_{ij}(\alpha,\beta)=a_{ik}(\alpha,\beta)A_{kj}; \quad a_{ik}(\alpha,\beta)=c_i(\alpha)c_k(-\beta).$$

It should be noted that Eq. (12) is valid for arbitrary temperatures (up to the Curie temperature), arbitrary values of OA constants, and arbitrary relations between $I_0$ and $K_0$. We shall confine our analysis to the case of low temperatures ($T\ll T_c$).

**4.** Let us analyze Eq. (12) for the case when the Heisenberg exchange constant exceeds the biquadratic exchange constant ($I_0>K_0$), and the wave vector $\mathbf{k}\|y$. In such a geometry, nonzero components of the unit vector of phonon polarization are $e_l^y, e_{\tau}^x, e_i^z$.

It was proved by Val'kov *et al.*[5] that in the system under investigation (in the absence of the ME interaction) four types of magnetic phases can exist, two of which are characterized by the vector order parameter ($FM_z$ for $\langle S\rangle\|z$ and $FM_x$ for $\langle S\rangle\|x$), and the other two by the tensor order parameter ($Q_1$ and $Q_2$).

In the case of low temperatures, $E_+$ is the lowermost energy level, and hence we can confine ourselves only to the inclusion of this level in subsequent calculations. It should be noted that in contrast to the situation analyzed earlier[21] and characterized by a simpler form of the OA energy operator, no inversion of energy levels is observed in the present case upon a transition to Q phases.

Let us analyze Eq. (12) for the $Q_1$ phase (near the $Q_1-FM_x$ and $Q_1-FM_z$ phase transition lines) and for the $Q_2$ phase (near the $Q_2-FM_x$ line).

In the $Q_1$ phase, the dispersion equation (12) splits into two equations

$$\{(1+x_{11})(1+2x_{55})-2x_{15}x_{51}\}$$
$$\times\{(1+2x_{22})(1+2x_{77})-4x_{27}x_{72}\}=0. \tag{13}$$

We consider the first equation

$$\{(1+x_{11})(1+2x_{55})-2x_{15}x_{51}\}=0. \tag{14}$$

whose solution has the form

$$\omega_1^2(k)=[E_{+-}+K(k)][E_{+-}+2I(k)-K(k)]$$
$$+a_0\frac{\omega_{\tau}^2(k)[E_{+-}+2I(k)-K(k)]}{\omega_{\tau}^2(k)-[E_{+-}+K(k)][E_{+-}+2I(k)-K(k)]}; \tag{15a}$$

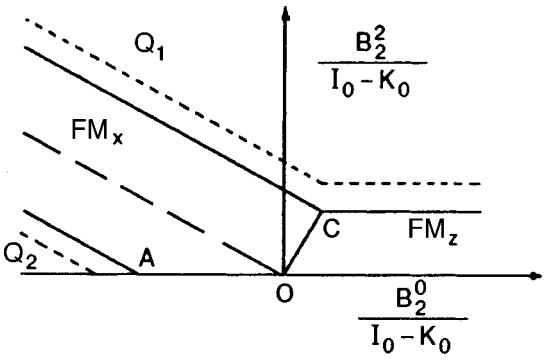


FIG. 1. Phase diagram of a biaxial FM for $I_0>K_0$. Dashed lines are PT lines without ME interaction, solid lines are PT lines taking into account ME interaction. At point $C$, the PT lines $Q_1-FM_x$-phase and $Q_1-FM_z$-phase average. The PT line $Q_2-FM_x$-phase passes through point $A$. The dot-and-dash line passing through the $FM_x$-phase and point $O$; the average value of magnetic moment is equal to unity.

$$\omega_2^2(k)=\omega_{\tau}^2(k)$$
$$-a_0\frac{\omega_{\tau}^2(k)[E_{+-}+2I(k)-K(k)]}{\omega_{\tau}^2(k)-[E_{+-}+K(k)][E_{+-}+2I(k)K(k)]}. \tag{15b}$$

It should be noted that only the amplitudes of transformations $T^{\alpha_4}(k,\tau)=-T^{\alpha_3}(k,\tau)$ have nonzero values in the case under investigation, i.e., only $\tau$-polarized phonons interact with the magnetic subsystem.

In Eqs. (15a) and (15b), we have introduced the following notation: $E_{+-}=E_+-E_-=-2B_2^2-K_0-a_0$; $a_0=\nu^2/\eta$; $\omega_{\tau}(k)=c_{\tau}k$ is the spectrum of a noninteracting $\tau$-polarized phonon, and $c_{\tau}^2=\eta/(2m)$ is the square of the velocity of sound.

It can easily be seen from (15a) that the quasimagnon spectrum has the form

$$\omega_1(k)=\sqrt{(2B_2^2+a_0+\gamma k^2)(B_2^2-I_0+K_0+a_0)}, \tag{16a}$$

while the spectrum of $\tau$-polarized quasiphonons is defined by formula (15b) and has the form

$$\omega_2^2(k)=\omega_{\tau}^2\left(1-\frac{a_0}{I_0-K_0}\right), \tag{16b}$$

where $\gamma=R_0^2K_0$, $R_0$ being the radius of biquadratic interaction.

Expression (16a) defines the PT line $Q_1-FM_z$-phase (Fig. 1)

$$B_2^2=I_0-K_0-a_0, \tag{17}$$

which is displaced by $a_0$ as compared to the case when the ME interaction is absent.[5] The magnon branch in this case plays the role of a soft mode, and the PT occurs along this excitation branch. It follows from (16b) that the quasiphonon branch weakly interacts with the magnon subsystem, which is manifested only in a slight renormalization of the velocity of sound:

$$\tilde{c}_{\tau}^2=c_{\tau}^2\left(1-\frac{a_0}{I_0-K_0}\right).$$

Besides, the second equation

$$\{(1+2x_{22})(1+2x_{77})-4x_{27}x_{72}\}=0. \tag{18}$$

in the vicinity of the PT line $Q_1-FM_z$-phase describes the high-frequency magnon branch which does not interact with the elastic subsystem. However, this equation becomes decisive in the behavior of the system in the vicinity of the PT line $Q_1-FM_x$-phase.

In this case, only the amplitudes of transformations $T^{\alpha_2}(k,t)=-T^{\alpha_1}(k,\tau)$ have nonzero values.

The solutions of Eq. (18) have the form

$$\omega_1^2(k)=[E_{+0}+K(k)][E_{+0}+2I(k)-K(k)] + a_0\frac{\omega_t^2(k)[E_{+0}+2I(k)-K(k)]}{\omega_t^2(k)-[E_{+0}+K(k)][E_{+0}+2I(k)-K(k)]}; \tag{19a}$$

$$\omega_2^2(k)=\omega_t^2(k) - a_0\frac{\omega_t^2(k)[E_{+0}+2I(k)-K(k)]}{\omega_t^2(k)-[E_{+0}+K(k)][E_{+0}+2I(k)-K(k)]}, \tag{19b}$$

where $E_{+0}=E_+-E_0=-3B_2^0-B_2^2-K_0-a_0$; $\omega_t(k)=c_tk$ is the spectrum of a $t$-polarized phonon.

Expression (19a) defines the magnon spectrum

$$\omega_1(k) = \sqrt{(3B_2^0+B_2^2+a_0+\gamma k^2)[3B_2^0+B_2^2-2(I_0-K_0)+a_0]},$$

and (19b) defines the spectrum of $t$-polarized phonons

$$\omega_2^2(k)=\omega_t^2\left(1-\frac{a_0}{I_0-K_0}\right).$$

These expressions show that the elastic and magnetic subsystems interact weakly. This interaction leads to a slight decrease in the velocity of $t$-polarized sound and to a displacement of the $Q_1-FM_x$-phase PT line by $a_0$ (relative to the case when ME coupling is absent[5]): $B_2^2=-3B_2^0+2(I_0-K_0)-a_0$.

In the vicinity of the $Q_1-FM_x$-phase PT line, Eq. (14) describes the high-frequency branch that does not interact with the elastic subsystem.

It can easily be seen that $\sin\tilde{\theta}=0$ and $\cos\tilde{\theta}=1$ for the PT $Q_1-FM_x$-phase and the $Q_1-FM_z$-phase, and hence the ground state realized on these PT lines is the state $\psi(+)=(1/\sqrt{2})(|1\rangle+|-1\rangle)$ in accordance with (1). The realization of such a ground state indicates that the $Q_1$ phase is formed as a result of a purely quantum effect of ''spin contraction.''[6,22] In this case, $\langle S\rangle$ decreases in magnitude at each site.

In addition, an analysis of formulas (15a) and (15b) on the line $B_2^2=I_0-K_0$, i.e., the line of the PT under investigation without the ME interaction,[5] shows that the quasiphonon spectrum assumes the form

$$\omega^2(k)=\omega_\tau^2(k)\frac{\gamma k^2+2B_2^2}{\gamma k^2+2B_2^2+a_0}.$$

and for $2B_2^2<\gamma k^2<2B_2^2+a_0$ we obtain $\omega^2(k)=\omega_\tau^2(k)\,\gamma k^2/(2B_2^2+a_0)$.

On the line $B_2^2=-3B_2^0+2(I_0-K_0)$, the quasiphonon spectrum can be presented in the form

$$\omega^2(k)=\omega_t^2(k)\frac{\gamma k^2+3B_2^0+B_2^2}{\gamma k^2+3B_2^0+B_2^2+a_0},$$

while for $3B_2^0+B_2^2<\gamma k^2<3B_2^0+B_2^2+a_0$ we have $\omega^2(k)=\omega_t^2(k)\,\gamma k^2/(3B_2^0+B_2^2+a_0)$.

In the quasimagnon spectrum, the above-mentioned PT lines acquire gaps defined as

$$\omega(0)=\sqrt{a_0(I_0-K_0+a_0)};$$

$$\omega(0)=\sqrt{a_0[2(I_0-K_0)+a_0]}.$$

A similar analysis of the dispersion equation (12) in the $Q_2$-phase leads to the following result.

The nonzero transformation amplitudes are $T^{\alpha_2}(k,t)=-T^{\alpha_1}(k,t)$, i.e., only $t$-polarized phonons interact with the magnetic subsystem.

The spectrum of coupled ME waves in the $Q_2$-phase has the form

$$\omega_1^2(k)=[E_{+0}+K(k)][E_{+0}+2I(k)-K(k)] + a_0\frac{\omega_t^2(k)[E_{+0}+2I(k)-K(k)]}{\omega_t^2(k)-[E_{+0}+K(k)][E_{+0}+2I(k)-K(k)]}; \tag{20a}$$

$$\omega_2^2(k)=\omega_t^2(k) - a_0\frac{\omega_t^2(k)[E_{+0}+2I(k)-K(k)]}{\omega_t^2(k)-[E_{+0}+K(k)][E_{+0}+2I(k)-K(k)]}, \tag{20b}$$

where $E_{+0}=E_+-E_0=3B_2^0+B_2^2-K_0-a_0$.

An analysis of these expressions similar to that carried out above shows that the magnetic and elastic subsystems interact weakly. This interaction leads to a small renormalization of the velocity of the $t$-polarized sound

$$\omega_2^2(k)=\omega_t^2\left(1-\frac{a_0}{2(I_0-K_0)}\right)$$

and to a displacement of the PT line $Q_2-FM_x$-phase by $a_0$: $B_2^2=-3B_2^0-2(I_0-K_0)+a_0$ as compared to the case when the ME coupling is absent.[5]

In this phase, $\sin\tilde{\theta}=1$ and $\cos\tilde{\theta}=0$, and hence the ground state of the system is $\psi(+)=|0\rangle$. Thus, in contrast to the $Q_1$-phase, the $Q_2$ phase is realized in the standard manner.[6,18] Moreover, no peculiarities in the quasiphonon spectrum, which take place in the $Q_1$-phase, are observed in the $Q_2$-phase on the line $B_2^2=-3B_2^0-2(I_0-K_0)$ line.

Consequently, the PT $FM_x-Q_2$-phase cannot occur as a reorientational PT, but is realized though a decrease in the modulus of $\langle S^x\rangle$ as the PT line $B_2^2=-3B_2^0-2(I_0-K_0)+a_0$ is approached.

The above analysis of the dispersion equation (12) (for $I_0>K_0$) makes it possible to construct the phase diagram of a biaxial ferromagnet with biquadratic exchange (Fig. 1).

Solid lines on the diagram correspond to the inclusion of the ME coupling, while the dashed lines correspond to the absence of ME coupling.[5] The *dot-and-dash* line in the $FM_x$-phase, we have $\langle S^x\rangle = 1$. As we move from this line to the PT lines $FM_x - Q_1$ and $FM_x - Q_2$-phase, $\langle S^x\rangle \to 0$, while $\langle S^x\rangle = 0$ on these lines. However, it was proved above that the mechanisms according to which $\langle S^x\rangle$ tends to zero as well as the ground states of the system for the PT under investigation are different for transitions to the $Q_1$- and $Q_2$-phases.

**5.** Let us now analyze the spectra of coupled ME waves in the case when the biquadratic interaction is stronger than the Heisenberg exchange ($I_0 < K_0$). As before, we shall consider the case of low temperatures and assume that the wave vector $\mathbf{k} \| y$.

According to (8), $\langle S\rangle = 0$ for $K_0 > I_0$, and hence only phases with tensor order parameters (Q-phases) can be realized in the system. It was proved in Ref. 5 (in the absence of the ME interaction) that in the $Q_1$ and $Q_2$-phases that can be realized in this case, the order parameters and the ways of realization are the same as in the case considered above ($I_0 > K_0$, see Sec. 4). Let us analyze the spectra of coupled ME waves in these phases.

Equation (12) for the $Q_1$ phase splits into two equations one of which describes the spectrum of high-frequency magnon branch that does not interact with the elastic subsystem. The second equation

$$(1+2x_{22})(1+2x_{77}) - 4x_{27}x_{72} = 0 \tag{21}$$

gives the spectra of coupled ME waves.

Using the notation introduced above, we can write the solutions of Eq. (21) in the form

$$\omega_1^2 = [E_{+0} + K(k)][E_{+0} + 2I(k) - K(k)] + \frac{a_0\omega_t^2(k)[E_{+0} + 2I(k) - K(k)]}{\omega_t^2(k) - [E_{+0} + K(k))(E_{+0} + 2I(k) - K(k)]}, \tag{22}$$

$$\omega_2^2(k) = \omega_t^2(k) - \frac{a_0\omega_t^2(k)[E_{+0} + 2I(k) - K(k)]}{\omega_t^2(k) - [E_{+0} + K(k))(E_{+0} + 2I(k) - K(k)]}, \tag{23}$$

where $E_{+0} = E_+ - E_0 = -3B_2^0 - B_2^2 - K_0 - a_0$.

Formula (22) determines the quasimagnon spectrum

$$\omega_1(k) = \sqrt{(\gamma k^2 + 3B_2^0 + B_2^2 + a_0)[3B_2^0 + B_2^2 + a_0 + 2(K_0 - I_0)]}, \tag{24}$$

and expression (23) defines the spectrum of *t*-polarized quasiphonons:

$$\omega_2^2(k) = \omega_t^2(k) \times \frac{(\gamma k^2 + 3B_2^0 + B_2^2)[3B_2^0 + B_2^2 + 2(K_0 - I_0)]}{(\gamma k^2 + 3B_2^0 + B_2^2 + a_0)[3B_2^0 + B_2^2 + 2(K_0 - I_0) + a_0]}. \tag{25}$$

It follows from (25) that the quasiphonon spectrum in the vicinity of the line $B_2^2/(K_0 - I_0) = -3B_2^0/(K_0 - I_0)$ is ''softened'' in the long-wave limit ($\gamma k^2 \ll a_0$) and acquires the form

$$\omega_2^2(k) = \omega_t^2(k)\frac{2\gamma k^2}{a_0[2(K_0 - I_0) + a_0]},$$

while the quasimagnon spectrum acquires the ME gap:

$$\omega_1(0) = \sqrt{a_0[2(K_0 - I_0) + a_0]}.$$

Thus, as we ''move'' in the $Q_1$-phase to the line $B_2^2/(K_0 - I_0) = -3B_2^0/(K_0 - I_0)$, the role of the ME coupling in the system becomes more significant, and the quasiphonon branch is ''softened'' on this line (in the long-wave limit), while the quasimagnon spectrum acquires an ME gap. Such a behavior of the spectra indicates that an orientational PT in the material parameters occurs in the system.

A similar analysis of Eq. (12) in the $Q_2$-phase makes it possible to determine the spectra of ME waves in this state:

$$\omega_1^2(k) = [E_{+0} + K(k)][E_{+0} + 2I(k) - K(k)] + \frac{a_0\omega_t^2(k)[E_{+0} + 2I(K) - K(k)]}{\omega_t^2(k) - [E_{+0} + K(k)][E_{+0} + 2I(k) - K(k)]}, \tag{26}$$

$$\omega_2^2(k) = \omega_t^2(k) - \frac{a_0\omega_t^2(k)[E_{+0} + 2I(k) - K(k)]}{\omega_t^2(k) - [E_{+0} + K(k)][E_{+0} + 2I(k) - K(k)]}, \tag{27}$$

where $E_{+0} = E_+ - E_0 = 3B_2^0 + B_2^2 - a_0 - K_0$.

Expression (27) for the quasiphonon spectrum shows that for $B_2^2/(K_0 - I_0) = -3B_2^0/(K_0 - I_0)$, the phonon branch in the $Q_2$-phase in the long-wave limit ($\gamma k^2 \ll a_0$) is ''softened,'' i.e.,

$$\omega_2^2(k) = \omega_t^2(k)\frac{2\gamma k^2}{a_0[2(K_0 - I_0) + a_0]},$$

while the quasimagnon spectrum acquires an ME gap:

$$\omega_1(0) = \sqrt{a_0[2(K_0 - I_0) + a_0]}.$$

The obtained results indicate that the system experiences an orientational PT $Q_1 - Q_2$-phase along the line $B_2^2/(K_0 - I_0) = -3B_2^0/(K_0 - I_0)$. In contrast to the case considered in Ref. 5 (without ME interaction), the role of the soft mode is played by the quasiphonon branch and not by the magnon branch. The phase diagram corresponding to this case in shown in Fig. 2.

**6.** Thus, in the case of a strong Heisenberg exchange interaction ($I_0 > K_0$), the system can exist in the magnetic phases ($FM_x$ and $FM_z$) as well as in phases with tensor order parameters. Phase transitions in this case occur only through

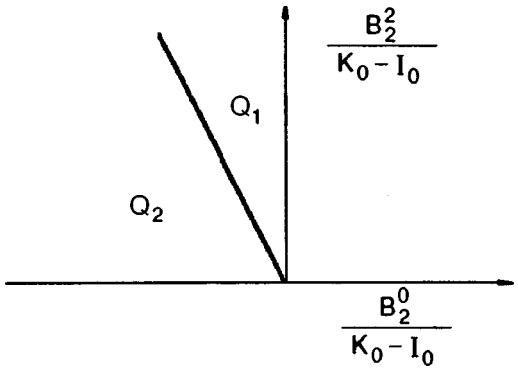


FIG. 2. Phase diagram of a biaxial FM for $K_0 > I_0$.

a decrease in $\langle S \rangle$ and not through the rotation of the magnetization vector. This is also manifested in spectral regularities of elementary excitations: the soft mode is the magnon branch along which PT occur, while only a weak renormalization of the velocity of sound occurs in the phonon spectrum. The inclusion of ME coupling displaces the PT lines by $\sim a_0/(I_0 - K_0)$.

A more interesting situation takes place for $K_0 > I_0$. In this case, the system contains only phases with tensor order parameters ($Q_1$ and $Q_2$). The quasiphonon mode is a soft mode in the PT, while the quasimagnon spectrum acquires an ME gap. Such a behavior of spectra is typical only for orientational PT. In the case under investigation, reorientation is reduced to the rotation of the principal axis of the tensor of quadrupole moments. Thus, orientational PT can be realized not only in systems with a vector order parameter, but also in more complicated situations. Consequently, the behavior of the spectra of ME waves can be used not only to judge about the presence of PT, but also to determine whether the transition is of the orientational type.

[1] E. L. Nagaev, *Magnets with Complex Exchange Interactions* [in Russian], Nauka, Moscow (1988).
[2] V. V. Val'kov, G. N. Matsulev, and S. G. Ovchinnikov, Preprint No. 418, Inst. Physics, Siberian Branch of the USSR Acd. Sci., Krasnoyarsk (1987).
[3] V. V. Val'kov, G. N. Matsulev, and S. G. Ovchinnikov, Preprint No. 596, Inst. Physics, Siberian Branch of the USSR Acd. Sci. Krasnoyarsk (1989).
[4] V. V. Val'kov, G. N. Matsulev, and S. G. Ovchinnikov, Preprint No. 645, Inst. Physics, Siberian Branch of the USSR Acd. Sci. Krasnoyarsk (1990).
[5] V. V. Val'kov, G. N. Matsulev, and S. G. Ovchinnikov, Fiz. Tverd. Tela **31**, 60 (1989) [Sov. Phys. Solid State **31**, 948 (1989)].
[6] V. M. Loktev and V. S. Ostrovskii, Fiz. Nizk. Temp. **20**, 983 (1994) [Low Temp. Phys. **20**, 775 (1994)].
[7] H. H. Chen, Phys. Rev. Lett. **27**, 1383 (1971).
[8] R. Aleonaro and P. Morin, Phys. Rev. B **19**, 3869 (1979).
[9] P. Morin, L. Rouchy, and D. Schitt, Phys. Rev. B **17**, 3684 (1978).
[10] E. A. Turov and V. G. Shavrov, Usp. Fiz. Nauk **140**, 429 (1983) [Sov. Phys. Usp. **26**, 593 (1983)].
[11] Yu. N. Mitsaĭ, A. N. Maiorova, and Yu. A. Fridman, Fiz. Tverd. Tela (St. Petersburg) **34**, 66 (1992) [Sov. Phys. Solid State **34**, 34 (1992)].
[12] H. F. Tiersten, J. Math. Phys. **5**, 1298 (1964).
[13] W. F. Brown, J. Appl. Phys. **36**, 994 (1965).
[14] V. G. Bar'yakhtar and E. A. Turov, in *Electron Structure and Electron Properties of Metals and Alloys* [in Russian], Naukova Dumka, Kiev (1988).
[15] I. M. Vitebskiĭ, N. M. Lavrinenko, A. N. Maiorova *et al.*, Ukr. Fiz. Zh. **39**, 597 (1994).
[16] V. G. Bar'yakhtar, V. M. Loktev, and S. M. Ryabchenko, Zh. Éksp. Teor. Fiz. **88**, 1752 (1985) [Sov. Phys. JETP **61**, 1040 (1985)].
[17] Yu. N. Mitsaĭ, Yu. A. Fridman, O. V. Kozhemyako, and B. L. Eingorn, Fiz. Nizk. Temp. **24**, 345 (1998) [Low Temp. Phys. **24**, 261 (1998)].
[18] V. M. Loktev and V. S. Ostrovskii, Fiz. Tverd. Tela (Leningrad) **20**, 3086 (1978) [Sov. Phys. Solid State **20**, 1779 (1978)].
[19] R. O. Zaitsev, Zh. Éksp. Teor. Fiz. **68**, 207 (1975) [Sov. Phys. JETP **41**, 100 (1975)].
[20] L. D. Landau and E. M. Lifshitz, *Statistical Physics* Part I, Pergamon Press, Oxford, 1980.
[21] Yu. N. Mitsaĭ and Yu. A. Fridman, Fiz. Tverd. Tela (Leningrad) **32**, 2316 (1990) [Sov. Phys. Solid State **32**, 1345 (1990)].
[22] V. V. Val'kov, T. A. Val'kova, and S. G. Ovchinnikov, Zh. Éksp. Teor. Fiz. **88**, 550 (1985) [Sov. Phys. JETP **61**, 323 (1985)].

Translated by R. S. Wadhwa

# On the theory of equilibrium magnetoelastic domain structure in easy-plane antiferromagnet

E. V. Gomonaj

*National Technical University of Ukraine KPI, 37, Ave., Peremogy, Kiev, 252056 Ukraine*

V. M. Loktev*)

*National Technical University of Ukraine KPI, 37, Ave., Peremogy, Kiev, 252056 Ukraine; Bogolyubov' Institute for Theoretical Physics, National Academy of Sciences of Ukraine, 14-b, Metrologichna str., Kiev, 252143 Ukraine*

(Submitted March 5, 1999)
Fiz. Nizk. Temp. **25**, 699–707 (July 1999)

Macroscopic magnetoelastic domain structure of the defectless layered antiferromagnet of $CoCl_2$-type with the ''easy-plane'' magnetic anisotropy is studied theoretically in the framework of phenomenological approach. In assumption of mobile domain walls, the finite-size effects are shown to result in the formation of a stable domain structure that changes reversibly under the action of the external magnetic field and can be treated as equilibrium. It is found that in antiferromagnets, where (in contrast to ferromagnets) long-range forces of magnetic origin are absent, the domain structure and its collective behavior are governed by elasticity. Field dependence of a domain structure, magnetostriction and low-frequency AFMR of poly- and monodomain samples are calculated, the external magnetic field being directed perpendicular to the main symmetry axis of the crystal. The results obtained are in qualitative agreement with the available experimental data.  [S1063-777X(99)00807-5]

## INTRODUCTION

The origin of equilibrium domain structure (DS) in antiferromagnetic (AFM) insulators is studied for a long time,[1,2] but the question is still obscure, despite a well developed theory for the close vicinity of the magnetic 1-st order phase transitions [in particular, for the field-induced spin-flop transitions in the easy-axis antiferromagnets (see the review[3] and recent paper[4] where this theory has been generalized for the case of the hexagonal AFM with the easy-plane magnetic anisotropy]. The DS of the pure antiferromagnets is usually treated as the result of structural imperfections (such as dislocations, twins, impurities, etc.) that cause the so-called sprout AFM domains (including 180° domains). Sometimes, the origin of the DS is attributed to the entropy factor, which decreases the free energy of the sample in the vicinity of the critical temperature in the case of spatially inhomogeneous ordering.

Both mentioned and some other possibilities were analyzed in a recent paper[5] where numerous experimental evidences of the equilibrium (almost insensitive to growth conditions) domain structure in dihaloids of transition metals $MX_2$ (M=Mn, Co, Ni:X=Cl, Br) were given. According to observations, the domain structure changes almost reversibly under the action of the external magnetic field; it gradually disappears when the field is switched on and recovers after it is switched off. Such a behavior evidently points to the equilibrium nature of the DS observed in these compounds.[1)]

The authors[5] also suggested that magnetoelastic interactions play a dominant role in formation of the equilibrium DS in the layered easy-plane antiferromagnets of $CoCl_2$-type. However, the only condition pointed out is not sufficient and there is an additional requirement necessary for DS formation, namely, the account of the sample surface. The finite size effects bring about the appearance of the DS during ferromagnetic and ferroelastic phase transitions as well as the magneto-elastic interactions.

These effects should play an important role in the AFM, and particularly, in dihaloids of transition metals, where the antiferromagnetic domains bear a magnetostrictive character and are of rather small size. In fact, the width of the antiferromagnetic domain wall can be evaluated as $\delta_0 \sim a(2H_E/H_A)^{1/2} \sim a(2H_E/H_{sf}) \sim 15-20a$, where $a$ is interatomic distance, $H_E$, $H_A$ and $H_{sf}$ are the exchange field, the interplane anisotropy field and the spin-flop field, correspondingly (for $CoCl_2$ $H_{sf}=2$ kOe[6] and spin-flip field $2H_E=32$ kOe).[7] Small thickness and low energy of the domain walls ($2.10^{-4}$ mJ/m$^2$, compared with the typical value 4 mJ/m$^2$ for a ferromagnet) give grounds for expecting the small size of AFM domains and assume that the surface properties of the sample do strongly depend upon the average strain.

It should be mentioned that an equilibrium DS is observed in the martensites in the course of a thermoelastic phase transition. It arises from the condition of strain compatibility of martensitic and austenitic phases. The peculiar feature of this structure is that the domain (twin) size is very small ($-1000$ Å see Ref. 8) and compatibility conditions relate only with the average-strain.

The present paper is aimed at the theoretical investigation of the macroscopic magnetoelastic domain structure of the defectless easy-plane layered AFM of $CoCl_2$-type with the account of finite-size (surface) effects. In the framework of the phenomenological model, we calculate the domain

 

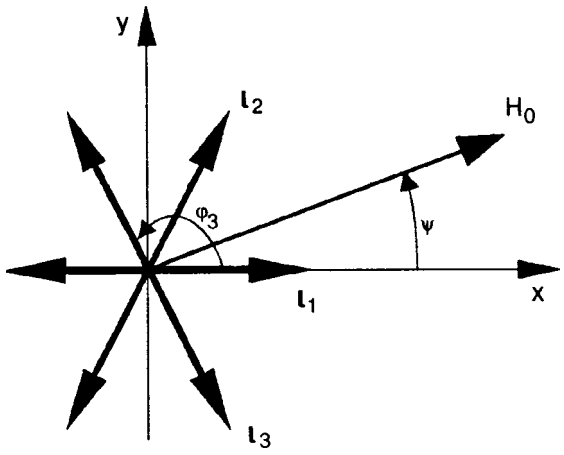


FIG. 1. Orientation of **1** vectors inside the domains, $\mathbf{H}_0$ is the external magnetic field.

structure, sample magnetostriction and AFMR frequency in the presence of an external magnetic field directed perpendicular to the main symmetry axis of the crystal.

### 1. Model

We consider a thin plate of a layered easy-plane rhombohedral antiferromagnet of $CoCl_2$-type. The crystal symmetry group is $D_{3d}^5$. The plate is oriented perpendicular to the 3-rd order crystal axis, labeled as $z$, $x$-axis is chosen along the 2nd order in-plane symmetry axis. Below the Néel temperature, the magnetic structure of the crystal can be described with two orthogonal dimensionless vectors: ferromagnetic, $\mathbf{m}$, and antiferromagnetic, $\mathbf{l}$, $\mathbf{m}^2+\mathbf{l}^2=1$. In the absence of external $\mathbf{m}=0$ and $\mathbf{l}$ has 3 equivalent orientations[2)] in the basis plane (directed along three 2nd order symmetry axes). In the in-plane external magnetic field, the magnetic structure is described by two parameters: the modulus $m$ of the ferromagnetic vector, and the angle $\varphi$ between the $\mathbf{l}$ and $x$-axes, neglecting small deflections of the magnetic vectors from the basis plane (see Fig. 1). The bulk free energy of the crystal in this case can be written in the simplest form (see, e.g., Ref. 9):

$$F_{\rm vol}=\int dv\Big\{2JM_0^2\mathbf{m}^2+2\beta^{(2)}M_0^2m_z^2-\frac{2}{3}\beta_\perp^{(6)}M_0^2\times(1-m^2)^3\cos 6\varphi+4M_0^2[\lambda_{me}^{(l)}(1-m^2)+\lambda_{me}^{(m)}m^2]\times[(u_{xx}-u_{yy})\cos 2\varphi+2u_{xy}\sin 2\varphi]+\frac{1}{2}c_{66}\times[(u_{xx}-u_{yy})^2+4u_{xy}^2]-2M_0H_0m\sin(\varphi-\Psi)\Big\}, \quad (1)$$

where the constant $J$ describes the interplanar AFM exchange; $\beta^{(2)}$, $\beta_\perp^{(6)}$ are the effective anisotropy constants; $2M_0$ is the saturation magnetization; $\lambda_{me}$ are the magnetostrictive constants; $u_{ik}$ $(i,k=x,y)$ are the strain tensor components; $c_{66}$ is the elastic modulus, principal for the case under consideration, and the external magnetic field is defined as $H_0=|\mathbf{H}_0|$, $\tan\Psi=H_{0y}/H_{0x}$. In the expression (1) we have omitted the isotropic part of strain tensor, $u_{xx}+u_{yy}$, qualitatively insignificant for the present problem. The effective magnetostrictive constants $\lambda_{me}^{(l)}$ and $\lambda_{me}^{(m)}$ originate from the relativistic (dipole-dipole or spin-orbit) interactions and, as was shown in Ref. 10, can essentially depend upon the concrete electronic and crystal structure of a compound.

Herein we consider the model in which the surface effects are accounted through the surface tension. The shape-dependent part of the surface energy for the simplest case of disk with radius $R$ and thickness $h$ is given by the expression

$$F_{\rm surf}=\frac{\pi Rh}{2}\sigma_{\rm surf}[\langle u_{xx}-u_{yy}\rangle^2+4\langle u_{xy}\rangle^2], \quad (2)$$

where $\sigma_{\rm surf}$ is the surface tension coefficient for the (100) and (010) faces, notion $\langle ...\rangle$ means the averaging over the sample volume:

$$\langle u_{ij}\rangle=\frac{1}{\pi R^2h}\int u_{ij}dv \quad (3)$$

and we have neglected the contribution from the disc sides (001) (which is appropriate if $h\ll R$). In the expression (1), (2) we have neglected the magnetostatic energy which contribution, as will be shown below, is much smaller than that from the surface energy.

For small external fields, $H_0\ll JM_0$, the ferromagnetic moment $m\ll 1$ can easily be excluded from (1). So, neglecting $\beta^{(2)}\ll J$,

$$F_{\rm vol}=\int dv\Big\{-\frac{2}{3}\beta_\perp^{(6)}M_0^2\cos 6\varphi-\frac{H_0^2}{2J}\sin^2(\varphi-\Psi)+4M_0^2\lambda_{me}^{(l)}[(u_{xx}-u_{yy})\cos 2\varphi+2u_{xy}\sin 2\varphi]+\frac{1}{2}c_{66}[(u_{xx}-u_{yy})^2+4u_{xy}^2]\Big\}. \quad (4)$$

The local orientation of the vector $\mathbf{l}$ can then be found by minimization of the functional

$$F=F_{\rm vol}+F_{\rm surf} \quad (5)$$

with respect to $\varphi(\mathbf{r})$, $u(\mathbf{r})$ functions. The corresponding integral equations have the form:

$$\begin{cases} u_{xx}-u_{yy}=-\dfrac{4M_0^2\lambda_{me}^{(l)}}{c_{66}}\cos 2\varphi+\dfrac{4M_0^2\lambda_{me}^{(l)}\sigma_{\rm surf}}{c_{66}(c_{66}R+\sigma_{\rm surf})}\langle\cos 2\varphi\rangle \\ 2u_{xy}=-\dfrac{4M_0^2\lambda_{me}^{(l)}}{c_{66}}\sin 2\varphi+\dfrac{4M_0^2\lambda_{me}^{(l)}\sigma_{\rm surf}}{c_{66}(c_{66}R+\sigma_{\rm surf})}\langle\sin 2\varphi\rangle \end{cases}, \quad (6)$$

$$\frac{1}{3}H_{sf}^2\sin 6\varphi=\sin 2\varphi[H_0^2\cos 2\Psi+2H_{MD}^2\langle\cos 2\varphi\rangle]-\cos 2\varphi[H_0^2\sin 2\Psi+2H_{MD}^2\langle\sin 2\varphi\rangle]. \quad (7)$$

Here we have introduced the characteristic fields convenient for further calculations: $H_{sf}=2M_0\sqrt{6\beta_\perp^{(6)}J}$—spin-flop field, and $H_{MD}=4M_0^2\lambda_{me}^{(l)}[(2J\sigma_{\rm surf})/c_{66}(c_{66}R+\sigma_{\rm surf})]^{1/2}$— the field of monodomenization.

Equation (7) evidently shows that the surface produces the same effect as an external magnetic field, the effective internal field being defined as

$$H_{\text{eff}}^2=\sqrt{H_0^4+4H_{MD}^4(\langle\cos 2\varphi\rangle^2+\langle\sin 2\varphi\rangle^2)+2H_0^2H_{MD}^2\langle\cos 2(\varphi-\Psi)\rangle^2} \tag{8}$$

$$\tan 2\Psi_{\text{eff}}=\frac{H_0^2\sin 2\Psi+2H_{MD}^2\langle\sin 2\varphi\rangle}{H_0^2\cos 2\Psi+2H_{MD}^2\langle\cos 2\varphi\rangle}.$$

Thus, it can be stressed that in the case of AFM it is the elastic strain that plays the role similar to the magneto-dipole interaction in ferromagnets.

Note, that for infinite sample ($R\to\infty$)$H_{MD}\to 0$ and effective field identically coincides with the external field $\mathbf{H}_0$; for such a situation $\Psi_{\text{eff}}\to\Psi$.

Equation (7) has different solutions depending on the physical situation considered below.

*1.1. Mobile domain walls*. In this case the average strain can follow the changes caused by an external magnetic field. Up to a certain field value, $H_0=H_{1c}$, specified below, the effect of the magnetic field is compensated by the average strains, so that the effective field inside the sample $\mathbf{H}_{\text{eff}}=0$.[3)] Equation (7) has three non-trivial solutions $\varphi_1=0$, $\varphi_{2,3}=\pm 2\pi/3$, corresponding to 3 equivalent equilibrium orientations of the **l** vector, i.e., to three magnetoelastic domains (as was already pointed out before). Evidently, each of them is distorted orthorhombically [in correspondence with Refs. 11 and 12, see formulas (6)]. Such a distortion for easy-plane AFM was observed in Ref. 13. Moreover, magnetoelasticity proves to be a crucial factor for the existence of an equilibrium DS.

In neglecting the domain wall energy, one can find the relative volume $\xi_j(j=1,2,3)$ of each domain from the following equations, obtained from (8):

$$H_0^2\cos 2\Psi+2H_{MD}^2\langle\cos 2\varphi\rangle=0 \tag{9}$$

$$H_0^2\sin 2\Psi+2H_{MD}^2\langle\sin 2\varphi\rangle=0, \tag{10}$$

we take it into account that:

$$\langle\cos 2\varphi\rangle=\sum_j \xi_j\cos 2\varphi_j, \quad \sum_j \xi_j=1. \tag{11}$$

The ultimate expression for $\xi_j$ is

$$\xi_j=\frac{1}{3}\left[1-\frac{H_0^2}{H_{MD}^2}\cos 2(\varphi_j-\Psi)\right], \quad j=1,2,3. \tag{12}$$

Note, that in this case $\xi_j$ are the thermodynamic variables as well as strain components and $\varphi$; the equality of the chemical potentials (free energy densities) of different ''phases'' (domains) is satisfied automatically.

According to (12), the volume fraction of the domains depends upon the value of the external magnetic field $H_0$. At zero field, $H_0=0$, all three types are equally distributed, so that the symmetry of the sample does not change after the transition into the polydomain antiferromagnetic state. In nonzero field the fraction of the most energetically ''unfavorable'' domain (**l** vector lies closely to the direction of the magnetic field, say, domain 1 for $0<\Psi<\pi/6$, see Fig. 1) diminishes. At $H_0=H_{1c}=H_{MD}/\cos 2\Psi)^{1/2}$ the domains of the 1st type disappear. Further behavior of the system at $H_0>H_{1c}$ can be found out from the equations (7), (10) and (11) with $j=2,3$. In this case the internal effective field is no longer zero, but it is directed along $x$-axis ($\Psi_{\text{eff}}=0$),[4)] so, $\varphi_2=-\varphi_3=\varphi$, and

$$\cos 2\varphi=\frac{3H_{MD}^2}{4H_{sf}^2}-\frac{1}{2}\left[\left(1+\frac{3H_{MD}^2}{2H_{sf}^2}\right)^2+3\frac{H_0^2-H_{1c}^2}{H_{sf}^2}\cos 2\Psi\right]^{1/2}, \tag{13}$$

$$\xi_{2,3}=\frac{1}{2}\left[1\mp\frac{H_0^2\sin 2\Psi}{H_{MD}^2\sin 2\varphi}\right]. \tag{14}$$

In other words, in the two-domain structure the **l** vectors inside the domains start to rotate and simultaneously the fractions of the different domains change. The process of monodomenization is completed at some critical field $H_0=H_c$ which can be found from equation (13) along with the condition $\xi_2=0$ or in other words,

$$H_c^2\sin 2\Psi=H_{MD}^2\sin 2\varphi. \tag{15}$$

For the case $\Psi=0$ both domains 2 and 3 disappear simultaneously at

$$H_0=H_{2c}\equiv\sqrt{H_{sf}^2+2H_{MD}^2}, \tag{16}$$

when all the **l** vectors achieve the direction perpendicular to the external field. Effective field (16) of monodomenization is defined both by the magnetic anisotropy (due to $H_{sf}$) and by the surface effect (due to $H_{MD}$). For the symmetric case $\Psi=\pi/6$ monodomenization is completed at $H_0=H_{1c}$ when domains 1 and 2 disappear and **l** vector in the third domain is aligned perpendicular to the external field. For the general case, $0<\Psi<\pi/6$, critical field $H_{1c}<H_c<H_{2c}$; after the process of monodomenization is finished, further change of $\varphi$ angle can be calculated from the equation

$$\frac{1}{3}H_{sf}^2\sin 6\varphi=H_0^2\sin 2(\varphi-\Psi). \tag{17}$$

The considered model gives rise to thermodynamically equilibrium domain structure at any magnetic field value. Really, the difference in free energy of the polydomain and monodomain state calculated from (1) and (2) at the same external field value,

$$F_{\text{poly}}-F_{\text{mono}}=-\frac{V}{2J}\left[H_{MD}^2+\frac{1}{2}H_0^2\cos 2(\varphi-\Psi)+\frac{1}{18}H_{sf}^2(1-\cos 6\varphi)\right]\leqslant 0 \tag{18}$$

is nonpositive, which makes the polydomain state thermodynamically preferable. So, in the model proposed the behavior of the DS in the external magnetic field is absolutely reversible.

*1.2. Immobile domain walls*. The domain walls cannot move freely, so, the ratio of the domains is fixed and only the rotational processes take place inside the domains. Orientation of **l** vectors can be calculated from equations (7) and (11) with the given $\xi_j$ values which are defined by technological factors. For small external field the equation (7) has 3 solutions corresponding to different domains. Monodomenization of the sample is completed when all the **l** vectors are aligned perpendicular to the external field direction.

For illustration let us consider the symmetrical case $\Psi=0$. If initially the domains have been produced by stray field at random, then $\xi_1=\xi_2=\xi_3=1/3$ and

$$\varphi_1=0,\ \ \varphi_2=-\varphi_3=\varphi,$$

$$\cos 2\varphi=\frac{H_{MD}^2}{2H_{sf}^2}-\frac{1}{2}\left[\left(1+\frac{H_{MD}^2}{H_{sf}^2}\right)^2+3\frac{H_0^2}{H_{sf}^2}\right]^{1/2}. \tag{19}$$

The field of monodomenization $H_c^{\text{immob}}=(H_{sf}^2+2/3H_{MD}^2)^{1/2}$ in this case is smaller than the corresponding value for the case of mobile domain walls [$H_c^{\text{immob}}<H_{2c}$, compare with formula (16)]. For arbitrary $\Psi$ the value of monodomenization field can be much greater.

After the magnetic field is removed, such a domain structure will not restore, at least, in principal, because **l** vectors will tend to lie along the nearest easy axis, which for general field orientation is the only one. So, once cycled in the magnetic field, the sample becomes monodomain and the behavior of the DS in this case is absolutely irreversible.

In the real experiments, the behavior of the DS in antiferromagnets of $CoCl_2$-type are partly irreversible, so, we can assume some intermediate case when most of the domain walls are mobile but some of them are pinned by the defects or different imperfections of a crystal and contribute to the certain irreversibility mentioned and observed.

### 2. Magnetostriction

In the experiments[5,7] the magnetic field was arbitrarily oriented in the easy plane of the crystal, and magnetostriction was measured along and perpendicular to the field direction. Corresponding macroscopic elongations, $(\Delta l/l)_{\parallel}$ and $(\Delta l/l)_{\perp}$ can be calculated according to the general formula

$$(\Delta l/l)_{\mathbf{n}}=\sum n_i\langle u_{ik}\rangle n_k, \tag{20}$$

where **n** is a unit vector in the direction of measurement, $\langle u_{ik}\rangle$ is the averaged strain tensor. Substituting (6) into (20) and neglecting of isomorphous strain $(u_{xx}+u_{yy})$ one readily obtains:

$$\left(\frac{\Delta l}{l}\right)_{\parallel}=-\left(\frac{\Delta l}{l}\right)_{\perp}=-\frac{4M_0^2R\left[\lambda_{me}^{(l)}+(\lambda_{me}^{(m)}-\lambda_{me}^{(l)})\left(\frac{H_0}{2H_E}\right)^2\right]}{c_{66}R+\sigma_{\text{surf}}}$$

$$\times\langle\cos 2(\varphi-\Psi)\rangle, \tag{21}$$

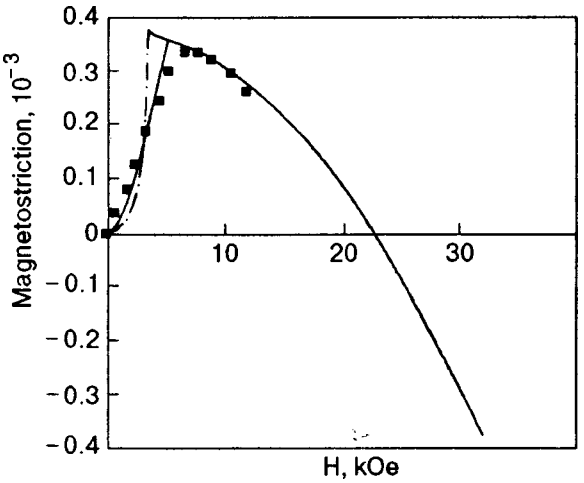


FIG. 2. Field dependence of magnetostriction of polydomain crystal: solid line—theoretical, mobile domain walls; dash line—theoretical, immobile domain walls; points—experimental.[7]

where $H_E=JM_0$, is the exchange field. In the formula (21) we have taken into account the dependence $m(H_0)\approx H_0/2H_E$, which is significant at $H_0\leqslant 2H_E$.

Field dependence of elongation $(\Delta l/l)_{\parallel}$ calculated from (21) for $CoCl_2$ with $\Psi=0$, $H_{sf}=2$ kOe; $H_{MD}=3.3$ kOe, $2H_E=32$ kOe, $4M_0^2\lambda_{me}^{(l)}=-4M_0^2\lambda_{me}^{(m)}=36$ MPa, $c_{66}=34.7$ GPa[7] is shown in Fig. 2. We have considered two cases: mobile (solid curve) and immobile (dash curve) domain walls. Figure 3 shows the same dependences vs squared magnetic field, $H_0^2$; the points correspond to experimental data.[7] The difference between two theoretical curves is significant at low field value. In the case of mobile domain walls the theoretical dependence (solid curve) is in good agreement with the experimental data. The $H_{MD}$ value was taken to fit the experimental slope $(\Delta l/l)_{\perp}$ vs $H_0^2$ at $H_0<3$ kOe.

The behavior of magnetostriction as seen from formula (21) and Fig. 2 is governed by two processes. At small field, $H_0\leqslant H_c\ll H_E$, magnetostriction of the sample is changed due to the process of monodomenization that influences the

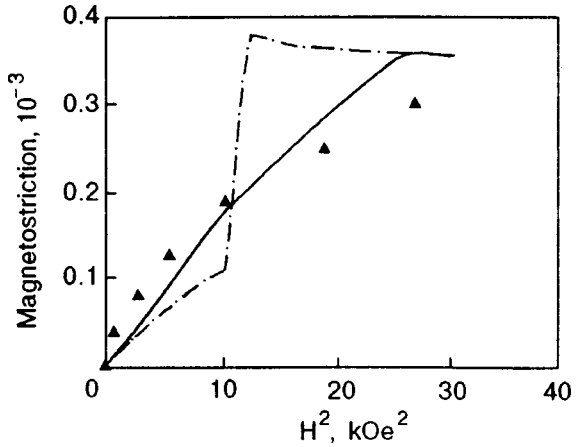


FIG. 3. Magnetostriction vs squared magnetic field in polydomain crystal: solid line—theoretical, mobile domain walls: dash line—theoretical, immobile domain walls; points—experimental.[7]

average $\cos 2(\varphi-\Psi)$ value (increasing section of the curve in Fig. 2). After this process is finished, variation of monodomain magnetostriction is defined only by an increase of magnetization in the external magnetic field (decreasing section of the curve in Fig. 2). It is seen from (21) that in the monodomain state the slope $(\Delta l/l)_\perp$ vs $H_0^2$ depends upon the difference $\lambda_{me}^{(m)}-\lambda_{me}^{(l)}$ only, that must be considered as a phenomenological parameter.

### 3. AFMR spectra

Experimentally measured field dependence of the low-frequency AFMR[7] shows that below 5 kOe the resonance frequency is approximately two times lower than the value extrapolated from measurements at higher frequency. In the interval $H_0\sim 5-7$ kOe field dependence of AFMR is practically vertical and starting from 7 kOe it turns out to be in agreement with high-frequency measurements. The characteristic field value coincides with the value of monodomenization field $H_c$ observed in magnetostriction experiments.

The observed peculiarity in the AFM spectra can be interpreted in the framework of the equilibrium magnetoelastic domain model developed above. Indeed, for the infinite samples the low AFMR frequency is contributed by the magnetic anisotropy field and magnetoelastic field as well, due to the fact, that the crystal lattice is ''frozen.'' On the other hand, it was shown by Gann and Zhukov[14] that for small samples the lattice relaxes together with the antiferromagnetic vectors, and then, the resonance frequency is defined mainly by the local anisotropy field.

The similar effect of ''unfreezing'' of crystal lattice can be achieved in the AFM with the magnetoelastic DS, if the domain size is quite small. To catch the effect, let us consider the in-plane oscillations of the magnetic moments together with acoustic waves in the polydomain sample with mobile domain walls. Low-frequency AFMR can be found on the basis of Lagrangian formalism with a Lagrangian taken in a standard form:[15]

$$L=\int d\nu\left(\frac{\dot\varphi^2}{2Jg^2}+\frac{1}{2}\rho\dot{\mathbf{u}}^2\right)-F_{\rm vol}, \tag{22}$$

where $g$ is gyromagnetic ratio, $\rho$ is a crystal density, $\mathbf{u}$ is a displacement vector $F_{\rm vol}$ is given by formula (4). Corresponding Euler–Lagrange equations have the form:

$$\begin{cases} \ddot\varphi-\dfrac{g^2}{2}H_0^2\sin 2(\varphi-\Psi)+\dfrac{g^2}{3}H_{sf}^2\sin 6\varphi-16g^2\lambda_{me}^{(l)} \\ \quad\times JM_0^2[(u_{xx}-u_{yy})\sin 2\varphi-2u_{xy}\cos 2\varphi]=0 \\ \ddot u_x-s^2\left[\dfrac{\partial^2}{\partial x^2}+\dfrac{\partial^2}{\partial y^2}\right]u_x-\dfrac{4\lambda_{me}^{(l)}M_0^2}{\rho}\left[\dfrac{\partial\cos 2\varphi}{\partial x}+\dfrac{\partial\sin 2\varphi}{\partial y}\right]=0 \\ \ddot u_y-s^2\left[\dfrac{\partial^2}{\partial x^2}+\dfrac{\partial^2}{\partial y^2}\right]u_y-\dfrac{4\lambda_{me}^{(l)}M_0^2}{\rho}\left[\dfrac{\partial\sin 2\varphi}{\partial x}-\dfrac{\partial\cos 2\varphi}{\partial y}\right]=0, \end{cases} \tag{23}$$

where $s=(c_{66}/\rho)^{1/2}$ is the in-plane sound velocity and equilibrium $\varphi$ value depends upon the $x$ and $y$ coordinates. Equations (23) describe the perturbations over inhomogeneous (polydomain) state of the sample.

The low-frequency branch of AFMR for $H_0<H_{1c}$ can be then calculated from the following equation

$$\omega^2=g^2\left\{H_{sf}^2+H_{ME}^2\left[1-\int\frac{\mathbf{k}^2(|a_{\mathbf{k}}|^2+|b_{\mathbf{k}}|^2)}{\mathbf{k}^2-(\omega^2/s^2)}d\mathbf{k}\right]\right\}, \tag{24}$$

where $H_{ME}=8M_0^2\lambda_{me}^{(l)}\sqrt{J/c_{66}}$ is a magnetostriction field; $a_{\mathbf{k}}$, $b_{\mathbf{k}}$ are the Fourrier components of the functions $\sin 2\varphi(\mathbf{r})$ and $\cos 2\varphi(\mathbf{r})$, correspondingly, $\int(|a_{\mathbf{k}}|^2+|b_{\mathbf{k}}|^2)d\mathbf{k}=1$.

The relation (24) shows that resonance frequency depends upon the average domain size $d$. For macroscopic domains with $d\gg\lambda\equiv s/(gH_{sf})$ characteristic value of $k\sim 1/d\ll s/\omega$ and the last term in (24) can be neglected. In this case the domain can be treated as infinite, corresponding AFMR frequency is

$$\Omega_{\rm AFMR}^{(\infty)}=g\sqrt{H_{sf}^2+H_{ME}^2} \tag{25}$$

and we arrive to a standard situation with the ''frozen'' lattice, AFMR gap is defined by anisotropy and magnetoelasticity as well. In the opposite case with $d\ll\lambda$, the Fourrier spectrum of functions $\sin 2\varphi(\mathbf{r})$ and $\cos 2\varphi(\mathbf{r})$ has two significant contributions with $k=0$ and $k=\pi/d$. The corresponding expression for AFMR frequency is

$$\Omega_{\rm AFMR}=g\left(H_{sf}^2+\frac{H_0^4H_{ME}^2}{4H_{MD}^4}\right)^{1/2}\left[1+\frac{g^2H_{ME}^2d^2}{2\pi^2s^2}\times(|a_{\pi/d}|^2+|b_{\pi/d}|^2)\right]<\Omega_{\rm AFMR}^{(\infty)}, \tag{26}$$

where we have taken into account that

$$|a_0|^2+|b_0|^2=\langle\cos 2\varphi\rangle^2+\langle\sin 2\varphi\rangle^2=\frac{H_0^4}{4H_{MD}^4}.$$

So, in the magnetically inhomogeneous sample the crystal lattice does follow the oscillations of the magnetic moments and thus diminishes the magnetoelastic contribution to the resonance frequency [see formula (26)]. This effect should be more pronounced in $CoCl_2$, where magnetoelastic contribution into AFMR spectrum is of the same order as an anisotropy one.

The field dependence of AFMR spectrum in $CoCl_2$ can be thus explained as follows. Suppose, at zero field the sample has a well developed DS with the average size $d\ll\lambda$ (for $CoCl_2$ $\lambda\sim 10^{-7}$ m). The lattice then proves to be partially ''unfrozen'' and frequency is defined mainly by anisotropy field [see expression (26)]. The external magnetic field affects the AFMR frequency in two ways: through the variation of average cosine and sine values and through the increase of the average domain size[4] $d(H_0)$ [last term in (26)]. As a result, the frequency grows smoothly with the field $H_0$. After the domain size achieves macroscopic value $d\sim R\gg\lambda$, the lattice becomes frozen, and resonance frequency steeply jumps to the value corresponding to infinite homogeneous sample [formula (25)]. Tentative behavior of AFMR vs magnetic field calculated from (25) and (26) with $g=6$, $H_{sf}=2$ kOe, $H_{ME}=1.5$ kOe, $H_{MD}=3.3$ kOe is shown in Fig. 4.

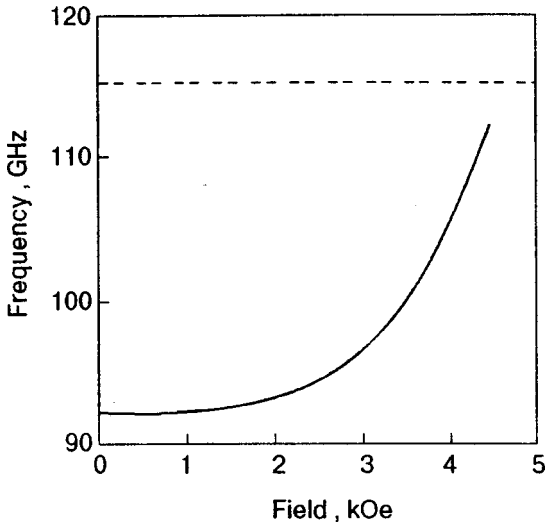


FIG. 4. Theoretical field dependence of resonance AFMR frequency (scheme): solid line—polydomain sample; dash line—infinite homogeneous sample.

Additional decrease of AFMR frequency in the polydomain sample can also result from the damping of the domain wall motion, stimulated by reassembling of the DS in the external magnetic field.[16] The ultimate value of AFMR frequency, $\tilde{\Omega}_{\mathrm{AFMR}}=\sqrt{\Omega^2_{\mathrm{AFMR}}-\delta^2}$, where $\delta$ is the damping coefficient, can be significantly lower than $\Omega^{(\infty)}_{\mathrm{AFMR}}$.

It can be shown that the model of immobile domain walls gives another form of spectrum which does not correlate with the experimental data.

#### 4. Discussion

Above we propose the model which naturally interprets the antiferromagnetic domains in the easy-plane antiferromagnets as equilibrium. The model is based on the magnetoelastic origin of the domains, supposition of mobile domain walls and additional condition imposed on the average strain of the sample. For illustration we have considered the simplest example when the condition in question was related with the surface tension of the sample which was the case if the surface energy made a significant contribution into free energy of the sample. As a consequence of the model, the value of monodomenization field depends upon the characteristic size $R$ of the sample and thus vanishes when $R$ tends to infinity.

The results obtained could be generalized if $R$ implies the characteristic size of substructure unit of the sample (i.e., dislocation-free region or crystallite), defined by the technological factors. In the case of fixed (glued) sample expression (2) should be substituted with corresponding boundary conditions for the sample faces. Anyway, finite-size effects can play a crucial role in the behavior of antiferromagnets with significant magnetostriction and should be taken into account in interpretation of experimental results.

The predicted behavior of the DS of AFM is analogous to that of ferromagnetic. Namely, up to some critical external field value, the effective internal magnetic field is compensated due to the reassembling of the domains. The value of critical field is defined by the geometry and size of the sample. It is interesting and important that in AFM model considered the long range interactions include no magnetic component and are completely provided by elasticity.

The size of the domains can be calculated with the account of short-wavelength contribution to the surface energy which compensates the increase of volume energy resulting from the domain walls.

In our calculations we have not considered the magnetostatic effects and domain walls themselves. Demagnetization factor influences the DS in the region of 1st order (spin-flop) phase transition which takes place in narrow interval of angle $\Psi\approx 0$ (see Ref. 4). For arbitrary orientation of the external magnetic field in the easy plane of AFM the magnetostatic contribution is $(H_{MD}/2H_E)\sim 0.06\ll 1$ times smaller than the surface energy and thus can be neglected.

The account of domain walls is necessary for evaluation of the domain size that is out of scope of the present paper. The structure of domain walls can be calculated in an analogy with general approaches (see Ref. 3) by taking into account magnetic and elastic subsystems. It should be noted that in the defect-free sample the interdomain boundary are ideally conjugated and no stresses appear because of compatibility conditions.

## CONCLUSIONS

1. The domain structure of easy-plane AFM with degenerated orientation of antiferromagnetic vector can be treated as equilibrium in the finite-size sample with the mobile domain walls. The effect originates from the magnetoelastic nature of the domains with the account of surface tension.

2. At zero magnetic field all types of the domains are equally represented. The external magnetic field effects the magnetic and elastic properties of the sample in two ways. At small field value variation of the domain structure gives rise to additional average strain field which compensates the external magnetic field, the orientation of the magnetic moments inside domains being fixed. At some critical value, $H_0=H_c$, the sample becomes monodomain and magnetic field results in reorientation of the magnetic moments.

3. Experimentally observed magnetostriction vs magnetic field dependence for $CoCl_2$ crystal is adequately described in terms of the model under consideration with mobile domain walls.

4. AFMR frequency of polydomain crystal can be significantly lowered due to ''unfreezing'' of the crystal lattice if the size of domain is quite small.

5. The above mentioned calculations can be considered as a basis for the following important and quite general supposition: variation of the surface energy (that is of Coulomb nature and so is not small) can result in the formation of equilibrium inhomogeneous state (or in other words, the equilibrium domain structure of magnetoelastic or elastic nature).

**ACKNOWLEDGEMENTS**

We are sincerely indebted to Prof. S. M. Ryabchenko, Dr. A. F. Lozenko and Dr. V. M. Kalita for stimulating and constructive discussions of the problem under consideration and for opportunity to get acquainted with the results of the manuscript[5] before publication. We are also grateful to Prof. V. G. Bar'yakhtar for the interest to the work and useful comments.

*)E-mail: malyshen@ukrpack.net; vloktev@bitp.kiev.ua

1)We cannot exclude another possibility, when, for example, due to the high defect concentration, the internal stresses govern the local equilibrium orientation of AFM vector. After the magnetic field is removed, this vector reverts to the initial state or to the nearest easy direction. On the other hand, observations[5] point to the regular DS rather than to the stochastic.

2)We don't distinguish between the states with 1 and $-1$. Besides these three directions are usually provided by hexagonal anisotropy, as it was suggested in Ref. 4: but in rhombohedral AFM this anisotropy can be also caused by the difference in strain components $u_{xz} \cdot u_{yz}$ that results in 60° in-plane anisotropy for **1** vector. In what follows, however, we shall suppose that there is an in-plane magnetic anisotropy which effectively includes both these factors. So, corresponding strain components will be omitted for simplicity.

3)The similar equality holds true for DS corresponding to the so-called intermediate state that exists in the vicinity of the 1st order spin-reorientation phase transition in the easy-axis AFM.[3]

4)It is easy to check that another solution of (7) and (8) with $\Psi_{\text{eff}} = \pi/2$ is energetically unfavorable.

5)We suppose that the change of the DS proceeds by the growth of the domains of certain type at the expense of others.

[1] M. M. Fartdzinov, Usp. Fiz. Nauk **84**, 611 (1964) [Sov. Phys. Usp. **7**, 853 (1964)].
[2] V. V. Eremenko and N. F. Kharchenko, Sov. Sci. Rev. **A5**, 1 (1984).
[3] V. G. Bar'yakhtar, A. N. Bogdanov, and D. A. Yablonskii, Usp. Fiz. Nauk **156**, 47 (1988) [Sov. Phys. Usp. **31**, 810 (1988)].
[4] A. N. Bogdanov and I. E. Dragunov, Fiz. Nizk. Temp. **24**, 1136 (1998) [Low Temp. Phys. **24**, 852 (1998)].
[5] V. M. Kalita, A. F. Lozenko, S. M. Ryabchenko, and P. A. Trotsenko, Ukr. Fiz. Zh. **43**, 1469 (1998).
[6] K. Wilkinson, J. W. Cable, E. O. Wollan, and W. C. Koehler, Phys. Rev. **113**, 497 (1959).
[7] A. F. Lozenko, P. E. Parkhomchuk, S. M. Ryabchenko, and P. A. Trotsenko, Fiz. Nizk. Temp. **14**, 941 (1988) [Sov. J. Low Temp. Phys. **14**, 317 (1988)].
[8] K. Otsuka, C. M. Wayman, K. Nakai, H. Sakamoto, and K. Shimizu, Acta Metall. **24**, 207 (1976).
[9] E. A. Turov, *Physical Properties of Magnetically Ordered Crystals*, Ed. AN SSSR, Moscow (1963).
[10] S. V. Maleev, JETP Lett. **68**, 71 (1998).
[11] A. S. Borovik-Romanov and E. G. Rudashevskii, Zh. Éksp. Teor. Fiz. **47**, 2095 (1964) [Sov. Phys. JETP **20**, 1407 (1965)].
[12] E. A. Turov and V. G. Shavrov, Fiz. Tverd. Tela **7**, 217 (1965) [Sov. Phys. Solid State **7**, 166 (1965)].
[13] A. V. Andrienko and L. A. Proeorova, Zh. Éksp. Teor. Fiz. **74**, 1527 (1978) [Sov. Phys. JETP **47**, 798 (1978)].
[14] V. V. Gann and A. I. Zhukov, Fiz. Tverd. Tela **24**, 2799 (1982) [Sov. Phys. Solid State **24**, 1584 (1982)].
[15] B. A. Ivanov and G. K. Oksyuk, Nonlinear Dynamics of the Weak Antiferromagnets, Preprint ITPh, ITF-84-8P, Kiev (1984).
[16] V. A. Loktev and Yu. B. Gaididei, Fiz. Nizk. Temp. **9**, 204 (1983) [Sov. J. Low Temp. Phys. **9**, 104 (1983)].

This article was published in English in the original Russian journal. It was edited by R. T. Beyer.

## ELECTRONIC PROPERTIES OF METALS AND ALLOYS

# Orientational effect in ultrasonic attenuation in metals under the conditions of magnetoacoustic resonance

A. V. Yeremenko, O. V. Kirichenko, and V. G. Peschanskiĭ*)

*B. Verkin Institute for Low Temperature Physics and Engineering, National Academy of Sciences of the Ukraine, 310164 Kharkov, Ukraine*

(Submitted January 5, 1999; revised March 2, 1999)
Fiz. Nizk. Temp. **25**, 708–711 (July 1999)

Ultrasonic absorption in metals (degenerate conductors) in a strong magnetic field is investigated theoretically. Peculiarities in the orientational magnetoacoustic resonance are discovered and compared with the known Reneker tilt effect. Special role of open Fermi surfaces is emphasized. © *1999 American Institute of Physics.* [S1063-777X(99)00907-X]

Absorption of ultrasonic waves in conducting media in a strong magnetic field **H** is of the resonance type if the radius of curvature $r$ of the trajectory of charge carriers is much smaller than their mean free path $l$, but exceeds significantly the acoustic wavelength $1/k$. Magnetoacoustic resonance in metals is connected with a drift of charge carriers along the acoustic wave vector **k** for

$$kl \gg kr \gg 1. \tag{1}$$

Charge carriers that move for a long time in phase with the acoustic wave interact effectively with its field. The region of effective interaction in the magnetic field is concentrated near the turning point on the electron orbit, where $\mathbf{k}\cdot\mathbf{v}=0$. The number of wavelengths over which the electron drifted along the wave vector to meet the wave at the same phase at the turning point is immaterial. Consequently, the condition of resonant interaction or charge carriers with the wave has the form

$$(\mathbf{k}\cdot\overline{\mathbf{v}}-\omega)T=2\pi n, \quad n=0,1,2,3, \tag{2}$$

where $T=2\pi/\Omega=2\pi m^*c/eH$ is the period of motion of a charge in the magnetic field, $e$, **v**, and $m^*$ are the charge, velocity, and cyclotron effective mass of electron in vacuum; the bar over the letter indicates averaging over the time $T$.

As a rule, the frequency $\omega$ of the acoustic wave is much smaller than the collision frequency $1/\tau$ of charge carriers and naturally much smaller than the frequency $\Omega$ of electron rotation in a strong magnetic field ($\Omega\tau \gg 1$) so that the quantity $\omega T$ for a nonzero $n$ can be disregarded in the resonant condition (2). In this case, the resonance is manifested most strongly when conduction electrons drift along **k** in open trajectories for $\mathbf{H}\perp\mathbf{k}$,[1] and charge carriers belonging to the entire layer of open cross sections of the Fermi surface $\varepsilon(\mathbf{p})=\varepsilon_F$ by the plane $p_H=\mathbf{p}\cdot\mathbf{H}/H=\text{const}$ participate in the formation of resonant peaks in the dependence of the damping decrement of acoustic waves on the magnitude of the magnetic field.

Resonance is observed for values of magnetic field, for which the drift along **k** over the time $T$, i.e.,

$$\mathbf{k}\cdot\overline{\mathbf{v}}T/k=\int_0^T dt\,\mathbf{k}\cdot\overline{\mathbf{v}}(t)/k=cP_0\sin\varphi/eH \tag{3}$$

is multiple to the acoustic wavelength: $\mathbf{k}\cdot\overline{\mathbf{v}}T/k=2\pi n$. Here $P_0$ is the period of the Fermi surface along the direction $p_x$ of its ''openness,'' i.e., the direction of drift of charge carriers along the trajectory in the momentum space $p_H=\text{const}$, and $\varphi$ is the angle between the $x$-axis and the acoustic wave vector.

For $kr \gg 1$, attenuation of acoustic waves in metals is mainly associated with electron viscosity and is determined by the deformation mechanism of dissipation.[2] Damping decrement for acoustic waves, i.e.,

$$\Gamma=Q/\rho\dot{u}^2 s \tag{4}$$

can be easily found from the dissipative function $Q$ determined by the nonequilibrium distribution function for charge carriers in a reference frame moving with the deformed crystal lattice with velocity $\dot{u}$. Here $\rho$ is the crystal density, $s$ the velocity of sound, and $u$ the displacement of ions under the action of deformation.

The solution of the kinetic equation for the charge carrier distribution function $f=f_0[\varepsilon(\mathbf{p})+i\omega\mathbf{p}\cdot\mathbf{u}]-\psi\partial f_0/\partial\varepsilon$ linearized in a weak perturbation of conduction electrons, i.e.,

$$\mathbf{v}\frac{\partial\psi}{\partial\mathbf{r}}+\frac{\partial\psi}{\partial t}+\left(\frac{1}{\tau}-i\omega\right)\psi=g \tag{5}$$

allows us to write the dissipative function in the form

$$Q=\int\frac{2d^3p}{(2\pi h)^3}\,\delta[\varepsilon(\mathbf{p})-\varepsilon_F]\psi\psi^*/\tau=\langle\psi\psi^*/\tau\rangle. \tag{6}$$

The collision operator in Eq. (5) is taken in the approximation of the relaxation time $\tau$ of charge carriers, $f_0$ is the equilibrium Fermi function of the conduction electron distribution, and

$$g=-i\omega\Lambda_{ij}(\mathbf{p})u_{ij}e\tilde{\mathbf{E}}\cdot\mathbf{v}. \tag{7}$$

 

The time $t$ determines the position of a charge on its trajectory in a magnetic field in accordance with the equation of motion

$$\frac{\partial \mathbf{p}}{\partial t} = \frac{e}{c}[\mathbf{v} \times \mathbf{H}]. \tag{8}$$

The renormalization of the energy spectrum of charge carriers under the action of crystal deformation, i.e.,

$$\delta\varepsilon = \lambda_{ij}(\mathbf{p}) u_{ij} \tag{9}$$

is contained in the kinetic equation in the form taking into account the conservation of charge carriers, namely,

$$\Lambda_{ik}(\mathbf{p}) = \lambda_{ik}(\mathbf{p}) - \langle \lambda_{ik}(\mathbf{p}) \rangle / \langle 1 \rangle. \tag{10}$$

Here $\lambda_{ij}(\mathbf{p})$ are the tensor components of the deformation potential, and the electric field

$$\tilde{\mathbf{E}} = \mathbf{E} - \frac{i\omega}{c}[\mathbf{u} \times \mathbf{H}] + \frac{m\mathbf{u}\omega^2}{e}, \tag{11}$$

accompanying the acoustic wave is taken into account in a reference frame moving with the vibrating crystal lattice.

Using relations (4)–(9), we can easily find the damping decrement of acoustic waves:

$$\Gamma(H) = \Gamma_0 \frac{r}{l} \int \frac{dp_H / p_F}{\cosh T/\tau - \cos(\mathbf{k} \cdot \overline{\mathbf{v}} T - \omega T)}. \tag{12}$$

Here $p_F$ is the characteristic Fermi momentum and $\Gamma_0 = \omega / v$ is the absorption coefficient of sound in zero magnetic field. In formula (12), we have omitted insignificant numerical factors of the order of unity as well as small corrections oscillating with $1/H$ and proportional to $(kr)^{-1/2}$.[3–6]

It follows from formula (3) that the drift of charge carriers along $\mathbf{k}$ over a period of motion in an open orbit in a plane orthogonal to the magnetic field is the same for all conduction electrons in the entire layer of open cross sections of the Fermi surface by the plane $p_H = \mathbf{p} \cdot \mathbf{H}/H$. According to formula (12), all charge carriers belonging to the layer of open cross sections of the Fermi surface for $\omega T \ll 1$ participate in the formation of a resonant peak of absorption of acoustic energy of height $\Gamma_0 l/r$ for

$$H_n = \frac{kcP_0 \sin\varphi}{2\pi ne}. \tag{13}$$

It should be borne in mind that this result is valid for a sufficiently wide layer of open electron trajectories, for which the contribution of charge carriers with open cross sections of the Fermi surface close to a self-intersecting orbit to acoustic energy absorption is negligibly small. The period of motion of charge carriers in a magnetic field increases unlimitedly as we approach the boundary self-intersecting cross sections of the Fermi surface, which separate the layer of open cross sections from closed electron orbits, attaining the minimum value somewhere inside this layer. Consequently, the function $T(p_H)$ always has at least one extremum (minimum $T_{\min}$). The divergence of $T(p_H)$ near a self-intersecting orbit is logarithmic, and hence the number of charge carriers for which $\omega T \geqslant 1$ is proportional to $\exp(-1/\omega T_{\min})$ for $\omega T_{\min} \ll 1$, and their contribution to the acoustic damping decrement is negligibly small. If the layer of open cross sections of the Fermi surface is narrow, i.e., the separation between self-intersecting orbits is rather small, the condition $\omega T \ll 1$ cannot be satisfied even for quite large values of magnetic field. In this case, the contribution of acoustic waves to damping comes mainly from charge carriers with close orbits.

For certain orientations of the wave vector, for which $\sin\varphi$ is of the same order of magnitude as the ratio of the velocity of sound $s = \omega/k$ to the Fermi velocity of conduction electrons, an absorption peak is observed for $n = 0$. This peak is of the same origin as the abrupt increase in the damping of sound in the absence of open cross sections of the Fermi surface in a strong magnetic field ($kr \ll 1$), which takes place when the vectors $\mathbf{H}$ and $\mathbf{k}$ deviate from orthogonality through a small angle $\theta$ of the order of the ratio of the velocity of sound $s$ to the extremal value of the drift velocity $\overline{v}_H$ of charge carriers along the magnetic field (tilting effect).[7–10]

In contrast to resonant absorption of acoustic energy for $n$ differing from zero, the zero line of absorption (peak at $n = 0$) is possible when the drift velocity of charge carriers coincides with the velocity of sound. Its position does not depend on the magnetic field and is determined only by the orientation of the acoustic wave vector relative to the magnetic field and the direction of charge carrier drift in open trajectories. In this case, the distance at which the amplitude of acoustic vibrations decreases by a factor of $e$ (and equal to $1/\Gamma$) is the same as for $H = H_n$.

When the orthogonality of the vectors $\mathbf{H}$ and $\mathbf{k}$ is violated, the condition of resonant interaction of conduction electrons with the acoustic wave assumes the form

$$\frac{c}{eH}\left( kP_0 \sin\varphi + k\frac{\partial S}{\partial p_H}\sin\theta - 2\pi m^* \omega \right) = 2\pi n, \tag{14}$$

where $S$ is the area of the cross section of the Fermi surface by the plane $p_H = \text{const}$.

For $kr \sin\theta \ll 1$ and $\omega T \ll 1$, the last two terms in formula (14) are small, and their inclusion does not affect significantly the shape of resonant curves in the energy absorption of acoustic waves with $n$ differing from zero. However, the height of absorption peaks decreases sharply for $kr \sin\theta \geqslant 1$. In the case when $\partial S/\partial p_H$ has an extremum at the Fermi surface, the peak height has the form

$$\Gamma_{\text{res}} = \frac{\Gamma_0 l/r}{(kl\sin\theta)^{1/2}}. \tag{15}$$

for

$$H_n = \frac{kc}{2\pi ne}\left( P_0 \sin\varphi + \frac{\partial S}{\partial p_H^0}\sin\theta \right). \tag{16}$$

This absorption peak is formed by a small fraction of electrons from the neighborhood of $p_H = p_H^0$, where the displacement of electrons over a period along the magnetic field has an extremum, i.e.,

$$\left.\frac{\partial^2 S}{\partial p_H^2}\right|_{p_H = p_H^0} = 0. \tag{17}$$

If $\partial^2 S/\partial p_H^2$ does not vanish anywhere and is bounded everywhere on the Fermi surface, the absorption coefficient for acoustic energy has the same form for $kr \sin\theta \geqslant 1$

$$\Gamma = \frac{\Gamma_0}{kr \sin\theta} \tag{18}$$

in the absence of open cross sections of the Fermi surface as well as in the presence of such cross sections for any orientation of charge carrier drift in a plane orthogonal to the magnetic field. A considerable decrease in the height of the resonant peak is due to the fact that the variation of $\theta$ ''shifts,'' the role of effective charge carriers from one type to another.

For $\omega\tau \geqslant 1$, the last term in formula (14) cannot be disregarded any longer. If the charge carrier drift along the wave vector **k** is associated only with the presence of open cross sections of the Fermi surface for a given orientation of magnetic field, i.e., for $\theta = 0$, the absorption peak is displaced and is observed for

$$H_n = \frac{kc}{2\pi ne}(P_0 \sin\varphi - 2\pi m_0 s), \tag{19}$$

where $m_0$ is the extremal effective mass of charge carriers, and the height $\Gamma$ of the peak decreases with increasing $\omega\tau$ by a factor of $(\omega\tau)^{1/2}$.

If the cyclotron effective mass has not one but several extrema, the number of acoustic energy absorption peaks decreases in the same proportion.

An orientational acoustic energy absorption peak independent of the magnitude of the magnetic field is observed when conduction electrons do not lead the acoustic wave, and their drift velocity along **k** is equal to the velocity of sound. When the orthogonality of the vectors **k** and **H** is violated, the resonant peak for $n = 0$ is formed by charge carriers corresponding to the extremal values of the quantity $(\partial s/\partial p_H)\sin\theta - 2\pi m^* s$, i.e., satisfying the condition

$$\frac{\partial^2 S}{\partial p_H^2}\sin\theta - s\frac{\partial^2 S}{\partial p_H \partial \varepsilon} = 0. \tag{20}$$

Thus, the height and position of resonant peaks of acoustic energy absorption by charge carriers in metals and degenerate conductors are very sensitive to the orientation of magnetic field and acoustic wave vector.

Magnetoacoustic effects sensitive to the shape of the Fermi surface[1,3,4,7] were successfully used as a reliable spectroscopic method for studying the electron energy spectrum of metals. The aim of this communication is to emphasize once again the potentialities of this method, which makes it possible to obtain additional information on the spectrum of charge carriers in metals and conductors with metal-type conductivity (in particular, to analyze in detail the effective masses of electrons with open trajectories in the momentum space).

This research was partly supported by the NATO scientific program (Grant CRG.CRGP 972846).

*)E-mail: vpeschansky@ilt.kharkov.ua

[1] E. A. Kaner, V. G. Peschansky, and I. A. Privorotskii, Zh. Éksp. Teor. Fiz. **40**, 214 (1961) [Sov. Phys. JETP **13**, 147 (1961).
[2] A. I. Akhiezer, Zh. Éksp. Teor. Fiz. **8**, 1330 (1938).
[3] A. B. Pippard, Philos. Mag. **2**, 1147 (1957).
[4] V. L. Gurevich, Zh. Éksp. Teor. Fiz. **37**, 71 (1960) [Sov. Phys. JETP **10**, 51 (1960).
[5] V. M. Gokhfeld and V. G. Peschansky, Sov. Sci. Rev. Phys. **A17**, 1 (1993).
[6] E. A. Kaner and F. Peres Rodrigues, Fiz. Nizk. Temp. **14**, 39 (1988) [Sov. J. Low Temp. Phys. **14**, 21 (1988).
[7] D. H. Reneker, Phys. Rev. **115**, 303 (1959).
[8] E. A. Kaner, L. B. Chebotarev, and A. V. Yeremenko, Zh. Éksp. Teor. Fiz. **80**, 1058 (1981) [Sov. Phys. JETP **53**, 540 (1981).
[9] A. M. Grishin, V. G. Skobov, L. M. Fisher, and A. S. Chernov, JETP Lett. **35**, 455 (1982).
[10] V. M. Kontorovich, Usp. Fiz. Nauk **142**, 265 (1984) [Sov. Phys. Usp. **27**, 134 (1984)].

Translated by R. S. Wadhwa

# Bifurcations and a chaos strip in states of long Josephson junctions

K. N. Yugay, N. V. Blinov, and I. V. Shirokov

*Omsk State University, 55a Mira Ave., 644077, Omsk, Russia*
(Submitted January 6, 1999)
Fiz. Nizk. Temp. **25**, 712–717 (July 1999)

Stationary and nonstationary, in particular, chaotic states in long Josephson junctions are investigated. Bifurcation lines on the parametric bias current-external magnetic field plane are calculated. The chaos strip along the bifurcation line is observed. It is shown that transitions between stationary states are the transitions from metastable to stable states and that the thermodynamical Gibbs potential of these stable states may be larger than for some metastable states. The definition of a dynamical critical magnetic field characterizing the stability of the stationary states is given. 
[S1063-777X(99)01007-5]

## INTRODUCTION

Dynamical chaos in long Josephson junctions is of great interest because it can be a source of a dynamical noise in devices based on them, in particular, in SQUIDs, limiting the sensitivity of these devices. Furthermore, dynamical chaos in long Josephson junctions (LJJ) is a very interesting physical phenomenon taking place in nonlinear systems in the absence of an external stochastic force.[1–9] Dynamical chaos in a LJJ is easily excited and therefore it may also be investigated experimentally rather easily.[10,11]

In our previous works[12,13] we have shown that among a set of solutions of the Ferrell–Prange equation describing stationary states of the LJJ in an external magnetic field[14] are both stable and unstable ones. At the same time, these stationary states are asymptotic solutions of the nonstationary sine-Gordon equation and we have also shown that a selection of the stable solutions can be governed by a rapid damping in time of the initial perturbation entering into the nonstationary sine-Gordon equation through the boundary conditions. Changing the intensity of this perturbation at fixed shape, we can obtain various stationary states for the LJJ without a bias current or three clusters of states (stationary, and time dependent regular and chaotic) in the presence of a bias current. It turned out that asymptotic states are very sensitive to an external perturbation, its value and shape define the state (stationary, regular or chaotic) to which the system will tend at $t\to\infty$ (we have called this influence on the selection of asymptotic states of the small rapidly damping initial perturbation in time an effect of memory). The fact of coexistence of all these three characteristic asymptotic states selected only by the form of the initial perturbation seems to be astonishing. It is evidently enough that the Ferrell–Prange equation will not have solutions at a large bias current $\beta$. Therefore the question arises: at which values of $\beta$ do stationary states of a LJJ disappear or what will be a boundary in the parametric $\beta$-$H_0$ plane ($H_0$ is an external magnetic field) that separates this plane on the regions where stationary states do and do not exist? Since the number of solutions of the Ferrell–Prange equation changes at variation of the parameters $(H_0,\beta)$, another question arises: what is the form of bifurcation lines in the plane $\beta-H_0$ that separate the parametric plane on the regions with a different number of stationary solutions of the Ferrell–Prange equation?

The existence of several stable solutions of the Ferrell–Prange equation is equivalent to the fact that thermodynamical Gibbs potential $G$ associated with the distribution of the magnetic field along the junction has minima, and each minimum corresponds to a certain solution of the Ferrell–Prange equation. Does a global minimum of $G$ correspond to the most stable state (e.g., in the Lyapunov sense)? In the case of the junction of the finite length both Meissner and one-fluxon states are thermodynamically advantageous simultaneously, so it is interesting to investigate dynamical properties of these states. Answering this question, we introduce a dynamical critical field that describes the stability characteristic of the junctions.

In Sec. 1 bifurcation lines on the parametric $\beta-H_0$ plane are calculated. In Sec. 2 the definition of the dynamical critical magnetic field is given and the dependence of this field on $\beta$ and the length of the junction $L$ is calculated. In Sec. 3 transitions between states are described. It is shown in Sec. 4 that a chaos strip arises along the bifurcation line on the parametric $\beta-H_0$ plane. The last Sec. 5 contains the discussion of our calculation and brief conclusions.

### 1. Bifurcation lines

Stationary states of a LJJ are investigated using the numerical integration of the Ferrell–Prange equation:

$$\varphi_{xx}(x)=\sin\varphi(x)-\beta, \tag{1}$$

where $\varphi(x)$ is the stationary Josephson phase variable, $\beta$ is the dc bias current density normalized to the critical current $j_c$, $x$ is the distance along the junction normalized to the Josephson penetration length $\lambda_J=\sqrt{C\Phi_0/8\pi^2 j_c d}$, $\Phi_0$ is the flux quantum, $d=2\lambda_L+b$, $\lambda_L$ is the London penetration length, $b$ is the thickness of the dielectric barrier. The boundary conditions for Eq. (1) have the form

$$\varphi_x(x)\big|_{x=0}=\varphi_x(x)\big|_{x=L}=H_0, \tag{2}$$

 

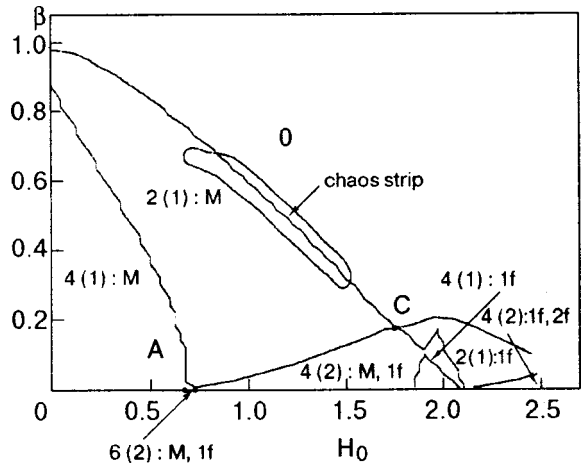


FIG. 1. Bifurcation lines. The number of solutions of the Ferrell–Prange equation (1)–(2) are pointed out. The number of stable states is indicated in brackets. $M$ denotes a stable Meissner state and $1f$ denotes a stable one-fluxon state $L=5$.

where $L$ is the total length of the junction normalized to $\lambda_J$ and $H_0$ is the external magnetic field perpendicular to the junction and normalized to $\tilde{H}=\Phi_0/2\pi\lambda_J d$.

Numerical integration of Eqs. (1)–(2) allows us to find the regions with a certain number of solutions on the parametric $\beta-H_0$ plane (Fig. 1). It is easy to show that the set of points corresponding to the even number of solutions forms two-dimensional domains on this plane, whereas the set corresponding to the odd ones may form just one-dimensional curves. Mostly, the lines corresponding to the odd number of the solutions of the Ferrell–Prange boundary problem coincide with the bifurcation lines. Using the shooting method for solving of the boundary problem one can prove that the $2\pi$-periodicity of the function $H(\varphi_0)$ expressing the dependence of the magnetic field at the right side of the junction $(x=L)$ on the phase taken at the left side $(x=0)$ results in the appearing of the odd number of solutions only when the $H(\varphi_0)$ touches the line $H=H_0$ in an extreme point, i.e., $\partial H(\varphi_0)/\partial\varphi_0=0$. As an illustration, we have plotted in Fig. 2

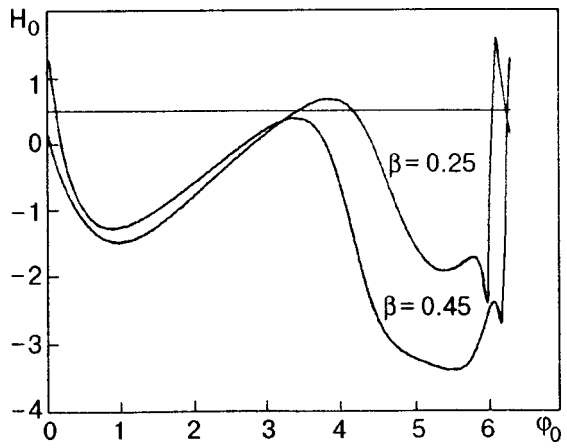


FIG. 2. Dependence of the magnetic field at $x=L$ on the phase taken at the left side of junction $x=0$ at $H_0=0.5$, $L=5$, $\beta=0.25$ and $\beta=0.45$.

the function $H(\varphi_0)$ at $H_0=0.5$, $L=5$, $\beta=0.25$ and $\beta=0.45$.

Boundaries between the regions—bifurcation lines—define an essential modification of the system. The bifurcation lines in Fig. 1 are obtained for $L=5$; here a step by $\beta$ is equal to $5\cdot10^{-3}$ and a step by $H_0$ is equal to $2.5\cdot10^{-3}$. In this figure the numbers of solutions of Eq. (1)–(2) are pointed out, the numbers of stable solutions are given in the brackets, while $M$ and $1f$ denote a stable Meissner and one-fluxon states, respectively. It is seen that a Meissner state is stable at small values of $H_0$ and at large values of $H_0$ a one fluxon state is stable. It should be noted that the region where there are no stationary solutions (region 0) bounds with the region having a minimum of stationary solutions, being equal to 2 (region 2). In approaching the boundary of region 0 and 2 the number of stationary solutions decreases: $6\rightarrow4\rightarrow2\rightarrow0$, on the other hand, a number of nonstationary states which are the asymptotic solutions of the sine-Gordon equation, increases. Our calculations have shown that one of two stationary solutions in region 2 is stable, and another is unstable (metastable). We noted earlier[12] that the stable states are symmetrical. The presence of bias current $\beta$ leads to a symmetry violation that results, evidently, in the instability of the states.

The problem of the stability of stationary states $\varphi(x)$ was solved in the following way:[13] the sine-Gordon equation was linearized in the vicinity of stationary solution: $\varphi(x,t)=\varphi(x)+\theta(x,t)$, where $\theta(x,t)$ is the infinitesimal perturbation. The equation for $\theta(x,t)$—the linearized sine-Gordon equation—we can solve by means of the expansion of this function in terms of a complete system of eigenfunctions of the Schrödinger operator with potential $\cos[\varphi(x)]$:

$$\theta(x,t)=\sum_n e^{\lambda_n t}u_n(x), \tag{3}$$

where $u_n(x)$ are eigenfunctions of the Schrödinger operator of the problem:

$$-u_{xx}(x)+u(x)\cos\varphi(x)=Eu(x), \tag{4}$$

$$u_x(x)|_{x=0}=u_x(x)|_{x=L}=0,$$

and

$$\lambda_n=-\gamma\pm\sqrt{\gamma^2-E_n}, \tag{5}$$

where $\gamma$ is the dissipative coefficient in the sine-Gordon equation. We note that values of $\lambda$ coincide with corresponding values of Lyapunov exponents in the case when perturbations are considered with respect to the stationary solutions. In the general case, Lyapunov exponents are calculated in the same way as in Ref. 13. Thus, in the presence of a bias current we have the different picture of a LJJ states than at $\beta=0$ (this case has been examined in Ref. 12). For example, at $H_0=1.9$ the increasing of $\beta$ from 0 to 0.22 leads to the changing of the stationary states number $6\rightarrow4\rightarrow2\rightarrow0$, i.e., to a consecutive losing of the stationary solutions. Simultaneously, an increasing of the number of nonstationary states occurs that we found by directly solving the nonstationary sine-Gordon equation.

### 2. Dynamic critical field

In the literature the critical magnetic field $H_{c1}$ in a LJJ is defined as a field value, at which an existence of a Josephson vortex (fluxon, soliton) becomes advantageous thermodynamically for the first time (see, for example, Refs. 10 and 11). In the case of an infinitely long junction the critical field is $H_{c1}(\infty)=4/\pi=1.274$. Essentially, this field corresponds to the global minimum of the thermodynamic Gibbs potential for the one-fluxon state. However, in a junction of finite length there are some local minima that coexist with the global one and every minimum corresponds to the solution of Eqs. (1)–(2). Some of these solutions are stable, another unstable in the sense discussed in Sec. 1.

We write down the thermodynamic Gibbs potential in the form

$$G=\int_0^L dx\left[\frac{1}{2}\varphi_x^2(x)+1-\cos\varphi(x)-\beta\varphi(x)-H_0\varphi_x(x)\right]. \tag{6}$$

Here $G$ is the thermodynamic Gibbs potential per unit length along an external magnetic field and normalized to $\tilde{G}=\Phi_0/16\pi^3\lambda_j d$. The Ferrell–Prange equation is an extremal of the functional (6). An investigation of the second variation of $G$ shows that all extrema of this functional satisfy to the necessary and sufficient conditions of a strong minimum.[15] Thus, all solutions of Eqs. (1)–(2) (both stable and unstable ones) correspond to minima of the thermodynamic Gibbs potential; one of them is global, the others are local. Our calculations of the thermodynamic Gibbs potential (6) show that, for example, at $\beta=0$, $L=5$ and $H_0=0.67$ the Meissner state has a global minimum ($G_M=-0.44$), but the stable one-fluxon state has a local one ($G_{1f}=4.03$). The one-fluxon state has a global minimum of $G$ starting at $H_0=1.57$ ($G_{1f}=-2.582$) and at the same value of $\beta$ and $L$. At this value of $H_0$ a Meissner state has a local minimum $G_M=-2.58$. At $H_0\geqslant 2.09$ the Meissner state disappears. Thus, at a field less than the critical one $H_{c1}$, the stable one-fluxon state exists. We shall further call the minimum value of a magnetic field at given $L$ and $\beta$, at which the stable one-fluxon state appears for the first time and which corresponds to the local minimum of the thermodynamic Gibbs potential as the dynamical critical field $H_{dc}$. It is interesting that the dynamical critical field $H_{dc}$ makes up on the parametric plane a line that coincides with the bifurcation line *BC* (see Fig. 1). Our calculations show that the bias current increases the dynamical critical field $H_{dc}$. Evidently, it is connected with a symmetry violation of a state by the bias current $\beta$. In Fig. 3 two stable one-fluxon states at $\beta=0$ and $\beta=0.1$ ($L=5, H_0=1.4$) are shown. It is seen that the state with $\beta=0.1$ is asymmetric. The dynamical critical field at $L=5$ are $H_{dc}=0.67$ at $\beta=0$ and $H_{dc}=1.4$ at $\beta=0.1$. Upon increasing $L$ the value of $H_{dc}$ is changed ($\beta=0$): $H_{dc}(L=5)=0.66$, $H_{dc}(L=6)=0.4$, $H_{dc}(L=7)=0.26$, $H_{dc}(L=8)=0.15$, $H_{dc}(L=10)=0.06$, i.e. the $H_{dc}$ decreases. In this case the critical field $H_{c1}$ has the values: $H_{c1}(L=5)=1.57$, $H_{c1}(L=6)=1.45$, $H_{c1}(L=7)=1.38$, $H_{c1}(L=8)=1.34$, $H_{c1}(L=10)=1.28$, i.e., the $H_{c1}$ decreases also approaching to the value of $H_{c1}(L=\infty)=1.274$.

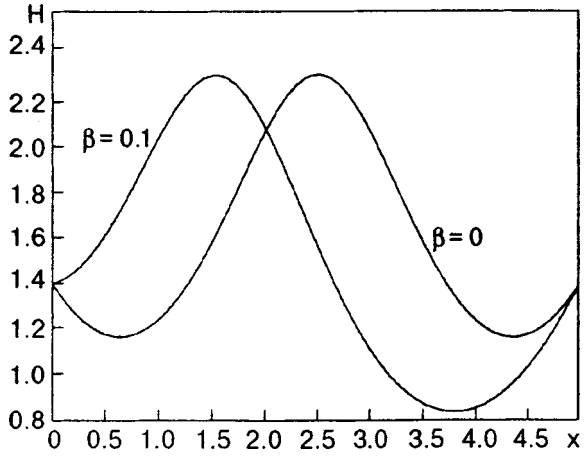


FIG. 3. One-fluxon states at $H_0=1.4$ and $L=5$ for $\beta=0$ and $\beta=0.1$.

### 3. Transitions between states

As it has been shown in the previous section, every stationary state of LJJ, i.e., the solution of Eqs. (1)–(2), corresponds to a minimum of the thermodynamic Gibbs potential and these minima are not equivalent with respect to the problem of instability. For example, in Fig. 4 stationary states of LJJ at $H_0=2.035$, $\beta=0.001$ and $L=5$ are shown. The values of the Gibbs potential calculated using Eq. (6) are as follows: $G_1=-5.03$, $G_2=-4.52$, $G_3=-4.61$, $G_4=-4.64$, $G_5=-4.61$, $G_6=-6.7$. States 4 (Meissner) and 6 (one-fluxon) are stable, the other ones are metastable. It should be noted that unstable state 1 corresponds to deeper minimum than the stable state 4. This property contradicts the naive idea that more stable states occur at deeper minima. Now we shall consider this question in detail.

The sine-Gordon equation with dissipation and bias current describing an evolution of the initial state has the form:

$$\varphi_{tt}(x,t)+2\gamma\varphi_t(x,t)-\varphi_{xx}(x,t)=-\sin\varphi(x,t)+\beta, \tag{7}$$

where $t$ is a time normalized to the inverse of the Josephson plasma frequency $\omega_J=\sqrt{2\pi c j_c/C\Phi_0}$, $C$ is the junction capacitance per unit area, $\gamma=\Phi_0\omega_J/4\pi cRj_c$ is the dissipative

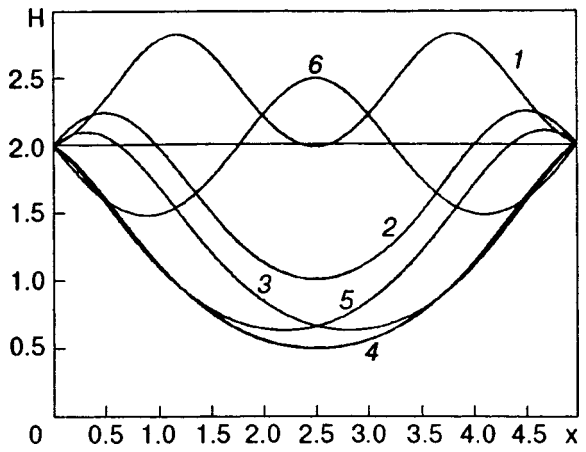


FIG. 4. Stationary states of LJJ at $H_0=2.035$, $\beta=0.001$ and $L=5$. States *1, 2, 3, 5* are unstable, states *4* and *6* are stable.

TABLE I. Transitions between states.

| Number of State | Stability | G | Transitions $m\to n$ | Sort of Stable States |
|---|---|---|---|---|
| 1 | unstable | 2.34 | 1→10 | |
| 2 | unstable | 2.78 | 2→8 | |
| 3 | unstable | 0.64 | 3→8 | |
| 4 | unstable | 14.69 | 4→10 | |
| 5 | unstable | 14.98 | 5→10 | |
| 6 | unstable | 14.69 | 6→10 | |
| 7 | unstable | 13.53 | 7→10 | |
| 8 | stable | −1.42 | 8→8 | Meissner |
| 9 | unstable | 0.64 | 9→8 | |
| 10 | stable | −0.44 | 10→10 | 1 fluxon |
| 11 | unstable | 2.34 | 11→10 | |
| 12 | stable | 2.29 | 12→12 | 2 fluxon |

coefficient per unit area, $R$ is the resistance of junction per unit area. We write down the boundary conditions for Eq. (7) in the form

$$\varphi_x(x,t)_{x=0}\equiv H(0,t)=\varphi_x(x,t)\big|_{x=L}\equiv H(L,t)$$
$$=H_0(1-a\mathrm{e}^{-t/2t_0}\cos 0{,}5t). \qquad (8)$$

The integration of Eqs. (7)–(8) for $H_0=2.035$, $\beta=0.001$, $L=5$ (the same as in Fig. 4) and $\gamma=0.26$ gives: the metastable state 1 passes to the stable state 6 at any values of perturbation parameter $a$, 2→4 at $a=0$, 2→6 at $a=1$, 3→4 at $a=0.05$, 3→6 at $a=0.07$, 4→6 at $a=0.5$ and so on. Every transition from the metastable state to the stable one, $m\to n$, is a transition from the state with the certain value of local minimum $G_m$ to another state with smaller value of minimum $G_n$. These transitions $m\to n$ with $G_m>G_n$ are realized by certain values of the parameter of the initial perturbation $a$ in expression (8). One can say that the local minima of $G_l$ are connected with each other by a certain disintegration channel along the coordinate $a$. From this point of view one can say also that stationary states contain a specific ''latent'' parameter, by which a connection with different local minima $G_l$ may be realized. In particular, the perturbation parameter $a$ appears here as a ''latent'' parameter. It is possible, there are several ''latent'' parameters connecting the stationary states. One of the most important characteristics of ''latent'' parameters is that the stationary state does not depend on them directly; however, the form of the asymptotic state and the rate of disintegration depend essentially on them. The presence of a ''latent'' parameter apparently explains, a nonequivalence of the different local minima with respect to the stability, especially in the case when a stable local minimum is above a nonstable local one. In Table I results of the integration of Eqs. (1), (2) and the calculation of $G$ for every one of these solutions at $H_0=1.174$, $\beta=0$, $L=8$ are represented. The transitions between states $m\to n$ are defined as follows: the $m$th solution of the stationary Ferrell–Prange equation (1)–(2) was taken as an initial condition of the sine-Gordon Eqs. (7) and (8). If this $m$th state was unstable then it fell into the $n$th stable state.

The scheme of the transitions between states $m\to n$ is represented in Fig. 5. It is seen that $G_m>G_n$ for all the transitions (we note that $G_3$ and $G_9$ for the metastable states *3* and *9* are less than $G_{12}$; the state *12* is stable). The stable states—Meissner, one-fluxon, and two-fluxon—are shown in Fig. 6 at the same parameters as in Fig. 5.

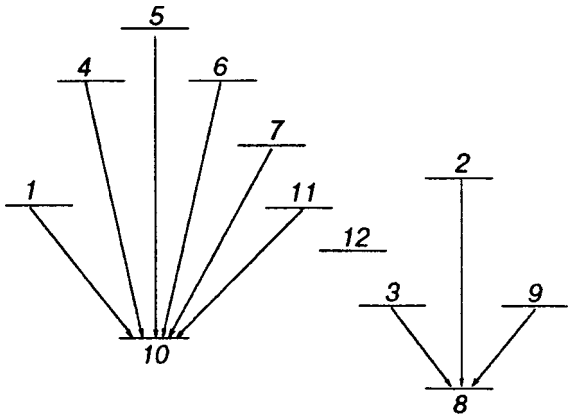


FIG. 5. The scheme of transitions between states $m\to n$. States *8*, *10* and *12* are stable (*8*—Meissner, *10*—one fluxon. *12*—two fluxon), others are unstable. $H_0=1.174$, $L=8$, $\beta=0$.

#### 4. Chaos strip

As we noted above, the number of stationary states decreases with approach to the bifurcation line 0–2, but the number of nonstationary asymptotic states is increased simultaneously. Changing the perturbation parameter $a$ we can obtain three sorts of typical states: stationary, regular and chaotic.[13] These states are distinguished not only by a form of the field distribution in the junction and a variation in time, but also by values of the Lyapunov exponent λ: for the stationary states $\lambda<0$, for the regular states $\lambda\leqslant 0$ and for the chaos states $\lambda>0$. The Lyapunov exponents were calculated in the same way as in Ref. 13. However, as the calculations have shown, chaotic states may be excited not in the whole region 2 (see Fig. 1), but only in the bounded region in close to the bifurcation line 0–2. This region is extended in the form of a narrow strip along the bifurcation line 0–2 approximately from 0.7 to 1.6 in $H_0$ and in the range of 0.002–

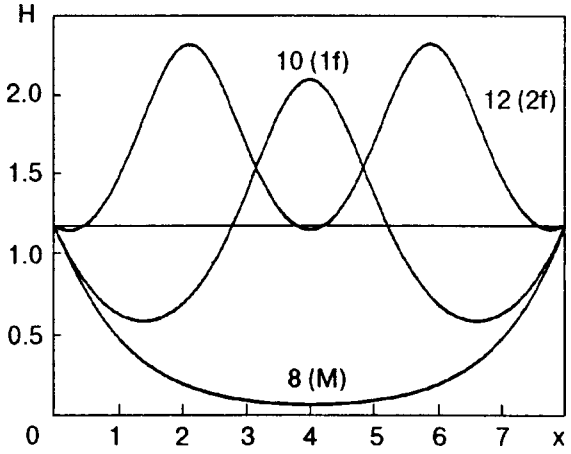


FIG. 6. The stable states: *M*—Meissner, 1*f*—one-fluxon, and 2 *f*—two-fluxon at the same parameters at those in Fig. 5.

0.015 in $\beta$. We note that the chaos strip is arranged mostly under the bifurcation line in the region 2, but not in the region 0, as it may be expected because of all states in the region 0 are nonstationary. The chaos strip is outlined on the parametric $\beta - H_0$ plane in Fig. 1.

This chaos strip along the bifurcation line 0–2 calls to mind (to a certain extent) the separatrix of a nonlinear oscillator, where a chaos motion is observed.

### 5. Discussion and conclusions

In the present work we have shown that the parametric $\beta - H_0$ plane of a LJJ is separated on series of regions with the different number of solutions of the stationary Ferrell–Prange equation. The boundaries between these regions—bifurcation lines—characterize an essential modification of the system. A chaos strip arises along the bifurcation line 0–2. We have found that the chaos strip is arranged in the main below the bifurcation line 0–2, where stationary states take place.

We have introduced the definition of a dynamical critical field as the lowest field at which the one-fluxon state becomes stable for the first time in the Lyapunov sense. In addition, the Meissner state may also be stable at some parameters. Because both the Meissner and the one-fluxon states may be thermodynamically advantageous simultaneously, our definition based on the stability in the Lyapunov sense characterizes an important feature of the stationary states of the LJJ.

We have shown that disintegration of the metastable states and the transition to some stable states $m \rightarrow n$ occur for $G_m > G_n$. A metastable state corresponds to the local minimum of the Gibbs potential, and also this minimum may be lower than this one of a stable state. A nonequivalence of these local minima we explain by means of existing of a ''latent'' parameter not detecting in a stationary state, by which, for example, two local minima may be connected and a channel of the disintegration of the upper state may arise. In our case the perturbation parameter plays a role of a ''latent'' parameter, however, the number of these parameters may be much greater. We note the analogy between the quantum transitions and the transitions mentioned above, although the system is described by the classical Ferrell–Prange and sine-Gordon equations.

We are aware that we could not touch upon all questions concerning the properties of a LJJ. We hope to return to the problems of a LJJ in our next work.

These investigations are supported by the Russian Fund for Fundamental Research (Project No. 96-02-19321).

[1] W. J. Yeh, O. G. Symko, and D. J. Zheng, Phys. Rev. B **42**, 4080 (1990).
[2] N. Gronbech-Jensen, P. S. Lomdahl, and M. R. Samuelsen, Phys. Rev. B **43**, 1279 (1991).
[3] N. Gronbech-Jensen, Phys. Rev. B **45**, 7315 (1992).
[4] G. F. Eriksen and J. B. Hansen, Phys. Rev. B **41**, 4189 (1990).
[5] X. Yao, J. Z. Wu, and C. S. Ting, Phys. Rev. B **42**, 244 (1990).
[6] L. E. Guerrero and M. Ostavio, Physica B **165–166**, 11657 (1990).
[7] I. H. Dalsgaard, A. Larsen, and M. Mygind, Physica B **165–166**, 1661 (1990).
[8] S. Rajasekar and M. Lakshmannn, Physica A **167**, 793 (1990).
[9] S. Rajasekar and M. Lakshmanan, Phys. Lett. A **147**, 264 (1990).
[10] A. Barone and G. Paterno, *Physics and Applications of the Josephson Effect*, Wiley-Interscience, New-York (1982).
[11] K. K. Likharev, Introduction to *Dynamics of Josephson Junctions*, Nauka, Moscow (1985) (in Russian).
[12] K. N. Yugay, N. V. Blinov, and I. V. Shirokov, Phys. Rev. B **49**, 12036 (1994).
[13] K. N. Yugay, N. V. Blinov, and I. V. Shirokov, Phys. Rev. B **51**, 12737 (1995).
[14] C. S. Owen and D. J. Scalapino, Phys. Rev. **164**, 538 (1967).
[15] I. M. Gelfand and S. V. Fomin, *Calculus of Variations*, *Fizmatgiz*, Moscow (1961) (in Russian).

This article was published in English in the original Russian journal. It was edited by R. T. Beyer.

## LOW-DIMENSIONAL AND DISORDERED SYSTEMS

# Helicons and magnetoimpurity waves in layered conductors

V. M. Gvozdikov,*) A. M. Ermolaev, and R. Vega-Monroy

*Department of Physics, Kharkov State University, 310077 Kharkov, Ukraine*
(Submitted January 28, 1999)
Fiz. Nizk. Temp. **25**, 718–724 (July 1999)

It is shown that local electron states, caused by impurities in a layered conductor placed in an external magnetic field, give rise to resonant corrections $\delta\sigma_{\alpha\beta}(\omega)$ to the high-frequency conductivity tensor $\delta\sigma_{\alpha\beta}(\omega)$ of the layers. These corrections appear due to the resonant transitions of electrons between the Landau levels and the local states and change dramatically the spectrum of collective electromagnetic oscillations in the system because of the ''branch crossing'' nearby the frequency $\omega_0$ ($\hbar\omega_0$ is the local state energy). As a result, a new magnetoimpurity wave, $\omega_-(k)$, appears in the spectrum in addition to the helicon mode, $\omega_+(k)$, which is known to exist in a pure layered conductor in a perpendicular magnetic field ($k$ is the wave vector along the magnetic field). In the long wavelength limit, $ka \ll 1$, the helicon-like mode $\omega_+(k)$ has a gap of the order of $\omega_0$, whereas the magnetoimpurity mode in this limit goes to zero $\omega_-(k) \sim (ka)^2$ ($a$ is the distance between adjacent layers). The small damping of these modes due to the broadening of the Landau levels and the magnetoimpurity levels are also calculated.  [S1063-777X(99)01107-X]

### 1. INTRODUCTION

Impurities in metals play a twofold role. First, they decrease the free path of electrons and thereby damp electromagnetic waves.[1,2] On the other hand, impurities may create bound states which result in a dramatic change in the electron energy spectrum and create new electromagnetic modes in conventional metals.

The effect of impurities on the electronic energy spectrum becomes much more pronounced in an external magnetic field which effectively decreases the dimensionality of the system and assists the localization of electrons by attractive impurities. Local and quasi-local magnetoimpurity states (i.e., the ones localized nearby the impurity in an external magnetic field) were studied long ago in conventional metals[3,4] and recently in two-dimensional (2D) conductors.[5]

Impurities break down the spatial homogeneity of a system, they lift up the degeneracy of the electronic energy spectrum on the Landau orbit center position and split off one local state from each Landau level. The magnitude of splitting, $\Delta$, is equal to the energy of a bound state. Thus, a new resonant frequency $\omega_s = \Delta + s\Omega$ ($\Omega = eH/mc$ is the cyclotron frequency and the integer $s = 0,1,...$ numerates the resonances) related to electron transitions between the Landau levels and the magnetoimpurity ones appears in the conductivity tensor $\sigma_{\alpha\beta}(\omega)$ and gives rise to the resonant attenuation of the electromagnetic waves in metals.[5]

The conductivity tensor, as is well known, is the key quantity in the theory of electromagnetic waves in metals; it determines the dispersion of the electromagnetic waves in conventional[1,2] and layered metals[6–13] and superconductors.[14]

The high-frequency conductivity tensor of a 2D electron gas with magnetoimpurity states in quantizing perpendicular magnetic field was calculated in Ref. 5 and we are going to apply in what follows the results of these calculations to studies of magnetoimpurity electromagnetic waves in layered conductors.

Electromagnetic waves in layered conductors and superlattices in a quantizing external magnetic field have been studied in a number of works.[6–13] It was found that a quasi-two-dimensional nature of layered conductors brings some specific features compared to the results obtained for conventional 3D metals. In particular, a new type of spiral waves in layered conductors under the conditions of the quantum Hall effect have been predicted theoretically.[9,11–13] In these works a model for layered electron gas was employed which ignores electron hopping across the layers because the quantum Hall effect takes place in purely 2D systems. Thus, the most interesting case of quasi-two-dimensional behavior of electrons in superlattices corresponds to the model without electron dispersion across the layers. In this model electromagnetic waves can propagate only owing to the interlayer electromagnetic correlations described by the Maxwell's equations. The relationship between the electromagnetic field and the current within the layer is determined by the conductivity tensor which depends on the layer structure and determines the shape of the electromagnetic wave dispersion in layered conductors.

The purpose of the present paper is to calculate the dispersion relation for a new weakly damped electromagnetic wave caused by the resonant transitions between magnetoimpurity levels and the Landau levels in layered conductors in perpendicular to layers quantizing magnetic field.

 

In Sec. 2 we discuss the physics of the high-frequency conductivity in a 2D conductor with magnetoimpurity states. Section 3 is devoted to calculations of the dispersion relations for helicons and magnetoimpurity electromagnetic waves in layered conductors. Summary of the results obtained and the discussion are given in Sec. 4.

## 2. THE CONDUCTIVITY TENSOR IN A 2D CONDUCTOR WITH MAGNETOIMPURITY STATES

The helicons in layered conductors at low temperatures have a dispersion along the magnetic field that is described by the function[9]

$$\omega(k)=\Omega W(ka). \tag{1}$$

It turned out that their damping[15] depends on the wave vector $k$ by dint of the same function $W(ka)$ (see Sec. 3 for details):

$$\gamma(k)=\nu W(ka), \tag{2}$$

where

$$W(ka)=\frac{\sin^2(ka/2)}{(\omega_*/2)^2+\sin^2(ka/2)}. \tag{3}$$

Here $\nu$ is the electronic collision frequency due to impurities and lattice defects; $\omega_*=\omega_p a/c$, $a$ stands for the interlayer spacing; $c$ is the velocity of light and $\omega_p$ is the plasma frequency. We have assumed above that $\nu$ is a smooth function of the energy near the Fermi level. This holds true, in particular, for potential scattering of electrons by impurities.

Generally, the role of impurities is more complicated, because of the possibility of creating bound states. This possibility is enhanced in an external magnetic field and in low-dimensional systems. In the 2D system, an isotropic potential-well of arbitrary small intensity produces a bound state with the energy[16]

$$\varepsilon_l=-\frac{\hbar^2}{2mb^2}\exp\left(-\frac{\hbar^2}{2mb^2U_0}\right). \tag{4}$$

Here $b$ is the radius and $U_0$ is the depth of the potential well; $m$ stands for the electron mass.

The external magnetic field applied perpendicular to a 2D conductor with impurities produces a host of local states. Impurities lift up the degeneracy on the Landau orbit center position and split off one level from each of the Landau levels. Depending on the sign of the potential the local impurity level may appear either above or below Landau level (correspondingly, for repulsive and attractive potentials). Therefore, the energy spectrum of considered systems consists of a series of two sets of levels: the impurity levels and the Landau ones. The separation between the impurity level and the nearest Landau level in case of a weak attractive potential $U_0\ll\hbar\Omega$ is equal to

$$\Delta=2U_0\left(\frac{b}{l}\right)^2, \tag{5}$$

here $l$ denotes the magnetic length $l=(\hbar c/eH)^{1/2}$.

The local energy levels $\varepsilon_k^l$ correspond to poles of the scattering amplitude of electrons on the complex energy plane and cannot be treated perturbatively. Therefore, it is necessary to take into account exact values of the scattering amplitude $\Psi(\varepsilon)$ for calculations of the conductivity tensor of a 2D conductor in the quantizing magnetic field.

Near the pole it becomes equal to

$$\Psi(\varepsilon)\approx\frac{R_k}{\varepsilon-\varepsilon_k^l}. \tag{6}$$

$R_k$ in Eq. (6) is the residue of the scattering amplitude $\Psi(\varepsilon)$ at the energy $\varepsilon=\varepsilon_k^l$. If $\Delta\ll\hbar\Omega$, then

$$R_k=2\pi(l\Delta)^2. \tag{7}$$

This quantity determines corrections to the conductivity tensor $\sigma_{\alpha\beta}(\omega,H)$ of a 2D electron gas in quantizing perpendicular magnetic field due to the localization of electrons nearby the impurity atoms. Such corrections in linear approximation on the impurities concentration $n_i$ have been calculated in the paper.[5] The corresponding results for the diagonal $\delta\sigma_{xx}$ and the Hall $\delta\sigma_{xy}$ components of the conductivity tensor are

$$\delta\sigma_{xx}=i\frac{e^2n_e}{m\omega}\left[\sum_{s=0}^{\infty}\alpha_{xx}^{(s)}\frac{\omega_s}{\omega-\omega_s+i\nu}+\sum_{p=1}^{\infty}\beta_{xx}^{(p)}\frac{\omega_p}{\omega-\omega_p+i\nu}\right], \tag{8}$$

$$\delta\sigma_{xy}=\frac{e^2n_e}{m\omega}\left[\sum_{s=0}^{\infty}\alpha_{xy}^{(s)}\frac{\omega_s}{\omega-\omega_s+i\nu}+\sum_{p=1}^{\infty}\beta_{xy}^{(p)}\frac{\omega_p}{\omega-\omega_p+i\nu}\right]. \tag{9}$$

Here $\omega_s$ and $\omega_p$ are the frequencies of electron transitions between the Landau and the local levels, $\Gamma=\hbar\nu$ stands for their broadening and determines thereby the quantity $\nu$. Symbols $\alpha_{ik}^{(s)}$ and $\beta_{ik}^{(p)}$ denote the oscillator strength for the resonant transitions. These quantities depend on the wave vector $q$ by dint of terms of the order $n_i(ql)^2$ which may be discarded in the limit $n_i(ql)^2\ll1$ ($q$ is the absolute value of the in-plane wave-vector).

Under above conditions, we have

$$\alpha_{xx}^{(s)}=\alpha_0\sum_k R_k[f(\varepsilon_k^l)-f(\varepsilon_{k+s})]P_{ks}^{+}, \tag{10}$$

$$\alpha_{xy}^{(s)}=\alpha_0\sum_k R_k[f(\varepsilon_k^l)-f(\varepsilon_{k+s})]P_{ks}^{-}, \tag{11}$$

$$P_{ks}^{\pm}=\left[\frac{k+s}{(\omega_s-\Omega)^2}\pm\frac{k+s+1}{(\omega_s+\Omega)^2}\right], \tag{12}$$

$$\alpha_0=\frac{n_i}{2\pi\hbar ml^4\omega_s n_e}. \tag{13}$$

Here $\varepsilon_n=\hbar\Omega(n+1/2)$ and $f(\varepsilon)$ is the Fermi function.

We do not use any specific form of the impurity potential in Eqs. (10)–(13) so that the quantities $\varepsilon_k^l$, $\Gamma$, and $R_k$ may be considered as fitting parameters of the theory or may be calculated for some particular scattering potential.

In all above equations, frequencies $\omega_s=\omega_0+s\Omega$ correspond to transitions from the local levels to Landau levels, whereas frequencies $\omega_p=p\Omega-\omega_0$ correspond to transitions in the opposite direction ($\omega_0=\Delta/\hbar$). The summation in Eqs. (10) and (11) is only taken over those local levels which are

involved into transitions at given frequency. Near the resonant frequency $\omega=\omega_0$ only resonant terms with $s=0$ are left, so that

$$\delta\sigma_{xx}\approx i\frac{e^2n_e}{m\omega}\alpha_{xx}^{(0)}\frac{\omega_0}{\omega-\omega_0+i\nu}. \tag{14}$$

$$\delta\sigma_{xy}\approx\frac{e^2n_e}{m\omega}\alpha_{xy}^{(0)}\frac{\omega_0}{\omega-\omega_0+i\nu}. \tag{15}$$

The number of the terms in the sum over $k$ in Eqs. (10) and (11) depends on the chemical potential value $\mu$. For example, in case of an attractive impurity potential and also under the condition $\varepsilon_N^l<\mu<\varepsilon_N$ only one term with $k=N$ contributes to the sums (10) and (11). Thus, taking into account Eq. (7) and the inequality $\omega_0\ll\Omega$ we have, from Eqs. (10) and (11),

$$\alpha_{xx}^{(0)}=-\frac{n_i}{n_e}\frac{\omega_0}{\Omega}(2N+1), \tag{16}$$

$$\alpha_{xy}^{(0)}=\frac{n_i}{n_e}\frac{\omega_0}{\Omega}. \tag{17}$$

$N$ is the number of filled Landau levels, $N=[\mu/\hbar\Omega]$. The symbol $[X]$ here denotes the integer part of $X$.

### 3. HELICONS AND MAGNETOIMPURITY WAVES

Having at hand the conductivity tensor of a 2D electron gas in quantizing magnetic field[17]

$$\sigma_{xx}=\sigma_0(1+\gamma^2)^{-1},\quad \sigma_{xy}=-\sigma_0+\gamma\sigma_{xx}, \tag{18}$$

$$\sigma_{xx}=\sigma_{yy},\quad \sigma_{xy}=-\sigma_{yx}, \tag{19}$$

where

$$\sigma_0(H)=\frac{n_ee^2}{m\Omega},\quad \gamma=(\nu-i\omega)/\Omega, \tag{20}$$

and corrections to $\sigma_{\alpha\beta}$ due to the magnetoimpurity bound states (14)–(17); we now turn to the problem of the electromagnetic wave propagation in layered conductors in an external magnetic field. The dispersion equation for electromagnetic waves in a uniform layered conductor in a perpendicular to conducting layers external magnetic field $H$ was obtained in a number of works.[9,10,15] According to Ref. 15, it says

$$\det\left[\delta_{\alpha\beta}-\frac{2\pi i\omega}{c^2q_\omega}\sigma_{\alpha\beta}(q,\omega,H)V_{\alpha\beta}S(q,k,\omega)\right]=0. \tag{21}$$

Here $\sigma_{\alpha\beta}$ is the 2D conductivity tensor of a layer (the model employed neglects electron hopping between the layers, so that they are correlated only via the electromagnetic fields); $S(q,k,\omega)$ stands for the structural factor:

$$S(q,k,\omega)=\frac{\sinh q_\omega a}{\cosh q_\omega a-\cos ka}, \tag{22}$$

$$q_\omega^2=q^2-\frac{\omega^2\varepsilon_0}{c^2}, \tag{23}$$

$$V_{11}=V_{12}=1,\quad V_{22}=V_{21}=-\frac{c^2q_\omega^2}{\omega^2\varepsilon_0}, \tag{24}$$

$q$ is the in-plane wave vector; $k$ is the wave vector component perpendicular to the layers (i.e., parallel to the field $H$); $\varepsilon_0$ is the dielectric constant of a substance between the layers.

The dispersion equation (21) is rather general since it determines the frequency $\omega=\omega(q,k,H)$ of a wave which can propagate in the volume of a layered conductor as a function of the wave vector $q$, $k$ and the field $H$ provided that the conductivity tensor of the constituent layers is known.

Substituting Eqs. (18)–(20), (14), and (15) in Eq. (21), we have

$$1+\gamma^2+i\gamma S\sigma_0(\beta-\alpha)+\alpha\beta(S\sigma_0)^2=V(\alpha_\parallel,\alpha_\perp), \tag{25}$$

$$V(\alpha_\parallel,\alpha_\perp)=-\alpha\beta(S\sigma_0)^2\left[2\frac{\gamma\alpha_\parallel-i\alpha_\perp}{\gamma+\gamma_0}+\frac{1+\gamma^2}{(\gamma+\gamma_0)^2}\times(\alpha_\parallel^2-\alpha_\perp^2)\right]-S\sigma_0(\beta-\alpha)\frac{i\alpha_\parallel(1+\gamma^2)}{\gamma+\gamma_0}. \tag{26}$$

We have introduced here the following notations:

$$\alpha=\frac{2\pi\omega}{q_\omega c^2},\quad \beta=\frac{2\pi q_\omega}{\omega\varepsilon},\quad \gamma_0=\frac{i\omega_0}{\Omega}, \tag{27}$$

$$\alpha_\perp=\frac{n_i}{n_e}\gamma_0,\quad \alpha_\parallel=\alpha_\perp(2N+1). \tag{28}$$

The left-hand side in Eq. (25) is nothing but the dispersion equation for electromagnetic waves in layered conductors without the corrections due to the magnetoimpurity bound states. The quantity $V(\alpha_\parallel,\alpha_\perp)$ depends on the impurities concentration $n_i/n_\varepsilon$ and vanishes when $n_i=0$.

Consider first the case of waves propagating along the magnetic field. These waves have zero component along the planes, $q=0$ and, therefore, the structure form-factor $S(q,k,\omega)$ (22) becomes

$$S(q,k,\omega)\approx\frac{i\omega_*\tilde{\omega}n_0}{1-\cos(ka)}, \tag{29}$$

where $\tilde{\omega}=\omega/\omega_p$, $\omega_p=4\pi n_ee^2/ma$ is the plasma frequency; $n_0=\sqrt{\varepsilon_0}$ is the refraction index of the matter between the layers.

The form-factor (29) is small elsewhere except for $ka\ll1$ because of the smallness of the parameter $\omega_*\tilde{\omega}n_0\ll1$. Putting $n_i=0$ and substituting Eq. (29) into (25) we found

$$1+(g-iX)^2-i(g-iX)2AX-A^2X^2=0, \tag{30}$$

$$g=\frac{\nu}{\Omega},\quad X=\frac{\omega}{\Omega},\quad A=\left(\frac{\omega_*}{2}\right)^2\sin^{-2}(ka/2). \tag{31}$$

The dispersion equation (30) has exact solutions (1) and (2), that is typical for helicons. The resonances at $\omega=\omega_0$ brought into the system, owing to the magnetoimpurity bound states, should modify the helicons dispersion near the intersection of the dispersion curves $\omega(k)$ (1) and $\omega=\omega_0$. Qualitatively, the impact of this ''crossing event'' on the

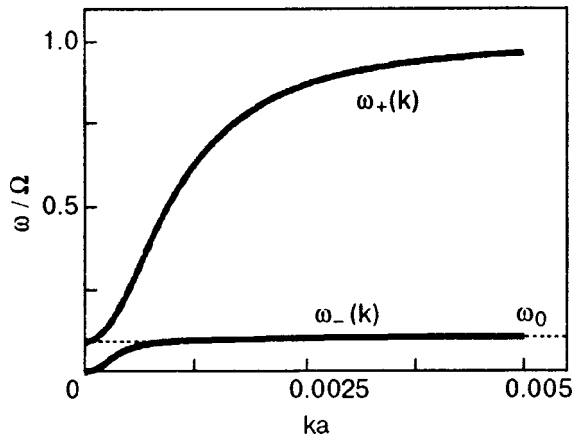


FIG. 1. The high-frequency helicon-like mode $\omega_+(k)$ and the low-frequency magnetoimpurity mode $\omega_-(k)$ calculated numerically from the dispersion equation (32) for $\omega_*=0.01$, $X_0=0.1$, $\alpha_\perp=0.1$, $\alpha_\parallel=10$, $g=g_0=0$.

wave spectrum is well known:[18] a twofold degeneracy is lifted up, causing the appearance of two new branches in the dispersion law of helicons, one above and another below $\omega_0$. To consider this phenomenon in more detail, we should include the $V$-term (26) in the right-hand side of dispersion equation (30).

Taking into account the smallness of the impurity concentration and the condition $\omega_0/\Omega \ll 1$, we have

$$1+(g-iX)^2-i(g-iX)2AX-A^2X^2 = \frac{2\alpha_\perp}{X-X_0+ig_0}AX(AX-B). \tag{32}$$

Here

$$B=2N+1, \quad X_0=\frac{\omega_0}{\Omega}, \quad g_0=\frac{\nu_0}{\Omega},$$

and $\nu_0$ is the broadening of the bound state $\omega_0$.

We see that the right-hand side of Eq. (32) (which is due to the magnetoimpurity bound states) enhances the degree of algebraic Eq. (32) compared with Eq. (30) and bring forth an additional root $X=X(k,A,g,g_0)$, i.e., a new branch in the wave dispersion equation.

The results of numerical calculations for the dispersion curves given by Eq. (32) are shown in Fig. 1.

The most dramatic changes are seen to take place near the crossing point of two branches: the helicon dispersion branch $\omega(k)$, given by Eq. (1), and the magnetoimpurity (bound state energy) branch $\omega=\omega_0$. They are shown in more detail in Fig. 2. We see that two new modes appear in consequence of this crossing: the low-frequency mode $\omega_-(k)$ and the high-frequency mode $\omega_+(k)$. The low-frequency mode dispersion for $ka \ll 1$, $g=0$, $g_0=0$ is given by

$$\omega_-(k)\approx\Omega^2(ka)^2\frac{2\alpha_\perp B}{\omega_*^2\omega_0}\left\{\left[1+\left(\frac{\omega_0}{\Omega\alpha_\perp B}\right)^2\right]^{1/2}-1\right\}. \tag{33}$$

For $ka\simeq 1$, $g=0$, $g_0=0$ it behaves as

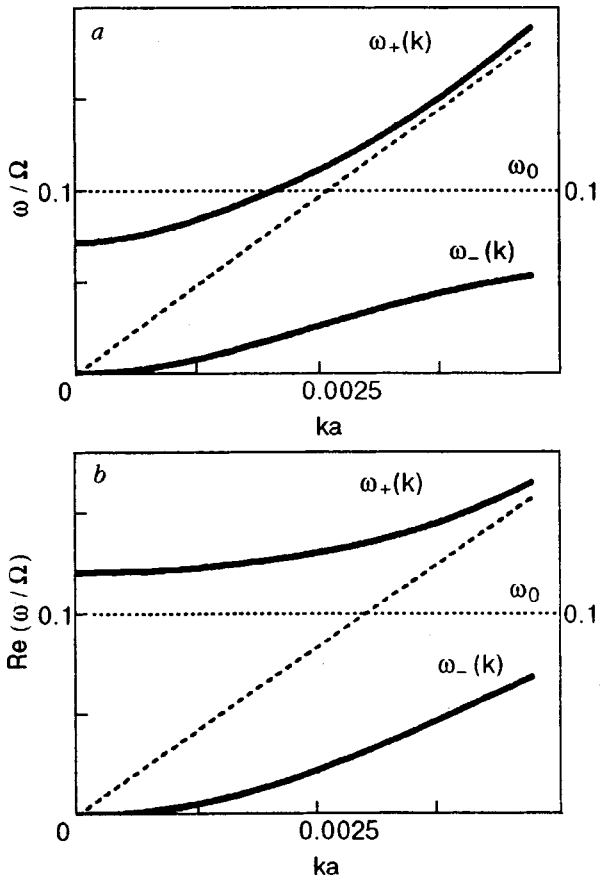


FIG. 2. The $\omega_+(k)$ and $\omega_-(k)$ modes (as in Figs. 1) shown in more detail near the crossing point of helicons (dashed line) with the magnetoimpurity frequency $\omega_0$ (dots). In difference to Fig. 1 parameters $\alpha_\perp$ and $\alpha_\parallel$ are taken to be $\alpha_\perp=0.01$ and $\alpha_\parallel=100$ for more descriptiveness of the picture. The absence of the gap between modes $\omega_+(k)$ and $\omega_-(k)$ is seen in Fig. 2a (where $g=0$) since $\omega_+(0)<\omega_0$. For slightly damped Landau levels $g\neq 0$ the above gap may appear, as is the case in Fig. 2b, where Re $\omega_+(0)>\omega_0$ and $g=0.01$.

$$\omega_-(k)\approx\omega_0-\frac{\Omega\omega_*^2\alpha_\perp B}{\sin(ka/2)}. \tag{34}$$

In the same fashion one can easily obtain explicit relations for the high-frequency mode $\omega_+(k)$. In the case of zero broadening ($g=g_0=0$), we have

$$\omega_+(k)\approx\omega_0-2\alpha_\perp\Omega\left[1-\frac{B\Omega}{\omega_0\omega_*^2}(ka)^2\right] \quad \text{for} \quad ka\ll 1 \tag{35}$$

and

$$\omega_+(k)\approx\Omega\left[1+\frac{\alpha_\perp B\omega_*^2}{4\sin^2(ka/2)}\right] \quad \text{for} \quad ka\simeq 1. \tag{36}$$

From the numerical calculations shown in Fig. 2, it follows that there is no gap between the branches $\omega_+(k)$ and $\omega_-(k)$ for $\nu=0$, since $\omega_+(0)<\omega_0$. This gap appears for nonzero Landau levels broadening as one can see from Fig. 2(b), where calculations are made for $\nu=0.01$ and it is found that $\omega_+(0)>\omega_0$, which is the upper limit of the low-frequency mode $\omega_-(k)$.

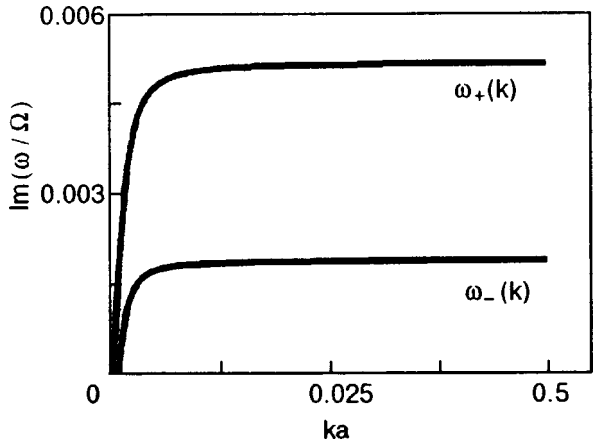


FIG. 3. The damping of the $\omega_+(k)$ and $\omega_-(k)$ modes shown in Fig. 1 calculated for $g=0.01$ and $g_0=0.01$.

In case of nonzero $g$ and $g_0$ both modes, $\omega_+(k)$ and $\omega_-(k)$, are damped. In fact, only weakly damped modes can propagate in a layered conductor, which implies parameters $g$ and $g_0$ should be much less than unity. Writing the wave frequency in the complex form $\omega=\mathrm{Re}\,\omega-i\,\mathrm{Im}\,\omega$ (i.e., taking into account its damping) we found from Eq. (30) in the linear on $g$ and $g_0$ approximation,

$$\mathrm{Im}\,\omega_\pm(k)=\frac{\Omega}{2}\left\{\frac{\omega_\pm(k)}{\Omega}\left[b-d\,\frac{\omega_\pm(k)}{\Omega}\right]+g_0\right\}\times\left\{a+2\,\frac{\omega_\pm(k)}{\Omega}\left[c-3e\,\frac{\omega_\pm(k)}{\Omega}\right]\right\}^{-1},\quad(37)$$

where

$$a=1+2\alpha_\perp AB,\quad b=2gX_0(1+A),$$
$$c=X_0(1+A)^2-2\alpha_\perp A^2,$$
$$d=g_0(1-2A-A^2)+2g(1+A),\quad e=(1+A)^2.\quad(38)$$

The numerical calculations for damping of the low-frequency, $\omega_-(k)$ and high-frequency, $\omega_+(k)$, modes are shown in Fig. 3.

## 4. SUMMARY AND CONCLUSIONS

We have shown above that magnetoimpurity states which appear in layered conductors in a quantizing external magnetic field are favorable for the propagation of the electromagnetic waves across the layers. These new modes come into being near the frequencies of the electron resonant transition between the magnetoimpurity level $\omega_0$ and the Landau levels. Physically, the magnetoimpurity modes do exist because of the electron localization at the impurity atoms which is favored by the external magnetic field and the two-dimensional nature of the electron dynamics within the layers. This localization made conductors closer to dielectrics which are known to be transparent for the electromagnetic waves. The magnetoimpurity waves in conventional 3D metals have been predicted by Kaner and Ermolaev[19,20] and then considered theoretically in the so-called noncompensated metals in which the electric charges are carried both by electrons and holes.[18] The quasi-two-dimensional character of the problem considered in this paper makes the whole phenomenon more pronounced, because of more strong van Hove singularities in the density of electronic states $g(\omega)$ in 2D systems compared to 3D ones. The latter facilitates the creation of a bound state $\omega_0$ (i.e., the eigenvalue of the Lifshitz equation, which we took for granted above) and, in particular, enhances the singularity in the frequency dependences of the $\delta\sigma_{xx}(\omega)$ in Eqs. (14)–(15) compared to the 3D case. Recall, that quantities $\delta\sigma_{xx}(\omega)$ and $\delta\sigma_{xy}(\omega)$ have square-root singularities in the 3D case that arise due to the appropriate singularities of the $g(\omega)$ at the Landau levels and do not depend on the details of the attractive potential of the impurities.

The spiral magnetoimpurity waves, to the best of our knowledge, have not yet been observed, although the existence of the magnetoimpurity bound states was surely established in some doped Bi compounds[21–23] and semiconductors.[24]

In layered conductors, the conditions for bonding of electrons by the attractive impurities in an external magnetic field are more favorable than in 3D metals, which enhances the chance of finding magnetoimpurity waves in such systems. Currently, a good deal of layered conductors (natural and artificially fabricated) are under study and attraction of researchers to the problem of magnetoimpurity waves in them is one of the purposes of this paper. Unfortunately, the most popular new layered systems, namely Bi- and Tl-based high-$T_c$ cuprates, should be, to all appearances, excluded from the list of candidates for observation of the magnetoimpurity modes in them because of the large damping $\nu\simeq\omega$ found in these materials above $T_c$.[25]

*)E-mail: vladimir.m.gvozdikov@univer.kharkov.ua

[1] E. A. Kaner and V. G. Skobov, Adv. Phys. **17**, 605 (1968).
[2] A. A. Abrikosov, *Fundamentals of the Theory of Metals*, North-Holland, Amsterdam (1988).
[3] V. G. Skobov, Zh. Éksp. Teor. Fiz. **37**, 1467 (1959) [Sov. Phys. JETP **10**, 1039 (1960)].
[4] Yu. A. Bychkov, Zh. Éksp. Teor. Fiz. **39**, 689 (1960) [Sov. Phys. JETP **12**, 483 (1961)].
[5] N. V. Gleizer and A. M. Ermolaev, Fiz. Nizk. Temp. **23**, 73 (1997) [Low Temp. Phys. **23**, 55 (1997)].
[6] F. G. Bass, A. A. Bulgakov, and A. P. Tetervov, High-frequency Properties of Semiconducting Superlattices, Nauka, Moskow (1989) [in Russian].
[7] V. M. Gohfeld, M. I. Kaganov, and V. G. Peschansky, Fiz. Nizk. Temp. **12**, 1173 (1986) [Sov. J. Low Temp. Phys. **12**, 661 (1986)].
[8] V. G. Peschansky, H. Kheir Bek, and S. N. Savel'eva, Fiz. Nizk. Temp. **18**, 1012 (1992) [Low Temp. Phys. **18**, 711 (1997)].
[9] A. Tselis and J. J. Quinn, Phys. Rev. B **29**, 3318 (1984).
[10] K. I. Golden and G. Kalman, Phys. Rev. B **52**, 14719 (1995).
[11] L. Wendler and M. I. Kaganov, Phys. Status Solidi B **142**, K63 (1987).
[12] B. N. Narahari, Phys. Rev. B **37**, 10423 (1988).
[13] I. D. Vagner and D. Bergman, Phys. Rev. B **35**, 9856 (1987).
[14] V. M. Gvozdikov, Physica C **224**, 293 (1994).
[15] V. M. Gvozdikov and R. Vega-Monroy, Vestnik Kharkovskogo Universiteta **118**, 4 (1998).
[16] L. D. Landau and E. M. Lifshitz, *Quantum Mechanics*, Nauka, Moskow (1989).
[17] T. Ando, A. B. Fowler, and F. Stern, Rev. Mod. Phys. **54**, 437 (1982).

[18] N. V. Gleizer, A. M. Ermolaev, and G. I. Rashba, Fiz. Nizk. Temp. **20**, 1169 (1994) [Low Temp. Phys. **20**, 919 (1994)].
[19] E. A. Kaner and A. M. Ermolaev, Pis'ma Zh. Eksp. Teor. Fiz. **44**, 3915 (1986) [*sic*].
[20] E. A. Kaner and A. M. Ermolaev, Zh. Éksp. Teor. Fiz. **92**, 2245 (1987) [Sov. Phys. JETP **65**, 1266 (1987)].
[21] A. M. Ermolaev and M. I. Kaganov, JETP Lett. **6**, 315 (1967).
[22] A. M. Ermolaev, Zh. Éksp. Teor. Fiz. **54**, 1259 (1968) [Sov. Phys. JETP **27**, 673 (1968)].
[23] N. B. Brandt and L. G. Lyubutina, Zh. Éksp. Teor. Fiz. **52**, 686 (1967) [Sov. Phys. JETP **25**, 450 (1967)].
[24] S. P. Andreev, Usp. Fiz. Nauk. **143**, 213 (1984) [Sov. Phys. Usp. **27**, 431 (1984)].
[25] J. Ruvalds, Supercond. Sci. Technol. **9**, 905 (1996).

This article was published in English in the original Russian journal. It was edited by R. T. Beyer.

# Hyperfine-driven persistent currents in mesoscopic rings based on a 2D electron gas with Rashba spin-orbit interaction

V. A. Cherkaskiy and S. N. Shevchenko

*Physical-Technical Department, Kharkov State University, 4 Svobody Square, 310077 Kharkov, Ukraine; B. Verkin Institute for Low Temperature Physics and Engineering, National Academy of Sciences of Ukraine, 47 Lenin Ave., 310164, Kharkov, Ukraine*

A. S. Rozhavsky,*)

*B. Verkin Institute for Low Temperature Physics and Engineering, National Academy of Sciences of Ukraine, 47 Lenin Ave., 310164 Kharkov, Ukraine; Grenoble High Magnetic Field Laboratory, Max-Planck-Institut für Festöperforschung and Centre National de la Recherche Scientifique B. P. 166, 38042 Grenoble Cedex 09, France*

I. D. Vagner**)

*Grenoble High Magnetic Field Laboratory, Max-Planck-Institut für Festkörperforschung and Centre National de la Recherche Scientifique B.P. 166, 38042 Grenoble Cedex 09, France*
(Submitted February 23, 1999)
Fiz. Nizk. Temp. **25**, 725–730 (July 1999)

We present a detailed theory of induced persistent current (PC) produced by hyperfine interaction in mesoscopic rings based on a 2D-electron (hole) gas in the absence of external magnetic field. PC emerges due to combined action of the hyperfine interaction of charge carriers with polarized nuclei, spin-orbit interaction and Berry phase. © *1999 American Institute of Physics.* [S1063-777X(99)01207-4]

## INTRODUCTION

The current situation in solid state physics is characterized in particular by a hectic search of various macroscopic topological quantum effects. The most popular of these are the persistent current (PC) phenomena (the oscillations of the diamagnetic moment) in a non-simply connected mesoscopic conductor. PC is produced by a sensibility of a single particle wave function to a force-free field which is taken into account via the twisted boundary conditions:

$$\Psi|_{\varphi=0}=e^{i\Delta\varphi}\Psi|_{\varphi=2\pi}, \tag{1}$$

where $\varphi$ is an angular variable, and $\Delta\varphi$ is the topological phase shift.

In multiparticle systems, Eq. (1) results in the oscillatory dependence of the thermodynamic and kinetic characteristics on $\Delta\varphi$. If $\Delta\varphi$ is governed by any varying external parameter $\gamma$, e.g. the magnetic field, the response of a system is the oscillatory function of $\gamma$.

Normally, the actual experiments are performed on thin quasi-one-dimensional submicron metallic or semiconductor based[1] loops pierced by a magnetic flux $\Phi$, and $\Delta\varphi$ reveals the Aharonov–Bohm effect (ABE)[2,3]

$$\Delta\varphi_{AB}=\frac{q}{\hbar c}\oint \mathbf{A}\cdot d\mathbf{l}=2\pi\frac{\Phi}{\Phi_0}, \tag{2}$$

where $\Phi_0=hc/q$, $q$ is the charge of a conduction particle.[1)]

The ABE-oscillations of the diamagnetic moment (the PCs) reflect the broken clockwise-anticlockwise symmetry of charge carriers momenta caused by the external vector potential. The PC is defined as

$$I_{\mathrm{PC}}=-c(\partial F/\partial\Phi), \tag{3}$$

where $F$ is the free energy of the loop.

In a recent publication,[4] we have proposed a new mechanism for the observation of adiabatically slow oscillations of PC with time specific for 2D quantum Hall systems. This mechanism does not apply to an external magnetic field, i.e., the oscillatory current $I_{\mathrm{PC}}$ [Eq. (3)] exists even at $\Phi=0$.[4] The bottomline physics behind these spontaneous PC can be understood along the following lines.

The time reversal symmetry breaking is in general achieved as the combined action of the ABF and topological spin-orbit interactions. It was shown in Ref. 5 that the topological phase shift $\Delta\varphi$ in Eq. (1) is the sum of the ABE, Aharonov–Casher[6] and Berry[7] phases providing the topologically nontrivial spatial charge carriers spins distribution:

$$\Delta\varphi=\Delta\varphi_{AB}+\Delta\varphi_{AC}+\Delta\varphi_{B}, \tag{4}$$

where

$$\Delta\varphi_{AC}=\frac{\mu_B}{\hbar c}\oint d\mathbf{l}\cdot(\mathbf{E}\times\sigma), \tag{5}$$

$$\Delta\varphi_{B}=s\pi(1-\cos\chi), \tag{6}$$

here $\mu_B$ is the Bohr magneton, $\mathbf{E}$ is the electric field, $\sigma$ is the charge carrier spin vector, $\chi$ is the tilt angle of a magnetic texture, $s=\pm1$ is the spin projection on a magnetic field.

As $(d/d\Phi)(\Delta\varphi)=2\pi/\Phi_0$, the PC can be a nonzero function of $\Delta\varphi_{AC}+\Delta\varphi_{B}$ even at $\Delta\varphi_{AB}=0$.

 

It was proposed in Ref. 4 to create a spatial distribution of the charge carriers spins through the hyperfine interaction with polarized nuclei. The contact hyperfine interaction is[8]

$$H_{hf}=\frac{8\pi}{3}g\mu_B\mu_n\sum_i \mathbf{I}_i\cdot\boldsymbol{\sigma}\delta(\mathbf{r}-\mathbf{R}_i), \tag{7}$$

where $\mu_n$ is the nuclear magneton, $g$ is the $g$-factor, $\mathbf{I}_i$, $\boldsymbol{\sigma}$, $\mathbf{R}_i$, $\mathbf{r}$ are the nuclear and the charge carrier spins and the position vectors, respectively. Once the nuclear spins are polarized, i.e., if $\langle\Sigma_i\mathbf{I}_i\rangle\neq 0$, the charge carriers feel the effective field $\mathbf{B}_{hf}(t)$ which lifts the spin degeneracy even in the absence of an external magnetic field. At low temperatures, the nuclear relaxation rates are inconveniently small,[9] in particular in GaAs/AlGaAs the nuclear spin relaxation times are of the order of $10^3$ sec.[10] The Zeeman splitting reaches one tenth of the Fermi energy.[11,12] The Aharonov–Casher phase (5) arises from the spin-orbit interaction[13] which in GaAs/AlGaAs 2D-gas has the form[14]

$$H_{SO}=\frac{\alpha}{\hbar}(\boldsymbol{\sigma}\times\mathbf{p})\cdot\mathbf{v}, \tag{8}$$

where $\mathbf{p}$ is the charge carrier momentum, $\mathbf{v}$ is the normal to the surface, $\alpha=0.25\cdot 10^{-9}$ eV·cm for holes[14] and $\alpha=0.6\cdot 10^{-9}$ eV·cm for electrons,[15] and

$$\Delta\varphi_{AC}=\frac{m^*}{\hbar^2}\oint\alpha(\mathbf{v}\times\boldsymbol{\sigma})\cdot d\mathbf{l}. \tag{9}$$

The combination $\Delta\varphi_{AC}+\Delta\varphi_B$ itself does not depend on $\mathbf{B}_{hf}$ explicitly, the oscillatory dependence on $\mathbf{B}_{hf}(t)$ emerges in the PC through the mesoscopic factor $\cos(2\pi\sqrt{\mu_s(\mathbf{B}_{hf})/\Delta})$[5] where $\mu_s(\mathbf{B}_{hf})$ is the Zeeman shifted chemical potential of the charge carriers with the spin projection $s$, and $\Delta$ is the spacing between the quantized electron levels in a 1D-ring. The effect of Berry phase in 2DEG based AlSb/InAs/AlSb heterostructure was observed in Ref. 16.

In this paper we consider PC in two cases: i) when nuclei are polarized along a certain direction in the plane and ii) when nuclear spins form an out-of-plane crown texture. We show that:

i). In this case $\Delta\varphi_B=0$, and $\Delta\varphi_{AC}\neq 0$ only if the spin-orbit coupling is inhomogeneous $[\alpha=\alpha(\varphi)]$ such that

$$\int_0^{2\pi}d\varphi\alpha(\varphi)e^{i\varphi}\neq 0. \tag{10}$$

The inhomogeneity of the spin-orbit coupling plays the same role as the topologically nontrivial spin texture.[4,17]

ii). In this case the PC exists at $\alpha=$const and even at $\alpha=0$ the PC is nonzero due to $\Delta\varphi_B$.

## CALCULATION OF PERSISTENT CURRENTS

The induced PC is given by the Eq. (3) at $\Phi=0$. The standard algebra (see the Appendix) gives the following equation for the $I_{\rm PC}$:

$$I_{\rm PC}\cong\frac{eT}{\hbar}\sum_{l=1}^{\infty}\sum_j\left.\frac{\sin(2\pi l n_F^{(j)})}{\sinh(lT/\tilde{T}^{(j)})}\right|_{\Phi=0}, \tag{11}$$

where $T$ is the temperature, index $j$ numerates the roots of the equation:

$$\varepsilon(n_F^{(j)})=\mu. \tag{12}$$

Here $\varepsilon$ is the eigenvalue of the Schrödinger equation, $\mu$ is the chemical potential and

$$\tilde{T}^{(j)}=\frac{1}{2\pi^2}\left|\frac{\partial\varepsilon}{\partial n}\right|_{n=n_F^{(j)}}, \tag{13}$$

is the crossover temperature.

In what follows we solve the Schrödinger equation for the charge carriers confined to a 1D-ring with the radius $\rho$, obtain $n_F^{(j)}$ and $\tilde{T}^{(j)}$, and analyze $I_{\rm PC}$ in various geometries.

*i). The in-plane polarized nuclei*, $\Delta\varphi_B=0$. The charge carriers Hamiltonian takes the form

$$\hat{H}=\frac{\hat{p}^2}{2m^*}+\frac{1}{2\hbar}\{\boldsymbol{\alpha}\boldsymbol{\sigma}\cdot\mathbf{n},\hat{p}\}_+-g\mu_B B_{hf}\boldsymbol{\sigma}_x, \tag{14}$$

here $\mathbf{B}_{hf}$ is oriented along the $x$-axis in the $xy$-plane, $m^*$ is the effective mass, $g$ is the $g$-factor, $\{\ldots\}_+$ stands for the anticommutator,

$$\boldsymbol{\sigma}\cdot\mathbf{n}=\sigma_x\cos\varphi+\sigma_y\sin\varphi,$$

$$\hat{p}=-(i\hbar/\rho)(\partial/\partial\varphi-i(\Phi/\Phi_0)),\quad \Phi_0=hc/e.$$

Consider weak spin-orbit coupling $\alpha\ll\Delta\rho$, where $\Delta=\hbar^2/2m^*\rho^2$.

The spectrum linear in $\alpha$ is

$$\varepsilon_n^{\pm}\cong\Delta\left(n-\frac{\Phi}{\Phi_0}\right)^2\mp g\mu_B B_{hf}\pm 2\Delta\left(n-\frac{\Phi}{\Phi_0}\right)\frac{\langle\alpha\cos\varphi\rangle}{2\Delta\rho}, \tag{15}$$

where

$$\langle\alpha\cos\varphi\rangle=\frac{1}{2\pi}\int_0^{2\pi}d\varphi\alpha(\varphi)\cos\varphi. \tag{16}$$

The PC takes the form

$$I_{\rm PC}\cong\frac{4\pi eT}{\hbar\Delta\rho}\langle\alpha\cos\varphi\rangle\sum_{l=1}^{\infty}l\frac{\sin(2\pi l\sqrt{\mu/\Delta})\sin(\pi lb/\sqrt{\Delta\mu})}{\sinh(\pi^2 lT/\sqrt{\Delta\mu})}, \tag{17}$$

where $b=g\mu_B B_{hf}(t)$.

At low temperatures $T\ll\sqrt{\Delta\mu}/\pi^2$ the r.h.s. of Eq. (17) takes the form of the series rectangles:

$$I_{\rm PC}\cong\frac{4e}{\hbar}\sqrt{\mu/\Delta}\frac{\langle\alpha\cos\varphi\rangle}{\rho}\left\{\tilde{\delta}\left[2\pi\sqrt{\mu/\Delta}\left(1-\frac{b}{2\mu}\right)\right]-\tilde{\delta}\left[2\pi\sqrt{\mu/\Delta}\left(1+\frac{b}{2\mu}\right)\right]\right\}, \tag{18}$$

where $\tilde{\delta}(x)$ is the rectangle with the height $\sqrt{\Delta\mu}/\pi T$ and the width $\pi^2T/\sqrt{\Delta\mu}\ll 1$ centered at the points $x=2\pi k$, where $k$ is an integer. The magnitude of $I_{\rm PC}$ (17) is of the order of

$$I_{\rm PC}\sim\frac{\alpha}{\Delta\rho}I_0, \tag{19}$$

where $I_0 = eV_F/2\pi\rho$ is the magnitude of a normal ABE persistent current. At high temperatures, $T \gg \sqrt{\Delta\mu}/\pi^2 \equiv \tilde{T}$, the PC decreases with temperature in a standard exponential way:

$$I_{\rm PC} \cong \frac{8\pi eT}{\hbar\Delta\rho}\langle\alpha\cos\varphi\rangle e^{-\pi^2 T/\sqrt{\Delta\mu}} \times \sin(2\pi\sqrt{\mu/\Delta})\sin(\pi b/\sqrt{\Delta\mu}). \quad (20)$$

In submicron rings, the opposite limit $\alpha \gtrsim \Delta\rho$ is more favorable. In this case we can perform the perturbation scheme over the ''parity'' of the spin-orbit coupling. One can achieve slowly varying on the scale of $k_F^{-1}$ coordinate dependent $\alpha(\varphi)$ by means of a controlled distribution of impurities. If the ''even'' component $\langle\alpha\cos\varphi\rangle$ is made much larger than the ''odd'' one $\langle\alpha\sin\varphi\rangle$ the unperturbed Hamiltonian takes the form

$$\hat{H} = \frac{\hat{p}^2}{2m^*} + \frac{1}{2\hbar}\{\alpha\sigma_x\cos\varphi, \hat{p}\}_+ - g\mu_B B_{hf}\sigma_x, \quad (21)$$

and the Schrödinger equation can be solved exactly. The spectrum is

$$\varepsilon_n^{\pm} = \Delta\left(n \pm \frac{\langle\alpha\cos\varphi\rangle}{2\Delta\rho}\right)^2 \mp g\mu_B B_{hf}. \quad (22)$$

The perturbation potential is

$$\hat{V} = \frac{1}{2\hbar}\{\alpha\sigma_y\sin\varphi, \hat{p}\}_+. \quad (23)$$

One can easily see that the first correction over $\hat{V}$ to the spectrum is zero, and the second correction is negligible at $b \gg (\alpha/\rho)\sqrt{\mu/\Delta}$.

The PC is

$$I_{\rm PC} \cong \frac{4eT}{\hbar} \times \sum_{l=1}^{\infty} \frac{\sin\left(\pi l \dfrac{\langle\alpha\cos\varphi\rangle}{\Delta\rho}\right)\sin(2\pi l\sqrt{\mu/\Delta})\sin(\pi lb/\sqrt{\Delta\mu})}{\sinh(\pi^2 lT/\sqrt{\Delta\mu})}. \quad (24)$$

In mesoscopic devices $b$ decreases with time exponentially $b \sim b_0\exp(-t/t_1)$. The time scale $t_1$ is macroscopically long at low temperatures.[10] The dependence of the $I_{\rm PC}$ on $b$ (i.e., on $t$) for Eq. (24) is shown at Fig. 1.

Equation (24) differs from Eq. (17) provided $\langle\alpha\cos\varphi\rangle \sim \Delta\rho$. If the fluctuating component $\langle\alpha\cos\varphi\rangle \ll \Delta\rho$, the result (24) is reduced to (17).

ii). The polarized nuclear spins form a crown, $\Delta\varphi_B \neq 0$. Consider $B_{hf}$ directed along the cylindrically symmetric crown (Fig. 2) tilted to the $z$-axis by the angle $\chi$. The electron spectrum can be obtained exactly following the paper.[18] We represent the Hamiltonian in the form

$$\hat{H} = \Delta\left(-i\frac{\partial}{\partial\varphi} + \frac{\Phi}{\Phi_0}\right)^2 + \frac{1}{2}\left\{\begin{pmatrix} 0 & e^{-i\varphi} \\ e^{i\varphi} & 0 \end{pmatrix}, \frac{\alpha}{\rho}\left(-i\frac{\partial}{\partial\varphi} + \frac{\Phi}{\Phi_0}\right) - b\sin\chi\right\}_+ - b\cos\chi\sigma_z. \quad (25)$$

The solution to the spectral equation is

$$\Psi = \begin{pmatrix} \Psi_1 e^{i(m-1/2)\varphi} \\ \Psi_2 e^{i(m+1/2)\varphi} \end{pmatrix}, \quad (26)$$

where $m = n + 1/2$, $n$ is an integer.

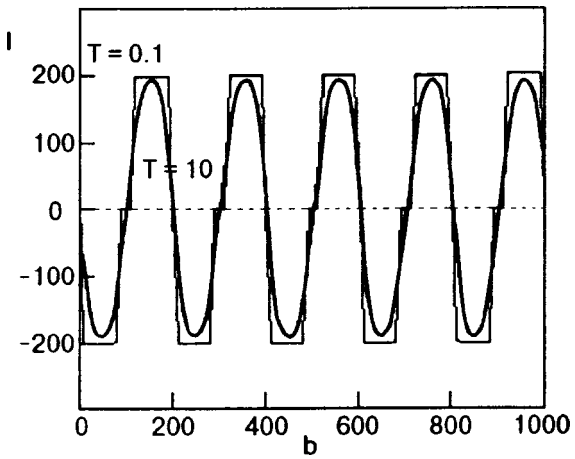


FIG. 1. Dependence of $I_{\rm PC}$ upon $b$ when nuclei are polarized along a certain direction in the plane for $\mu \sim 10^4$, $\alpha/\rho \sim 2$. ($\mu$, $\alpha/\rho$, $b$ and $T$ are expressed here in units of $\Delta$; $I$ in units of $I_0$; for real submicron rings $\Delta = 10^{-3}$–$10^{-2}$ K.)

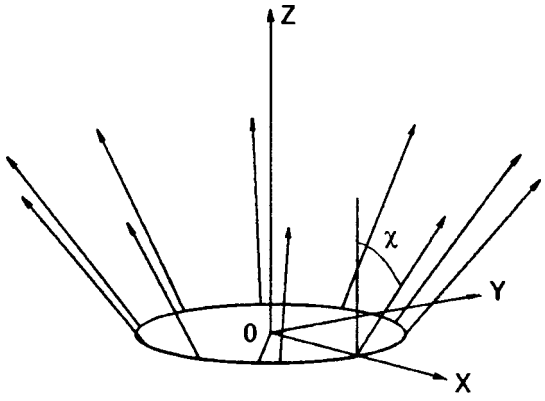


FIG. 2. $\mathbf{B}_{hf}$ directed along the cylindrically symmetric crown tilted to the $z$-axis by the angle $\chi$.

The spectrum is

$$\varepsilon_m^{\pm}=\Delta\left(\lambda_m^2+\frac{1}{4}\right)\pm\left[\left(\Delta^2+\frac{\alpha^2}{\rho^2}\right)\lambda_m^2+2\Delta\kappa b\lambda_m+b^2\right]^{1/2}, \tag{27}$$

where $\lambda_m=m+(\Phi/\Phi_0)$, $\kappa=\cos\chi-(\alpha/\Delta\rho)\sin\chi$. The dependence of the PC [Eq. (36)] on $b$ calculated numerically with the spectrum (27) is plotted at Fig. 3.

After some straightforward but cumbersome calculations we get at $\kappa<1$ the asymptotic expression for $I_{\rm PC}$

$$I_{\rm PC}\cong\frac{4eT}{\hbar}\sum_{l=1}^{\infty}(-1)^l\frac{\sin(\pi l\kappa/\sqrt{1+(\mu\alpha^2/\Delta\rho^2b^2)})\sin(2\pi l\sqrt{\mu/\Delta})\sin(\pi lb/\sqrt{\Delta\mu})}{\sinh(\pi^2 lT/\sqrt{\Delta\mu})}. \tag{28}$$

Consider the case of a ''strong'' Zeeman splitting $b\gg(\alpha/\rho)\sqrt{\mu/\Delta}$. In this limit one can easily see that

$$(-1)^l\sin(\pi l\kappa)=\sin(\Delta\varphi_{AC}+\Delta\varphi_B), \tag{29}$$

where

$$\Delta\varphi_{AC}=2\pi\frac{\alpha m^*}{\hbar^2}\rho\sin\chi. \tag{30}$$

Equation (30) is evidently obtained from the general definition (5) by the substitutions

$$(\mathbf{v}\times\boldsymbol{\sigma})\to\sigma_\rho\to\sin\chi, \tag{31}$$

which means that in a ''strong'' hyperfine field all the spins are aligned to the crown direction.

In a ''weak'' hyperfine field $b\ll(\alpha/\rho)\sqrt{\mu/\Delta}$, the topological phases are expressed in terms of averaged spin components:

$$\Delta\varphi_{AC}=2\pi\frac{\alpha m^*}{\hbar^2}\rho\langle\sigma_\rho\rangle, \tag{32}$$

where $\langle\sigma_\rho\rangle\cong b\sqrt{\Delta/\mu}(\rho/\alpha)\sin\chi\ll1$, and

$$\Delta\varphi_B=\pi(1-\cos\chi)\langle\sigma_\chi\rangle, \tag{33}$$

where $\langle\sigma_\chi\rangle\equiv b\sqrt{\Delta/\mu}(\rho/\alpha)\ll1$.

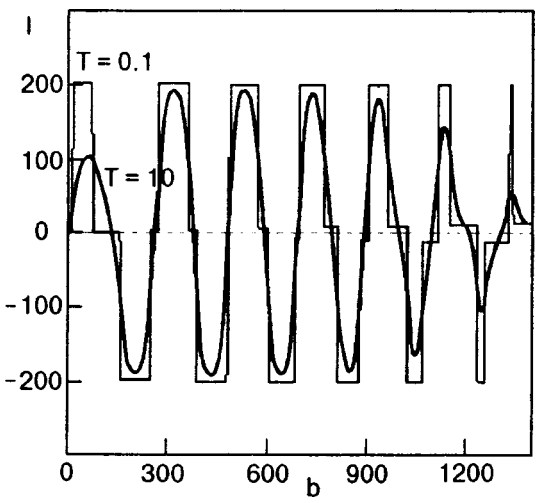


FIG. 3. Dependence of $I_{\rm PC}$ upon $b$ in the case when nuclear spins form an out-of-plane crown texture. ($\kappa\sim0.5$, $\mu\sim10^4$, $\alpha/\rho\sim2$, quantities $b$, $T$, $\mu$, $\alpha/\rho$ are expressed here in units of $\Delta$; $I$ in units of $I_0$).

The remarkable feature of the Eq. (28) is that $I_{\rm PC}\neq0$ even at $\alpha=0$ when $\Delta\varphi_B\neq0,\pm\pi$, i.e. at $\chi\neq0$, $\pi/2$, $(\mathrm{mod}\,\pi)$.

## APPENDIX

In this chapter, following the lines of Ref. 19 we perform the derivation of the PC for the arbitrary dispersion law of charge carriers.

At a fixed chemical potential, the PC is

$$I_{\rm PC}=\sum_{n=-\infty}^{\infty}\frac{i_n}{e^{(\varepsilon_n-\mu)/T}+1}, \tag{A1}$$

where $i_n$ is the partial current of the $n$th orbital:

$$i_n=\frac{e}{h}\frac{\partial\varepsilon}{\partial n}. \tag{A2}$$

Making use of the Poisson summation formula were present the r.h.s. in (A1) in the form

$$\begin{aligned}I_{\rm PC}&=\frac{e}{h}\int_{-\infty}^{\infty}dn\frac{\partial\varepsilon/\partial n}{e^{(\varepsilon(n)-\mu)/T}+1}\\&\quad+2\frac{e}{h}\sum_{l=1}^{\infty}\int_{-\infty}^{\infty}dn\frac{(\partial\varepsilon/\partial n)\cos(2\pi nl)}{e^{(\varepsilon(n)-\mu)/T}+1}\\&=-\frac{eT}{h}\log(e^{-(\varepsilon(n)-\mu)/T}+1)\Big|_{-\infty}^{\infty}\\&\quad+4\pi T\frac{e}{h}\sum_{l=1}^{\infty}\sum_{\mathrm{Im}(n_k)>0}\mathrm{Im}\,e^{2\pi iln_k},\end{aligned} \tag{A3}$$

where $\varepsilon(n_k)=\mu+2i\pi T(2k-1)$, which gives at $T\ll\mu$:

$$n_k\cong n_F+\frac{i\pi T(2k-1)}{\partial\varepsilon/\partial n|_{n=n_F}}. \tag{A4}$$

Eventually, we arrive to Eqs. (11)–(13):

$$I_{\rm PC}\cong\frac{eT}{\hbar}\sum_{l=1}^{\infty}\sum_j\left.\frac{\sin(2\pi\ln_F^{(j)})}{\sinh(lT/\tilde{T}^{(j)})}\right|_{\Phi=0}, \tag{A5}$$

where

$$\tilde{T}^{(j)}=\frac{1}{2\pi^2}\left|\frac{\partial\varepsilon}{\partial n}\right|_{n=n_F^{(j)}},\quad \varepsilon(n_F^{(j)})=\mu. \tag{A6}$$

Since $\tilde{T}^{(j)}$ for various $j$ vary insignificantly,[2)] we safely replace $\tilde{T}^{(j)}$ by some averaged $\tilde{T} \cong \tilde{T}^{(j)}$ and get

$$I_{\mathrm{PC}} \cong \frac{eT}{\hbar} \sum_{l=1}^{\infty} \sinh^{-1}\left(\frac{lT}{\tilde{T}}\right) \sum_{j} \sin(2\pi l n_F^{(j)}). \tag{A7}$$

*)Deceased
**)E-mail: vagner@labs.polycnrs-gre.fr

1)The external flux is swept adiabatically slowly with time, and, in fact, one observes oscillations with a certain temporal period connected with $\Phi_0$.

2)E.g. for in-plane $\mathbf{B}_{hf}$-configuration $\tilde{T}^{\pm} = \sqrt{\mu \pm b}$, so the difference between different $\tilde{T}^{(j)}$ is of the order of $B_{hf}/\mu$.

[1] D. Mailly, C. Chapelier, and A. Benoit, Phys. Rev. Lett. **70**, 2020 (1993).
[2] L. P. Levy, G. Dolan, J. Dunsmuir, and H. Bouchlak, Phys. Rev. Lett. **64**, 2074 (1990); V. Chandrasekhar, K. A. Webb, M. J. Brady, M. B. Ketchen, W. J. Gallagher, and A. Kleinsasser, Phys. Rev. Lett. **67**, 3578 (1991).
[3] Y. Aharonov and D. Bohm, Phys. Rev. **115**, 485 (1959).
[4] I. D. Vagner, A. S. Rozhavsky, P. Wyder, and A. Yu. Zyuzin, Phys. Rev. Lett. **80**, 2417 (1998).
[5] E. N. Bogachek, I. V. Krive, I. O. Kulik, and A. S. Rochavsky, Mod. Phys. Lett. B **5**, 1607 (1991).
[6] Y. Aharonov and A. C. Casher, Phys. Rev. Lett. **53**, 319 (1984).
[7] M. V. Berry, Proc. R. Soc. London, Ser. A **392**, 45 (1984); D. Loss, P. Goldbart, and A. V. Balatsky, Phys. Rev. Lett. **65**, 1655 (1990); D. Loss and P. Goldbart, Phys. Rev. B **45**, 13544 (1992).
[8] C. P. Slichter, *Principles of Magnetic Resonance*, Springer-Verlag, Berlin (1991), 2nd eddition.
[9] F. Bloch, Phys. Rev. **70**, 460 (1946).
[10] A. Berg, M. Dobers, R. R. Gerhardts, and K. V. Klitzing, Phys. Rev. Lett. **64**, 2563 (1990); I. D. Vagner and T. Maniv, Phys. Rev. Lett. **61**, 1400 (1998).
[11] K. Wald, L. P. Kouwenhoven, P. L. Euen, N. C. Van der Vaart, and C. T. Foxon, Phys. Rev. Lett. **73**, 1011 (1994).
[12] S. E. Barret, A. Schmeller, J. P. Elsemstein, L. N. Pfeiffer, and K. W. West, Phys. Rev. Lett. **75**, 4290 (1995).
[13] H. Mathur and A. D. Stone, Phys. Rev. Lett. **68**, 2964 (1992).
[14] Yu. A. Bychkov and E. I. Rashba, J. Phys. C **17**, 6039 (1984); P. Pfeiffer and W. Zawadzki, Phys. Rev. B **32**, R14332 (1995).
[15] D. Stein, K. v. Klitzing, and G. Weimann, Phys. Rev. Lett. **51**, 130 (1983).
[16] A. F. Morpargo, -J. P. Heide, B. J. van Wess, -J. J. Kulpers, T. M. Klapwijk, and G. Borghs, Phys. Rev. Lett. **80**, 1050 (1998).
[17] A. G. Aronov and Y. B. Lyanda-Geller, Phys. Rev. Lett. **70**, 343 (1993).
[18] A. V. Chaplik and L. I. Magaril, Superlattices Microstruct. **18**, 321 (1995).
[19] H. F. Cheung, Y. Gefen, E. K. Riedel, and W. H. Shih, Phys. Rev. B **37**, 6050 (1988).

This article was published in English in the original Russian journal. It was edited by R. T. Beyer.

## LATTICE DYNAMICS

# Thermal disorder of proustite cationic sublattice

N. A. Borovoĭ, Yu. P. Gololobov, and I. N. Salivonov

*Taras Shevchenko University, 252127 Kiev, Ukraine*
(Submitted November 30, 1998; revised March 9, 1999)
Fiz. Nizk. Temp. **25**, 731–736 (July 1999)

Temperature dependences of acoustic emission and relative intensity of some structural x-ray peaks for proustite ($Ag_3AsS_3$) samples are investigated in the temperature range 100–300 K. Anomalous behavior of the obtained dependences is observed at $T\sim150$ K. The experimental results have been analyzed by using different models of positional disorder of the silver sublattice. The entire body of the obtained data can be explained assuming that an increase in temperature starting from $T\sim150$ K leads to predominant disordering of the part of the cationic sublattice of proustite, that is formed by right spirals $(AgS)_\infty$. © *1999 American Institute of Physics.* [S1063-777X(99)01307-9]

Unique physical properties of proustite ($Ag_3AsS_3$) crystals at low temperatures are mainly due to it labile cationic sublattice. For example, the instability of the silver ionic subsystem is responsible for the well-known phase transitions (PT), namely, PT-1 ($T_1\sim60$ K) leading to the formation of the incommensurate phase, PT-2 ($T_2\sim50$ K) accompanied by a change in the magnitude and direction of the structure modulation vector, and PT-3 ($T_3\sim28$ K), viz., a ferroelectric transition resulting in a field-reoriented spontaneous polarization. In addition, Smolenskii *et al.*,[1] who discovered the splitting of $E$-mode in the Raman spectra at $T\sim150$ K, concluded that proustite crystals also display PT-4 accompanied by a lowering of symmetry to the monoclinic symmetry (hypothetically, $C_{3V}\rightarrow C_S$). The PT-4 temperature ($T\sim200$ K) was determined by extrapolation of the obtained experimental dependences to higher temperatures.[1,2] At the same time, independent analysis based on the same Raman scattering method did not confirm the existence of this PT in $Ag_3AsS_3$ crystals.[3,4] Thus, not only the origin, but also the existence of PT-4 remain unclear. In this connection, we decided to carry out a complex investigation of proustite in the temperature range 100–300 K.

Since the PT-4 is determined by external effects such as the electromagnetic field,[5] we chose the acoustic emission method for our experiments. It was proved earlier that this method is not only extremely sensitive to various PT, but also makes it possible to make measurements without any external effect on the sample.[6,7] Moreover, x-ray diffraction patterns of proustite (in particular, temperature dependences of the relative intensity of a number of structural peaks) were investigated in the temperature range indicated above.

Synthetic single crystals of $Ag_3AsS_3$ were grown in Uzhgorod (Ukraine) by the Bridgman–Stockburger technique. The samples intended for acoustic measurements were in the form of plane-parallel plates of a Y- or Z-cut of thickness 0.8–1.7 mm and the surface area 30–56 $mm^2$. The method of measurements of temperature dependences of acoustic emission is described in detail in Ref. 6. X-ray measurements were made on polycrystalline samples obtained by grinding proustite single crystals. $Ag_3AsS_3$ powders were sieved through a screen with 400 mesh/inch. The samples were prepared by using nitrocellulose varnish in the form of disks of 1 mm thickness and 15 mm diameter. X-ray diffraction patterns were obtained on monochromatized Co $K_\alpha$ radiation (operating conditions for the x-ray tube BSV-29 Co are as follows: $U=35$ kV and $I=30$ mA) in the scanning mode with a step $\Delta(2\theta)=0.02°$, build-up time 10–30 s, and sample rotation in the plane of the reflecting surface at a frequency of 2 $s^{-1}$ (on a diffractometer DRON-4-07 with Bragg-Bretano focussing). The integral intensity of structural peaks was determined as the area under the corresponding curve on diffraction patterns. The error in determining the peak intensity did not exceed 5%. In the temperature range 100–293 K, diffraction patterns were obtained on the low-temperature attachment URNT-180 in the standard form. The error in maintaining the temperature did not exceed $\pm0.5$ K. The x-ray measuring technique was on the whole similar to that used earlier in Ref. 8.

The temperature dependence $N(T)$ of the acoustic emission intensity of a proustite crystal obtained for a relatively slow variation of temperature ($\sim1$ K/min) is shown in Fig. 1. It can be seen that the $N(T)$ dependence has a clearly manifested peak at $T\sim150$ K (which is reproduced successfully in repeated measurements), indicating structural variations occurring in proustite at this temperature.

In order to determine the possible variation of the proustite structure, we analyzed its x-ray diffraction patterns at four different temperatures: 100, 130, 170, and 293 K. The analysis of the diffraction pattern geometry carried out by us leads to the conclusion that the spatial group $C_{3V}^6$ of the crystals $Ag_3AsS_3$ does not change in the temperature range 100–293 K, which is in accord with the results obtained earlier.[9] At the same time, along with the conventional decrease in the intensity of diffraction peaks upon heating

 

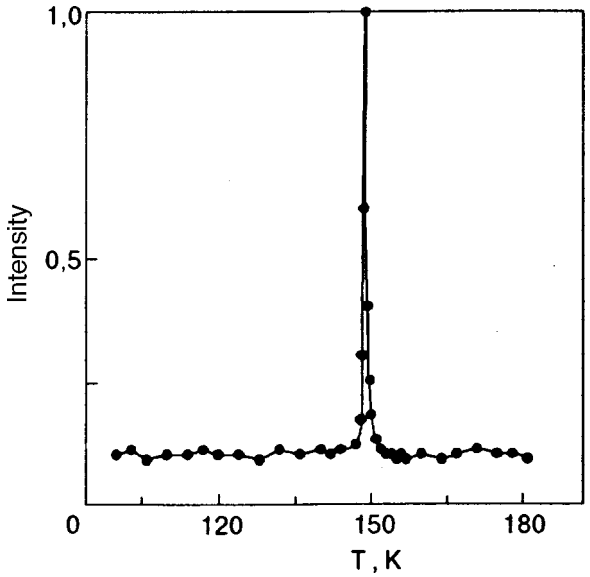


FIG. 1. Temperature dependence of the acoustic emission intensity of a proustite crystal with $Z$-cut. The heating rate is $\approx 1$ K/min.

(which is typical of most of reflexes for proustite), we observed an anomalous temperature dependence of the relative intensity of four structural peaks with indices (12.2), (23.2), (31.2), and (20.2). For each of these reflexes, we obtained the temperature dependences of relative intensity with a temperature step 6–8 K (Fig. 2). It can be seen that there are two temperature regions with basically different types of this dependence:the relative intensity decreases as the temperature increases from 100 to 140–160 K (normal region), and increases at higher temperatures (anomalous region). This is manifested especially clearly for the diffraction peak (23.2) whose intensity changes by more than 25%.

Let us analyze the obtained experimental data. Hexagonal unit cell of $Ag_3AsS_3$ contains six structural units. The core of a cell is determined by anionic pyramidal groups $AsS_3$ whose vertices are oriented in the direction of the polar axis $C$. Octahedral voids located between $AsS_3$ complexes form helical channels parallel to the $C$-axis. A hexagonal unit cell contains 36 voids of this type, only 18 of them being occupied by $Ag^+$ ions. A completely ordered silver sublattice corresponds to the equilibrium position of $Ag^+$ at the center of every second void. As a result, $Ag^+$ ions form right and left helical chains $(AgS)_\infty$ with a step $c/3$, which are parallel to the third-order axis. The nearest ions in two neighboring chains are not coupled with one another and are displaced by $c/2$ in the direction of the $C$-axis. Thus, two mutually penetrating sublattices are formed in the structure of proustite, one of which (denoted by $A$) contains only left spirals $(AgS)_\infty$, and the other ($B$) contains only right spirals. Vacant crystallographic positions and those occupied by $Ag^+$ ions alternate in the case of complete ordering. We denote by $VA$ and $VB$ the combinations of vacant positions in the sublattices $A$ and $B$, respectively. Consequently, in the crystal structure of proustite we can single out four groups of positions for silver ions, two of which ($A$ and $B$) are completely occupied by $Ag^+$ ions in a perfect crystal, while the other two ($VA$ and $VB$) are vacant (see the figures in Refs. 2 and 4).

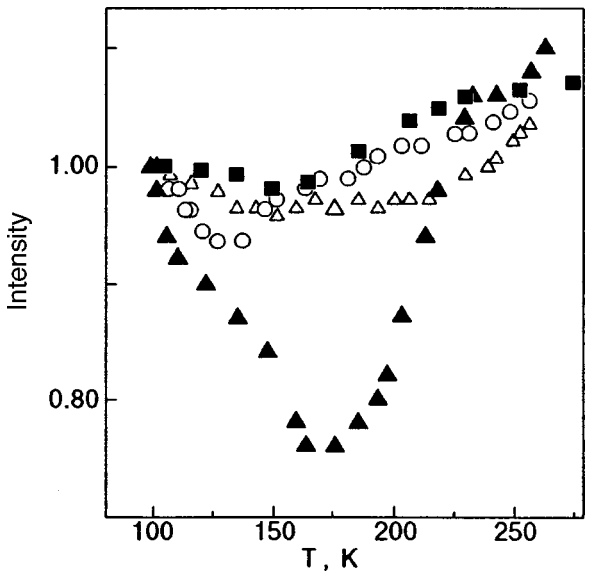


FIG. 2. Temperature dependences of relative integral intensity of diffraction peaks for proustite with different ($hkl$) indices: (23.2) (dark triangles), (20.2) (△), (31.2) (○), and (12.2) (■).

However, some of vacant positions in a real crystal are occupied by $Ag^+$ ions.[3] For this reason, the ionic occupancy of each sublattice will be specified by the average occupancy of the positions $P_i = n_i/N_i$, where $n_i$ is the average number of $Ag^+$ ions in the $i$th sublattice and $N_i$ the number of available crystallographic positions in the given sublattice. For a hexagonal unit cell of proustite, we can obviously write $N(A) = N(B) = N(VA) = N(VB) = 9$. Then the structural amplitude $\mathbf{S}_{Ag}(\mathbf{q})$ of the silver sublattice we can present in the form of four terms reflecting the filling of the indicated groups of positions. Consequently, the structural amplitude $\mathbf{S}(\mathbf{q})$ of proustite has the form

$$\begin{aligned}\mathbf{S}(\mathbf{q}) = \mathbf{S}_{Ag}(\mathbf{q}) + \mathbf{S}_{As}(\mathbf{q}) + \mathbf{S}_{S}(\mathbf{q}) = f_{Ag}(\mathbf{q})B_{Ag}(\mathbf{q}) \\ \times \Bigg[ P_A \sum_{j=1}^{9} \exp[-2\pi i \mathbf{q}\cdot\mathbf{R}(A)_j] \\ + P_B \sum_{j=1}^{9} \exp[-2\pi i \mathbf{q}\cdot\mathbf{R}(B)_j] \\ + P_{VA} \sum_{j=1}^{9} \exp[-2\pi i \mathbf{q}\cdot\mathbf{R}(VA)_j] \\ + P_{VB} \sum_{j=1}^{9} \exp[-2\pi i \mathbf{q}\cdot\mathbf{R}(VB)_j] \Bigg] \\ + f_{As}(\mathbf{q})B_{As}(\mathbf{q}) \sum_{j=1}^{6} \exp(-2\pi i \mathbf{q}\cdot\mathbf{R}(\mathrm{As})_j) \\ + f_{S}(\mathbf{q})B_{S}(\mathbf{q}) \sum_{j=1}^{18} \exp(-2\pi i \mathbf{q}\cdot\mathbf{R}(\mathrm{S})_j), \qquad (1)\end{aligned}$$

where $\mathbf{q}$ is the scattering vector, $B_{Ag}(\mathbf{q}) = \exp(-M_{Ag})$, $M_{Ag}$ being the Debye–Waller factor for $Ag^+$ ions, $\mathbf{R}(A)_j$,

TABLE I. Possible limiting types of disorder of cationic sublattice for proustite crystals.

| Type | Transition | Population of positions |
|---|---|---|
| I | $A+B\rightarrow VA+VB$ | $P=P_A=P_B,\ P_{VA}=P_{VB}=1-P_A$ |
| II | $A+B\rightarrow VA$ | $P=P_A=P_B,\ P_{VB}=0,\ P_{VA}=2(1-P_A)$ |
| III | $A+B\rightarrow VB$ | $P=P_A=P_B,\ P_{VA}=0,\ P_{VB}=2(1-P_A)$ |
| IV | $A+B\rightarrow$surface | $P=P_A=P_B,\ P_{VA}=P_{VB}=0$ |
| V | $A\rightarrow VA+VB$ | $P=P_A,\ P_B=1,\ P_{VA}=P_{VB}=0{,}5(1-P_A)$ |
| VI | $A\rightarrow VA$ | $P=P_A,\ P_B=1,\ P_{VB}=0,\ P_{VA}=1-P_A$ |
| VII | $A\rightarrow VB$ | $P=P_A,\ P_B=1,\ P_{VA}=0,\ P_{VB}=1-P_A$ |
| VIII | $A\rightarrow$surface | $P=P_A,\ P_B=1,\ P_{VA}=P_{VB}=0$ |
| IX | $B\rightarrow VA+VB$ | $P=P_B,\ P_A=1,\ P_{VA}=P_{VB}=0{,}5(1-P_B)$ |
| X | $B\rightarrow VA$ | $P=P_B,\ P_A=1,\ P_{VB}=0,\ P_{VA}=1-P_B$ |
| XI | $A\rightarrow VB$ | $P=P_B,\ P_A=1,\ P_{VA}=0,\ P_{VB}=1-P_B$ |
| XII | $B\rightarrow$surface | $P=P_B,\ P_A=1,\ P_{VA}=P_{VB}=0$ |

*Remark*. $A$ and $B$ are sublattices with left and right spirals, $VA$ and $VB$ vacant positions in sublattices $A$ and $B$, $P_i=n_i/9$ is the average population of positions in the $i$th sublattice. $n_i$ the average number of silver ions in the $i$th sublattice (the number of positions for each sublattice is 9).

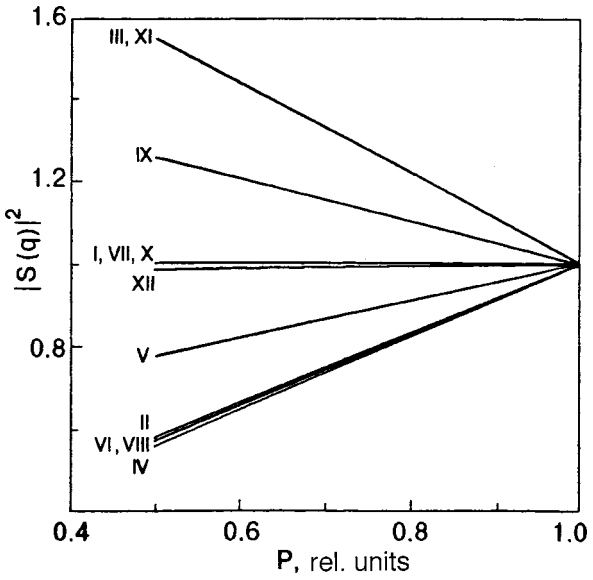


FIG. 3. Dependences of the structural factor on the population of positions by $Ag^+$ ions for the diffraction peak (23.2). The figures on the curves indicate the number of the corresponding type of disorder (see Table I).

$\mathbf{R}(B)_j$, $\mathbf{R}(VA)_j$, $\mathbf{R}(VB)_j$ are the radius-vectors of crystallographic positions of the corresponding sublattices, and $f_{\mathrm{Ag}}(\mathbf{q})$ is the atomic scattering function for the $Ag^+$ ion. The corresponding quantities for S and Ag are denoted in the same way. The values of the Debye–Waller factor and the coordinates of all atoms of each species required for calculating $|\mathbf{S}(\mathbf{q})|^2$ are determined in Refs. 10 and 11. The coordinates of vacancies for $Ag^+$ ions were calculated on the basis of the results reported in these publications.

The effect of the temperature dependence of the Debye–Waller factor (in the Debye approximation) on the relative intensity of each of the four peaks indicated above for invariable occupancies of atomic positions in the proustite structure was analyzed at the first stage. Calculations based on formula (1) proved that, from the four diffraction peaks, an anomalous behavior of relative intensity can be due to inverse temperature dependence only for the peak (20.2) (the same dependence was observed earlier for some other compounds).[12] As regards the reflexes (12.2), (23.2), and (31.2), an increase in their relative intensity with temperature can be explained only by a change in population of crystallographic positions by individual atoms. Arsenic and sulfur atoms in $Ag_3AsS_3$ crystals are coupled through a quite strong covalent bond, while silver atoms are coupled by a relatively weak ionic bond, which is manifested, for example, in a high ionic conductivity of proustite, attaining values $\sim 10^{-3}$ Sm/m at room temperature.[13] For this reason, we considered the influence of possible migration of silver ions on the structural amplitude of proustite. An analysis of various possible types of disordering in the cationic sublattice of proustite made it possible to single out twelve limiting versions of disordering presented in Table I. Unfortunately, we cannot analyze directly the temperature dependence of $|\mathbf{S}(\mathbf{q})|^2$ for each type of disordering since the temperature dependence $P(T)$ of population of the main positions by $Ag^+$ ions for $Ag_3AsS_3$ crystals differs from the exponential dependence and has not been determined in the general form to our knowledge. For this reason, we calculated the dependences of $|\mathbf{S}(\mathbf{q})|^2$ of the reflexes (23.2), (12.2), and (31.2) on the population $P$ of the main positions in the range of $P=0.5-1.0$ for each type of disordering for the same Debye–Waller factor. Figure 3 shows the calculated dependences of $|\mathbf{S}(\mathbf{q})|^2$ on $P$ for the reflex (23.2). It can be seen that an increase in the intensity of this reflex with temperature is possible only in three cases (we assume that the heating of the crystal is accompanied by a decrease in $P$). Subsequent calculations proved that an increase in the intensity of diffraction peaks (23.2), (12.2), and (31.2) with temperature and a simultaneous decrease in relative intensity of the remaining observed reflexes can be explained only for one of the three types of disordering, namely, III, IX, or XI.

Moreover, for each of the types indicated above, we calculated the dependences of $|\mathbf{S}(\mathbf{q})|^2$ on the population of positions for all other structural peaks observed on x-ray diffraction patterns. It was found that for the case III, an increase in the relative intensity of the reflex (51.1) with temperature must be almost an order of magnitude higher than the increase in the relative intensity of the reflex (23.2), which contradicts the experimental data. Thus, the anomalous behavior of the intensity of diffraction peaks can be explained for the IX or XI type of disordering. It is interesting to note that both these models are connected with disordering of $Ag^+$ ions with right spirals. In the former case, disordering occurs equiprobably over all vacant positions, while in the latter case it takes place only over free positions in right spirals. A numerical comparison of experimental results (see Fig. 2) with calculated values of the change in the intensity of peak (23.2) (see Fig. 3) speaks in favor of the XI model of disordering. Thermal disorder occurs in all probability over all possible positions, but the probabilities of populating vacant positions in different spirals are obviously different.

Since the motion of ensembles of point defects is a powerful source of acoustic emission,[7] the onset of thermal disorder for right spirals must be accompanied by the emer-

gence of considerable acoustoemission noises. This probably explains the peak on the $N(T)$ dependence observed at $T \sim 150$ K.

Thus, our experimental results provide a qualitative explanation under the assumption that the part of the cationic sublattice of proustite crystals, which is formed by right spirals $(AgS)_\infty$ is predominantly disordered upon an increase in temperature starting from $T \sim 150$ K. If this is true, only a fraction of the cationic sublattice of proustite undergoes at 150 K a sort of the phase transition typical of superionic crystals of class III according to O'Keefe classification.[14] It should be noted that the approach proposed here does not claim to unambiguity, and the verification of its validity requires additional investigations.

At the same time, structural changes in proustite at $T \sim 150$ K also follow from the results obtained earlier by other authors, for example, a change in the activation energy of charge carriers at this temperature,[15] a considerable increase in the pyroelectric coefficient,[16] and also the clearly manifested kink on the temperature dependence of the velocity of longitudinal ultrasonic waves propagating along the $C$-axis.[17]

The authors are grateful to S. M. Ryabchenko for valuable remarks made during the discussion of the results of this research.

[1] G. A. Smolenskiĭ, I. G. Siniĭ, E. G. Kuz'minov, and A. A. Godovikov, Fiz. Tverd. Tela (Leningrad) **21**, 2332 (1979) [Sov. Phys. Solid State **21**, 1343 (1979)].

[2] G. A. Smolenskiĭ, I. G. Siniĭ, S. D. Prokhorova *et al.*, Crystallografiya **27**, 140 (1982) [Sov. Phys. Crystallogr. **27**, 86 (1982)].

[3] L. A. Rebane and K. E. Khaller, Fiz. Tverd. Tela (Leningrad) **25**, 1789 (1983) [Sov. Phys. Solid State **25**, 1030 (1983)].

[4] W. Taylor, P. J. S. Ewen, and T. Han, Ferroelectrics **55**, 751 (1984).

[5] L. A. Kot, S. D. Prokhorova, Yu. M. Sandler *et al.*, Fiz. Tverd. Tela (Leningrad) **25**, 1535 (1983) [Sov. Phys. Solid State **25**, 884 (1983)].

[6] Yu. P. Gololobov and I. N. Salivonov, Fiz. Tverd. Tela (Leningrad) **33**, 298 (1991) [Sov. Phys. Solid State **33**, 172 (1991)].

[7] Yu. P. Gololobov, V. M. Perga, I. N. Salivonov, and E. E. Shchigol, Fiz. Tverd. Tela (St. Petersburg) **34**, 115 (1992) [Sov. Phys. Solid State **34**, 59 (1992)].

[8] N. A. Borovoy and Yu. P. Gololobov, Fiz. Tverd. Tela (St. Petersburg) **39**, 1652 (1997) [Phys. Solid State **39**, 1474 (1997)].

[9] I. M. Shmyt'ko, V. Sh. Shekhtman, B. Sh. Bagautdinov, and N. S. Afonnikova, Fiz. Tverd. Tela (Leningrad) **32**, 2441 (1990) [Sov. Phys. Solid State **32**, 1416 (1990)].

[10] D. Harker, J. Chem. Phys. **4**, 381 (1936).

[11] P. Engel and W. Nowacki, N. Jahr. Min. Monatsh. **6**, 181 (1966).

[12] M. A. Krivoglaz, *Diffraction of X-rays and Neutrons in Nonideal Crystals* [in Russian], Naukova Dumka, Kiev (1983).

[13] V. B. Zlokazov, L. Ya. Kobelev, and S. V. Karpachev, Dokl. Akad. Nauk SSSR **259**, 344 (1981) [Sov. Phys. Dokl. **26**, 684 (1981)].

[14] M. Salamon, *Physics of Superionic Conductors*, Springer Verlag, New York, 1979.

[15] A. N. Babushkin, V. B. Zlokazov, and L. Ya. Kobelev, Fiz. Tverd. Tela (Leningrad) **25**, 573 (1983) [Sov. Phys. Solid State **25**, 324 (1983)].

[16] S. L. Bravina, L. S. Kremenchugskiĭ, N. V. Morozovskiĭ *et al.*, Preprint No. 26, Inst. of Physics, Ukrainian Academy of Sciences, Kiev (1982).

[17] A. D. Belyaev, Yu. P. Gololobov, V. F. Machulin, and E. G. Miselyuk, Fiz. Tverd. Tela (Leningrad) **26**, 1349 (1984) [Sov. Phys. Solid State **26**, 820 (1984)].

Translated by R. S. Wadhwa

# Peculiarities of dynamics of one-dimensional discrete systems with interaction extending beyond nearest neighbors, and the role of higher dispersion in soliton dynamics

A. M. Kosevich*) and S. E. Savotchenko

*B. Verkin Institute for Low Temperature Physics and Engineering, National Academy of Sciences of the Ukraine, 310164 Kharkov, Ukraine*
(Submitted February 12, 1999)
Fiz. Nizk. Temp. **25**, 737–747 (July 1999)

In the analysis of dynamics of an ideal system as well as a system with point defects, the role of interaction is considered not only for the nearest neighbors. The Green's function is constructed for steady-state vibrations of a chain at all possible frequencies. It is shown that, if the interaction with the next-to-nearest neighbors is taken into account, the Green's function inevitably becomes double partial, the nature of its two components depending significantly on its eigenfrequency. It is found that the Green's function for frequencies of the continuous spectrum of small vibrations has one component of the plane wave type, while the other component is localized near the source of perturbations. Such a Green's function describes the so-called quasilocal vibrations. At certain discrete frequencies falling in the continuous spectrum, the quasilocal vibration is transformed into local vibration (that does not propagate to infinity). The conditions of applicability of differential equations with fourth spatial derivative are analyzed for describing the longwave vibrations of the atomic chain. Relations between parameters of atomic interactions permitting the use of such equations are formulated. Asymptotic forms of soliton fields in a nonlinear medium with spatial dispersion are discussed. It is shown that most of the soliton parameters are determined by the dispersion relation for the linearized equation. 
[S1063-777X(99)01407-3]

## INTRODUCTION

An important question in the recent investigations of the nonlinear mechanics of discrete one-dimensional systems concerns the manifestations of discreteness in soliton dynamics.[1] Nonlinear dynamics of an isolated soliton in a discrete chain is determined to a considerable extent by the spatial structure, and hence a moving soliton experiences the influence of a certain effective potential. This potential generates a Peierls force for a soliton in classical dynamics, and a free quasiparticle motion band in quantum dynamics (see Ref. 2). As regards soliton interaction, the possibility of formation of nonradiative soliton complexes, nature of regression of the corresponding fields, as well as admissible values of soliton parameters, they are mainly determined by the dispersion relation for linearized equations. Consequently, the first stage of investigation of this problem requires an analysis based on linear dynamic equations whose dispersion relations can be derived quite easily in discrete as well as continual models. This requires the discussion of certain relations between the discreteness of mechanical systems and the specific features of the functional dynamic equations describing these systems.

On account of the discreteness of the system, the dispersion relation for small vibrations differs from that for the continual description of a distributed one-dimensional system. In the longwave approximation, this difference is taken into account by higher dispersion, i.e., higher powers of the wave numbers $k$ in the expansion of the frequency $\omega$ (or energy) in powers of $ak$, where $a$ is the period of the discrete structure (lattice constant). In the coordinate representation, higher dispersion is taken into account by supplementing the ordinary differential equations of mathematical physics with spatial derivatives of, say, the fourth order.

It is well known that the limiting longwave description of the mechanics of a discrete system, which is based on the use of differential equations with second-order spatial derivatives, remains the same for any number of interacting neighbors. Hence such an approximation can be developed quite effectively by using the model involving the interaction of only the nearest neighbors and containing one parameter of interaction between particles. If, however, the aim of investigations is to study the supplementary higher dispersion, the latter must be characterized by an independent parameter. Such a parameter can be ''earned'' only if we take into account the interaction of not just the nearest neighbors. This circumstance prompted the authors to undertake the present analysis of the role of interaction of second neighbors in the crystal lattice.

We shall confine the discussion to the dynamics of one-dimensional systems described by equations obtained mainly as a result of linearization of the following two finite- difference equations:

(1) generalization of the well-known equation of the dy-

 

namics of a discrete atomic chain, which leads to the sine Gordon equation

$$\frac{\partial^2 u_n}{\partial t^2}+\omega_0^2 \sin u_n+\alpha(2u_n-u_{n+1}-u_{n-1}) -\beta(2u_n-u_{n+2}-u_{n-2})=0, \quad (1)$$

where $\alpha$ and $\beta$ are the constants of interaction with the next-to-nearest neighbor;

(2) a discrete analog of the nonlinear Schrödinger equation (NSE)

$$i\frac{\partial \psi_n}{\partial t}-E_0\psi_n+|\psi_n|^2\psi_n-\alpha'(2\psi_n-\psi_{n+1}-\psi_{n-1}) +\beta'(2\psi_n-\psi_{n+2}-\psi_{n-2})=0, \quad (2)$$

where the parameters $\alpha'$ and $\beta'$ apparently have dimensionalities differing from those of the corresponding constants in Eq. (1).

In Sec. 1, we shall study the dynamics of the system defined by the linearized equation (1). Note that the Green's function for such a system is always double-partial, i.e., consists of two independent components. In Green's function of steady-state vibrations with frequencies lying in the continuous spectrum, one of the component belongs to the localized states. This means that quasilocal vibration is the typical state of the system under consideration. The double-partial Green's function causes an interesting peculiarity of the forced vibrations in the system. The forced harmonic vibration with a frequency lying in the continuous spectrum may have distributions which result in the generation of localized vibrations. This is due to the fact that the interference of diverging waves away from the region of application of the distributed force leads to a complete mutual suppression of these waves.

Section 2 is devoted to the derivation of continual dynamic equations in the longwave approximation. It is shown that while differential equations with second-order spatial derivatives always have a region of applicability as the longwave approximation for discrete equations, the applicability of equations with fourth-order spatial derivatives is confined by rigid constraints imposed on the parameters of the initial equation. In particular, a consistent derivation of the functional equations with fourth-order spatial derivatives can be carried out in the description of steady-state vibrations by taking into account the interaction with nearest as well as next-to-nearest neighbors in the atomic chain.

It is shown by considering a simple example that the main parameters of the soliton solution of the NSE (if such an equation exists) are determined by the linearized equation, irrespective of the structure of the nonlinear term in the equation.

## 1. LINEAR DYNAMICS OF A DISCRETE ATOMIC CHAIN

*Green's function of a discrete system.* For the harmonic steady-state atomic vibrations $u_n(t)=u_n\exp(-i\omega t)$, the linearized equation (1) can be written in the form

$$(\omega_0^2-\omega^2)u_n+\alpha(2u_n-u_{n+1}-u_{n-1}) -\beta(2u_n-u_{n+2}-u_{n-2})=0. \quad (3)$$

The dispersion relation for these vibrations, corresponding to the solution $u_n=u_0\exp(ikn)$ is defined as

$$\omega^2(k)=\omega_0^2+4\alpha\sin^2\frac{k}{2}-4\beta\sin^2 k, \quad (4)$$

where it is assumed that the atomic spacing $a=1$. The continuous vibrational spectrum is the frequency band $\omega_0<\omega<\omega_m$, where $\omega_m^2=\omega_0^2+4\alpha$.

In the $n$-representation, the Green's function for the equation of steady-state vibrations of an infinite atomic chain can be presented as follows:

$$G_n(\omega)=\frac{1}{2\pi}\int_{-\pi}^{\pi}\frac{dke^{ikn}}{\omega^2-\omega^2(k)}. \quad (5)$$

The peculiarities of the Green's function are defined by the poles of the integrand on the complex $k$ plane, i.e., by the roots of the characteristic equation

$$16\beta z^4+4s^2z^2+\omega_0^2-\omega^2=0, \quad (6)$$

where $z=\sin(k/2)$ and $s^2=\alpha-4\beta$. Equation (6) has the following roots:

$$z_{1,2}^2=\frac{1}{8\beta}[-s^2\pm\sqrt{s^4-4\beta(\omega_0^2-\omega^2)}], \quad (7)$$

where the subscript 1 corresponds to the plus sign and 2 to the minus sign. We shall assume that $s^2=\alpha-4\beta>0$.

The roots of the characteristic equation determine the type of the Green's function (5). Depending on the frequency range of vibrations, the roots (7) may be real, complex, or purely imaginary.

Let us first consider the peculiarities of the dynamics of a chain in the frequency range outside the continuous spectrum band. We begin with the frequencies $\omega<\omega_0$. Such frequencies are important in the description of the dynamics of an atomic chain in the presence of a defect or asymptotic forms of bion-type soliton fields. Localized vibrations may emerge in this case.

In the frequency interval $\omega_c<\omega<\omega_0$, where $\omega_c^2=\omega_0^2-s^4/4\beta$, the roots (7) will be purely imaginary:

$$z_j=i\zeta_j=i\sinh\frac{\kappa_j}{2}\quad (j=1,2),$$

$$\zeta_{1,2}^2=\frac{1}{8\beta}[s^2\pm\sqrt{s^4-4\beta(\omega_0^2-\omega^2)}]. \quad (8)$$

The Green's function (5) for frequencies below the continuous spectral band in the interval $\omega_c<\omega<\omega_0$ can be calculated easily:

$$G_n(\omega)=\frac{1}{16\beta(\zeta_1^2-\zeta_2^2)}\left\{\frac{e^{-\kappa_1|n|}}{\zeta_1(1+\zeta_1^2)^{1/2}}-\frac{e^{-\kappa_2|n|}}{\zeta_2(1+\zeta_2^2)^{1/2}}\right\}, \quad (9)$$

where $\kappa_j=2\sinh^{-1}\zeta_j$ $(j=1,2)$ are the parameters characterizing the spatial regression of the amplitudes of local vibrations with increasing distance from the defect. Note that if

next- to-nearest neighbors are considered in the atomic chain, the Green's function becomes double-partial, i.e., it consists of two partial components that decrease exponentially in different ways.

Note that in addition to the uniform vibration with $\kappa_1=0$, which is the only one existing for a purely quadratic dispersion law, a nonuniform state with $\kappa_2\neq 0$ ($\sinh^2(\kappa_2/2)=s^2/4\beta$) supported by certain boundary conditions may exist at the limiting frequency $\omega=\omega_0$ corresponding to the lower edge of the continuous spectrum. In particular, this means that there exists a basic possibility of the existence of dynamic solitons for nonlinear equations of the type (1) or (2) even with an eigenfrequency $\omega=\omega_0$.

For $\omega<\omega_c$, the roots (8) become complex, i.e., $\kappa_{1,2}=\kappa\pm iq$, where $\kappa$ and $q$ are defined by the relations

$$\cosh\kappa\cos q=\frac{\alpha}{4\beta},\quad \sinh\kappa\sin q=\left(\frac{\omega_c^2-\omega^2}{4\beta}\right)^{1/2}.$$

Beginning from the frequencies lower than $\omega_c$, a transition takes place from ordinary to generalized local vibrations. By generalized local vibrations we mean vibrations whose amplitude decreases in an oscillating manner with increasing distance from the defect. In this case, the Green's function can be presented in the form

$$G_n(\omega)=-\frac{\exp(-\kappa|n|)\sin(q|n|+\varphi)}{(\omega_c^2-\omega^2)^{1/2}(\omega_0^2-\omega^2)^{1/4}(\omega_m^2-\omega^2)^{1/4}},\quad (10)$$

where the phase $\varphi$ is defined by the relation

$$\tan 2\varphi=\frac{\sinh 2\kappa\sin 2q}{2(\sinh^2\kappa\cos^2 q-\cosh^2\kappa\sin^2 q)}.\quad (11)$$

Let us now analyze Green's function for steady state vibrations with frequencies higher than the continuous spectral band $\omega>\omega_m$. In this frequency range, one of the wave numbers is complex ($k_1=\pi+i\kappa_1$), while the other is purely imaginary ($k_2=i\kappa_2$). In this case, the Green's function is defined as

$$G_n(\omega)=\frac{1}{16\beta(\zeta_1^2+\zeta_2^2)}\left\{\frac{(-1)^n e^{-\kappa_1|n|}}{\zeta_1(1+\zeta_1^2)^{1/2}}+\frac{e^{-\kappa_2|n|}}{\zeta_2(\zeta_2^2-1)^{1/2}}\right\},\quad (12)$$

where $\zeta_1=\sinh(\kappa_1/2)$ and $\zeta_2=\cosh(\kappa_2/2)$, and the parameters $\zeta_j$ $(j=1,2)$ are defined by the relations

$$\zeta_1^2=\frac{1}{8\beta}\{\sqrt{(\alpha+4\beta)^2+4\beta(\omega^2-\omega_m^2)}-\alpha-4\beta\},\quad (13)$$

$$\zeta_2^2=\frac{1}{8\beta}\{\sqrt{(\alpha+4\beta)^2+4\beta(\omega^2-\omega_m^2)}+\alpha+4\beta\}.\quad (14)$$

For $\beta=0$, the second term in (12) vanishes, and the Green's function naturally coincides with the expression for the Green's function of a discrete chain in which only the nearest neighbors interact.

Note that the second term in (12) is not typical for the vibrations of a chain with interaction between nearest neighbors only (when $\beta=0$). Even at the limiting frequency corresponding to the upper edge of the continuous spectrum $\omega^2=\omega_m^2=\omega_0^2+4\alpha$, it describes nonuniform vibrations in which adjacent atoms vibrate in phase.

*Problem of natural local vibrations of a chain with a point defect.* Let us consider harmonic vibrations of a chain in the presence of a point defect which is an isotopic impurity at the site $n=0$. In other words, we shall assume that this site contains an atom of mass $M$ which differs from the mass $m$ of the remaining atoms in the chain. In this case, we must consider instead of (3) the equation

$$(\omega_0^2-\omega^2)u_n+\alpha(2u_n-u_{n+1}-u_{n-1})-\beta(2u_n-u_{n+2}-u_{n-2})=fu_n\delta_{n0},\quad (15)$$

where $f=(M-m)\omega^2/m$ is the parameter characterizing the defect, and $\delta_{n0}$ is Kronecker's delta. The formal solution of Eq. (15) can be written in the following form with the help of Green's function (5):

$$u_n=-fu_0G_n(\omega).\quad (16)$$

The dispersion relation defining the frequencies of local vibrations can be obtained from (16) by putting $n=0$[3]:

$$1+fG_0(\omega)=0.\quad (17)$$

In this case, we can use Green's function (9) to obtain the dispersion relation for local frequencies falling in the interval $\omega_c<\omega<\omega_0$:

$$f=16\beta(\zeta_1^2-\zeta_2^2)\left\{\frac{\zeta_1\zeta_2\sqrt{1+\zeta_1^2}\sqrt{1+\zeta_2^2}}{\zeta_1\sqrt{1+\zeta_1^2}-\zeta_2\sqrt{1+\zeta_2^2}}\right\},\quad (18)$$

where the parameters $\zeta_j$ $(j=1,2)$ are defined by relation (8).

In the frequency range $\omega<\omega_c$, we can use Green's function (10) and write the dispersion relation for the frequencies of generalized local vibrations in the form

$$f\sin\varphi=-(\omega_c^2-\omega^2)^{1/2}(\omega_0^2-\omega^2)^{1/4}(\omega_m^2-\omega^2)^{1/4}.\quad (19)$$

Naturally, local vibrations with frequencies lower than the continuous spectrum can emerge only for $f>0$, i.e., in the presence of a heavy impurity.

Similarly, substitution of Green's function (12) into Eq. (17) leads to the dispersion relation for high-frequency local vibrations:

$$f=-16\beta(\zeta_1^2+\zeta_2^2)\left\{\frac{\zeta_1\zeta_2\sqrt{1+\zeta_1^2}\sqrt{\zeta_2^2-1}}{\zeta_1\sqrt{1+\zeta_1^2}+\zeta_2\sqrt{\zeta_2^2-1}}\right\},\quad (20)$$

where the parameters $\zeta_j$ $(j=1,2)$ are defined by relations (13) and (14).

Local vibrations with frequencies higher than the continuous spectral band emerge in the presence of a light impurity (for $f<0$).

*Forced local vibrations.* Let us now assume that the atoms in a chain are subjected to certain distributed forces $F_n\exp(-i\omega t)$ localized in the vicinity of $n=0$. In this case, the steady state solution of the dynamics of a chain can be written with the help of Green's function in the form

$$u_n=-\sum_{n'}G_{n-n'}(\omega)F_{n'}.\quad (21)$$

Let us assume that the distribution of forces has the form

$$F_n=(\delta_{0n}+\delta_{1n})F, \tag{22}$$

i.e., two adjacent sites of the chain (say, $n=0$ and $n=1$) are subjected to identical (in magnitude and sign) external forces oscillating with frequency $\omega\geqslant\omega_m$. If the frequency $\omega$ is equal to the limiting frequency $\omega_m$, the chain may undergo local vibrations with all the atoms in the same phase:

$$u_n=-\frac{F(1+e^{\kappa_2})}{16\beta\zeta_2(\zeta_1^2+\zeta_2^2)(\zeta_2^2-1)^{1/2}}e^{-\kappa_2 n}, \tag{23}$$

whose parameter $\kappa_2$ is defined by the relation

$$\sinh^2\frac{\kappa_2}{2}=\frac{\alpha}{4\beta}. \tag{24}$$

Obviously, one of the terms in (12) may not ''operate'' for some types of coercive external force. For example, let us consider the action of oscillating forces applied to the sites $n=0$ (force $F_0$) and $n=\pm1$ (force $F_1$), i.e.,

$$F_n=F_0\delta_{0n}+F_1(\delta_{1n}+\delta_{-1n}). \tag{25}$$

In this case, we obtain from (21) the following solution by taking into account the distribution of forces (25) and Green's function (12):

$$u_n=-\frac{1}{16\beta(\zeta_1^2+\zeta_2^2)}\left\{\frac{(-1)^n(F_0-2F_1\cosh\kappa_1)e^{-\kappa_1|n|}}{\zeta_1(1+\zeta_1^2)^{1/2}}+\frac{(F_0+2F_1\cosh\kappa_2)e^{-\kappa_2|n|}}{\zeta_2(\zeta_2^2-1)^{1/2}}\right\}. \tag{26}$$

If forces $F_0$ and $F_1$ have opposite signs and $|F_0|>2|F_1|$, there exists a frequency $\omega$ for which

$$\cosh\kappa_2=\left|\frac{F_0}{2F_1}\right|. \tag{27}$$

In this case, Eq. (26) is simplified and assumes the form

$$u_n=\frac{(-1)^{n+1}2F_1(\cosh\kappa_1+\cosh\kappa_2)e^{-\kappa_1|n|}}{16\beta\zeta_1(\zeta_1^2+\zeta_2^2)\sqrt{1+\zeta_1^2}}. \tag{28}$$

Such a solution can describe the asymptotic forms of an enveloping soliton for high-frequency localized vibrations. It can be seen that such a soliton can emerge at quite specific eigenfrequencies.

If the forces $F_0$ and $F_1$ have the same sign, localized vibrations

$$u_n=-\frac{2F_1(\cosh\kappa_1+\cosh\kappa_2)e^{-\kappa_2|n|}}{16\beta\zeta_2(\zeta_1^2+\zeta_2^2)\sqrt{\zeta_2^2-1}}, \tag{29}$$

corresponding to the motion of atoms in the same phase emerge at a certain frequency $\omega$ defined by the equation

$$\cosh\kappa_1=\frac{F_0}{2F_1}. \tag{30}$$

*Peculiarities of vibrations with frequencies lying in the continuous spectrum band.* The inclusion of interaction with next-to-nearest neighbors leads to the emergence of additional peculiarities of vibrations with frequencies lying inside the continuous spectral band $\omega_0<\omega<\omega_m$. In this case, vibrations emerge with one mode localized in the vicinity of the defect, the other being a standing wave. Such vibrations are called quasilocal vibrations. In the frequency range under consideration, the characteristic equation (6) has two real roots

$$z_1^2=\frac{1}{8\beta}[\sqrt{s^4+4\beta(\omega^2-\omega_0^2)}-s^2], \tag{31}$$

and two imaginary roots

$$\zeta_2^2=\frac{1}{8\beta}[\sqrt{s^4+4\beta(\omega^2-\omega_0^2)}+s^2]. \tag{32}$$

Hence one of the wave numbers $k_1=2\sin^{-1}z_1$ will be real and the other $k_2=i\kappa_2$ ($\kappa_2=2\sinh^{-1}\zeta_2$) will be imaginary.

Using formulas (31) and (32), we can calculate Green's function (5) in the frequency range of quasilocal steady state vibrations:

$$G_n(\omega)=iB(\omega)e^{ik_1|n|}+M(\omega)e^{-\kappa_2|n|}, \tag{33}$$

where

$$B(\omega)=[16\beta z_1(z_1^2+\zeta_2^2)\sqrt{1-z_1^2}]^{-1},$$

$$M(\omega)=[16\beta\zeta_2(z_1^2+\zeta_2^2)\sqrt{1+\zeta_2^2}]^{-1}.$$

Taking Green's function (33) into consideration, we can use the familiar relation

$$g(\omega^2)=\frac{1}{\pi}\operatorname{Im}G_0(\omega)$$

to calculate the density of vibrations (distribution of states in squares of frequencies) of a defect-free chain:

$$g(\omega^2)=\frac{1}{16\pi\beta(z_1^2+\zeta_2^2)z_1(1-z_1^2)^{1/2}}. \tag{34}$$

For a certain distribution of forces $F_n$, the solution in the region of the continuous spectrum can be obtained from (21) with the help of the Green's function (33):

$$u_n=\begin{cases}-iB(\omega)F^*(k_1)e^{-ik_1n}-M(\omega)Q(-\kappa_2)e^{\kappa_2 n}, & n<0;\\ -iB(\omega)F(k_1)e^{ik_1n}-M(\omega)Q(\kappa_2)e^{-\kappa_2 n}, & n>0,\end{cases} \tag{35}$$

where $F(k)=\Sigma_n F_n e^{-ikn}$ and $Q(\kappa)=\Sigma_n F_n e^{\kappa_2 n}$.

Let us assume that $F_n=F_{-n}$. There may exist a symmetric distribution $F_n$ for which the condition

$$F(k)=\sum_n F_n\cos kn=0, \tag{36}$$

is satisfied for a certain value of $k$, i.e., the Fourier component of spatial distribution of forces vanishes. In this case, the solution is localized for an appropriate frequency $\omega$ defined by the condition (36):

$$u_n=-M(\omega)Q(\kappa_2)e^{-\kappa_2|n|}, \tag{37}$$

where the parameter $\kappa_2$ corresponds to such a frequency.

Thus, interference of waves excited by the chosen distribution $F_n$ of force leads to mutual suppression of vibrations away from the region of application of such forces. In other

words, a localized state appears in the continuous frequency spectrum, which cannot be expected in a distributed dynamic system with interaction of nearest neighbors only.

Let us suppose that $F_n$ has the form of a two-hump distribution:

$$F_n=\varphi(n-n_0)+\varphi(n+n_0), \tag{38}$$

where $\varphi(n)=\varphi(-n)$ is an even function. In this case, Eq. (36) holds for all values of $k$ satisfying the condition $\cos kn_0=0$, i.e., for $k=(2p+1)\pi/2n_0$, where $p=0,\pm1,\pm2,...,\pm(n_0-1)$.

Even if we do not require that the function $\varphi(n)$ be even, it can easily be shown that there exists at least one value of $k$ for which condition (36) is satisfied.

It is obvious that there exists a discrete set of frequencies falling in the continuous spectrum, for which the force that depends harmonically on time and has a spatial distribution (38) does not excite any radiation at infinity. Distribution of the type (38) simulates the behavior of the nonlinear term in (1) or in (2) for the case when such an equation has a two-soliton solution. If such a solution does exist, it corresponds at certain frequencies to the steady state of a pair of solitons. Such a situation was discussed in Ref. 4. It should be emphasized that the possibility of existence of such a solution in the continuous frequency spectrum is determined entirely by the form of the dispersion relation for small vibrations.

It should be remembered that the localized states described above belong to the quasicontinuous spectrum of the atomic chain, and hence the weight of each of them is quite small and proportional to $1/\sqrt{N}$, where $N$ is the number of atoms in the chain. However, the weight of such states may be finite in nonlinear dynamics.

*Scattering of a wave by a point defect.* Let us return to the case of an isotopic point defect for $F_n=f\delta_{n0}u_0$. The possibility of obtaining the explicit form of Green's function for the investigated system makes it possible to study easily the problem of scattering of the vibration of an ideal chain by a point defect. It is well known that the solution of the scattering problem can be written in the form

$$u_n=u_0e^{ik_1n}+\chi_n, \tag{39}$$

while the field $\chi_n$ can be the presented in terms of the Green's function[2]

$$\chi_n=-u_0f\frac{G_n(\omega)}{D(\omega)}, \tag{40}$$

where $D(\omega)=1+fG_0(\omega)$. In this solution, we must choose the Green's function corresponding to waves in the form (33) diverging at infinity. In this case, the solution (39) can be written in the form

$$u_n=\begin{cases} u_0e^{ik_1n}-\dfrac{u_0f}{D(\omega)}[iB(\omega)e^{-ik_1n}+M(\omega)e^{\kappa_2n}], & n<0,\\ u_0e^{ik_1n}-\dfrac{u_0f}{D(\omega)}[iB(\omega)e^{ik_1n}+M(\omega)e^{-\kappa_2n}], & n>0. \end{cases} \tag{41}$$

It is interesting to note that if the condition

$$iB(\omega)f=D(\omega) \tag{42}$$

is satisfied, the incident wave is reflected completely at the defect and an asymmetric state corresponding to a standing wave which exists only along one of the semi-axes, and to modes localized on both sides of the defect is realized:

$$u_n=\begin{cases} u_0\left(2i\sin(k_1n)-f\dfrac{M(\omega)}{D(\omega)}e^{\kappa_2n}\right), & n<0;\\ -u_0f\dfrac{M(\omega)}{D(\omega)}e^{-\kappa_2n}, & n>0. \end{cases} \tag{43}$$

It follows from Eq. (42) that asymmetric states (43) can be realized at frequencies defined by the relation

$$f=-16\beta\zeta_2\sqrt{1+\zeta_2^2}(z_1^2+\zeta_2^2). \tag{44}$$

The emergence of such an asymmetric state (43) with frequencies in the continuous spectrum was detected in Ref. 5, where the scattering of an elastic wave at a plane defect was considered in an isotropic medium. Similar peculiarities were observed for the discrete model of an fcc crystal in Ref. 6, where the results of numerical calculations were analyzed. It should be remembered, however, that an elastic wave consists of two independent components (longitudinal and transverse), while the field considered by us has only one component. Consequently, the role of two components in the present case is played by two types of eigenvibrations corresponding to different roots of the characteristic equation.

As far as the weight of the state (43) is concerned, the statement made about the solution (37) can be repeated.

## 2. LONGWAVE VIBRATIONS OF A SYSTEM WITH SPATIAL DISPERSION

*Linear equations of motion and Green's functions in the functional approximation.* If interaction with next-to-nearest neighbors in a discrete chain is taken into consideration, a significant change is observed in the longwave vibrations for $k\ll1$ (it should be recalled that $a=1$). In this limit, the discrete equation (3) leads to the differential equation

$$\frac{\partial^2u}{\partial t^2}+\omega_0^2u-s^2\frac{\partial^2u}{\partial x^2}+A^2\frac{\partial^4u}{\partial x^4}=0, \tag{45}$$

whose parameters are connected with the interaction constants of nearest and next-to-nearest neighbors: $s^2=\alpha-4\beta$, $A^2=(16\beta-\alpha)/12$. We shall assume that the condition $\alpha/16<\beta<\alpha/4$ is satisfied.

The dispersion relation for steady-state vibrations of a system without defects can be obtained easily from (45) or from an expansion of the dispersion relation (4) in the discrete model up to fourth-order terms in $k$:

$$\omega^2(k)=\omega_0^2+s^2k^2+A^2k^4. \tag{46}$$

The wave numbers $k$ corresponding to a fixed frequency $\omega$ can be determined from (46):

$$k_{1,2}^2=\frac{1}{2A^2}[-s^2\pm\sqrt{s^4-4A^2(\omega_0^2-\omega^2)}], \tag{47}$$

where the subscripts 1 and 2 correspond to plus and minus sign, respectively.

Since the requirement $k_{1,2}^2 \ll 1$ must be satisfied for all roots of (47) in the longwave approximation, the approximation based on (46) can be used for describing the steady-state vibrations of a discrete chain only at frequencies $|\omega_0-\omega| \ll A$ if the parameters of the chain satisfy the condition $s^2 \ll A^2$. However, in this case $A^2 \equiv \beta - s^2/12 \approx \beta$ and it can be seen that Eq. (45) can be used only if the next-to-nearest neighbors are taken into consideration.

Let us consider the peculiarities of localized vibrations with frequencies below the continuous spectrum $\omega < \omega_0$. In the frequency range $\omega_c < \omega < \omega_0$, where $\omega_c^2 = \omega_0^2 - s^4/4A^2$, the wave numbers (47) are purely imaginary $k_j = i\kappa_j$ ($j=1,2$), and Green's function for Eq. (45) in the frequency range under consideration is defined as

$$G(x) = \frac{1}{2A^2(\kappa_1^2-\kappa_2^2)}\left(\frac{e^{-\kappa_1|x|}}{\kappa_1} - \frac{e^{-\kappa_2|n|}}{\kappa_2}\right). \tag{48}$$

Green's function (48) is the longwave limit of function (9) under the assumption $\zeta_j = \kappa_j/2 \ll 1$ and $A^2 = \beta$. It can be verified once again that if additional dispersion is taken into account in Eq. (45), the results match for $A^2 = \beta \gg s^2$.

In the frequency range $\omega < \omega_c$, Green's function in the continual approximation follows naturally from the discrete Green's function (10):

$$G(x) = -\frac{\sin(q|x|-\varphi)\exp(-\kappa|x|)}{2A^{1/2}(\omega_c^2-\omega^2)^{1/2}(\omega_0^2-\omega^2)^{1/4}}, \tag{49}$$

where

$$\kappa^2 = \frac{1}{4A^2}(2A\sqrt{\omega_0^2-\omega^2}+s^2)$$

and

$$q^2 = \frac{1}{4A^2}(2A\sqrt{\omega_0^2-\omega^2}-s^2),$$

and the phase $\varphi$ of vibrations is defined by the relation $\tan\varphi = \kappa/q$.

Generalization of formula (49) to the spherically symmetric case of a three-dimensional system was carried out by Buzdin *et al.*[7] (see Appendix).

At frequencies $\omega > \omega_0$, quasilocal vibrations may emerge in the continuous spectrum since one of the roots (47) will be real:

$$k^2 = \frac{1}{2A^2}[-s^2 + \sqrt{s^4+4A^2(\omega^2-\omega_0^2)}], \tag{50}$$

and the other will be imaginary:

$$\kappa^2 = \frac{1}{2A^2}[s^2 + \sqrt{s^4+4A^2(\omega^2-\omega_0^2)}]. \tag{51}$$

In this case, Green's function is defined as

$$G(x) = iB(\omega)e^{ik|x|} + M(\omega)e^{-\kappa|x|},$$
$$B(\omega) = [2A^2k(k^2+\kappa^2)]^{-1},$$
$$M(\omega) = [2A^2\kappa(k^2+\kappa^2)]^{-1}. \tag{52}$$

Green's function (52) demonstrates the properties of quasilocal vibrations: it is double-partial, one of its portions being localized in space and the other being a standing wave in the entire space. Function (52) reflects an interesting peculiarity of the physical properties of the system with the above-mentioned dispersion, viz., the presence of an additional spatially localized field component (portion of Green's function), which may appear in a linear chain with defects, as well as in soliton problems of a nonlinear chain. This peculiarity admits the existence of localized vibrations with frequencies belonging to the continuous spectrum of the chain under consideration. The conditions of realization of such states in a distributed system are analogous to those obtained in Sec. 1 for a discrete chain.

*Problem of high-frequency vibrations.* The standard technique of continual description of high-frequency ($|\omega - \omega_m| \ll \omega_m$) eigenvibrations of a discrete chain boils down to the introduction of envelopes of atomic displacements for which adjacent atoms vibrate in antiphase. Presenting the solution of Eq. (3) in the form

$$u_n = (-1)^n\Phi_n, \tag{53}$$

we find that the function $\Phi_n$ depends weakly on $n$ in the indicated frequency range, and obtain the following equation in the continual approximation:

$$(\omega_m^2-\omega^2)\Phi + s_1^2\frac{\partial^2\Phi}{\partial x^2} + B^2\frac{\partial^4\Phi}{\partial x^4} = 0, \tag{54}$$

where $s_1^2 = \alpha + 4\beta$ and $B^2 = (\alpha+16\beta)/12$. Obviously, $\Phi(x)$ has the meaning of the envelope of high-frequency vibrations.

The dispersion relation corresponding to Eq. (54) can be obtained easily from (4) by putting $k = \pi + q$ and expanding (4) up to fourth powers in small $q$:

$$\omega^2(q) = \omega_m^2 - s_1^2q^2 + B^2q^4. \tag{55}$$

Obviously, Eq. (55) follows directly from (54) as a result of the substitution $\Phi(x) = \Phi_0\exp(iqx)$. It can be seen that for large values of $q$, the dispersion relation of the type (55) corresponds to nonphysical behavior of vibrational frequencies of an atomic chain in the vicinity of the upper edge of the continuous spectral band. The last term, which is proportional to the fourth power of $q$, ''distorts'' the dispersion relation. Hence we must confine ourselves to just the quadratic approximation in $q$.

Since we assumed that $\alpha > 4\beta > 0$, it means that the inclusion of the fourth derivative in Eq. (54) is incorrect for this model, and the longwave description of steady-state vibrations with frequency $\omega \approx \omega_m$ must be restricted to the second spatial derivative in Eq. (54). Small values of $q$ correspond to the condition $|\omega_m^2-\omega^2| \ll \alpha$, which determines the range of applicability of the second-order differential equation for the envelope of high-frequency vibrations.

*Role of higher dispersion in soliton dynamics.* The fact that the asymptotic form of Green's function (48) consists of two exponents allows us to make certain remarks about the soliton solutions of the corresponding nonlinear equation, e.g., Eq. (2). We can write this equation for the steady-state solution $\Psi = z(x)\exp(-iEt)$ in the dimensionless form

$$\frac{d^4z}{dx^4}-\frac{d^2z}{dx^2}+\Omega z=z^3, \tag{56}$$

containing only one parameter $\Omega$ which is proportional to $E-E_0$.

Suppose that (56) has an even soliton solution $z(x)=\varphi_s(x)=\varphi_s(-x)$. An analysis of all the terms in Eq. (56) gives

$$\varphi_s(x)=\frac{M}{\cosh^2 \kappa x}, \quad M=\text{const}. \tag{57}$$

The expansion of this equation at infinity can obviously be presented in the form

$$\varphi_s(x)=4M(e^{-2\kappa|x|}-2e^{-4\kappa|x|}). \tag{58}$$

Comparing the exponents in (58) and (48) where we have made the substitutions $A^2=s^2=1$ and $\Omega=\omega_0^2-\omega^2$, we obtain

$$4\kappa^2=\kappa_1^2=\frac{1}{2}(1-\sqrt{1-4\Omega}),$$

$$16\kappa^2=\kappa_2^2=\frac{1}{2}(1+\sqrt{1-4\Omega}). \tag{59}$$

This gives

$$\kappa^2=0.5 \quad \text{and} \quad \Omega=0.16. \tag{60}$$

Thus, if a soliton solution exists for the nonlinear equation, its basic parameters are defined by the linearized equation. Naturally, the solution itself follows from the nonlinear equation (56). Solution (57) with parameters (60) was obtained first by Hook and Karlsson.[8]

*Analysis of eigenfrequencies of a medium with higher dispersion of opposite signs.* The situation involving the use of Eq. (45) changes if $\beta<0$. In this case, $s^2=\alpha+4|\beta|$, $A^2=-(|\beta|+s^2/12)<0$, and the condition $|A^2|\gg s^2$ formulated above cannot be satisfied. Hence the linear equation (45) is inapplicable for describing longwave steady-state vibrations of a discrete chain. One of the reasons behind this is that the dispersion relation (46) with $A^2<0$ displays a nonphysical behavior for large $k$. In this case, the continual description with the help of an equation of the type (45) is admissible only when a differential equation with second-order spatial derivative is used.

However, a situation exists in which Eq. (3) has a continual equivalent for $\beta<0$. his concerns the description of dynamic excitation of a chain moving steadily with a velocity $V$, for which the solution $u(x,t)=u(x-Vt)$. In this case, we obtain instead of (45) the equation

$$\omega_0^2 u-\gamma^2\frac{\partial^2 u}{\partial x^2}-B^2\frac{\partial^4 u}{\partial x^4}=0, \tag{61}$$

where $\gamma^2=s^2-V^2$, $s^2=\alpha+4|\beta|$ and $B^2=(\alpha+16|\beta|)/12$. The wave numbers $k$ corresponding to the given velocity $V$ are obtained from the dispersion relation

$$\omega_0^2+\gamma^2k^2-B^2k^4=0 \tag{62}$$

and are defined by the expressions

$$k_{1,2}^2=\frac{1}{2B^2}(\gamma^2\pm\sqrt{\gamma^4+4B^2\omega_0^2}). \tag{63}$$

It can be seen that the longwave condition $k\ll 1$ is satisfied if $\gamma^2\ll B^2$ and $\omega_0^2\ll B^2$.

Equation (61) has a double-partial solution as before: one portion is in the form of a plane wave with the squares of wave numbers defined as

$$k_1^2=\frac{1}{2B^2}(\sqrt{\gamma^4+4B^2\omega_0^2}+\gamma^2), \tag{64}$$

while the other is localized, and the coefficient of attenuation of its amplitude with distance is defined by the expression

$$\kappa_2^2=\frac{1}{2B^2}(\sqrt{\gamma^4+4B^2\omega_0^2}-\gamma^2). \tag{65}$$

Obviously, the second (localized) portion has a physical meaning either for an external force applied to the chain moving with a velocity $V$, or in the analysis of the asymptotic forms of the field of a soliton moving with the given velocity. It is interesting to note that relations (64) and (65) have a meaning for $V<s$ as well as for $V>s$, but inevitably under the condition $|\gamma^2|\ll B^2$. As regards the necessary conditions, they can be satisfied even for $\beta=0$. In other words, Eq. (61) has a physical meaning under these conditions even for a chain in which only the nearest neighbors interact. This justifies the longwave description of the nonradiative motion of a soliton in the generalized Frenkel-Kontora model.[9,10]

The situation in which the higher spatial dispersion is taken into account in the continual approximation for describing vibrations with frequencies close to the upper edge of the continuous spectral band also varies for $\beta<0$. Putting $k=\pi+q$ in (4) and expanding it in small $q$, we obtain the dispersion relation

$$\omega^2(q)=\omega_m^2-s^2q^2-C^2q^4, \tag{66}$$

where $s^2=\alpha-4|\beta|>0$ and $C^2=(16|\beta|-\alpha)/12>0$. This gives the wave numbers in which we are interested:

$$q_{1,2}^2=\frac{1}{2A^2}[-s^2\pm\sqrt{s^4-4C^2(\omega^2-\omega_m^2)}]. \tag{67}$$

Since the requirement $q_{1,2}\ll 1$ must be met for all the roots defined by (67), the continual approximation based on the use of higher dispersion in (66) is applicable for describing the vibrations of a discrete linear chain of atoms at frequencies $|\omega_m^2-\omega^2|\ll C^2$ under the condition $s^2\ll C^2$. Hence it would be expedient to take into consideration the fourth spatial derivative in the differential equation for the envelope of high-frequency vibrations in this case.

The authors are obliged to M. M. Bogdan for fruitful discussions of the results. This research was supported by the project 2.4/163 of the Ukrainian Ministry of Science and Technology.

## APPENDIX: GENERALIZATION OF GREEN'S FUNCTION TO THE THREE-DIMENSIONAL SPHERICALLY SYMMETRIC CASE

Generalization of Eq. (45) for the model of a three- dimensional medium in the continual approximation can be represented in the form[7]

$$\frac{\partial^2 u}{\partial t^2}+\omega_0^2 u-s^2\Delta u+A^2\Delta\Delta u=0, \tag{A1}$$

where the Laplace operator $\Delta=(1/r^2)\partial(r^2\partial/\partial r)/\partial r$ in the spherically symmetric case. Obviously, the harmonic solutions of Eq. (A1) have a dispersion relation for steady-state vibrations in the form (46), where $k$ stands for the modulus of the wave vector.

Green's function for a three-dimensional crystal is defined as

$$G(r)=\frac{1}{(2\pi)^3}\int\frac{e^{i\mathbf{k}\cdot\mathbf{r}}d^3k}{\omega^2-\omega^2(k)}. \tag{A2}$$

For steady-state vibrations with dispersion relation (46), we can easily calculate Green's function for various frequency intervals.

At frequencies below the continuous spectrum $\omega_c<\omega<\omega_0$, where $\omega_c^2=\omega_0^2-s^4/4A^2$, the wave numbers (47) are purely imaginary, $k_j=i\kappa_j$ $(j=1,2)$, and the Green's function is defined as

$$G(r)=-\frac{1}{4\pi A^2}\frac{e^{-\kappa_1 r}-e^{-\kappa_2 r}}{(\kappa_1^2-\kappa_2^2)r}. \tag{A3}$$

For $\omega<\omega_c$, wave numbers (47) become complex $(\kappa_{1,2}=\kappa\pm iq)$, and

$$G(r)=\frac{1}{8\pi A^2}\frac{\sin(qr)}{q\kappa}\frac{e^{-\kappa r}}{r}. \tag{A4}$$

For the continuous spectral frequencies $\omega>\omega_0$, we obtain one real wave number $k$ (50) and one purely imaginary wave number $i\kappa$ (51). In this case, Green's spherical symmetric function has the form

$$G(r)=\frac{1}{4\pi A^2}\frac{e^{ikr}-e^{-\kappa r}}{(k^2+\kappa^2)r}. \tag{A5}$$

Using this equation, we can easily calculate the density of vibrations:

$$g(\omega^2)=\frac{1}{(2\pi)^2}\left\{\frac{\sqrt{s^4+4A(\omega^2-\omega_0^2)}-s^2}{2A^2[s^4+4A(\omega^2-\omega_0^2)]}\right\}. \tag{A6}$$

The Green's functions obtained in this way can be used for studying the vibrations of a crystal with a point defect.

*)E-mail: kosevich@ilt.kharkov.ua

[1] S. Flach and C. Willis, Phys. Rep. **295**, 181 (1998).
[2] A. M. Kosevich, *Theory of Crystal Lattice* [in Russian], Vishcha Shkola, Khar'kov (1988).
[3] I. M. Lifshitz and A. M. Kosevich, Rep. Progr. Phys. **29.1**, 217 (1966).
[4] A. V. Buryak and N. N. Akhmediev, Phys. Rev. E **51**, 3572 (1995).
[5] A. M. Kosevich and A. V. Tutov, Phys. Lett. A **248**, 271 (1998).
[6] A. M. Kosevich, D. V. Matsokin, and S. E. Savotchenko, Fiz. Nizk. Temp. **25**, 63 (1999) [Low Temp. Phys. **25**, 48 (1999)].
[7] A. I. Buzdin, V. N. Men'shov and V. V. Tugushev, Zh. Éksp. Teor Fiz. **91**, 2204 (1986) [Sov. Phys. JETP **64**, 1310 (1986)].
[8] A. Hook and M. Karlsson, Opt. Lett. **18**, 1390 (1993).
[9] M. Bogdan and A. Kosevich, in: *Nonlinear Coherent Structures in Physics and Biology* (Ed. by K. H. Spatschek and F. G. Mertens), Plenum Press, New York (1994).
[10] M. Bogdan and A. Kosevich, Proc. Estonian Acad Sci. Phys. Mat. **46**, 14 (1997).

Translated by R. S. Wadhwa

## LOW-TEMPERATURE PHYSICS OF PLASTICITY AND STRENGTH

# Effect of plastic deformation on the shape and parameters of the low-temperature peak of internal friction in niobium

V. D. Natsik, P. P. Pal-Val, L. N. Pal-Val,*) and Yu. A. Semerenko

*B. Verkin Institute for Low Temperature Physics and Engineering, National Academy of Sciences of the Ukraine, 310164 Kharkov, Ukraine*

(Submitted January 28, 1999)
Fiz. Nizk. Temp. **25**, 748–757 (July 1999)

Temperature dependences of the decrement of longitudinal vibrations are studied at moderately low temperatures in polycrystalline niobium with the residual resistivity ratio $RRR=60$ at frequencies 78 and 363 kHz. A peak of internal friction is detected in the vicinity of 200 K. The height, width, and temperature of the peak change significantly upon a variation of vibrational frequency and as a result of changes in the defect structure of the sample under thermocycling, plastic deformation, or prolonged low-temperature recovery. It is shown that the absorption peak is due to the interaction of elastic vibrations of the sample with a system of identical thermally activated relaxators with an activation energy of 0.15 eV and an attack frequency of $1\times10^{10}\,s^{-1}$ in a nearly perfect crystal. A theory is proposed for describing the variation of the shape and parameters of the internal friction peak due to statistical dispersion of the values of activation energy of the relaxators. 
[S1063-777X(99)01507-8]

### 1. INTRODUCTION

Peaks of mechanical relaxation were detected by many authors who studied the temperature dependence of internal friction in niobium samples of various purity and structural perfection at moderately low temperatures. The temperature $T_p$ of peak localization increased from 90 to 200 K upon a change in the vibrational frequency in a wide frequency range from infrasonic frequencies of the order of $10^{-3}$ Hz to ultrasonic frequencies of the order of $10^5$ Hz.[1–12] It was noted in some publications that plastic deformation of samples prior to acoustic measurements led to an increase in the height and width of the peaks as well as to a shift of $T_p$ towards higher temperatures. The results obtained on the dependence $T_p(\omega)$ of the temperature of peak localization on the cyclic frequency $\omega$ are systematized in Fig. 1. It can be seen that the internal friction peaks under consideration in the first approximation correspond to a certain thermoactivated relaxation process with a relaxation time depending exponentially on temperature $T$:

$$\tau(T)=\tau_0\exp\left(\frac{U}{kT}\right), \tag{1}$$

where $U$ is the activation energy, $\tau_0$ the period of attacks, and $k$ the Boltzmann constant. The complete set of experimental data presented in Fig. 1 corresponds to the relaxation resonance $\omega\tau(T_p)=1$ for typical values of activation energy $U\approx0.27$ eV and the attack period $\tau_0\simeq10^{-13}$ s (straight line *1* in Fig. 1). However, a wide spread of experimental points which is apparently associated partially with differences in the structure of samples leads to considerable uncertainty in determining the empirical values of the parameters of relaxation process and complicates its microscopic interpretation.

We can state that the nature of the given relaxation process remains unclear. Moreover, we cannot be sure that all the data presented in Fig. 1 correspond to the same relaxation process and are not the result of superposition of several processes with different activation parameters.[13] A thoroughly developed theory that would describe the effect of structural inhomogeneities, e.g., statistical ensemble of dislocations and random fields of internal stresses introduced in crystalline samples during plastic deformation on the shape and parameters of internal friction relaxation peak has not been developed. The available theoretical publications concerning this problem are mainly devoted to an analysis of the joint effect of random spread in the activation energy $U$ and the preexponential factor $\tau_0$ or the relaxation time $\tau$ on the peak width (see, for example, Refs. 14 and 15). The shift in the peak temperature $T_p$ as well as the change in the height of the peak and its asymmetry, which are clearly manifested in experiments, have not been investigated.

In the present work, we obtain additional experimental data on internal friction of polycrystalline niobium in the range of moderately low temperatures. We observed in our experiments an internal friction peak in the temperature range near 200 K by using longitudinal ultrasonic vibrations at frequencies $\omega/2\pi=78$ and 363 kHz. The effect of preliminary plastic deformation and sample recovery on the location temperature, height, and shape of the peak is analyzed. We also propose a theoretical interpretation of the observed regularities, which is based on assumptions on the statistical nature of the parameters of elementary relaxators responsible

 

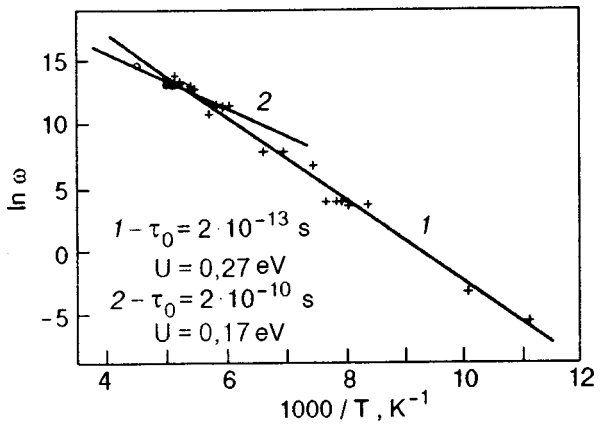


FIG. 1. Activation curve for the system of internal friction peak in niobium observed experimentally by different authors in the range of moderately low temperatures: the results of previous experiments (+) and the results obtained in this research (○,●), $U$ and $\tau_0$ are the parameters of straight lines drawn through the corresponding set of points with minimum standard deviations.

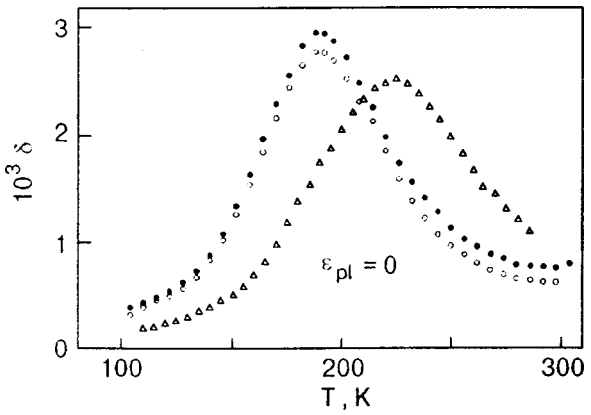


FIG. 2. Internal friction peak in polycrystalline undeformed niobium and its variation upon an increase in the amplitude $\varepsilon_0$ and frequency $\omega/2\pi$ of acoustic vibrations: $\omega/2\pi = 78$ kHz, $T_p = 190$ K, $\varepsilon_0 = 3\times10^{-8}$ (○) and $3\times10^{-5}$ (●); $\omega/2\pi = 363$ kHz, $T_p = 225$ K, $\varepsilon_0 = 3\times10^{-8}$ (△).

for the given peak and on the effect of dislocations on the activation energy dispersion and volume density of relaxators.

## 2. EXPERIMENTAL PROCEDURE AND RESULTS OF MEASUREMENTS

The sample was spark cut from polycrystalline niobium, lapped with abrasive powders to attain the required shape and geometrical dimensions size, and then subjected to chemical polishing to remove surface layers damaged during mechanical treatment. The final size of the sample was $3\times3\times21$ mm. The grain size of the sample did not exceed 0.1 mm, which was much smaller than the sample section. The initial density of dislocations was $\sim10^6$ cm$^{-2}$.

The integral measure of sample purity was the residual resistivity ratio $RRR = R_{300}/R_0 \simeq 60$, which was determined by measuring the temperature dependence of the sample resistance in the temperature range 2–300 K. The obtained experimental data were extrapolated to 0 K and to zero value of the external magnetic field used for the conversion of the samples to the normal state at temperatures below the superconducting transition temperature $T_c \simeq 9.3$ K.

In order to find the relation between acoustic properties of niobium and the dislocation structure of the samples, fresh dislocations were introduced in the sample by preliminary torsion at room temperature around the longitudinal axis to a residual plastic strain $\sim5\%$. After the deformation, the sample was lapped again to restore the shape of parallelepiped and subjected to chemical polishing. Measurements were made immediately after the deformation and after a time period about one year, which allowed us to detect changes in the acoustic properties of the sample as a result of prolonged holding at room temperature.

Acoustic measurements were made by the two-composite vibrator technique.[16,17] Longitudinal standing waves were excited in the sample at frequencies $\omega/2\pi = 78$ and 363 kHz. The amplitude of ultrasonic deformation $\varepsilon_0$ varied in the interval $3\times10^{-8} < \varepsilon_0 < 3\times10^{-5}$. Temperature dependences of logarithmic decrement $\delta$ of vibrations were measured in the temperature range 90–310 K during cooling and heating of the sample at a rate $\sim1$ K/min.

Figure 2 shows the temperature dependences $\delta(T)$ of decrement at vibrational frequency 78 kHz for two limiting deformation amplitudes: $\varepsilon_0 = \varepsilon_{0\,\min} = 3\times10^{-8}$ and $\varepsilon_0 = \varepsilon_{0\,\max} = 3\times10^{-5}$. A clearly manifested broad internal friction peak is observed at $T \approx 190$ K. An increase in the ultrasound amplitude by three orders of magnitude leads to an insignificant increase in $\delta(T)$ in the entire temperature range under investigation, as a result of which the peak height increases slightly. The shape of the peak and its position on the temperature axis remain almost unchanged. These changes suggest that the peak is associated with the linear resonant interaction of elastic vibrations with the system of identical elementary relaxators. An increase in the ultrasonic frequency leads to a shift of the peak temperature $T_p$ towards higher temperatures.

The dislocation structure of the sample under investigation can be changed noticeably in several ways. The most effective method is a considerable preliminary plastic deformation leading to an increase in the dislocation density. Another method is prolonged recovery of preliminary deformed samples, which leads as a rule to a decrease in dislocation density. The density of defects can also be increased by multiple thermocycling of the sample in a wide range of low temperatures at a high rate of temperature variation. The role of external deforming stress is played by thermoelastic stresses emerging in the sample. The influence of the above three factors on the internal friction peak under investigation is illustrated in Fig. 3. The figure shows the temperature dependences $\delta(T)$ of the decrement of vibrations at a frequency $\omega/2\pi = 78$ kHz in four cases: during first thermocycling of an undeformed sample in the temperature interval 300 K–6–300 K at a rate of 1 K/min; during repeated thermocycling at the same rate; immediately after deformation at room temperature to the residual strain $\varepsilon_{pl} = 5\%$, and after the 1-year holding of the deformed sample at room temperature.

The structural changes caused by thermoelastic stresses

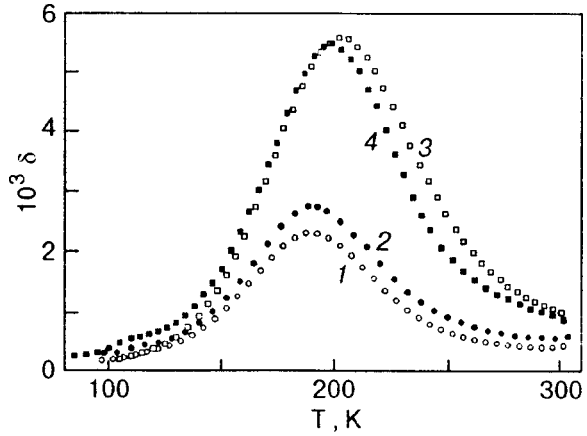


FIG. 3. Effect of variation of the defect structure of the sample on the internal friction peak in niobium detected in our experiments: undeformed sample subjected to single thermocycling (○), undeformed sample subjected to repeated thermocycling (●), immediately after plastic deformation (□), plastically deformed sample after 1-year holding at room temperature (■).

as well as external stresses lead to the following qualitative changes in the shape and parameters of the peak:

—the peak height $\delta_p = \max \delta(T)$ increases;

—the position $T_p$ of the peak on the temperature axis is displaced towards high temperatures;

—the peak width increases;

—the asymmetry of the peak increases due to its elevation above the background or an increase in the length of its high-temperature tail;

—the absorption background in the peak localization region increases weakly, but noticeably.

Prolonged low-temperature recovery of a deformed sample leads to opposite manifestations of the effects listed above.

The values of $T_p$ on the activation curve obtained in our experiments (see Fig. 1) coincide (to withing the spread in experimental values) with the array of points obtained by other authors. However, independent application of these values for determining the parameters of a relaxation process gives the values $U \approx 0.17\,\text{eV}$ and $\tau_0 \approx 2\times 10^{-10}\,\text{s}$ (straight line *2* in Fig. 1) that differ significantly from the values typical of the entire array of data on the $T_p(\omega)$ dependence. This circumstance emphasizes once again the difficulties emerging when the activation curve is used for microscopic interpretation of the relaxation resonance under investigation.

It is natural to assume that a possible reason behind the spread in points in Fig. 1 and the observed ambiguity in the empirical values of the parameters $U$ and $\tau_0$ is the influence of random inhomogeneities of the structure (primarily, dislocations) on the local values of these parameters in the bulk of the sample. Consequently, the first step in overcoming these difficulties must be the analysis of peculiarities of relaxational resonance, which are due to statistical nature of the parameters of elementary relaxators in real crystals.

## 3. THEORETICAL ANALYSIS OF THE EFFECT OF STATIC SPREAD IN ACTIVATION ENERGY OF ELEMENTARY RELAXATORS ON THE CONDITIONS OF RELAXATION RESONANCE

In this publication, we shall not consider specific microscopic models of an elementary relaxator whose interaction with elastic vibrations generates the internal friction peak under investigation. We shall only make a few remarks in this connection.

According to the aggregate of the main properties of the peak, it can be attributed to Bordoni peaks observed in the range of low temperatures for a number of fcc and bcc metals (in the case of bcc metals, such peaks are referred to as $\alpha$- and $\gamma$-peaks[8,15,18–20]). The typical values of the parameters $U$ and $\tau_0$ as well as the strong dependence of the peak height $\delta_p$ on the density of dislocations (growth dislocations or those introduced as a result of preliminary plastic deformations and vanishing in the course of recovery) allows us to consider as most probable microscopic models of a relaxator the following two elementary dislocation processes: thermoactivated generation of dislocation kinks pairs on rectilinear dislocation segments located in the valleys of the first-order Peierls relief, and thermoactivated diffusion of solitary kinks along dislocation lines through second-order Peierls barriers. It is important that an elementary relaxator of this type is strongly localized in the bulk of the crystal (in a region of the order of $10-10^2$ atomic spacings). In perfect crystals, it can be characterized by three parameters whose values in the first approximation are determined by energy and geometric parameters of a defect–free crystal: the activation energy $U_0$, the period of attacks $\tau_0$, and the characteristic elementary contribution $\Delta_0$ to the decrement of vibrations. If we denote by $C_r$ the relative volume concentration of such relaxators interacting with the vibrational mode of the sample under investigation, the expression defining their contribution to decrement of vibrations in the linear response approximation has the form of the Debye peak:

$$\delta(T,\omega) = 2\,\delta_p\,\frac{\omega\tau(u_0)}{1+\omega^2\tau^2(u_0)}, \tag{2}$$

where

$$\delta_p = C_r\Delta_0, \quad \tau(u_0) = \tau_0 \exp\left(\frac{U_0}{kT}\right).$$

The coordinate $T_p^{(0)}$ of the peak on the temperature axis is determined by the relations

$$\omega\tau(u_0) = 1, \quad T_p^{(0)} = -\frac{U_0}{k\ln(\omega\tau_0)}. \tag{3}$$

The peak height $\delta_p$ is naturally proportional to the contribution $\Delta_0$ from an individual relaxator as well as to the concentration $C_r$ of relaxators.

If a crystal contains a complex system of local structural inhomogeneities and long-range fields of internal stresses associated with a random distribution of various defects, the elementary relaxator parameters $U_0$, $\tau_0$, and $\Delta_0$ acquire random corrections in various regions of the crystal, and we must consider instead of these parameters random quantities

and distribution functions corresponding to them. The decrement of vibrations of a macroscopic sample is transformed in this case into a certain complex function $\overline{\delta}(T,\omega)$ obtained by statistical averaging of formula (2). The structure of formula (2) shows that averaging over the distribution of activation energy and attack period must produce the strongest effect on the temperature and frequency dependence $\overline{\delta}(T,\omega)$. Since the relaxation time $\tau$ also becomes a random quantity, we can introduce the distribution function for $\tau$ (the so-called relaxation spectrum) and average the Debye peak over this distribution.[15]

The phenomenological theory of mechanical relaxation in materials with random structural parameters[15] considers a set of distribution functions for these parameters as the basic problem. The application of these functions makes it possible to describe regularities of relaxation detected in experiments to the desired degree of accuracy. From the point of view of physics of thermoactivated processes, it is expedient to consider the activation energy and attack period as initial random parameters while using relation (1) for describing an elementary relaxation act, and seek the distribution function for these quantities. Obviously, such a distribution function will be determined only by the structure of the material and must be independent of temperature, and $\overline{\delta}(T,\omega)$ will be calculated using the explicit form of the temperature dependence of the function being averaged. On the contrary, while choosing the distribution function for relaxation time $\tau$, the temperature and structural characteristics are regarded as formally equivalent parameters that must determine this function, which obviously masks the physical role of temperature.

We shall not carry out a microscopic analysis of relaxation spectra here. Using the phenomenological approach developed in Ref. 15, we shall seek the distribution function which would make it possible to describe correctly the main peculiarities in the relaxation properties of the material under investigation (niobium), detected in experiments and described in the previous section. A specific feature of our analysis is that we essentially use the following three assumptions. First, we shall consider only a thermoactivated relaxation process and assume that only the structural parameters appearing in relations (1) and (2) are random quantities. Second, we shall confine our analysis to the region of low temperatures $kT \ll U_0$. Finally, we shall assume that the energy activation dispersion $D^2$ is quite small ($D \ll U_0$), i.e., consider relatively weak effects on the crystal structure leading to random variations of the initial value of activation energy. These assumptions allow us to take into account in the first approximation only the statistical nature of activation energy and disregard the dispersion of the parameters $\Delta_0$ and $\tau_0$ to an exponential accuracy.

Thus, taking into account the remarks made above, we shall assume that the only random parameter of the problem is the activation energy $U$ of an elementary relaxator. As a statistical characteristic of this quantity, we introduce the function $P(U)$, viz., the probability density for values of $U$, which is defined on the interval $(0,\infty)$ and satisfying the normalization condition

$$\int_0^\infty P(U)dU = 1. \tag{4}$$

In the case of statistical distribution of activation energy, the Debye peak (2) is transformed into a more complex function $\overline{\delta}(T,\omega)$ defined as

$$\overline{\delta}(T,\omega) = 2\Delta_0 C_r \int_0^\infty dU p(U) \frac{\omega\tau_0 \exp(U/kT)}{1+\omega^2\tau_0^2 \exp(2U/kT)}. \tag{5}$$

By way of a concrete simple example of the distribution $P(U)$, we consider a function of the form

$$P(U) = \frac{1}{\sqrt{2\pi D}} \left(\frac{U}{U_0}\right) \exp\left[-\frac{(U-U_0)^2}{2D^2}\right], \quad D \ll U_0. \tag{6}$$

It can be easily proved that a distribution of the quasi-Gaussian type (6) satisfies the normalization condition (4) to within a term of the order of $\exp(-U_0^2/2D^2)$, and the average value and dispersion corresponding to it to the first approximation in $D^2$ are given by

$$\overline{U} = \int_0^\infty UP(U)dU \cong U_0 + \frac{D^2}{U_0},$$

$$\overline{(U-\overline{U})^2} \cong \overline{(U-U_0)^2} = \int_0^\infty (U-U_0)^2 P(U)dU \cong D^2. \tag{7}$$

For $D \to 0$, distribution (6) is transformed to the Dirac delta-function $P(U) = \delta(U-U_0)$, which ensures the transition of the function $\overline{\delta}(T,\omega)$ (5) to the Debye peak (2) for low values of dispersion. At the same time, an increase in the parameter $D$, which broadens the distribution (6) and displaces its peak to high energies, leads to a broadening of the maximum of the temperature dependence of averaged decrement $\overline{\delta}(T,\omega)$ and to its displacement to high temperatures. It should also be noted that the asymmetry in distribution (6) relative to the value $U_0$ due to the factor $U$ in the preexponential factor leads to additional asymmetry of the temperature dependence $\overline{\delta}(T,\omega)$ relative to its peak.[1)] Consequently, the application of the distribution function (6) for calculating the averaged decrement of vibrations $\overline{\delta}(T,\omega)$ (5) creates all the premises required for the interpretation of the peculiarities of the mechanical relaxation peak in polycrystalline niobium samples described in the previous section. In the long run, the explanation of the properties of the peak boils down to the natural assumption that the relaxator concentration $C_r$ and the activation energy dispersion $D^2$ of an individual relaxator increase with the density of structural defects (e.g., dislocations) as a result of thermocycling or plastic deformation, while sample recovery decreases the values of these parameters.

Since the substitution of (6) into (5) leads to an integral that cannot be evaluated by using analytical methods, it is expedient to illustrate the validity of the above statements by using numerical integration. In order to transform the integral to a form convenient for numerical integration, we go

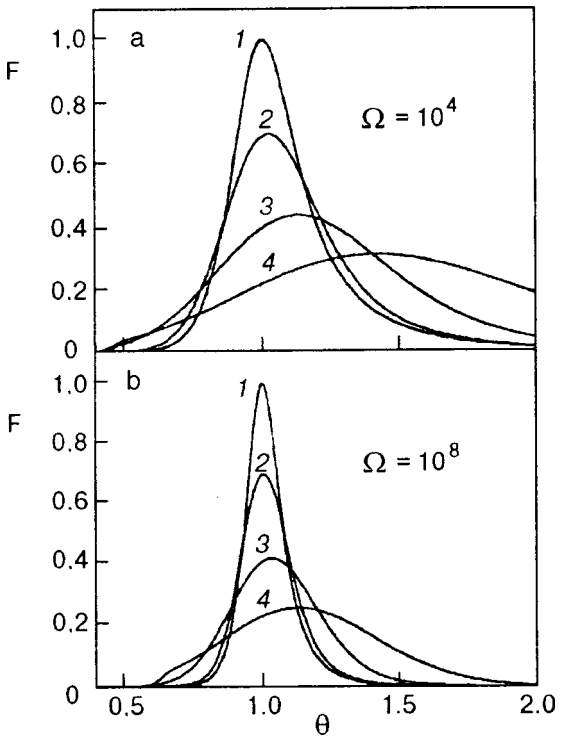


FIG. 4. Transformation of a Debye peak upon an increase in the dispersion of the activation energy of a relaxator: the result of numerical integration in formula (9) for essentially different values of the frequency parameter $\Omega$ ($10^4$ (a) and $10^8$ (b)) and different values of the dispersion parameter $d=0$ (curve *1*), 1 (curve *2*), 2.5 (curve *3*), and 5 (curve *4*).

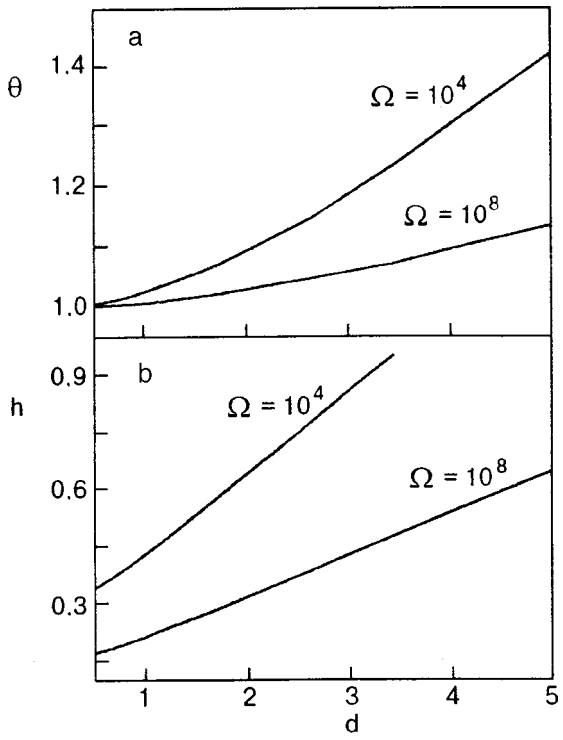


FIG. 5. Dependences of dimensionless localization temperature $\theta_p$ (a) and width $h$ (b) of the relaxation peak on the dispersion parameter $d$, obtained as a result of numerical integration in formula (9).

over to a new integration variable $x$ and a new set of the parameters of the problem, defining them by the relations

$$\ln x=\frac{U}{kT},\quad \theta=\frac{T}{T_p^{(0)}},\quad \Omega=\frac{1}{\omega\tau_0},\quad U_0=kT_p^0\ln\Omega,$$

$$d=\frac{\sqrt{2}D}{kT_p^{(0)}}=\frac{\sqrt{2}D}{U_0}\ln\Omega. \tag{8}$$

Here we have introduced the dimensionless temperature $\theta$, the reciprocal dimensionless frequency $\Omega$, and the dimensionless characteristic dispersion $d$. As a result of such a substitution, the averaged decrement of vibrations $\overline{\delta}(T,\omega)$ assumes the form

$$\overline{\delta}=C_r\Delta_0F(\theta,\Omega,:d),$$

$$F=\frac{2\Omega\theta^2}{\sqrt{\pi}d\ln\Omega}\int_1^\infty dx\,\frac{\ln x}{x^2+\Omega^2}\exp\left[-\left(\frac{\theta\ln x-\ln\Omega}{d}\right)^2\right]. \tag{9}$$

We are mainly interested in the variation of the temperature dependence of the decrement (relaxation peak on the temperature axis) upon an increase in the dispersion of activation energy of relaxators: the absence of dispersion corresponds to the limit $d\to 0$, while a relatively high dispersion is defined by the inequality $d\geqslant 1$. It should be noted that $\ln\Omega=-\ln(\omega\tau_0)\geqslant 10$ in actual practice, and hence our initial assumption concerning the fulfillment of the inequality $D\ll U_0$ permits an analysis of the inequality $d>1$. We choose two values of the parameter $\Omega=10^4$ and $10^8$ typical of ultrasonic experiments and consider the temperature dependence of the function $F(\theta)$ for several essentially different values of the parameter $d$. Numerical integration gives for the function $F(\theta,\Omega,d)$ the family of the curves shown in Fig. 4. For low values of $d$, the temperature dependence of the function $F(\theta,\Omega,d)$ has a peak at the point $\theta\approx 1$ and virtually coincides with the Debye peak (curve *1* in Fig. 4), while an increase in the parameter $d$ leads to a displacement of the peak towards high temperatures, its broadening, and an increase in asymmetry. For a quantitative characteristic of peak broadening, we can use the parameters

$$T_h=T_p^{(+)}-T_p^{(-)},\quad h=\frac{T_h}{T_p^{(0)}}=\theta_h^{(+)}-\theta_h^{(-)}, \tag{10}$$

where $\theta_h^{(+)}$ and $\theta_h^{(-)}$ are the values of temperature for which $F(\theta^{(+)})=F(\theta^{(-)})=0.5F(\theta_p)$ and $\theta_p$ is the peak of the function $F(\theta)$. The variation of the parameters $\theta_p$ and $h$ of the peak upon an increase in $d$ is illustrated in Fig. 5.

The curves in Fig. 5 describing the functions $\theta_p(d,\Omega)$ and $h_p(d,\Omega)$ permit simple analytic approximations whose accuracy is of the order of a few percent:

$$\theta_p=1+2\left(\frac{d}{\ln\Omega}\right)^2, \tag{11}$$

$$h=\frac{2(1+d)}{\ln\Omega}. \tag{12}$$

Using relations (8) and (10)–(12), we can easily obtain a system of two equations connecting the parameters $U_0$, $\tau_0$, and $D$ of the theory with the experimentally measured quantities $T_p$ and $T_h$:

$$U_0^2+4D^2+kT_pU_0(\ln\tau_0+\ln\omega)=0;$$

$$U_0-\sqrt{2}D(\ln\tau_0+\ln\omega)-\frac{1}{2}kT_h(\ln\tau_0+\ln\omega)^2=0. \quad (13)$$

It is convenient to write the first of these equations in the form of the relation corresponding to the activational curve $\ln\omega$ vs. $T_p^{-1}$:

$$\ln\omega=\ln\tau_0^{-1}-\frac{U_0^2+4D^2}{kU_0}\frac{1}{T_p}. \quad (14)$$

Recording the dependence $T_p(\omega)$ in a wide frequency range and plotting the activation curve, we can obtain empirical estimates for the parameter $\tau_0$ and effective activation energy $U_{\text{eff}}$ whose role is played by the factor in front of $T_p^{-1}$. The values of these parameters can also be estimated in the conventional way by measuring the values of $T_p$ for two close values of frequencies $\omega_1$ and $\omega_2$:

$$\tau_0^{-1}=\omega_0\exp\left[T_p\left(\frac{\partial T_p}{\partial\ln\omega}\right)^{-1}\right]$$

$$\cong\omega_1\exp\frac{T_p(\omega_2)\ln(\omega_2/\omega_1)}{T_p(\omega_2)-T_p(\omega_1)}, \quad (15)$$

$$U_{\text{eff}}=U_0\left(1+\frac{4D^2}{U_0^2}\right)=kT_p^2\left(\frac{\partial T_p}{\partial\ln\omega}\right)^{-1}$$

$$\cong\frac{kT_p(\omega_1)T_p(\omega_2)\ln(\omega_2/\omega_1)}{T_p(\omega_2)-T_p(\omega_1)}. \quad (16)$$

It should be noted that, in order to ensure the correctness of the procedure of determining $\tau_0$ and $U_{\text{eff}}$, we must use the empirical dependence $T_p(\omega)$ obtained for a constant value of $D$, i.e., for a invariable structure of the crystal.

Equations (13) also make it possible to determine empirical values of the initial activation energy $U_0$ and dispersion $D^2$ using the measurements of the temperature $T_p$ of the peak and its width $T_h$ for any fixed value of frequency $\omega$. The solution of the system of equations (13) for $U_0$ and $D$ to within the terms of the order $2(\ln\tau_0\omega)^{-2}\ll 1$ has the form

$$U_0=\frac{k(T_h^2-T_p^2)\ln(\tau_0\omega)}{T_p}+2kT_h, \quad (17)$$

$$D=-\frac{1}{2\sqrt{2}}[T_h\ln(\tau_0\omega)+2T_p]. \quad (18)$$

Concluding this section, we note that while using formulas (9) and (14)–(18) for interpreting experimental data, it should be borne in mind that various effects exerted on the crystal and changing the statistical parameters of relaxators can also lead in some cases to a change in the concentration $C_r$ of relaxators. This can result in the emergence of additional peculiarities in the behavior of the relaxation peak height that are absent in Fig. 4, e.g., an increase in $\max\overline{\delta}$ accompanied by a displacement of the peak towards high temperatures in the cases when the increase in $C_r$ is more significant than the decrease in $\max F$.

## 4. THEORY AND EXPERIMENT

Taking into account the phenomenological nature of the proposed theory, we must compare its results with experimental data using a correctly selected distribution function $P(U)$ and chosing the values of the parameters $\tau_0$, $U_0$, $D$, and $C_r\Delta_0$ which makes it possible to put in correspondence the temperature dependences shown in Figs. 2 and 3 to the dependences defined by formulas (9).

Expression (9) describes the contribution of attenuation of the statistical ensemble of identical thermoactivated relaxators with a quasi-Gaussian distribution function (6) for values of activation energy to the absorption of elastic vibrations. This expression can be used to describe all the main peculiarities in the behavior of the acoustic relaxation peak in niobium studied by us and described in Sec. 2 if we make the natural assumption that thermocycling and plastic deformation of the sample increases the density of structural defects as well as the activation energy dispersion $D^2$ and concentration $C_r$ of relaxators, while prolonged recovery must reduce these parameters.

A separate problem emerging when we compare the results of proposed theory with experimental data is the correct subtraction of the absorption background for all peaks in Fig. 3. Taking into account the small value and weak temperature dependence of the background at the foot of the peaks on the side of low temperatures, we can replace the background in the region of peaks in Fig. 3 by constants whose values are determined only by the structural state of the samples. For such constants, we can use the experimental values of the decrement $\delta$ at $T=100$ K. Thus, we shall speak on the verification of the applicability of the relation

$$\delta-\delta_{100\text{ K}}=C_r\Delta_0F(\theta,d,\Omega) \quad (19)$$

to the description of experimental data presented in Figs. 2 and 3.

Going over to an analysis of experimental data, we must primarily consider the displacement of the absorption peak on the temperature axis upon a change in the vibrational frequency (see Fig. 2). Using the data presented in this figure and formula (15), we obtain an empirical estimate for one of the principal microscopic parameters of the relaxation process, viz. the attack frequency $\tau_0^{-1}$ whose value is given in the last row of Table I.

In order to obtain empirical estimates of the ''initial'' activation energy $U_0$ and the parameter $D$ characterizing the statistical spread in the activation energy in a certain structural state of the sample, we must use the data presented in Fig. 3. For each peak presented in this figure, we can estimate the temperature $T_p$ of the peak and its width $T_h$ and to substitute these values into formulas (17) and (18). However, the accuracy of these estimates is not very high in view of considerable uncertainty in the values of $T_h$. In order to improve the accuracy of estimates of the parameters $U_0$ and $D$ and to verify the quantitative agreement between the ex-

TABLE I. Dependences of the parameters of absorption peak at vibrational frequency $\omega/2\pi=78$ kHz on the structural state of the sample and empirical values of the parameters of the theory parameters.

| Parameters of peak | Structural state of samples | | | |
|---|---|---|---|---|
| | 1 | 2 | 3 | 4 |
| $T_p$, K | 190 | 191 | 202 | 198 |
| $T_h$, K | 66 | 66 | 75 | 65 |
| $[\delta(T_p)-\delta(100\,\mathrm{K})]\cdot 10^3$ | 2.0 | 2.3 | 5.2 | 4.8 |
| $(C_r\Delta_0)\cdot 10^3$ | 2.54 | 2.97 | 7.02 | 5.92 |
| $d$ | 0.69 | 0.70 | 0.87 | 0.58 |
| $D$, $10^{-3}$ eV | 7.79 | 7.91 | 9.83 | 6.55 |
| $U_{\mathrm{eff}}$, eV | 0.152 | 0.152 | 0.153 | 0.151 |
| $U_0$, eV | 0.15 | | | |
| $\tau_0$, s | $1\times 10^{-10}$ | | | |

*Remark*. Numeration of structural states of the samples is the same as in Fig. 3.

perimental values and formula (19), we can use the potentialities of computer numerical analysis. Proceeding from the rough estimates of $T_p$ and $T_h$ obtained from Fig. 3 and the values of $U_0$ and $D$ calculated on their basis, we can select the refined values of the parameters $U_0$, $D$, and $C_r\Delta_0$, which make it possible to match experimental points on the $\delta(T)$ dependences with the curves describing the function (19) to a high degree of accuracy. The possibility of such a matching is illustrated in Fig. 6, and the corresponding fitting values of the parameters of the theory are given in the bottom rows of the table. In Fig. 6, the experimental points presented in Fig. 3 are normalized to the scale of dimensionless temperature $\theta=kT\ln\Omega/U_0$, and the values of $U_0$, $D$, and $C_r\Delta_0$ are chosen so that the theoretical curves in their central parts match the experimental points to the maximum possible extent. It should be noted that deviations of experimental points from the curves on the tails of the peaks are in all probability due to errors made as a result of application of extremely simplified procedure for substracing the background absorption.

The values of the parameters $C_r\Delta_0$ and $D$ given in Table I indicate that the volume density of elementary relaxators and the dispersion of their activation energy increase as a result of thermocycling and plastic deformation of the samples, while sample recovery is accompanied by a slight increase in the relaxator density and a quite strong decrease in the activation energy dispersion.

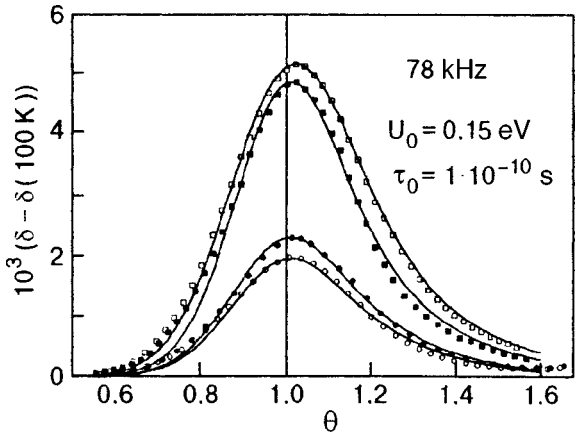


FIG. 6. Comparison of experimental data on temperature dependences of the decrement of vibrations for various structural states of the sample (see Fig. 3) with the theoretical dependence (19) constructed for a set of specially selected values of the parameters $U_0$, $\tau_0$, $D$, and $C_r\Delta_0$ given in Table I.

It should be noted that the refined values of activation parameters of the peak under investigation contained in Table I differ slightly from the preliminary rougher estimates obtained on the basis of the activation curve (straight line *2* in Fig. 1). The difference between these values and the mean values typical of the entire system of peaks observed earlier in experiments on internal friction in niobium in the range of moderately low temperatures (straight line *1* in Fig. 1) is much stronger. This circumstance indicates that several (at least two) thermoactivated relaxation processes can occur in niobium in this temperature range.

## 5. CONCLUSIONS

The results of our experiments and their theoretical analysis lead to several important conclusions.

—The internal friction peak detected and studied by us for polycrystalline niobium in the temperature range $\sim 200$ K possesses the properties of a thermally activated relaxation peak and emerges due to the interaction of elastic vibrations of the sample with a system of identical elementary relaxators characterized by the activation energy $U_0\approx 0.15$ eV and the attack frequency $\tau_0^{-1}\approx 1\times 10^{10}\,\mathrm{s}^{-1}$ for structurally erfect samples.

—The activation parameters of the peak differ significantly from the parameters of other peaks observed earlier for single crystals of niobium as well as polycrystalline samples in the range of moderately low temperatures (see Fig. 1).

—the position of the peak on the temperature axis and its shape are noticeably sensitive to the structural state of niobium samples. The parameters of the peak vary as a result of thermocycling, plastic deformation, and recovery.

—Structural sensitivity of the parameters of the peak is due to a change in the volume density of relaxators and statistical distribution of activation energy upon a change in the defect structure of the samples.

—In all the cases analyzed in our experiments, the statistical spread of activation energy values for relaxators is quite small and is successfully described by a function of the quasi-Gaussian type (6) with a low dispersion determined by the structural state of the sample.

The authors are grateful to S. N. Smirnov for fruitful discussions and advice concerning the problem touched upon in this publication.

*)E-mail: palval@ilt.kharkov.ua

1)The asymmetry of the distribution $P(U)$ and of the function $\overline{\delta}(T,\omega)$ can be varied by choosing other powers of the variable $U$ in the preexponential factor in formula (6).

[1] L. J. Bruner, Phys. Rev. **118**, 399 (1960).
[2] R. H. Chambers and J. Schultz, Acta Metall. **8**, 585 (1960).
[3] R. H. Chambers and J. Schultz, Phys. Rev. Lett. **6**, 273 (1961).

[4] P. G. Bordoni, M. Nuovo, and L. Verdini, Phys. Rev. **123**, 1204 (1961).
[5] H. Schultz and R. H. Chambers, Bull. Am. Phys. Soc. **9**, 214 (1964).
[6] E. J. Kramer and C. L. Bauer, Phys. Rev. **163**, 407 (1967).
[7] F. M. Mazzolai and M. Nuovo, Solid State Commun. **7**, 103 (1969).
[8] R. Chambers, in Physical Acoustics, *Principles and Methods*, vol. 3 (Ed. by W. Mason), New York (1968).
[9] R. Klam, H. Schultz, and H.-E. Schaefer, Acta Metall. **27**, 205 (1979).
[10] N. Kuramochi, H. Mizubayashi, and S. Okuda, Scr. Metall. **14**, 1047 (1980).
[11] V. V. Zoninashvili, I. A. Naskidashvili, U. Messerschmidt *et al.*, Phys. Status Solidi A **75**, K205 (1983).
[12] N. Kuramochi, H. Mizubayashi, and S. Okuda, Phys. Status Solidi A **104**, 453 (1987).
[13] S. Okuda, T. Motoyama, N. Kuramochi, and T. Arai, J. Phys. (Paris), Colloq. **46**, C10 (1985).
[14] R. de Batist, *Internal Friction of Structural Defects in Crystalline Solids*, Elsevier, New York (1972).
[15] A. S. Nowick and B. S. Berry, *Anelastic Relaxation in Crystalline Solids*, Academic Press, New York, 1972.
[16] P. P. Pal-Val and H.-J. Kaufmann, Fiz. Nizk. Temp. **9**, 325 (1983) [Sov. J. Low Temp. Phys. **9**, 163 (1983)].
[17] V. D. Natsik, P. P. Pal-Val, and S. N. Smirnov, Akust. Zh. **44**, 640 (1998) [Acoust. Phys. **44**, 553 (1998)].
[18] A. Seeger and C. Wüthrich, Nuovo Cimento B **33**, 38 (1976).
[19] P. P. Pal-Val, V. D. Natsik, and S. Kadeckova, Philos. Mag. A **56**, 407 (1987).
[20] P. P. Pal-Val, V. D. Natsik, and S. Kadeckova, Phys. Status Solidi A **105**, K37 (1988).

Translated by R. S. Wadhwa

## BRIEF COMMUNICATIONS

# On the origin of optical conductivity of HTSC in infrared spectral region

V. N. Samovarov*)

*B. Verkin Institute for Low Temperature Physics and Engineering, National Academy of Sciences of the Ukraine, 310164 Kharkov, Ukraine*

(Submitted January 29, 1999; revised March 15, 1999)
Fiz. Nizk. Temp. **25**, 758–762 (July 1999)

An expression for the frequency dependence of the anomalous component of optical conductivity $\sigma_{\mathrm{MIR}}(\omega)$ of cuprate superconductors is derived for the entire range of non-Drude intraband excitations $0<\hbar\omega<\hbar\omega_g\approx 1.5-2$ eV. The derivation is based on the assumption on finite probability of penetration of an electron (hole) from the hole band to the upper conduction band through the optical gap $\hbar\omega_g$, ensuring the correlated coupling between intraband and interband excitations. It is shown that the available experimental data are in good agreement with the two-component model, taking into account the total contribution of the anomalous component $\sigma_{\mathrm{MIR}}$ and the conventional Drude component $\sigma_D$ to the conductivity of the metal phase.  [S1063-777X(99)01607-2]

In contrast to traditional BCS superconductors, the optical conductivity of HTSC materials contains a considerable contribution of the non-Drude conductivity component $\sigma_{\mathrm{MIR}}(\omega)$, which does not obey the Drude classical law $\sigma_D(\omega)\propto\omega^{-2}$.[1] The anomalous component $\sigma_{\mathrm{MIR}}(\omega)$ is observed in the spectral region from zero frequency to the boundary energy $\hbar\omega_g=1.5-2$ eV, which is equal to the optical gap between the Fermi level located deep in the valence band and the upper (vacant) conduction band. The dependence $\sigma_{\mathrm{MIR}}(\omega)$ in the metal phase with a small number of charge carriers displays a clearly manifested peak in the middle IR frequency range $\sim 0.3-0.5$ eV, which allows us to call it the MIR component of the spectrum. As a result, the conductivity of the active $CuO_2$ plane in the energy range $<\hbar\omega_g$ can be presented b.y the two-component model

$$\sigma(\omega)=\sigma_D(\omega)+\sigma_{\mathrm{MIR}}(\omega)=\frac{1}{4\pi}\frac{\omega_P^2\Gamma_D}{\omega^2+\Gamma_D^2}+\sigma_{\mathrm{MIR}}(\omega), \tag{1}$$

where $\omega_P$ is the plasma frequency and $\Gamma_D$ the absorption for Drude charge carriers. The total conductivity $\sigma(\omega)$ gives the spectrum of intraband hole excitations. An interband conductivity component $\sigma_{\mathrm{CT}}(\omega)$ associated with photo-induced transfer of an electron from oxygen to copper ($Cu^{2+}O^{2-}\rightarrow Cu^{+}O^{-}$) emerges at frequency exceeding the optical gap width $\hbar\omega\geqslant\hbar\omega_g$. This component of the excitation spectrum associated with charge transfer (CT-component) determines the emergence of additional holes in the valence band.

Several explanations of the origin of the MIR-component of conductivity offered at present include the model of a marginal Fermi liquid,[2] Luttinger liquid,[3] and polaron[4] and bipolaron models.[5] A comparative analysis with experimental data does not allow us to give preference to any of the above models (see, for example, Ref. 6), which would be equally applicable for all cuprate HTSC upon variation of temperature and doping level. It should be noted in this connection that the available models are not based on the experimental result common for all cuprates, i.e., the existence of a correlated coupling between intraband and interband transitions. However, the crucial point for HTSC is the existence of interrelation between oscillator forces of MIR- and CT-transitions rather than the emergence of the anomalous component $\sigma_{\mathrm{MIR}}(\omega)$.

The gap width for cuprate HTSC formed by states with charge transfer remain virtually unchanged upon an increase in the doping level to the optimal value, but the integral value of interband conductivity decreases, while the integral value of intraband conductivity increases (e.g., for Y- and La-based samples).[7,8] Such an evolution of conductivity spectrum reflects in the purest form the interrelation of oscillator forces of transitions. (The optical gap for $Ba_{1-x}K_xBiO_3$ and similar compounds, which emerges due to excitation of charge density waves, decreases upon doping, and the interband component is shifted to the IR region, preserving its spectral area[9]).

The correlation coupling of MIR and CT excitations was observed for Bi-, Y-, and La-based compounds not only upon a change in the chemical doping level, but also upon cooling (photo-induced doping and structural ordering of YBCO).[10,11] For example, optical absorption during CT-transitions is suppressed upon cooling of YBCO, BSCCO, and LaCO samples in the entire spectral range, while the integral intensity increases during MIR-transitions.[4,5,11] A response of absorption to the superconducting transition is observed in the frequency range of MIR- and CT-excitations,[4,5,10,11] which was initially detected in absorption of YBCO films in the visible frequency range.[12] The response at MIR- and CT-frequencies has opposite polarities[4,11] in analogy with opposite signs of variations of

 

MIR and CT-spectra upon a change in temperature or doping level.

The interrelation between excitations observed upon a change in the doping level[13] can be traced quantitatively most exactly from the results of optical experiments with $La_{2-x}Sr_xCuO_4$ single crystals[7] containing only one $CuO_2$ plane in a unit cell:

$$\Delta_x\left(\int \sigma_{\mathrm{MIR}}(\omega)d\omega\right) = -\Delta_x\left(\int \sigma_{\mathrm{CT}}(\omega)d\omega\right). \tag{2}$$

This equation indicates that as a result of doping (increase in the number of holes $n \propto x$), the CT conductivity is completely converted into the MIR conductivity. This interrelation is preserved from the beginning of metallization ($x \simeq 0.05$) up to the optimal value $x \simeq 0.15$, above which the relative contribution of the Drude spectral component increases strongly, and the samples start losing their superconducting properties. Ultimately, a change in the conductivity indicates the pumping of excitation energy since, according to the rigorous sum rule,[1] $\int \sigma(\omega)d\omega \propto \langle T\rangle$, where $\langle T\rangle$ is the kinetic energy of the system.

The above arguments allow us to analyze the intraband MIR-conductivity by using the model of two coupled oscillators with oscillatory modes at frequencies $\omega_1$ and $\omega_2$. From the quantum-mechanical point of view, the coupling of oscillators is due to finite probabilities for an electron (hole) to be in two states at instant $t$:

$$|\Psi|^2_{1,2} = \frac{1}{2}[1 \pm \cos(\omega_1 - \omega_2)t]. \tag{3}$$

The difference in the oscillatory frequencies for HTSC can be naturally assumed to be equal to the optical gap width $\hbar\omega_g = \hbar(\omega_1 - \omega_2)$, which suggests that an electron can experience interband ''tunneling'' through the optical gap along the oxygen–copper bond with the formation of a hole in the valence band. Consequently, in order to find the frequency dependence of conductivity, we can proceed from the following equation:

$$\frac{d(|\Psi|^2 v)}{dt} + (|\Psi|^2 v)\gamma = -\frac{e}{m_0}E(\omega)|\Psi|^2, \tag{4}$$

where $v$, $e$, and $m_0$ are the electron velocity, charge, and mass, $E(\omega)$ is the field of a light wave, and the quantity $\gamma$ characterizes attenuation which is determined by the energy blurring of energy levels. Generally speaking, the blurring of energy levels can be included in the expression (3) for probability density,[14] but we shall take it into account subsequently in attenuation. On the basis of Eq. (4), we obtain the following expression for the real conductivity component:

$$\sigma(\omega) = \frac{2A\gamma}{2(\omega+\omega_g)^2 + 2\omega_g(\omega+\omega_g) + \omega_g^2 + 2\gamma^2}, \tag{5}$$

where $A$ is a constant that will be determined later. First, we shall define $\gamma$ on the basis of the following considerations. The harmonic type of (3) can be disturbed due to random transitions of an electron (hole) through the optical gap, which lead to recombination of charge carriers. As a result, attenuation of intraband current must be proportional to the probability of a transition between two states: $\gamma = \gamma_0[1 - \exp^{-(\varepsilon/\hbar)t}]$, where the parameter $\varepsilon = \varphi(\mathrm{const} - \varepsilon_F)$ characterizes the energy level blurring and hence is a function of the hole gap width $\varepsilon_F$, which is proportional to the number $n$ of charge carriers ($\varepsilon_F = 10^{-1}$ eV). We must substitute into (5) the value of $\gamma$ for the time interval equal to the period of the applied field. In this case, we can put the attenuation at zero frequency equal to $\gamma_0 = 2\omega_g\lambda(n)$ proceeding from the uncertainty relation, where the dimensionless parameter $\lambda(n) \sim 1$ also depends on the number of charge carriers. This gives

$$\gamma = 2\omega_g\lambda(n)[1 - \exp(-\varepsilon(n)/\hbar\omega)].$$

In order to determine the constant $A$, we can use the standard approach, assuming that it is equal to the square of a certain effective plasma frequency $\Omega_{\mathrm{eff}}(m^*)$, which is a function of effective mass $m^*$. However, we shall use a different approach[13] that does not require the introduction of the additional parameter $m^*$ for describing the frequency dependence of conductivity in the case of correlated coupling of intraband and interband excitations in HTSC. Let us suppose that a mobile hole is formed only in the lower band of the system. We assume that in this case the conductivity $\sigma(0)$ in the lowermost energy state for $\hbar\omega = 0$ is equal to the minimum conductivity realized due to the charge transfer along the oxygen–copper bond of length $a_0$: $\sigma(0) \equiv \sigma_{\min} = e^2/ha_0$, where $h/e^2$ is the resistance quantum ($\sigma_{\min} = 2100\,\Omega^{-1}\cdot\mathrm{cm}^{-1}$ for $La_{2-x}Sr_xCuO_4$). In this case, $A = \sigma(0)\omega_g(5 + 8\lambda^2)/4\lambda$. If the system contains $n$ mobile holes in the lower band and accordingly $n$ electrons in the upper band, $A$ must be multiplied by $2n$ (we can assume that the effective number of charge carriers participating in this case in the creation of intraband current is $N_{\mathrm{eff}} = 2n$). For primitive cells of Y- and La-based compounds, $n = x$, where $x$ is the level of doping of the sample by oxygen or strontium. Thus, the final expression for intraband conductivity emerging as a result of interband ''tunneling'' of charge carriers has the form

$$\sigma_{\mathrm{MIR}}(\omega) = \frac{2x\sigma(0)\omega_g^2(5 + 8\lambda^2)[1 - \exp(-\varepsilon/\hbar\omega)]}{2(\omega+\omega_g)^2 + 2\omega_g(\omega+\omega_g) + \omega_g^2[1 + 8\lambda^2(1 - \exp(-\varepsilon/\hbar\omega))^2]}. \tag{6}$$

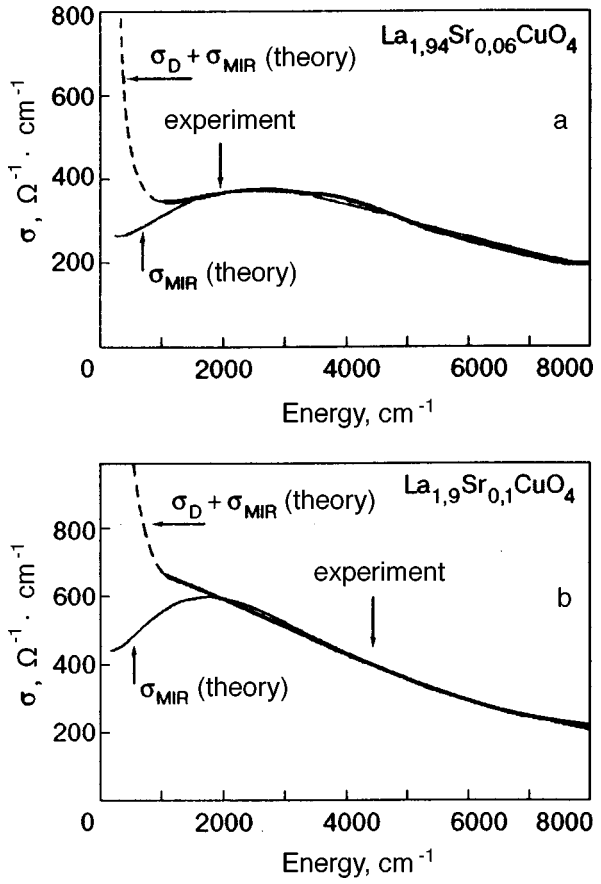


FIG. 1. Optical conductivity spectrum for the $CuO_2$ plane of a $La_{2-x}Sr_xCuO_4$ single crystal: $x=0.06$ (a) and $x=0.1$ (b). Experimental data were obtained at 300 K[7] (bold curves), the behavior of MIR conduction band calculated by formula (6) (solid curves), and joint contributions of the Drude and MIR conductivity components according to our results (dashed curves).

Pay attention to the fact that Eq. (6) acquires non-Lorentzian terms $(\omega+\omega_g)^2$ and $(\omega+\omega_g)$ determining the behavior of the high-frequency branch of (6). It was proved earlier on the basis of analysis of integral conductivity of HTSC[13] that the intraband conductivity of Y- and La-based samples contains a noticeable contribution $\sigma_{MIR} \propto (\omega+\omega_g)^{-2}$, but the reasons for the emergence of such a peculiar frequency dependence were not indicated.

A comparison of the results obtained by using Eq. (6) with experimental data was carried out for a series of available results on the optical conductivity of Y- and La-based compounds in a wide range of doping. By way of an example, Figs. 1a and 1b show the results of comparison for $La_{2-x}Sr_xCuO_4$ ($\hbar\omega_g=1.7$ eV) for $x=0.06$ and 0.1, when the contribution of the Drude component weakly masks the frequency dependence of the MIR component of the spectrum. A good agreement with experiment is observed, the values of $\lambda=2.2$ and $\varepsilon=0.18$ eV for $x=0.06$, and $\lambda=2$ and $\varepsilon=0.13$ eV for $x=0.1$. Slight discrepancy in the low-frequency spectral region for $\hbar\omega<0.2$ eV can be eliminated easily by adding the Drude term with the following typical parameters: $\omega_P=5300\,cm^{-1}$ and $\Gamma_D=100\,cm^{-1}$ for $x=0.06$, $\omega_P=6800\,cm^{-1}$, $\Gamma_D=200\,cm^{-1}$ for $x=0.1$. It should be noted that the given values of $\omega_P^2=4\pi ne^2/Vm^*$, where $V=95\cdot10^{-24}\,cm^{-3}$ is the volume per structural unit, corresponds to the quantities $n=x$ and $m^*=2m_0$. Dashed curves show the overall spectrum of intraband conductivity in this two-component model. The values of $\lambda$ and $\varepsilon$ change in this case insignificantly. The agreement with experimental results is observed up to the energy of $8000\,cm^{-1}$ ($\approx1$ eV) with an error smaller than 2% (for this reason, the experimental and theoretical curves virtually coincide for $\hbar\omega>1500\,cm^{-1}$). It can be seen that the expression (6) for conductivity component simulates not only the emergence of an asymmetric MIR peak, but also its displacement to the low-frequency region upon an increase in the doping level ($\approx2500\,cm^{-1}$ for $x=0.06$ and $\sim1500\,cm^{-1}$ for $x=0.1$), which is observed in experiments with HTSC.[15] A comparison with experimental results for YBCO[8] shows that the values of parameters lie near $\lambda=1$ and $\varepsilon=0.3$ eV for various levels of doping.

It is interesting to compare the results with the experimental data for the standard choice of the constant $A$ in formula (5): $2A=\Omega_{eff}^2=e^2 2x/Vm^*$, which can be presented in the form $e^2(2x)_S/m^*d$ for the two-dimensional case, where $(2x)_S\simeq(1-2)\cdot10^{14}\,cm^{-2}$ is the ''surface'' charge carrier density in the conducting $CuO_2$ layer for $x\leqslant0.1$, and $d$ is a certain effective thickness of the conducting layer. For $m^*=m_0$, the agreement with experimental results is attained for values of $d$ of the atomic scale $\approx1$ Å, which is comparable with or even smaller than the length $a_0=1.9$ Å of the oxygen–copper bond. Such a qualitative analysis shows that the proposed mechanism of formation of the intraband conductivity component is realized in a system with clearly pronounced two-dimensional nature. In the doping range above the optimal, the three-dimensionality is enhanced (the conductivity across $CuO_2$ layers acquires features of metal-type conductivity)[16] and the contribution to conductivity of isotropic Drude carriers whose plasma frequency corresponds to the condition $d\gg a_0$ increases significantly. As a result, the operation of the ''tunnel'' mechanism is weakened considerably ($\varepsilon\to0$) for strong doping, as superconductivity is suppressed. Apparently, a narrow $2D$-hole band is involved in this mechanism (narrow peak of the density of states), in which heavy charge carriers are subjected to strong $Cu^{2+}O^{2-}$–$Cu^{+}O^{-}$ fluctuations. Light carriers mainly determine the Drude conductivity. As the doping level increases, the peak of the density of states becomes blurred, fluctuations are suppressed, and as a result, the probability of interband transfer of charge carriers through the optical gap decreases sharply.

The author is grateful to I. Ya. Fugol for fruitful discussions and to V. L. Vakul for his assistance in carrying out a comparative analysis of experimental and theoretical results.

*)E-mail: samovarov@ilt.kharkov.ua

[1] E. Dagotto, Rev. Mod. Phys. **66**, 763 (1994).
[2] C. M. Varma, P. B. Littlewood, S. Schmitt-Rink *et al.*, Phys. Rev. Lett. **63**, 1996 (1989).
[3] P. W. Anderson, Physica C **185–189**, 11 (1991).
[4] C. H. Rüscher and M. Götte, Solid State Commun. **85**, 393 (1993).

[5] H. I. Kaufmann, E. K. H. Salie, Y. Yagil, and O. V. Dolgov, J. Supercond. **10**, 299 (1997).
[6] C. Baraduc, A. Azrak, and N. Bontemps, J. Supercond. **9**, 3 (1996).
[7] S. Uchida, T. Ido, H. Takagi *et al.*, Phys. Rev. B **43**, 7942 (1991).
[8] S. L. Cooper, D. Reznik, A. Kots *et al.*, Phys. Rev. B **47**, 8233 (1993).
[9] S. H. Blanton, R. T. Collins, K. H. Kelleher *et al.*, Phys. Rev. B **47**, 996 (1993).
[10] I. Ya. Fugol and V. N. Samovarov, Fiz. Nizk. Temp. **22**, 1241 (1996) [Low Temp. Phys. **22**, 945 (1996)].
[11] I. Ya. Fugol, V. N. Samovarov, and M. Yu. Libin, Fiz. Nizk. Temp. **25**, 459 (1999) [Low Temp. Phys. **25**, 335 (1999)].
[12] I. Ya. Fugol, V. N. Samovarov, Yu. I. Rybalko *et al.*, Sverkhprovodimost': Fiz., Khim., Tekhn. **4**, 109 (1991) [Supercond., Phys. Chem. Technol. **4**, 94 (1991)].
[13] V. N. Samovarov, Fiz. Nizk. Temp. **24**, 1043 (1998) [Low Temp. Phys. **24**, 782 (1998)].
[14] A. S. Davydov, *Quantum Mechanics*, Pergamon Press, Oxford, 1976.
[15] P. Calvani and S. Lupi, Solid State Commun. **85**, 665 (1993).
[16] J. Schutzmann, S. Tajima, S. Miyamoto, and S. Tanaka, Phys. Rev. Lett. **73**, 174 (1994).

Translated by R. S. Wadhwa